

UNIVERSITY OF CALIFORNIA

Santa Barbara

Interactions of tectonics, climate, and deposition in intermontane basins on the margin of the  
Puna Plateau, NW Argentina

A dissertation submitted in partial satisfaction of the  
requirements for the degree Doctor of Philosophy  
in Earth Science

by

Rebecca Lydia Jirón

Committee in charge:

Professor Douglas Burbank, Chair

Professor John Cottle

Professor Alexander Simms

December 2015

The dissertation of Rebecca Lydia Jirón is approved.

---

Alexander Simms

---

John Cottle

---

Douglas Burbank, Committee Chair

August 2015

Interactions of tectonics, climate, and deposition in intermontane basins on the margin of the  
Puna Plateau, NW Argentina

Copyright © 2015

by

Rebecca Lydia Jirón

## ACKNOWLEDGEMENTS

To everyone who shared with me your collaboration, guidance, discussions, friendship, and support over the years:

Thank you.

I would like to give special thanks to my advisor, Doug Burbank, for challenging me intellectually and guiding my development as a scientist. Additional thanks to the many other people in the UCSB geology department who helped me with this work in one form or another. In particular, I would like to thank Andrew Kylander-Clark and John Cottle for their guidance in U-Pb geochronology; Kate Zeiger, Luke Merrill, and Justin LaForge for their assistance with field work in Argentina; my fellow members of the Burbank lab and other friends in the department for many stimulating discussions; and Susannah Porter and Lorraine Lisiecki for being supportive role models for myself and other women in the Earth Sciences. I would also like to acknowledge our collaborators, Manfred Strecker and Ricardo Alonso, and thank Joe Kirschvink, Sarah Slotznick, and Steven Skinner at the Caltech Paleomagnetism Lab for lab access and support with paleomagnetic measurements.

I could not have completed this dissertation without the support of my parents Tom and Chris, my sisters Lisa and Laura, and my husband Franklin, who together provided me with the right combination of encouragement, commiseration, problem-solving, laughter, hugs, and fresh juice needed to complete a PhD.



VITA OF REBECCA LYDIA JIRÓN, NÉE STREIT  
September 2015

**EDUCATION**

Ph.D. in Earth Science, December 2015  
with Certificate in College and University Teaching  
University of California Santa Barbara

Bachelor of Science with Honor in Geology, June 2007  
California Institute of Technology, Pasadena, California

**PROFESSIONAL EMPLOYMENT**

Aera Energy LLC, Geology intern (summer 2013)

**TEACHING EXPERIENCE**

Teaching Associate, UCSB:

Mountains, Boots & Backpacks: intro to field geology for non-majors (Fall 2013)  
Physical Geology (Summer 2012)

Teaching Assistant, UCSB:

Introduction to Environmental Science (Winter 2015)  
Geologic Catastrophes (Winter 2014, Fall 2008)  
Dinosaurs (Spring 2010)  
Geomaterials (Fall 2009)

Instructor, School for Scientific Thought, UCSB:

If Rocks Could Talk (Winter 2012)

Teaching Assistant, Caltech:

Earth & Environment (Spring 2006, Spring 2007)

**PUBLICATIONS**

**Streit, R.L.**, D.W. Burbank, M.R. Strecker, R. Alonso, J.M. Cottle, A.R.C. Kylander-Clark, (2015). Controls on intermontane basin filling, isolation, and incision on the margin of the Puna Plateau, NW Argentina (~23°S). *Basin Research*. doi: 10.1111/bre.12141

**AWARDS**

2012 Richard V. Fisher Scholarship (UCSB department award)  
2011 Lloyd and Mary Edwards Field Studies Fellowship (UCSB dept. award)  
2010 NSF Graduate Research Fellowship  
2010 Award for outstanding contribution to UCSB ScienceLine  
2008 Clare Boothe Luce Fellowship (UCSB)  
2006 Fritz Burns Prize – Caltech undergraduate geology award  
2006 Carnation scholarship – Caltech upper class merit award  
2005 Summer Undergraduate Research Fellowship, Caltech

## ABSTRACT

Interactions of tectonics, climate, and deposition in intermontane basins on the margin of the  
Puna Plateau, NW Argentina

By

Rebecca Lydia Jirón

Intermontane basins are illuminating stratigraphic archives of deformation, denudation, and environmental conditions within the heart of actively growing mountain ranges. Commonly, however, it is difficult to determine from the sedimentary record of an individual basin whether basin formation, aggradation, and dissection were controlled primarily by climatic, tectonic, or lithological changes and whether these drivers were local or regional in nature. By comparing the onset of deposition, sediment-accumulation rates, incision, deformation, changes in fluvial connectivity, and sediment provenance in two interrelated intermontane basins, we can identify diverse controls on basin evolution. This work focuses on the Humahuaca basin and the Casa Grande basin, two adjacent intermontane basins currently connected by a bedrock gorge through the Sierra Alta, in the Eastern Cordillera of NW Argentina at ~23-24°S. We combine detailed geologic mapping, stratigraphic analysis of measured sections, provenance data, and geochronology to reconstruct the history of deformation, deposition, basin isolation, and incision in these basins. The exceptional time control provided by U-Pb geochronology of numerous volcanic

ashes contained within the Neogene-Quaternary basin fill combined with an unambiguous magnetostratigraphic record in the Humahuaca basin enables the comparison of multiple types of datasets, e.g., sediment-accumulation rates, timing of deformation on individual faults, detrital zircon provenance, paleocurrents, and sedimentary facies, from both basins to discriminate between potential controls on specific events in each basin's history.

In both basins, sediment accumulation occurred ~4 – 0.8 Ma in response to renewed uplift of ranges that had already experienced an earlier phase of deformation. Both basins experienced temporary channel defeat at the outlet of the basin ~2.5 Ma as a result of increased aridity in the rain shadow of the growing ranges to the east. In the Humahuaca basin, channel defeat resulted in ponding at the outlet, deposition of fine-grained fluvial and lacustrine strata over a larger area, and an increase in sediment-accumulation rates from 2.5 Ma until 2.1 Ma. This event apparently contributed to the integration of the northern Humahuaca subbasin with the southern Humahuaca subbasin, such that rivers previously flowing east into the Andean foreland were diverted south. In the Casa Grande basin, its isolation is recognized from the loss of a distinctive, Casa Grande-specific detrital zircon age peak in the downstream Humahuaca basin. Casa Grande's isolation lasted from ~2.4-2.1 Ma until <1.7 Ma. Despite the similar timing of deposition, sediment-accumulation rates in the Humahuaca basin were an order of magnitude higher than in the Casa Grande basin. Additionally, the Casa Grande basin strata are relatively undeformed, whereas faults in the Humahuaca basin were active from ~4.4-5 Ma until <1.6 Ma. Segmentation of faults on the western side of the Humahuaca basin results from the presence of E-W-striking Cretaceous normal faults that bounded Mesozoic grabens. The timing of deformation in the Humahuaca basin and bounding ranges is similar to the main phases of deformation in the Eastern

Cordillera and broken foreland ~200 km to the south, and large-scale differences in the style and spatial distribution of deformation in these two regions probably reflect differences in the position of each region relative to the Cretaceous Salta rift and the orientation of rift-related normal faults.

## TABLE OF CONTENTS

|  |     |
|--|-----|
| Acknowledgements.....  | iv  |
| Curriculum Vitae .....   | v   |
| Abstract.....  | vi  |
| Introduction .....   | 1   |
| Chapter 1.....   | 11  |
| <i>Controls on intermontane basin filling, isolation, and incision on the margin of the Puna Plateau, NW Argentina (~23°S)</i> |     |
| Tables & Figures .....   | 59  |
| Chapter 2.....   | 74  |
| <i>Neogene – Quaternary stratigraphy of the northern Humahuaca basin</i>   |     |
| Tables & Figures .....   | 112 |
| Chapter 3.....   | 125 |
| <i>Neogene – Quaternary deformation in the Humahuaca basin</i>   |     |
| Tables & Figures .....   | 175 |
| Appendices   |     |
| Appendix A: Effect of basin geometry on sediment-accumulation rate.....  | 189 |
| Appendix B: supplemental files available online .....  | 190 |

## INTRODUCTION

Intermontane basins provide a record of deformation, range uplift and exhumation, climate, and the response of the sedimentary system during orogenic development. Along the flanks of a growing orogen, intermontane basins form as deformation propagates into the foreland, uplifting ranges outboard of the existing topographic front. Intermontane basins may also form well inboard of the topographic front, particularly in settings where crustal heterogeneities promote the unsystematic propagation of deformation (e.g., Burbank & Reynolds, 1988; Strecker *et al.*, 2009). In contrast to foreland basins, where sediment accommodation is attributed to flexural subsidence driven by the topographic load of thrust sheets and the sediment load of the deposits in the foreland basin (Jordan, 1981), accommodation in intermontane basins is also created by uplift of the downstream range (Ori & Friend, 1984). The fluvial system in the basin is typically graded to a local base level that is controlled by the balance between rock uplift and incision at the basin outlet, where rivers exit the basin and traverse the downstream range. Hence, sediment accumulation in intermontane basins is sensitive to the tectonic, climatic, and lithological factors that control this balance.

Studies of intermontane basins flanking the Puna-Altiplano Plateau have illuminated the timing and pattern of Cenozoic deformation and range uplift in northwestern Argentina, as well as the effects of uplift on climate and on sediment routing from the orogen into the foreland (Strecker *et al.*, 1989; Marrett & Strecker, 2000; Bossi *et al.*, 2001; Kleinert & Strecker, 2001; Hilley & Strecker, 2005; Carrapa *et al.*, 2006; Coutand *et al.*, 2006; Mortimer *et al.*, 2007; Carrapa *et al.*, 2008; Strecker *et al.*, 2009; Bywater-Reyes *et al.*, 2010; Carrapa *et al.*, 2011; Siks & Horton, 2011; Carrapa *et al.*, 2012; Pingel *et al.*, 2013; Schoenbohm *et*

*al.*, 2015). These studies highlight the diachronous uplift of individual ranges and unsteady propagation of deformation across the Eastern Cordillera and broken foreland at ~24-27°S since the late Eocene (e.g., Hain *et al.*, 2011). Whereas this style of deformation is promoted by the reactivation of inherited high-angle faults (Strecker *et al.*, 2011), the presence of thick Paleozoic deposits farther north has promoted the development of a thin-skinned fold-and-thrust belt in the Subandes (Allmendinger *et al.*, 1983).

This dissertation focuses on the development of two adjacent intermontane basins, the Humahuaca and Casa Grande basins, in the Eastern Cordillera of NW Argentina at ~23-24°S, to investigate the relationships between tectonics, climate and intermontane basin deposition. The Humahuaca basin lies directly downstream of the Casa Grande basin and the two basins are connected by the narrow bedrock gorge of the Río Yacoraite, which traverses the Sierra Alta (Figure 1). This work combines detailed geologic mapping, stratigraphic analysis of measured sections, provenance data, and geochronology to reconstruct the history of deformation, deposition, basin isolation, and basin incision in these basins. The exceptional time control provided by U-Pb geochronology of numerous volcanic ashes contained within the Neogene-Quaternary basin fill combined with an unambiguous magnetostratigraphic record in the Humahuaca basin enables the comparison of multiple types of datasets, e.g., sediment-accumulation rates, timing of deformation, detrital zircon provenance, paleocurrents, and sedimentary facies, from both basins to discriminate between potential controls on specific events in each basin's history. Each of the following three chapters was prepared as a stand-alone research paper.

The first chapter investigates the controls on sediment accumulation, basin isolation, and basin incision in the Casa Grande basin. We analyze 120 m of fluvial and lacustrine

strata that were deposited in the Casa Grande basin between 3.8 and 0.8 Ma. By comparing the timing of events in the Casa Grande basin, including deposition above a basal unconformity, changes in sediment-accumulation rates and final incision, with the timing of events in the Humahuaca basin, we are able to assess whether these events were controlled by local or regional processes. For example, although uplift of the Sierra Alta along faults on the western margin of the Humahuaca basin appears to have been a necessary driver of deposition in the Casa Grande basin, we infer from the synchronous deposition above unconformities in both basins that regional changes in climate and sediment supply, rather than changes in local uplift rates, probably triggered the onset of deposition. Additionally, intervals of fluvial connectivity versus isolation of the Casa Grande basin were identified from detrital zircon provenance analysis of sandstones deposited in the downstream Humahuaca basin near the mouth of the Río Yacoraite. This application of detrital zircon analysis relies on the observation that sediment from the Casa Grande basin contains zircons derived from a Cretaceous pluton with unique ages that are not found elsewhere in the Humahuaca basin catchment. We relate the history of deposition, basin isolation, and basin incision in the Casa Grande basin to the changing balance of rock uplift rates, fluvial incision, and aggradation at the outlet of the basin.

The second of these three research chapters focuses on the stratigraphy of the northern Humahuaca basin. Based on their work in the southern Humahuaca basin, Pingel *et al.* (2013) proposed that lithological differences between the Plio-Pleistocene deposits in the northern and southern parts of the Humahuaca basin represent deposition in two subbasins. In this chapter, the boundary between the two subbasins is delineated on the basis of paleoflow directions and the maximum extent of fine-grained fluvial and lacustrine deposits, which are



confined to the northern subbasin. New zircon U-Pb geochronology of 35 ash samples in the Humahuaca basin, combined with the magnetostratigraphy and U-Pb geochronology presented in the previous chapter, facilitates calculations of sediment-accumulation rates in measured stratigraphic sections, correlation between stratigraphic sections distributed throughout the northern Humahuaca basin, identification of temporally constrained lateral facies variations, and comparison of the timing of events in the Humahuaca basin with events in nearby regions. Two events in the northern Humahuaca subbasin are of particular interest: the ~4.3 Ma onset of deposition of the Tilcara Fm above the Maimará Fm; and the ~2.5-2.1 Ma interval of high sediment-accumulation rate and finer-grained deposits. We find that uplift of the Tilcara ranges east of the Humahuaca basin deflected former eastward fluvial transport to the north in the northern Humahuaca basin at approximately the same time (~4.3 Ma) that it deflected flow southward in the southern subbasin (Pingel *et al.*, 2013). The timing of this event is similar to the onset of deformation on the western margin of the Humahuaca basin, the inferred acceleration of rock uplift rates in the Santa Victoria range ~60 km to the north (Amidon *et al.*, 2015), out-of-sequence deformation in the Subandes (Echavarría *et al.*, 2003; Uba *et al.*, 2009), and uplift and exhumation of the central ranges of the Eastern Cordillera following a westward shift in the location of deformation in the broken Salta foreland (Hain *et al.*, 2011; Pearson *et al.*, 2013). Such synchrony suggests the deformation and stratigraphic change in the Humahuaca basin is related to a regional-scale (100s of km) tectonic event. Based on the distribution of lacustrine deposits, the increase in sediment-accumulation rates, and isotopic evidence for an increase in aridity in the Humahuaca basin between 3.5 and 2.5 Ma (Pingel *et al.*, 2014), we propose that, in the face of ongoing rock uplift, decreased stream power led to channel defeat and ponding at the

outlet of the northern Humahuaca subbasin from ~2.5 Ma until 2.1 Ma. The appearance of southward paleocurrents toward the end of this interval suggests that this ponding eventually resulted in the integration of the northern subbasin into the southern subbasin.

The third research chapter addresses the style and timing of Late Miocene – Pleistocene deformation in the Humahuaca basin, its interaction with deposition in the basin, and its relationship to regional spatiotemporal patterns of deformation. Geologic mapping in the Humahuaca basin reveals that along-strike changes in the style of hanging-wall deformation on the western side of the basin are coincidence with thickness and facies changes in the Cretaceous rift-related rocks in the hanging walls of these faults. We propose that the E-W-trending Cretaceous normal faults that likely controlled the original thickness of these rift-related deposits were reactivated as oblique tear faults that formed the boundaries between these thrust segments with different styles of Plio-Pleistocene hanging-wall deformation. Cross-cutting relationships between several faults and Neogene-Quaternary basin deposits containing ashes dated with zircon U-Pb geochronology place unusually tight constraints on the timing of displacement on individual faults since ~5 Ma. Ashes that are offset across a fault also serve as marker beds that are used to estimate the amount of displacement on that fault over a given time interval. Comparison of the timing of deformation on the western side of the Humahuaca basin with changes in sedimentary facies and sediment-accumulation rates supports the hypothesis that sediment-accumulation rates are controlled primarily by the balance of uplift and incision at the outlet of the basin, rather than by thrusting in and on the western margin of the basin. We note that the timing of deformation in the Humahuaca basin and its bounding ranges is similar to the main phases of deformation in the broken Salta foreland (Hain *et al.*, 2011; Pearson *et al.*, 2013) and that

differences in the style and spatial distribution of deformation in these two regions probably reflect differences in the position of each region relative to the Cretaceous Salta rift and the orientation of rift-related normal faults.

This work highlights the dynamic nature of these intermontane basins and the response of the sedimentary system to changing tectonic and climatic conditions during the past 6 Myr. The collection and analysis of diverse stratigraphic and structural datasets, as well as the clear integration of these datasets through the excellent time control provided by U-Pb dating of numerous ashes, are essential to reconstructing the evolution of these intermontane basins. We find that the history of deposition, isolation, and incision in these intermontane basins can be understood in terms of the dynamic balance between rock uplift of the downstream range, fluvial incision through the uplifting zone, and aggradation upstream of the uplift (Burbank *et al.*, 1996; Humphrey & Konrad, 2000; Sobel *et al.*, 2003; Hilley & Strecker, 2005). The interpretation of which combination of local or regional changes in rock uplift rates, climate, and sediment supply drives changes in this balance for a particular event in the basin history is aided by comparisons between the northern and southern Humahuaca subbasins, between the Humahuaca basin and the upstream Casa Grande basin, and between these intermontane basins and other locations in NW Argentina. Whereas a regional acceleration of uplift in the ranges of central Eastern Cordillera of NW Argentina ~5 Ma was essential to onset of intermontane basin deposition; increased aridity – interpreted as a result of the growing ranges reaching elevations sufficient to block moisture transport from the foreland – around 2.5 Ma appears to have driven channel defeat at the outlets of both the northern Humahuaca subbasin and the Casa Grande basin.

## REFERENCES

- ALLMENDINGER, R.W., RAMOS, V.A., JORDAN, T.E., PALMA, M. & ISACKS, B.L. (1983) Paleogeography and Andean structural geometry, Northwest Argentina. *Tectonics*, **2**, 1-16.
- AMIDON, W.H., LUNA, L.V., FISHER, G.B., BURBANK, D.W., KYLANDER-CLARK, A.R.C. & ALONSO, R. (2015) Provenance and tectonic implications of Orán Group foreland basin sediments, Río Iruya canyon, NW Argentina (23°S). *Basin Research*, 10.1111/bre.12139.
- BOSSI, G.E., GEORGIEFF, S.M., GAVRILOFF, I.J.C., IBANEZ, L.M. & MURUAGA, C.M. (2001) Cenozoic evolution of the intramontane Santa Maria basin, Pampean Ranges, northwestern Argentina. *Journal of South American Earth Sciences*, **14**, 725-734.
- BURBANK, D., MEIGS, A. & BROZOVIC, N. (1996) Interactions of growing folds and coeval depositional systems. *Basin Research*, **8**, 199-223.
- BURBANK, D.W. & RAYNOLDS, R.G.H. (1988) Stratigraphic keys to the timing of thrusting in terrestrial foreland basins: Applications to the Northwestern Himalaya. In: *New Perspectives in Basin Analysis* (Ed. by K. L. Kleinspehn, and Paola, C.), 331-351. Springer-Verlag, New York.
- BYWATER-REYES, S., CARRAPA, B., CLEMENTZ, M. & SCHOENBOHM, L. (2010) Effect of late Cenozoic aridification on sedimentation in the Eastern Cordillera of northwest Argentina (Angastaco basin). *Geology*, **38**, 235-238.
- CARRAPA, B., STRECKER, M.R. & SOBEL, E.R. (2006) Cenozoic orogenic growth in the Central Andes: Evidence from sedimentary rock provenance and apatite fission track thermochronology in the Fiambala Basin, southernmost Puna Plateau margin (NW Argentina). *Earth and Planetary Science Letters*, **247**, 82-100.
- CARRAPA, B., HAUER, J., SCHOENBOHM, L., STRECKER, M.R., SCHMITT, A.K., VILLANUEVA, A. & GOMEZ, J.S. (2008) Dynamics of deformation and sedimentation in the northern Sierras Pampeanas: An integrated study of the Neogene Fiambala basin, NW Argentina. *Geological Society of America Bulletin*, **120**, 1518-1543.
- CARRAPA, B., TRIMBLE, J.D. & STOCKLI, D.F. (2011) Patterns and timing of exhumation and deformation in the Eastern Cordillera of NW Argentina revealed by (U-Th)/He thermochronology. *Tectonics*, **30**, 30.
- CARRAPA, B., BYWATER-REYES, S., DECELLES, P.G., MORTIMER, E. & GEHRELS, G.E. (2012) Late Eocene-Pliocene basin evolution in the Eastern Cordillera of northwestern Argentina (25 degrees-26 degrees S): regional implications for Andean orogenic wedge development. *Basin Research*, **24**, 249-268.
- COUTAND, I., CARRAPA, B., DEEKEN, A., SCHMITT, A.K., SOBEL, E.R. & STRECKER, M.R. (2006) Propagation of orographic barriers along an active range front: insights from sandstone petrography and detrital apatite fission-track thermochronology in the intramontane Angastaco basin, NW Argentina. *Basin Research*, **18**, 1-26.
- ECHAVARRIA, L., HERNANDEZ, R., ALLMENDINGER, R. & REYNOLDS, J. (2003) Subandean thrust and fold belt of northwestern Argentina: Geometry and timing of the Andean evolution. *AAPG Bulletin*, **87**, 965-985.
- HAIN, M.P., STRECKER, M.R., BOOKHAGEN, B., ALONSO, R.N., PINGEL, H. & SCHMITT, A.K. (2011) Neogene to Quaternary broken foreland formation and sedimentation

- dynamics in the Andes of NW Argentina (25 degrees S). *Tectonics*, **30**, TC2006, doi:2010.1029/2010TC002703.
- HILLEY, G.E. & STRECKER, M.R. (2005) Processes of oscillatory basin filling and excavation in a tectonically active orogen: Quebrada del Toro Basin, NW Argentina. *Geological Society of America Bulletin*, **117**, 887-901.
- HUMPHREY, N.F. & KONRAD, S.K. (2000) River incision or diversion in response to bedrock uplift. *Geology*, **28**, 43-46.
- JORDAN, T.E. (1981) Thrust loads and foreland basin evolution, Cretaceous, Western United States. *AAPG Bulletin*, **65**, 2506-2520.
- KLEINERT, K. & STRECKER, M.R. (2001) Climate change in response to orographic barrier uplift: Paleosol and stable isotope evidence from the late Neogene Santa Maria basin, northwestern Argentina. *Geological Society of America Bulletin*, **113**, 728-742.
- MARRETT, R. & STRECKER, M.R. (2000) Response of intracontinental deformation in the central Andes to late Cenozoic reorganization of South American Plate motions. *Tectonics*, **19**, 452-467.
- MORTIMER, E., CARRAPA, B., COUTAND, I., SCHOENBOHM, L., SOBEL, E.R. & GOMEZ, J.S. (2007) Fragmentation of a foreland basin in response to out-of-sequence basement uplifts and structural reactivation: El Cajon-Campo del Arenal basin, NW Argentina. *Geological Society of America Bulletin*, **119**, 637-653.
- ORI, G.G. & FRIEND, P.F. (1984) Sedimentary basins formed and carried piggyback on active thrust sheets. *Geology*, **12**, 475-478.
- PEARSON, D.M., KAPP, P., DECELLES, P.G., REINERS, P.W., GEHRELS, G.E., DUCEA, M.N. & PULLEN, A. (2013) Influence of pre-Andean crustal structure on Cenozoic thrust belt kinematics and shortening magnitude: Northwestern Argentina. *Geosphere*, **9**, 1766-1782.
- PINGEL, H., STRECKER, M.R., ALONSO, R.N. & SCHMITT, A.K. (2013) Neotectonic basin and landscape evolution in the Eastern Cordillera of NW Argentina, Humahuaca Basin (similar to 24 degrees S). *Basin Research*, **25**, 554-573.
- PINGEL, H., ALONSO, R.N., MULCH, A., ROHRMANN, A., SUDO, M. & STRECKER, M.R. (2014) Pliocene orographic barrier uplift in the southern Central Andes. *Geology*, **42**, 691-694.
- SCHOENBOHM, L.M., CARRAPA, B., MCPHERSON, H.M., PRATT, J.R., BYWATER-REYES, S. & MORTIMER, E. (2015) Climate and tectonics along the southern margin of the Puna Plateau, NW Argentina: Origin of the late Cenozoic Punaschotter conglomerates. *Geological Society of America Memoirs*, **212**, 251-260.
- SIKS, B.C. & HORTON, B.K. (2011) Growth and fragmentation of the Andean foreland basin during eastward advance of fold-thrust deformation, Puna plateau and Eastern Cordillera, northern Argentina. *Tectonics*, **30**, TC6017, doi: 6010.1029/2011TC002944.
- SOBEL, E.R., HILLEY, G.E. & STRECKER, M.R. (2003) Formation of internally drained contractional basins by aridity-limited bedrock incision. *Journal of Geophysical Research-Solid Earth*, **108**, 2344, doi:2310.1029/2002JB001883.
- STRECKER, M.R., CERVENY, P., BLOOM, A.L. & MALIZIA, D. (1989) Late Cenozoic tectonism and landscape development in the foreland of the Andes: Northern Sierras Pampeanas (26- 28°S), Argentina. *Tectonics*, **8**, 517-534.

- STRECKER, M.R., ALONSO, R., BOOKHAGEN, B., CARRAPA, B., COUTAND, I., HAIN, M.P., HILLEY, G.E., MORTIMER, E., SCHOENBOHM, L. & SOBEL, E.R. (2009) Does the topographic distribution of the central Andean Puna Plateau result from climatic or geodynamic processes? *Geology*, **37**, 643-646.
- STRECKER, M.R., HILLEY, G.E., BOOKHAGEN, B. & SOBEL, E.R. (2011) Structural, Geomorphic, and Depositional Characteristics of Contiguous and Broken Foreland Basins: Examples from the Eastern Flanks of the Central Andes in Bolivia and NW Argentina. In: *Tectonics of Sedimentary Basins* (Ed. by, 508-521. John Wiley & Sons, Ltd.
- UBA, C.E., KLEY, J., STRECKER, M.R. & SCHMITT, A.K. (2009) Unsteady evolution of the Bolivian Subandean thrust belt: The role of enhanced erosion and clastic wedge progradation. *Earth and Planetary Science Letters*, **281**, 134-146.

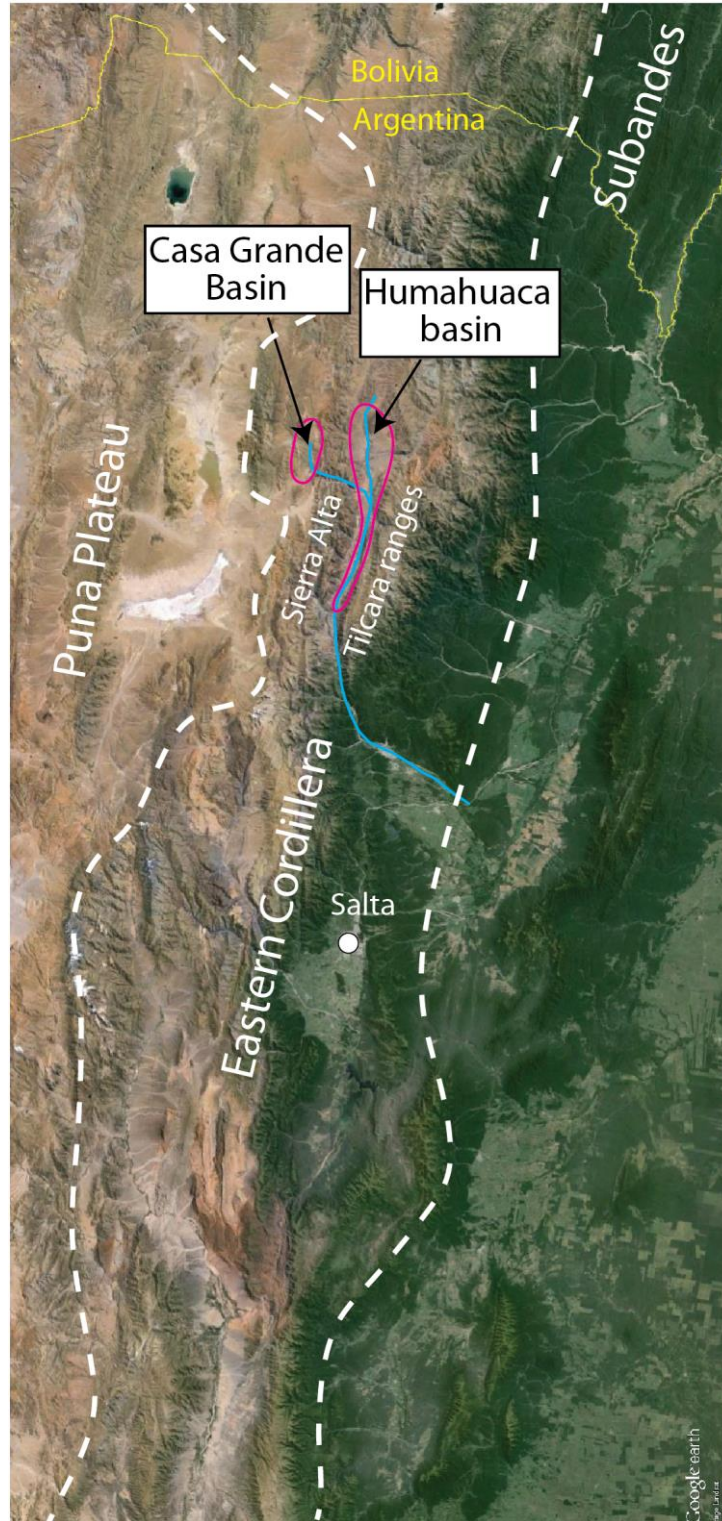


Figure 1. Location of the Humahuaca and Casa Grande basins in the Eastern Cordillera of NW Argentina.

## CHAPTER 1

### **Controls on intermontane basin filling, isolation, and incision on the margin of the Puna Plateau, NW Argentina (~23°S)**

Published as: Streit, R.L., D.W. Burbank, M.R. Strecker, R. Alonso, J.M. Cottle, A.R.C.

Kylander-Clark, (2015). Controls on intermontane basin filling, isolation, and incision on the margin of the Puna Plateau, NW Argentina (~23°S). *Basin Research*. doi:10.1111/bre.12141

#### **ABSTRACT**

Intermontane basins are illuminating stratigraphic archives of uplift, denudation, and environmental conditions within the heart of actively growing mountain ranges. Commonly, however, it is difficult to determine from the sedimentary record of an individual basin whether basin formation, aggradation, and dissection were controlled primarily by climatic, tectonic, or lithological changes and whether these drivers were local or regional in nature. By comparing the onset of deposition, sediment-accumulation rates, incision, deformation, changes in fluvial connectivity, and sediment provenance in two interrelated intermontane basins, we can identify diverse controls on basin evolution. Here we focus on the Casa Grande basin and the adjacent Humahuaca basin along the eastern margin of the Puna Plateau in northwest Argentina. Underpinning this analysis is the robust temporal framework provided by U-Pb geochronology of multiple volcanic ashes and our new magnetostratigraphic record in the Humahuaca basin. Between 3.8 Ma and 0.8 Ma, ~120 m of fluvial and lacustrine sediments accumulated in the Casa Grande basin as uplift of the Sierra Alta, the bounding range to its east, outpaced fluvial incision by the Río Yacoraite,



which presently flows eastward across the range into the Humahuaca basin. Detrital zircon provenance analysis indicates a progressive loss of fluvial connectivity from the Casa Grande basin to the downstream Humahuaca basin between 3 Ma and 2.1 Ma, resulting in the isolation of the Casa Grande basin from 2.1 Ma to <1.7 Ma. This episode of basin isolation is attributed to aridification due to uplift of the ranges to the east. Enhanced aridity decreased sediment supply to the Casa Grande basin to the point that aggradation could no longer keep pace with the rate of surface uplift at the outlet of the basin. Synchronous events in the Casa Grande and Humahuaca basins suggest that both the initial onset of deposition above unconformities at ~3.8 Ma and the re-establishment of fluvial connectivity at ~0.8 Ma were controlled by climatic and/or tectonic changes affecting both basins. Reintegration of the fluvial network allowed subsequent incision in the Humahuaca basin to propagate upstream into the Casa Grande basin.

## **INTRODUCTION**

In tectonically active orogens, the stratigraphic and paleoenvironmental records preserved within intermontane basins can reveal the history of uplift and erosion of nearby ranges. Unconformities, changes in sediment-accumulation rates, variations in grain size and depositional environment, and changes in sediment provenance record both tectonic and climatic forcing (e.g., Burbank & Raynolds, 1988; Jordan *et al.*, 1988; Bookhagen & Strecker, 2012). The complex relationships between these parameters typically render an unambiguous assessment of climatic versus tectonic signals in the depositional record difficult. For example, in addition to directly driving changes in the sedimentary system (e.g., fluvial connectivity, exposure of erodible or resistant rocks, and stream gradients), tectonics

can cause fundamental climatic changes that affect the system when surface uplift of bounding ranges enhances orographic precipitation on a range's windward side, while creating a rain shadow that induces a long-term shift to more arid conditions on its leeward side. Such relationships, including pronounced gradients in topography, rainfall, and surface processes across the orogen, are well illustrated along many flanks of Cenozoic plateaus worldwide, (e.g., Uba *et al.*, 2007; Strecker *et al.*, 2009; Hough *et al.*, 2011; Yildirim *et al.*, 2011; Burbank *et al.*, 2012; Lease *et al.*, 2012; Schildgen *et al.*, 2014), and provide insight into the characteristics of the sediment-routing system between the orogen interior and adjacent foreland regions. In addition, if basin deposits can be chronologically constrained, such basin fills may help understand the spatiotemporal patterns of tectonic deformation along orogenic plateau margins. The eastern margin of Puna Plateau in Argentina, the southern sector of the intra-orogenic Andean Altiplano-Puna Plateau, is such a region where sedimentary archives are preserved in intermontane basins that are parallel to the plateau margins.

Studies of intermontane basins on the eastern margin of the Puna Plateau have provided useful constraints on Cenozoic Andean deformation, uplift of bounding ranges, tectonically-driven orogen-scale climate change, and more regionally limited effects of climate response to surface uplift. Variations in sediment accumulation in Andean intermontane basins straddling the Puna margin have been attributed to increasing accommodation in the footwall of active thrust faults (Coutand *et al.*, 2006; Deeken *et al.*, 2006; Mortimer *et al.*, 2007), exhumation of different lithologies in the bounding ranges (Sobel & Strecker, 2003; Deeken *et al.*, 2006), channel defeat and basin isolation as a result of surface uplift of downstream ranges (Hilley & Strecker, 2005; Hain *et al.*, 2011; Bonorino

& Abascal, 2012), climatic changes (Bywater-Reyes *et al.*, 2010), and the combination of both aridity and deformation within the basin (Starck & Anzótegui, 2001; Strecker *et al.*, 2009; Schoenbohm *et al.*, 2015). Despite broad similarities among these basins, in detail, deposits within the basins straddling the eastern flanks of the Puna are diachronous, reflecting the asynchronous uplift of individual ranges spanning the Late Miocene to Pleistocene (Ramos, 1999; Strecker *et al.*, 2009). Notably, several of these basins have experienced intermittent basin isolation or episodes of severed drainage (Hilley & Strecker, 2005; Pingel *et al.*, 2013).

Whether an intermontane basin experiences aggradation or incision and whether it maintains downstream fluvial connectivity or becomes hydrologically isolated depends on the balance of rock-uplift rates, a river's ability to incise its bed, and sediment supply (Fig. 1). Aggradation will occur behind a rising bedrock barrier where river incision cannot keep pace with rock-uplift rates (Fig. 1B). Nonetheless, fluvial connectivity with downstream watersheds can be maintained if the rate of aggradation equals the rate of surface uplift of the bedrock channel (i.e., rock-uplift rate minus incision rate) within the zone of uplift (Burbank *et al.*, 1996). Otherwise, the channel is defeated and the basin will become isolated (Fig. 1C). If uplift increases the channel steepness through the bedrock portion of the river that lies downstream of an isolated basin, eventually a knick zone may propagate upstream and breach the barrier (Fig. 1D), thereby causing aggradation to cease within the formerly isolated basin (Burbank *et al.*, 1996; Humphrey & Konrad, 2000). Basin reintegration may also occur if the rate of aggradation increases relative to uplift, allowing sediment to overtop the barrier (Sobel *et al.*, 2003).

This study focuses on the role of these processes in the evolution of the Casa Grande basin, a Plio-Pleistocene intermontane basin on the eastern margin of the Puna Plateau at ~23°S latitude (Fig. 2). New U-Pb geochronology of numerous volcanic ashes contained within the strata throughout this region combined with an unambiguous magnetostratigraphic record provide exceptional control on the timing of events within the Casa Grande basin and the adjacent Humahuaca basin, which is located directly downstream (Fig. 3). Both basins are connected by the narrow bedrock gorge of the Río Yacoraite, which traverses the Sierra Alta. In turn, the north-south oriented Humahuaca basin drains southward into the broken foreland. Comparison of the timing of the episodes of filling, changes in provenance and sediment-accumulation rates, and incision in each basin allows us to infer how the interplay between tectonic and climatic processes may have controlled these events. Additionally, the history of fluvial connectivity between the Casa Grande and the Humahuaca basins is recorded by the zircon provenance of sedimentary deposits in the Humahuaca basin. We find that, although tectonic uplift of the range bounding the downstream margin of the Casa Grande intermontane basin was essential for its filling, both the onset of deposition above a basal unconformity and the loss of fluvial connectivity between the Casa Grande basin and the Humahuaca basin can likely be attributed to changes in sediment supply to the basin.

## **GEOLOGIC SETTING**

The southern central Andes are divided into several morphotectonic provinces (Fig. 2): the Western Cordillera, which comprises the modern volcanic arc, the low-relief Altiplano-Puna Plateau to its east, the high-relief, reverse-faulted Eastern Cordillera, the thin-skinned Subandean fold-and-thrust belt, and the basement-cored uplifts of the Santa Barbara

System and Sierras Pampeanas in the broken foreland (Jordan *et al.*, 1983). The Puna Plateau has an average elevation of ~4400 m and consists of internally drained, partially coalesced basins with intervening reverse fault-bounded ranges up to 5000-6000 m high (Turner & Méndez, 1979; Whitman *et al.*, 1996). Intermontane basins within the Eastern Cordillera and northern Sierra Pampeanas are structurally similar, but were only transiently isolated from the foreland during their development in late Miocene to Pleistocene time (Strecker *et al.*, 1989; Bossi *et al.*, 2001; Strecker *et al.*, 2007; Carrapa *et al.*, 2008; Bonorino & Abascal, 2012; Pingel *et al.*, 2013).

Located on the eastern margin of the Puna Plateau and lying at the southern end of the Tres Cruces basin, the Casa Grande basin (Fig. 3) is bounded by the Sierra Aguilar to the west and the Sierra Alta to the east. The basin lies at an elevation of ~3500 m, but is not considered part of the Puna Plateau because it is externally drained. Within the Casa Grande basin, the Río Yacoraite flows southward and exits the basin at its southeastern end through a bedrock gorge. From there, the Río Yacoraite flows eastward through the Sierra Alta into the Quebrada de Humahuaca (Humahuaca basin), where it joins the Río Grande. The Humahuaca basin is now a long narrow valley within the Eastern Cordillera bounded by the Sierra Alta to the west and the Tilcara ranges and Sierra Hornocal to the east. The northern portion of the basin lies at an elevation of ~2500-3000 m, whereas the bounding ranges exceed 5000 m above sea level. The Río Grande trunk stream flows southward along the axis of the valley and exits the basin into the foreland ~90 km south of the town of Humahuaca.

Uplift along the bivergent thrust- and reverse-fault system of the Sierra Alta and primarily east-vergent thrust faults of the Tilcara ranges exposes Neoproterozoic to Eocene rocks (Fig. 4) (Rodríguez Fernández *et al.*, 1999; Gonzalez *et al.*, 2004). The most abundant

units exposed are the Neoproterozoic to lower Cambrian shales, slates and phyllites of the Puncoviscana Formation, and the unconformably overlying Cambrian shelfal quartzites of the Mesón Group (Turner, 1960; Turner & Mon, 1979). The Mesón Group is overlain by the marine sandstones and shales of the Ordovician Santa Victoria Group (Turner, 1960). Lying above a major unconformity, the Cretaceous – Paleogene Salta Group includes the Cretaceous rift-related red sandstones of the Pirgua Subgroup, the Late Cretaceous – Paleocene post-rift Balbuena Subgroup (most notably the yellow-weathering marine carbonates of the Yacoraite Formation), and the fluvial and lacustrine mudstones, siltstones, and sandstones of the upper Paleocene to middle Eocene Santa Bárbara Subgroup, which have been interpreted as belonging to either thermal-subsidence basins (Moreno, 1970) or foreland basins (DeCelles *et al.*, 2011). Late Jurassic – early Cretaceous plutons (Figs. 3, 4) (Zappettini, 1989; Cristiani *et al.*, 2005; Insel *et al.*, 2012) within the Sierra Alta (Fundición granite) and Sierra Aguilar (Abra Laite and Aguilar granites) provide an important signature of source areas in these ranges for our provenance analysis. Hereafter, we refer to the Abra Laite and Aguilar granites collectively as the “Aguilar granite” because their close proximity and indistinguishable U-Pb zircon ages,  $153 \pm 4$  Ma and  $150.4 \pm 0.9$  Ma, respectively (Cristiani *et al.*, 2005; Insel *et al.*, 2012), allow them to be treated as a single source of detrital zircons for provenance analysis.

In the Casa Grande basin, the Santa Bárbara Subgroup is overlain by the upper Eo-Oligocene alluvial strata of the Casa Grande Formation (Boll & Hernández, 1986). A prominent angular unconformity separates the Casa Grande Formation from the overlying Plio-Pleistocene intermontane basin fill that is the focus of this study. In the Humahuaca basin, the upper Miocene – Pliocene sandstones and conglomerates of the Maimará

Formation were deposited in an unrestricted foreland basin setting (Salfity *et al.*, 1984; Gabaldón *et al.*, 1998; Pingel *et al.*, 2013). The Maimará Formation is overlain by the Plio-Pleistocene intermontane basin deposits of the Uquía Formation in the northern portion of the basin and the Tilcara Formation in the southern portion of the basin (Marshall *et al.*, 1982; Pingel *et al.*, 2013). In the sections below, we present a more refined analysis of this Plio-Pleistocene stratigraphy.

Within the context of the overall tectonic evolution of the southern central Andes, the Plio-Pleistocene intermontane basin fills of the Casa Grande and Humahuaca basins represent a response to a phase of hinterland-stepping deformation. Shortening commenced along the western flank of the Andes ~60-40 Ma and moved into the Eastern Cordillera ~40 Ma (Horton, 2005; Hongn *et al.*, 2007; Jordan *et al.*, 2007; Carrapa & DeCelles, 2015). Deformation in the Bolivian Eastern Cordillera continued until ~10 Ma (Gubbels *et al.*, 1993) and shifted to the Subandes ~12-9 Ma (Echavarría *et al.*, 2003; Uba *et al.*, 2009). Farther south, at ~25°S latitude, deformation in the Santa Barbara System began around 10 Ma and was coeval with uplift in the western sectors of the Eastern Cordillera, but most of the deformation in the Santa Barbara System occurred < 4 Ma (Hain *et al.*, 2011; Pearson *et al.*, 2013). Shortening lasted until <4 Ma in the Puna Plateau and has continued into the Quaternary in the Eastern Cordillera (Salfity *et al.*, 1984; Marrett *et al.*, 1994; Marrett & Strecker, 2000; Sancho *et al.*, 2008). Although paleo-elevation data for the Puna Plateau remain scarce, the uplift of ranges in the present-day sectors of the western Puna is inferred to have occurred >38 Ma and present-day elevations of the southern plateau margin are argued to have persisted since at least 9 Ma (Carrapa *et al.*, 2006; Canavan *et al.*, 2014; Carrapa *et al.*, 2014a; Montero-López *et al.*, 2014; Quade *et al.*, 2015). Despite the overall

west-to-east propagation of deformation, in detail, this propagation was unsteady and out-of-sequence deformation was common (Rodríguez Fernández *et al.*, 1999; Echavarría *et al.*, 2003; Elger *et al.*, 2005; Mortimer *et al.*, 2007; Strecker *et al.*, 2009; Uba *et al.*, 2009; Carrapa & DeCelles, 2015).

In the Tres Cruces basin (Fig. 3), evidence of synsedimentary thrusting is recorded by upper Eocene and lower Oligocene stratal thickening in the footwall of major thrusts (Coutand *et al.*, 2001). Oligocene deformation is also recorded by rapid exhumation and cooling ( $\sim 5^\circ\text{C}/\text{Myr}$ ) in the Sierra Aguilar 34-25 Ma (Insel *et al.*, 2012). Exhumation in the Sierra Alta is recorded by mid-Miocene ( $\sim 14$  Ma) apatite fission-track cooling ages from the Fundición granite (Deeken *et al.*, 2005). Additionally, Siks and Horton (2011) interpreted the early Oligocene to middle Miocene (by  $\sim 12$  Ma) loss of western detrital zircon sources in the Cianzo basin, located within the Sierra Hornocal east of the town of Humahuaca (Fig. 3), to reflect growing topography in the westernmost Eastern Cordillera, e.g., the Sierra Alta. The Cianzo thrust and Hornocal fault (Fig. 4) were active in the middle to late Miocene (Siks & Horton, 2011). It is unknown whether the thrust faults within the Tilcara ranges to the east of the Humahuaca basin were also active at this time, but any surface uplift of the Tilcara ranges was insufficient to interrupt fluvial connectivity with the foreland before  $\sim 4.2$  Ma (Pingel *et al.*, 2013).

A second generation of thrusting in the Eastern Cordillera – including thrusting within the Humahuaca basin – developed between 8.5 Ma and the present day (Rodríguez Fernández *et al.*, 1999; Sancho *et al.*, 2008; Pingel *et al.*, 2013). East of the Humahuaca basin, uplift of the Tilcara ranges formed a topographic barrier to eastward flow of the fluvial system into the foreland  $\sim 4.2$  Ma, when the Río Grande was deflected southward (Pingel *et*



*al.*, 2013; Amidon *et al.*, 2015). Additionally, Pingel *et al.* (2014) interpret hydrogen isotope ratios of hydrated volcanic glass ( $\delta D_g$ ) from the Humahuaca basin to reflect surface uplift of the basin between 6.0 and 3.5 Ma.

Today the Casa Grande and Humahuaca basins have a semi-arid to arid climate, receiving less than 250 mm/yr of rainfall over most of their area (e.g., Bookhagen & Strecker, 2012). In contrast, the humid foreland east of the Tilcara ranges receives >1000 mm/yr of precipitation (Bookhagen & Strecker, 2008), resulting in pronounced surface-process gradients (Bookhagen & Strecker, 2012). High precipitation on the eastern flanks of the southern central Andes is attributed to the transport of moisture from the Amazon Basin by the South American Low Level Jet (LLJ) during the summer monsoon (Vera *et al.*, 2006). Uplift of individual ranges results in orographic rainfall on the windward side of the range, increased aridity on the leeward side, and commonly pronounced erosion gradients (Kleinert & Strecker, 2001; Coutand *et al.*, 2006; Galewsky, 2009; Bookhagen & Strecker, 2012; Pingel *et al.*, 2014; Rohrmann *et al.*, 2014). The transition to the present arid conditions in the Humahuaca basin must have occurred sometime after ~3 Ma because the presence of capybara and crocodile fossils in the middle unit (~3-2.5 Ma) of the Uquía Formation indicates that the Humahuaca basin was more humid at that time (Reguero *et al.*, 2007). Furthermore, Pingel *et al.* (2014) attribute an abrupt deuterium enrichment in the hydrogen isotopic composition of hydrated volcanic glass between 3.5 Ma and 2.5 Ma to the onset of semiarid conditions in the Humahuaca basin as a result of the Tilcara ranges attaining threshold elevations for blocking moisture transport from the east.

## **METHODS**

Stratigraphic analysis of three measured sections (0.1- to 1-m resolution) was used to characterize the depositional setting of the Plio-Pleistocene sediments in the Casa Grande basin (Fig. 5). U-Pb geochronology of zircons from five volcanic ashes interbedded with these strata provides a temporal framework that enables reliable correlations between the sections and defines average sediment-accumulation rates. To assess changes in provenance, conglomerate compositions were determined by counting at least 100 clasts >1 cm in size within a 1-m<sup>2</sup> area. Where possible, paleocurrent directions were determined from the orientation of imbricated clasts or channel margins.

To track the degree of fluvial connectivity between the Casa Grande basin and the Humahuaca basin, an additional stratigraphic section (hereafter called the “Río Yacoraite section”) was measured through the Plio-Pleistocene strata in the Humahuaca basin near the mouth of the Río Yacoraite, and detrital zircon samples were collected at regular intervals through this section. The Río Yacoraite section was dated with magnetostratigraphy pinned by a high-resolution tephra date. Within this chronologic framework, temporal changes in both undecompressed sediment-accumulation rates in the Humahuaca basin and relative changes in amount of sediment transported from the Casa Grande basin to the Humahuaca basin were compared with sediment-accumulation rates in the Casa Grande basin.

Comparisons between the timing of events in the Casa Grande basin and the ages of unconformities and faulting events in the Humahuaca basin allow us to assess the role tectonics and climate in controlling changes in the Casa Grande basin. Our geologic mapping in Humahuaca basin documents cross-cutting relationships between Neogene-Quaternary strata, unconformities, and faults (Fig. 6). The timing of deformation on individual structures is constrained by U-Pb dating of intercalated ash layers within the faulted basin fill.

U-Pb dates on zircons from volcanic ashes within the Plio-Pleistocene strata were obtained by laser-ablation multi-collector inductively coupled mass spectrometry (LA-MC-ICPMS), following the ‘conventional’ LA-ICPMS methods described by Cottle *et al.* (2012). Data reduction, including corrections for baseline, instrumental drift, mass bias, and down-hole fractionation and uncorrected age calculations, was carried out using Iolite version 2.21 (Paton *et al.*, 2010). The 91500-reference zircon ( $1065.4 \pm 0.6$  Ma  $^{207}\text{Pb}/^{206}\text{Pb}$  ID-TIMS and  $1062.4 \pm 0.8$  Ma  $^{206}\text{Pb}/^{238}\text{U}$  ID-TIMS (Wiedenbeck *et al.*, 1995)) was used to monitor and correct for mass bias, as well as Pb/U fractionation. To monitor data accuracy, a secondary reference zircon – either ‘GJ-1’ ( $601.7 \pm 1.3$  Ma  $^{206}\text{Pb}/^{238}\text{U}$  ID-TIMS age,  $608.5 \pm 0.4$  Ma  $^{207}\text{Pb}/^{206}\text{Pb}$  ID-TIMS age) (Jackson *et al.*, 2004) or ‘SL-1’ ( $563.5 \pm 3.2$  Ma ID-TIMS age) (Gehrels *et al.*, 2008) – was analyzed once every ~ 8 unknowns and was mass bias- and fractionation-corrected based on measured isotopic ratios of the primary reference zircon. To account for the external reproducibility of the secondary reference zircons, an additional 2% uncertainty was propagated into the uncertainty on the measured  $^{207}\text{Pb}/^{206}\text{Pb}$  ratios.

Because many of these ashes show some degree of fluvial reworking, preference was given to grains that showed no signs of rounding or abrasion and especially to zircons with glass still adhering to their surfaces to try to avoid zircons recycled from older strata. Zonation within zircon grains was imaged with a cathodoluminescence (CL) detector mounted on a scanning electron microscope (SEM) at the University of California, Santa Barbara. For each ash, 30-40 zircons were dated, each with one 19-30  $\mu\text{m}$  analysis spot placed as close to the rim of each grain as possible to minimize the potential effect of older cores or protracted crystal growth.

Measured U-Pb ratios were corrected for initial  $^{230}\text{Th}$  disequilibrium and common lead. The measured  $^{238}\text{U}/^{206}\text{Pb}$  and  $^{207}\text{Pb}/^{206}\text{Pb}$  ratios for each analysis were corrected for initial  $^{230}\text{Th}$  disequilibrium (Scharer, 1984) following the method of Crowley *et al.* (2007). The main source of uncertainty in the disequilibrium correction is the Th/U ratio of the magma, which we estimated to be between 1 and 4 based on the range of values measured in glass adhering to 11 zircons from three different ashes; a value of  $2.5 \pm 1.5$  ( $2\sigma$ ) was used for the calculation. The Isoplot 3.0 Excel plug-in (Ludwig, 2012) was then used to calculate the  $^{207}\text{Pb}$ -corrected age for each analysis, using the disequilibrium-corrected  $^{207}\text{Pb}/^{206}\text{Pb}$  and  $^{238}\text{U}/^{206}\text{Pb}$  ratios and an assumed common lead  $^{207}\text{Pb}/^{206}\text{Pb}$  ratio of 0.836, which is the Stacey & Kramers bulk silicate Earth estimate at 3 Ma (Stacey & Kramers, 1975), with a 1% uncertainty on the assumed common lead composition. Because many of the ashes contain multiple age populations that likely reflect fluvial recycling of older ashes, as well as protracted crystal residence time in the magma chamber, we use a subset of the youngest ages to calculate the likely minimum age of each sample (Fig. 7). As a conservative estimate, the age we report for each sample is the weighted average of the five youngest analyses (excluding highly discordant analyses and analyses with large uncertainties on  $^{238}\text{U}/^{206}\text{Pb}$  or  $^{207}\text{Pb}/^{206}\text{Pb}$  ratios), and the uncertainty we report is two times the standard deviation of these five ages. All uncertainties are quoted at the 95% confidence or  $2\sigma$  level and include contributions from the external reproducibility of the primary reference material for the  $^{207}\text{Pb}/^{206}\text{Pb}$  and  $^{206}\text{Pb}/^{238}\text{U}$  ratios.

Due to a paucity of volcanic ashes preserved within the Río Yacoraite section of the Humahuaca basin, we used magnetostratigraphy to date this section (Fig. 8). Where possible, three oriented block samples of siltstone, mudstone, or fine sandstone were collected at

intervals of 10-20 m. Measurements were performed on 2-4 specimens from each site using a DC SQUID magnetometer in the Caltech paleomagnetism lab (Kirschvink *et al.*, 2008). After the natural remanent magnetization (NRM) was measured, specimens were cooled in liquid nitrogen to remove multidomain viscous remanent magnetism, and then subjected to stepwise thermal demagnetization in 22-31 steps up to 600-690 °C (Fig. 9A). Using PaleoMag 3.1d35 (Jones, 2002), we identified the high-temperature component of the magnetization from the Zijderveld diagram (Fig. 9A) for each specimen and applied principal component analysis (Kirschvink, 1980) to at least 5 points (typically 10-20) to calculate the direction of each specimen's characteristic remanent magnetization (ChRM) (Fig. 9B) and its virtual geomagnetic pole (VGP). All specimens with mean angular deviations (MAD) of  $\leq 15^\circ$  were utilized, as were 17 specimens with MADs between 15 and  $30^\circ$  because of their consistency with adjacent specimens. The resultant VGP latitudes define magnetic polarity zones through the Río Yacoraite section that we then correlate to the Geomagnetic Polarity Timescale (GPTS) (Lourens *et al.*, 2004) with the aid of one dated ash (Fig. 8).

The provenance of detrital zircons in the Río Yacoraite section was used to track temporal changes in the amount of sediment coming from the Casa Grande basin relative to other sources (see Fig. 3 for locations). For each sample, ~200 zircon grains were dated with LA-MC-ICPMS U-Pb geochronology. We discarded ages less than 12 Ma, because these ages are likely derived from widespread ashes that greatly vary in abundance through time and provide little information about sediment provenance. Sediment from modern channels was used to (i) characterize the detrital zircon signatures of sediment coming from the Casa Grande basin versus the Río Grande (the trunk stream) in the Humahuaca basin and (ii) distinguish specific source areas, such as plutons, with distinctive age signatures. Next,

detrital zircon ages from medium-grained sandstones collected at ~100 m intervals within the Río Yacoraite section and complemented by changing conglomerate compositions were used to deduce changes in the relative contributions of different source areas. Specifically, the relative abundance of zircons from the Aguilar granite (on the eastern border of the Puna Plateau) and Fundición granite (in the Sierra Alta) was used to track the sediment flux from the Casa Grande basin over time. Potential complications to this interpretation are addressed in the results section and include the possibility that Cretaceous-Neogene strata could contain recycled zircons with ages similar to the plutons, that the areal extent of certain rock units exposed at the surface may have changed, or that drainage patterns may have changed.

Finally, topography along Río Yacoraite was analyzed to provide constraints on incision through the Sierra Alta. Elevation data were drawn from the 30-m Advanced Spaceborne Thermal Emission and Reflection Radiometer (ASTER) Global Digital Elevation Model Version 2 (GDEM V2). We used the maximum elevation across narrow swaths (0.5-1 km wide) to extract the elevation profiles of ridgelines striking perpendicular to the Río Yacoraite (Fig. 10). Abrupt increases in mean slope in these profiles were identified (Fig. 10C), and the elevations of these slope breaks were plotted against distance downstream from the outlet of the Casa Grande basin (Fig. 10D). These slope breaks are interpreted as forming as a result of an increase in the rate of fluvial incision, causing steeper slopes adjacent to the incising river. Channels set the local base level for adjacent hillslopes, and higher incision rates produce steeper hillslope gradients, up to the threshold angle for landsliding, but the entire hillslope does not adjust instantly to changes in incision rate (e.g., Burbank, 2002). Thus, after an increase in incision rate, the lower part of hillsides adjacent to the channel may be oversteepened whereas their upper parts still retain the original lower slope. The height

(above the channel) of the break in slope between these contrasting regions of the hillside should be related to the amount of incision that has occurred since the increase in incision rate.

## **RESULTS**

### **Casa Grande stratigraphy**

In the Casa Grande basin, 120 m of Plio-Pleistocene fill (Fig. 5) lies above an extensive angular unconformity with the red sandstones of the Eo-Oligocene Casa Grande Formation (Boll & Hernández, 1986). A 3-meter-thick volcanic ash (CG250307-01) at the base of the fill yielded a U-Pb zircon age of  $3.74 \pm .04$  Ma. Deposition continued until about 0.8 Ma, as indicated by a  $0.80 \pm .02$  Ma ash (CG220311-02) lying two meters below the top of the fill in the southern measured section (Fig. 5). Since 0.8 Ma, the river has incised >150 m through the Plio-Pleistocene fill and underlying Casa Grande Formation.

The basin fill consists of mostly fluvial strata with some intervals (~15% of total thickness) of lacustrine deposits (Fig. 5). Fluvial facies include clast-supported, well-sorted granule, pebble, and cobble conglomerates in the northern and center sections and reddish siltstones and fine- to medium-grained sandstones with 10-30 cm horizontal beds in all three sections. The conglomerates typically display 10- to 40-cm-thick bedding and include thinner interbedded sandstone layers 5-10 cm thick. Lacustrine facies consist of laminated gray to tan mudstones with occasional thin vertical rootlets in the central and southern sections.

Paleoflow directions (Fig. 5) in the fluvial units inferred from measurements of channel margins and imbricated pebbles indicate average flow in the direction of the modern outlet, i.e., towards the south or south-southeast in the northern and central portion of the basin and

toward the east in the southwestern portion of the basin. Downstream fining of clast size from north to south is also consistent with flow toward the present-day outlet. The northernmost section consists of pebble-cobble conglomerates (62%) interbedded with medium- to fine-grained sandstones (25%) and with muddy debris flows (massive mudstones with matrix-supported pebbles and lenses of pebble conglomerates, ~20-cm-thick beds) (14%) in the upper part of the section. In the center of the basin, mostly pebble conglomerates (38%) and sandstones (29%) prevail with some siltstones (8%) and a few intervals of laminated mudstones (16%), whereas the southern measured section is dominated by medium to fine sandstones (78%) with intervals of laminated mudstones (13%) and uncommon pebble conglomerates (3%). Pebble clast counts in the northern section (taken at 2 m, 46 m, and 112 m in the section) demonstrate that conglomerate compositions remain fairly constant through time, consisting of 42-48% shale, 12-17% quartzite, 1-3% limestone, 9-11% red sandstone, and 29-31% granitic clasts (Fig. 5).

Five new U-Pb ash ages (Fig. 5) provide a chronologic framework that allows us to calculate average sediment-accumulation rates and to correlate between the measured sections and with events in the Humahuaca basin. Although three of these ashes were highly reworked and contained multiple age populations, the youngest grain ages approximate the depositional age of the sediments (Fig. 7, Table 1, Table S1). The ash at 80 m in the center section (CG210311-02) and the ash at 18.5 m in the southern section (CG220311-01) both yielded the same age ( $2.13 \pm .08$  Ma and  $2.14 \pm .14$  Ma), allowing robust correlation of these sections (Fig. 5). Averaged over million-year timescales, undecompressed sediment-accumulation rates decreased 50% from  $68 \pm 12$  m/Myr between 3.7 - 3.0 Ma to  $35 \pm 8$  m/Myr from 3.0 - 2.1 Ma, and then remained at  $33 \pm 7$  m/Myr until 0.8 Ma. These sediment-



accumulation rates are an order of magnitude lower than sediment-accumulation rates in other intermontane basins in the Eastern Cordillera of Argentina (Bywater-Reyes *et al.*, 2010; Schoenbohm *et al.*, 2015) and Andean foreland basins (Reynolds *et al.*, 2000; Reynolds *et al.*, 2001; Echavarría *et al.*, 2003; Horton, 2005; Uba *et al.*, 2007; DeCelles *et al.*, 2011; Galli *et al.*, 2014), but are comparable to the rates from intermontane basins in the Bolivian Eastern Cordillera (Horton, 2005). Similar to other intermontane basins in the Eastern Cordillera of Argentina (Bywater-Reyes *et al.*, 2010; Schoenbohm *et al.*, 2015), no clear correlation exists between accumulation rates and average grain size within the basin.

The Plio-Pleistocene strata within the Casa Grande basin are generally flat-lying and undeformed. On the eastern side of the basin, however, the basal unconformity and overlying ash at the fill's base dip  $\sim 5^\circ$  west, suggesting differential rock uplift of the Sierra Alta range on the eastern margin of the basin. Such uplift undoubtedly influenced late Pliocene-Pleistocene sedimentary processes within the Casa Grande basin.

### **Magnetostratigraphy & sediment-accumulation rates in the Río Yacoraite section**

Analysis of the Río Yacoraite stratigraphic section in the Humahuaca basin (Fig. 8) illuminates changes in the amount of sediment being transported from the Casa Grande basin to the Humahuaca basin and permits comparison of the timing of deposition in the two basins. Truncated by thrust faults at the top and the base of the section, these strata comprise 715 m of fluvial conglomerates and siltstones dipping  $\sim 10\text{-}30^\circ$  west. Paleoflow directions from imbricated clasts at 45 m and 174 m in the section indicate flow toward the east, but the relative contributions of the east-flowing Río Yacoraite and the south-flowing Río Grande (Fig. 3) likely vary throughout the section.

The Río Yacoraite section was dated with magnetostratigraphy (Fig. 8). Stepwise thermal demagnetization reveals a low-temperature component and a high-temperature component of NRM (Fig. 9). Whereas the low-temperature component (interpreted as a viscous overprint) is removed by 250°C, the high-temperature component (interpreted as the characteristic remanent magnetization: ChRM) typically decays stably toward the origin between 250°C and ~600°C, although many specimens retain some remanence until 680°C. This variable behavior suggests that both magnetite and hematite are magnetic carriers (O'Reilly, 1984).

Following tilt corrections, the ChRM directions obtained for 88 specimens from 35 sites cluster into two antipodal groups (Fig. 9, Table 2, Table S2). Note that 17 of these 88 ChRM directions had a mean angular deviation (MAD) (Kirschvink, 1980) between 15° and 30°, but were included in our analysis because they reveal orientations consistent with nearby “well-behaved” specimens. These data pass a B-level reversal test (McFadden & McElhinny, 1990), but fail the fold test, most likely due to the small variation in bedding orientations throughout the section (average dip is 21°, with a standard deviation of 6.4°).

The Río Yacoraite section's magnetic polarity stratigraphy (Fig. 8) comprises three normal and four reversed polarity zones, with each zone defined by  $\geq 3$  specimens. Correlation to the Geomagnetic Polarity Timescale (Lourens *et al.*, 2004) was aided by U-Pb dating of a  $2.54 \pm .06$  Ma reworked volcanic ash (HU190412-01) at 200 m in the section. This correlation assigns an age of 3.03 Ma (top of the Kaena subchron in the Gauss chron) to the lowest reversal at  $45 \pm 30$  m and an age of 1.78 Ma (top of the Olduvai subchron) to the highest reversal at  $622 \pm 31$  m in the section. Assuming constant sediment-accumulation rates, the top of the section dates from ~1.6 Ma.

Undeformed sediment-accumulation rates for the Río Yacoraite section were calculated using stratigraphic thicknesses and the age of bounding magnetic polarity reversals within the section (Fig. 8). Accounting for the uncertainties in the position of reversal boundaries, the average sediment-accumulation rate of  $330 \pm 90$  m/Myr from 3.03 Ma to 2.58 Ma increases to  $\sim 550$  m/Myr from 2.58 Ma to 1.78 Ma. The average sediment-accumulation rate between 2.58 and 1.95 Ma (the most tightly constrained reversals) is  $550 \pm 80$  m/Myr. Whereas these sediment-accumulation rates are similar to the rates in other intermontane basins in Eastern Cordillera (Bossi *et al.*, 2001; Bywater-Reyes *et al.*, 2010; Schoenbohm *et al.*, 2015), they are  $\sim 10$ -fold greater than the contemporaneous rates in the nearby Casa Grande basin ( $\sim 30$ -70 m/Myr). Notably, the observed changes in rates in the two basins are asynchronous and opposite, i.e., rates decrease through time in the Casa Grande basin and increase in the Humahuaca basin.

### **Provenance analysis of sediment in the Río Yacoraite section**

The primary difference between the modern detrital zircon age spectra coming from the Río Yacoraite as it descends eastward from the edge of the Puna Plateau through the Sierra Alta versus those of the Río Grande flowing southward along the axis of the Humahuaca valley is the presence or absence of a population of ages between 130 and 170 Ma (Fig. 11B, Table S3) that typify two plutons: the Aguilar granite on the border of the Puna Plateau and the Fundición granite in the Sierra Alta (Fig. 3). Zircons from small catchments draining the Aguilar granite on the west side of the Casa Grande basin are dominated by a unique 140-155 Ma age peak (Fig. 11C, Table S3). In contrast, the Fundición granite lying between Casa Grande and the Río Yacoraite section is dominated by 155-170 Ma ages (Fig. 11C, Table S3). As expected, the modern sediment from the mouth of the Río

Yacoraite contains both of these populations, whereas modern sediment from the outlet of the Casa Grande basin contains the Aguilar age population but not the Fundición age population (Fig. 11D, Table S3). Despite similarity of these Mesozoic ages, their distinctive populations (when defined using >150 detrital ages) permit discrimination between (i) sediment provenance from the Casa Grande basin catchment (which contains the Aguilar granite), indicative of fluvial connectivity across the Sierra Alta versus (ii) sediment provenance limited to the proximal (east) flank of the Sierra Alta where the Fundición granite is exposed.

A potential complication in interpreting the presence of these age signals as indicating sediment sourced directly from these plutons is that the Cretaceous-Neogene strata (i.e., Salta Group and Orán Group) could contain recycled zircons with similar ages. Luckily, these units do not appear to contain many zircons with ages matching our narrowly defined Aguilar and Fundición age populations (145-155 Ma and 155-170 Ma, respectively). This inference is supported by the absence of this age population in our sample from the modern Río Grande, which includes in its catchment outcrops of Salta Group and Orán Group rocks in the Sierra Hornocal. Additionally, none of the detrital zircon samples from the Salta Group and Orán Group analyzed by DeCelles *et al.* (2011) and Siks and Horton (2011) contained more than one zircon grain with an age between 140 and 170 Ma.

Before interpreting the provenance data in terms of fluvial connectivity across the Sierra Alta, other processes that could affect the fraction of Aguilar-derived zircons in the Río Yacoraite stratigraphic section should be assessed. Because the deposits within our measured section likely result from mixing between the Río Yacoraite and the Río Grande, the relative abundance of sediment from the Casa Grande basin and the Sierra Alta also depends on the proportion of sediment delivered by the Río Grande. A relative increase in

sediment from the Río Grande, due to either increasing sediment flux into that catchment or to the Río Grande migrating to the west side of the Humahuaca basin, should result in the same fractional decrease in the number of zircons from the Aguilar granite and the number of zircons from the Fundición granite. Thus, a key indicator of reduced sediment transport from the Casa Grande basin to the Humahuaca basin is a decrease in the fraction of Aguilar zircons relative to Fundición zircons. Second, a relative decrease in sediment derived from the Aguilar granite could also result from a decrease in the contribution of the Aguilar granite as a source of sediment to the Casa Grande basin. However, clast counts of conglomerates in the northern measured section in the Casa Grande basin (Fig. 5) show little temporal change in the abundance of granitic clasts (~30%), rendering this alternative hypothesis unlikely. We cannot completely rule out the possibility of either changes in the exposed area of Fundición granite or changes in drainage patterns affecting the amount of sediment eroded from that pluton and deposited in the Río Yacoraite section. Given the relatively slow pace of erosion implied by the preservation of a >4.3 Ma low-relief surface, however, it seems unlikely that very large changes would have occurred between 3 and 1.5 Ma. Third, the provenance data for a single sample could be biased either by short-term variability in deposition or by extreme events such as landslides. Notably, the abundance of granitic clasts in pebble-cobble conglomerates in the Río Yacoraite section follows the same decreasing trend as the fraction of detrital zircons from the Aguilar or Fundición granite (Fig. 12B). Clast counts from five sites through the Río Yacoraite section show a 10-fold decrease in the abundance of igneous clasts from 7% to <1% between ~3 Ma and ~1.9 Ma, equivalent to 45 m and 565 m in the section. The general agreement between these two data sets (Fig. 12) suggests that the detrital zircons are representative of long-term changes in sediment provenance.

The detrital zircon data records a decrease in the amount of sediment transported out of the Casa Grande basin and across the Sierra Alta to the Humahuaca basin between 3 Ma and 2.1 Ma. The lowest detrital zircon sample in the measured section (~3 Ma) has a detrital age distribution similar to the modern Río Yacoraite, with the peak at 140-170 Ma accounting for ~10% of detrital zircons >12 Myr old and an approximately 1:1 ratio of Sierra Aguilar-derived grains (140-155 Ma) to Sierra Alta-derived grains (155-170 Ma) (Fig. 12A, Table S3). Thus, the Casa Grande basin still maintained fluvial connectivity with the Humahuaca basin at 3 Ma. From ~3 Ma to ~2.7 Ma, the fraction of Aguilar grains decreased sharply while the fraction of Fundición (Sierra Alta) grains remained constant. Between ~2.7 Ma to ~2.1 Ma, the relative abundance of both Sierra Aguilar and Sierra Alta zircons decreased, and the fraction of Sierra Aguilar zircons relative to Sierra Alta zircons also decreased. Between 2.1 and 1.7 Ma, Aguilar-derived zircons accounted for <1% of each detrital zircon sample, indicating that little or no sediment from the Casa Grande basin reached the Humahuaca basin during that time.

### **Unconformities, incision, and deformation in the Humahuaca basin**

Comparison of the timing of the onset of deposition above unconformities and incision at the end of the filling cycle in the Casa Grande and Humahuaca basins provides insight into the tectonic and climatic conditions responsible for these events. We have identified an extensive unconformity (red lines: Fig. 6) with ~4-Ma ashes lying <10 m above it at multiple locations in the northern Humahuaca basin. West of Huacalera (5 km south of the Río Yacoraite), an angular unconformity separates the Maimará Formation dipping 40-45° to the west from the overlying Tilcara Formation dipping 15-25° to the west. Two ash samples above the unconformity (HU240307-01 and HU180411-03) yielded U-Pb ages of

4.24 ± .08 Ma and 4.38 ± .11 Ma, respectively, whereas an ash within the Maimará Formation ~10 m below the unconformity yielded an age of 5.05 ± .14 Ma. In this same area, the Cretaceous Pirgua Subgroup has been thrust eastward over the Maimará and lowermost Tilcara formations, and is unconformably overlain by a conglomerate with a 3.86 ± .04 Ma ash (HU080410-01) at its base. One kilometer to the west, a conglomerate with a 3.80 ± .05 Ma ash (HU190311-01) at its base unconformably overlies Salta Group rocks in the hanging wall of a younger fault that was active after 3.8 Ma. Near Uquía (8 km north of the Río Yacoraite), two ash layers (UQ280307-01 and UQ160512-01) in the conglomerate above an unconformity with faulted Cretaceous and Precambrian rocks were dated to 4.12 ± .05 Ma and 3.97 ± .05 Ma, respectively.

Terrace abandonment and incision in the Humahuaca basin likely occurred around the same time that the filling of the Casa Grande basin ceased (after 0.8 Ma). The timing of Pleistocene incision in the Humahuaca basin must be younger than the 0.87 ± .03 Ma ash (HU230412-01) situated 20 m below the top of a 240-m-high fill terrace on the east side of the valley across from the Río Yacoraite. Lying a few meters below this 0.87-Ma ash in the Humahuaca basin, an unconformity truncates finer-grained siltstone and sandstone deposits (Uquía Fm.) that contain a 2.21 ± .08 Ma ash (HU230412-02). This superposition suggests that the gravel containing the 0.87-Ma ash was deposited during a pulse of aggradation following an earlier period of erosion. The presence of an analogous 300-m-high fill terrace ~20 km to the south (near Tilcara: Fig. 3) with an 800-ka ash located in the lower third of the fill (Strecker *et al.*, 2007; Pingel *et al.*, 2013) suggests that this episode of aggradation followed by incision in the Humahuaca basin was a significant basin-wide event.

The deformation history of the Sierra Alta provides information about potential tectonic controls on filling, basin isolation, and incision in the Casa Grande basin. Although the main phase of deformation within the Sierra Alta occurred during the Miocene (Deeken *et al.*, 2005; Siks & Horton, 2011), more recent deformation along the eastern edge of the Sierra Alta has been previously documented in the Humahuaca basin (Rodríguez Fernández *et al.*, 1999; Pingel *et al.*, 2013). We mapped several west-dipping Plio-Pleistocene reverse faults in the Humahuaca basin (Fig. 6). Slip on these faults would have promoted rock uplift of the Sierra Alta. Because these faults crosscut ash-bearing Plio-Pleistocene strata, the U-Pb ages of the ashes serve to bracket intervals of slip along individual fault strands (Fig. 6). Reverse faults on the west side of the Humahuaca basin were active from at least 3.9 Ma, and likely from >4.1 Ma, until <1.6 Ma. Near the village of Uquía, the ~4.1 Ma ash above the unconformity is offset ~65 m vertically across the fault that thrusts Paleozoic rocks over Salta Group rocks, and this same fault is sealed by the 3.8 Ma ash above the unconformity west of Huacalera (Fig. 6). The thrust fault ~2 km west of Huacalera with Maimará Fm. and lowermost Tilcara Fm. rocks in the footwall and Salta Group rocks in the hanging wall, must have been active between 4.2 Ma and 3.9 Ma, based on the ages of the footwall strata and the conglomerate unconformably overlying the Salta Group rocks in the hanging wall (Fig. 6). Thrusting on the west side of the Humahuaca basin continued until <1.6 Ma: the age at the top of the Río Yacoraite section, which lies in the footwall of a thrust fault. Sometime after 1.8 Ma, active faulting shifted eastward to the fault in the center of the Humahuaca basin, as shown by the ~15-45° westward tilting of strata as young as 1.8 Ma west of the Río Grande, whereas coeval strata east of the Río Grande typically dip less than 10° west. Thus, west-dipping reverse faults east of the Sierra Alta were active both before and during the filling of



the Casa Grande basin. Other faults within the Sierra Alta may have been active during the last 4 Ma, but no cross-cutting relationships with ash-bearing Neogene-Quaternary sediments have been found.

### **Topographic constraints on uplift and incision along the Río Yacoraite**

Topographic analysis of hillslopes flanking the Río Yacoraite provides constraints on the incision and uplift of the Sierra Alta. The ridge crest directly east of the Casa Grande basin has two abrupt breaks in slope, defining the bedrock gorge at the outlet of the Casa Grande basin (Fig. 10A,C). Similar slope breaks are observed on many ridge crests along the Río Yacoraite (Fig. 10B,D) and cluster into three groups on the basis of their heights above the modern channel: one set of upper slope breaks lie ~500-700 m above the channel; and two sets of lower slope breaks lie ~200 m and ~300-400 m above the channel, respectively. Additionally, we observe gravels overlying small straths at two locations on the south side of the Río Yacoraite (labeled “7-cgl” and “11-cgl” on Fig. 10D). The bases of these gravels also lie ~200 m above the modern channel. Remnants of the gravel in swath 11 can be seen as high as 350 m above the modern channel. Given (i) the similar heights above the modern channel of the straths along the Río Yacoraite and the unconformity between the Uquía Fm. (2.2 Ma) and the terrace fill (0.9 Ma) on the east side of the Humahuaca basin and (ii) the thickness (>100 m) of the gravels in swath 11, we suggest that the deposition of these gravels along the Río Yacoraite was coeval with the 0.9 - <0.8 Ma pulse of aggradation in the Humahuaca basin.

At the outlet of the Casa Grande basin, the higher break in slope lies ~600 m above the modern channel. We interpret this upper slope break to reflect incision of the pre-existing topography in response to renewed rock uplift beginning >4.1 Ma. Notably, on the eastern

flank of the range, the elevated low-relief surface just north of the Río Yacoraite lies ~700 m above the modern river (Fig. 10B,C). The similar height of the low-relief surface and upper slope breaks above the modern river implies a relatively uniform amount of uplift across the Sierra Alta, suggesting that the uplift is primarily due to the faults on the eastern side of the range rather than faulting within the range. The onlap of the 4.1 Ma conglomerate onto the low-relief surface (Fig. 6) implies that this surface formed prior to 4.1 Ma and was subsequently uplifted.

Whereas the height of the upper slope breaks is interpreted to indicate the total amount of incision during the Plio-Pleistocene uplift of the Sierra Alta, the lower slope breaks are interpreted to reflect an episode of rapid incision after 0.8 Ma (Fig. 10E). At the outlet of the Casa Grande basin, this lower slope break lies ~340 m above the modern channel, at an elevation slightly above the top of the Casa Grande basin fill. The incision below this lower slope break at the Casa Grande outlet must have occurred after 0.8 Ma, or else it would have disrupted basin filling. Lower slope breaks occur at the same height on ridge crests flanking the Río Yacoraite for ~4 km downstream from the Casa Grande basin. Farther downstream, the lower slope break steps down to around 200 m above the modern channel. This contrast indicates that the upstream portion of the Río Yacoraite had not incised as much as the downstream portion prior to this final episode of incision.

## **DISCUSSION**

### **Reconstruction of intermontane basin history**

Evidence of Plio-Pleistocene uplift of the Sierra Alta (including thrusting on the east side of the range abutting the Humahuaca basin and tilting of basin-filling strata on the

western flanks of the range in the Casa Grande basin) suggests that aggradation within the Casa Grande basin resulted when incision of the Río Yacoraite was unable to fully keep pace with rock uplift in the Sierra Alta. Fluvial connectivity with the Humahuaca basin would have been sustained as long as sediment supply was sufficient for the rate of aggradation to keep up with the rate of local surface uplift at the outlet (as in Fig. 1B). The Plio-Pleistocene evolution of the Casa Grande basin therefore depended on competition between the rate of uplift of the downstream range (Sierra Alta), the rate of incision at the basin's outlet, and the rate of aggradation in the basin itself (e.g., Fig. 1); a scenario akin to the situation in the Toro basin 150 km to the southwest of Humahuaca (Hilley & Strecker, 2005). In this context, events in the basin's history can be interpreted as responses to evolving tectonic, climatic, and topographic conditions that affected the balances between sediment flux, transport capacity, incision, uplift, local base level, and aggradation (Fig. 13). Specifically, we further explore the onset of deposition, changes in sediment-accumulation rates, basin isolation and subsequent reintegration, and final incision.

### ***3.8 Ma Onset of deposition above an unconformity***

The initiation of deposition above an unconformity requires the sediment flux to exceed the transport capacity. A change in this ratio could result from localized or regional rock uplift or from a climate change. The synchronous onset of deposition above the unconformity in the Casa Grande and Humahuaca basins around 3.8 Ma suggests that this event was controlled by regional, rather than strictly local, conditions (Fig. 13B). Given that uplift of the Sierra Alta was accommodated along thrust faults within the Humahuaca basin, increased uplift rates should have promoted further erosion in the hanging walls of these faults, instead of the renewed deposition above the unconformity that formed between 5 and

4 Ma. Conversely, a regional increase in rock-uplift rates in both the Sierra Alta and the Tilcara ranges, perhaps related to deeper seated structure(s) could have driven aggradation in both basins by affecting the balance between rock uplift and incision at the outlet of each basin. Increased uplift rates could also promote deposition by increasing the caliber and/or flux of sediment to the basins. Alternatively, a change in climate affecting both basins could have driven the onset of deposition above the unconformity. Although a shift to a drier climate could drive deposition by decreasing discharge and, hence, transport capacity, the shift to semi-arid conditions in the Humahuaca basin did not occur until between 3.5 and 2.5 Ma (Reguero *et al.*, 2007; Pingel *et al.*, 2014). Conversely, a shift to a wetter climate or an increase in climate variability could drive deposition by increasing the sediment flux to the basin. For example, Schoenbohm *et al.* (2015) suggest that the onset of Punaschotter conglomerates in several basins around 4 Ma could be related to a global increase in climate variability 4-3 Ma (e.g., Zachos *et al.*, 2001; Lisiecki & Raymo, 2005), which could have increased erosion rates as a result of increased landscape disequilibrium (Godard *et al.*, 2013).

Previous studies of other basins in the Eastern Cordillera of NW Argentina (Kleinert & Strecker, 2001; Starck & Anzótegui, 2001; Bywater-Reyes *et al.*, 2010; Schoenbohm *et al.*, 2015) do not support a broader regional shift to more humid conditions around 4 Ma. On the other hand, a more local shift to wetter conditions as a result of localized range uplift is consistent with limited constraints on the uplift history of the Sierra Alta and Tilcara ranges. Initial uplift of a range typically results in increased precipitation due to an orographic rainfall effect and, as uplift continues, the range becomes a barrier to precipitation, leading to more arid conditions on its downwind side (Galewsky, 2009). The relationship between

modern precipitation patterns (Bookhagen & Strecker, 2012) and the elevations of ranges in the Santa Barbara System and Sierra Pampeanas indicates that ranges with elevations of ~1-2 km experience increased rainfall across the entire range, whereas ranges with elevations > 2.5 km produce enhanced rainfall on the windward sides and a rain shadow on the leeward side. Consistent with an orographically-enhanced precipitation effect, the onset of coarse-grained deposition in the Casa Grande basin occurred during the early stages of the Pliocene-Pleistocene uplift of the Sierra Alta and the Tilcara ranges, soon after both the ~4.2-Ma drainage reorganization in Humahuaca basin in response to uplift of the Tilcara Ranges (Pingel *et al.*, 2013) and the earliest evidence of faulting on the west side of the Humahuaca basin between 5.0 – 4.3 Ma. This interpretation implies that, despite Miocene deformation in the Sierra Alta and Sierra Hornocal (along strike with the Tilcara ranges), these ranges remained relatively low (<2.5 km) into Pliocene times, or that deep, E-W valleys acted as topographic conduits for moisture into the range (Barros *et al.*, 2004). Although perhaps surprising, this interpretation is consistent with paleocurrent and provenance data from the Maimará Formation in the Humahuaca basin, which indicate that, at 6 Ma, uplift of the Sierra Alta had not yet disrupted rivers flowing eastward from the Puna Plateau and that uplift of the Tilcara ranges did not disrupt eastward fluvial transport in the Humahuaca basin until ~4.2 Ma (Pingel *et al.*, 2013).

The onset of deposition may have been driven by a regional increase in uplift rates, a shift to more variable climate, or orographically enhanced precipitation in the early stages of range uplift. Although we cannot eliminate any of these hypotheses, we favor a tectonically driven increase in orographic precipitation, because it is consistent with constraints on the

timing of Plio-Pleistocene uplift of the Sierra Alta and Tilcara ranges (Pingel *et al.*, 2013; Pingel *et al.*, 2014).

### ***Rock uplift outpaces incision***

Sustained sediment accumulation in the Casa Grande basin is interpreted to have occurred when rock-uplift rates in the Sierra Alta persistently outpaced fluvial incision at the outlet of the basin. This imbalance caused local surface uplift of the bedrock channel immediately downstream of the outlet of the Casa Grande basin and drove aggradation behind this rising barrier. The increase of sediment supply relative to transport capacity could have decreased the river's ability to incise through the uplifting Sierra Alta by increasing the fraction of the bedrock channel protected by sediment cover (e.g., Sklar & Dietrich, 2001). This effect, however, likely would be transient: the reduction of bedrock incision due to cover would cause the channel to steepen with continued uplift, thereby resulting in a new equilibrium with both a steeper channel slope and a likely decrease in cover above the bedrock channel.

### ***3 Ma to 2.1 Ma loss of fluvial connectivity***

In the Río Yacoraite stratigraphic section, detrital zircons sourced from the Aguilar granite (Fig. 3) indicate persistent fluvial connectivity between the Casa Grande and downstream Humahuaca basins between 3 Ma and 2.5 Ma (Fig. 12A, Fig. 13C). Therefore, aggradation in Casa Grande basin must have approximately balanced the pace of local surface uplift at the basin's outlet (Fig. 1B). During this period, however, the relative abundance of detrital zircons of Aguilar age (140-155 Ma) from the Casa Grande basin catchment decreased, and by 2.1 Ma, almost no sediment from the Casa Grande basin

reached the Humahuaca basin (only a single zircon with Aguilar age out of ~200 dated grains: Fig. 12).

Between 3 Ma and 2.1 Ma, the sediment flux out of the Casa Grande basin diminished while the basin's sediment-accumulation rate remained constant (Fig. 5). These synchronous effects imply a long-term decrease in the amount of sediment entering the Casa Grande basin: a change that may reflect a transition to a more arid climate due to an enhanced rain shadow driven by continuing uplift of the Sierra Alta and Tilcara ranges (Figs. 13D, 13E). For basins with gently sloping margins, sediment-accumulation rates in a vertical stratigraphic section could remain constant while the amount of sediment transported out of the basin decreased even if the amount of sediment delivered into the basin did not decrease. For the geometry of the Casa Grande basin with its relatively wide, flat bottom and steep sides, however, this effect would be small (Appendix A1). Secondly, if only a small fraction of the sediment flux into the basin is transported out of the basin, then even a dramatic *relative* decrease in the amount of sediment transported out of the basin will have only a small effect on the rate of sediment accumulation in the basin.

We argue, however, that at 3 Ma, a large fraction of the sediment flux into the Casa Grande basin was likely transported out of the basin. Given that (1) the relative abundance of detrital zircons sourced from the Aguilar granite (easternmost Puna) and Fundición granite (Sierra Alta) in the Río Yacoraite section at 3 Ma is very similar to that of modern sediment near the mouth of the Río Yacoraite and (2) very little sediment is being trapped in the Casa Grande basin today, we infer that a significant fraction of the sediment entering the Casa Grande basin was also transported out of the basin 3 Ma. Whereas this conclusion would be invalid if the Aguilar granite accounted for a much larger fraction of sediment entering the

basin in the past than today, this scenario is unsupported. The fraction of granite pebbles in ~3-Ma conglomerates in the Casa Grande basin (30% in the northern measured section) are not dramatically different from today (15% at the outlet of the basin), and this difference could be due to location within the basin, rather than to changes in the amount of granite entering the basin. Thus, having discounted these alternative explanations, we invoke a decrease in sediment supply to explain the combined observations of (i) a decrease in the amount of sediment transport out of the Casa Grande basin between 3 Ma and 2.1 Ma with (ii) a concurrent decrease in the sediment-accumulation rates in the Casa Grande stratigraphic sections.

Such a decrease in sediment flux in response to increased aridity is consistent with the onset of semiarid conditions in the Humahuaca basin between 3.5 Ma and 2.5 Ma (Pingel *et al.*, 2014). The ~50% decrease in average sediment-accumulation rates in the Casa Grande basin during this same interval (Fig. 5) may also reflect this decrease in sediment supply. As the Casa Grande basin's sediment supply decreased, a larger fraction of that sediment was trapped in the basin by the local surface uplift at the outlet of the basin, resulting in the decrease in the abundance of Aguilar-derived zircons in the Río Yacoraite section between 3 and 2.7 Ma. By 2.1 Ma, Casa Grande's sediment flux had decreased to the point that aggradation could no longer keep pace with this uplift, resulting in a loss of fluvial connectivity with the Humahuaca basin.

### ***2.1 Ma to <1.7 Ma continued basin isolation***

From 2.1 Ma to the end of our detrital zircon record at ~1.7 Ma in the Río Yacoraite section, the Casa Grande basin remained largely isolated from the Humahuaca basin (Figs. 12, 13E). Even during this period of basin isolation, the deposits preserved within the Casa



Casa Grande basin constitute dominantly fluvial facies (Fig. 5). These facies imply that any lake that formed as a result of channel defeat at the basin's outlet was likely limited in extent to the southeastern portion of the basin near the modern outlet: a region where few Plio-Pleistocene sediments are currently preserved. Lacustrine intervals in the measured sections in the southwest and center of the Casa Grande basin could reflect either fluctuations in the extent of that lake or the formation of separate small lakes. The presence of lacustrine facies in the center of Casa Grande basin prior to 3 Ma (Fig. 5) also raises the possibility of an earlier cycle of basin isolation and reintegration. However, we cannot test this scenario with detrital zircon data because dated deposits older than ~3 Ma are not known near the mouth of the Río Yacoraite in the Humahuaca basin (Fig. 8).

With little or no sediment leaving the Casa Grande basin, the segment of the Río Yacoraite immediately downstream of the basin would have lacked tools to erode its bed, resulting in decreased incision rates (Sklar & Dietrich, 2001). Farther downstream, sediment eroded from the Sierra Alta would have provided tools to maintain higher incision rates. This contrast could have resulted in the greater incision of the downstream portion of the Río Yacoraite prior to 0.8 Ma and the development of a 150-m-high knickpoint, as inferred from the height of slope breaks along ridge crests (Figs. 10D,E).

#### ***<0.8 Ma reintegration and incision***

Deposition in the Casa Grande basin ceased after ~0.8 Ma (age of an ash 2 m below the top of southern measured section), and incision likely followed soon after. A pulse of filling followed by incision also occurred in the Humahuaca basin around this time, as recorded by fill terraces up to 300 m thick containing ashes dated to 0.9 – 0.8 Ma. If the Casa Grande basin also experienced a pulse of sediment accumulation at that time, this enhanced

flux could have allowed the fill to overtop the barrier at the outlet of the basin and reestablish fluvial connectivity between the Casa Grande and Humahuaca basins (Fig. 13F). This overflow would have increased the tools available to erode the bed along the steepened bedrock channel portion of the Río Yacoraite through the deformed Sierra Alta, thereby allowing a wave of incision to propagate across the Sierra Alta into the Casa Grande basin.

With the reestablishment of fluvial connectivity, post-0.8-Ma incision in the Humahuaca basin following terrace abandonment could propagate upstream into the Casa Grande basin (Fig. 13G). The final ~200 m of bedrock incision, i.e., incising beneath the lower slope break in the downstream portion of the Río Yacoraite (Fig. 10D,E), was likely driven by incision in the Humahuaca basin. This interpretation is consistent with both preserved straths along the lower Río Yacoraite and the unconformity underlying the 0.8-Ma fill in the Humahuaca: all located ~200 m above the modern channel.

Given that the reestablishment of fluvial connectivity was key to the incision of the Casa Grande basin fill after 0.8 Ma, one might ask why incision did not occur during earlier periods of fluvial connectivity, e.g., at 3 Ma. Increasing aridity around 3Ma (Pingel *et al.*, 2014) and resultant decreases in discharge and stream power may have hindered incision rates from coming into balance with rock uplift at Casa Grande's outlet. A second factor that may have contributed to incision rates outpacing rock uplift rates at ~ 0.8 Ma is that faulting in the Humahuaca valley had shifted farther east by that time (Fig. 10), which could have resulted in decreased rates of rock uplift in the Sierra Alta.

### **Regional context**

Whereas individual events in the Casa Grande basin history can be explained by climatically-driven changes in sediment supply (e.g., basin isolation) or the upstream

response to base-level change in the Humahuaca basin (e.g., final incision through the fill), more generally, Plio-Pleistocene sediment accumulation in the Casa Grande basin was driven by uplift of the Sierra Alta. This phase of renewed uplift, which also included deformation within the Humahuaca basin and uplift of the Tilcara ranges (Pingel *et al.*, 2013; Pingel *et al.*, 2014), occurred from >4.3 Ma until <1.7 Ma. This episode of range building occurred several million years after the arrival of deformation in this area by the middle Miocene, i.e., by ~14-10 Ma in the Sierra Alta and Sierra Hornocal (Deeken *et al.*, 2005; Siks & Horton, 2011; Insel *et al.*, 2012).

Much of the surface uplift of the Tilcara ranges occurred during this Plio-Pleistocene phase of deformation (Pingel *et al.*, 2013; Pingel *et al.*, 2014) and apatite (U-Th)/He cooling ages around 5.6 Ma from the Sierra Hornocal to the northeast (Reiners *et al.*, 2015) suggest that Plio-Pleistocene exhumation was also significant in these ranges. In the Sierra Alta, on the other hand, both mid-Miocene apatite fission-track cooling ages (Deeken *et al.*, 2005; Insel *et al.*, 2012) and the topographic constraints on incision along the Rio Yacoraite (Fig. 10), which suggest <600 m of Plio-Pleistocene surface uplift, imply lower rock uplift rates in the Sierra Alta than in the Tilcara ranges. Perhaps climate and sediment supply played such an important role in the Plio-Pleistocene evolution of the Casa Grande basin because deformation rates in the Sierra Alta were relatively low. That this later phase of deformation produced relatively minor uplift of the Sierra Alta may also explain why the rates of sediment accumulation in the Casa Grande basin are nearly an order of magnitude lower than in the Humahuaca basin and other intermontane basins in the Eastern Cordillera (e.g., Bossi *et al.*, 2001; Bywater-Reyes *et al.*, 2010; Galli *et al.*, 2014; Schoenbohm *et al.*, 2015).

The higher rates of sediment accumulation in the Humahuaca basin are probably due primarily to higher rock uplift rates in the Tilcara ranges compared to the Sierra Alta and secondarily to additional accommodation created in the footwall of thrust faults on the west side of the basin. In the Casa Grande basin, which lacked active basin-bounding faults, accommodation was generated solely by the uplift of the downstream barrier (e.g., Fig. 1B). Furthermore, this type of accommodation is temporary: once uplift ceases downstream, the channel should adjust to a lower channel slope, incising through the basin fill. Indeed, a large fraction of the fill in both the Casa Grande and Humahuaca basins has already been removed.

## **CONCLUSIONS**

Comparison of the timing of events at the 100-kyr timescale between the Casa Grande basin and the neighboring, downstream Humahuaca basin allows discrimination between local controls on basin evolution that affect each basin independently and regional controls that result in synchronous events in both basins. Furthermore, detrital zircon provenance of sediment in the Humahuaca basin records changes in its fluvial connectivity with the Casa Grande basin. By integrating stratigraphic analysis of intermontane basin fill, provenance data, sediment-accumulation rates, observations of cross-cutting relationships that constrain the timing of deformation along bounding ranges, and topographic evidence of incision history, we are able to assess the controls on the initial onset of deposition, sediment-accumulation rate, basin isolation, reintegration of the fluvial network, and subsequent incision. The main conclusions of this study include the following:

1. The 120-m-thick Plio-Pleistocene sedimentary fill in the intermontane Casa Grande basin was deposited between 3.8 Ma and 0.8 Ma. The dominantly fluvial strata

aggraded in response to local surface uplift at the outlet of the basin as rock uplift in the Sierra Alta outpaced the rate of channel incision. Rock uplift of the Sierra Alta was accommodated along east-vergent thrust faults that were active from  $>4.3$  Ma to  $< 1.7$  Ma on the west side of the Humahuaca basin. Following reintegration of the fluvial network at  $\sim 0.8$  Ma, the river incised  $>150$  m through the Plio-Pleistocene fill and the underlying Casa Grande Formation.

2. Along a given reach of a river system, aggradation or incision may be controlled by regional or local processes. The synchronous return to deposition above a widespread unconformity around 4 Ma in both basins suggests regional forcing, which we attribute to a hypothesized increase in sediment supply in response to enhanced precipitation in the early stages of range uplift and/or increased uplift rates in the Sierra Alta and Tilcara ranges. On the other hand, asynchronous changes in sediment-accumulation rates are locally controlled. In the Humahuaca basin, sediment-accumulation rates nearly double (from 330 m/Myr to 540 m/Myr) around 2.5 Ma, whereas in the Casa Grande basin, rates are halved (from 68 m/Myr to 35 m/Myr) around 3 Ma.
3. To discriminate between basin isolation or sustained fluvial connectivity, well-preserved stratigraphic sections with robust temporal frameworks, reliable provenance data, and distinct sedimentary facies are commonly required. However, as is the case in the Casa Grande basin, lacustrine facies associated with basin isolation may be limited in lateral extent and located close to the basin outlet, where preservation potential is low during dissection of the basin following reintegration of the fluvial network. Thus, the provenance of sediment deposited downstream from

- the basin can underpin successful identification of periods of basin isolation, as such provenance data will indicate the loss of distinctive source areas located within the catchment area of the basin. Detrital zircon provenance data indicates that fluvial connectivity between the Casa Grande basin and the Humahuaca basin persisted at 3 Ma, but by 2.1 Ma, the Casa Grande basin became isolated from the downstream drainage system and remained isolated until at least 1.7 Ma and possibly until 0.8 Ma.
4. By comparing relative changes in the amount of sediment transported out of the Casa Grande basin to sediment-accumulation rates in the Casa Grande basin, we conclude that basin isolation was accompanied by a decrease in sediment supply to the basin. Given independent evidence for a shift from humid to semi-arid conditions in the Humahuaca basin around this time (Reguero *et al.*, 2007; Pingel *et al.*, 2014), we argue that aridity decreased sediment supply to the point that aggradation was no longer able to keep pace with local surface uplift at the outlet of the Casa Grande basin, resulting in basin isolation.

## **ACKNOWLEDGEMENTS**

We thank Kate Zeiger, Luke Merrill, and Justin LaForge for their assistance with fieldwork and Sarah Slotznick, Steven Skinner, and Joe Kirschvink at the Caltech Paleomagnetism Lab for lab access and support with paleomagnetic measurements. We thank Barbara Carrapa, Delores Robinson, and Brian Horton for their constructive reviews. This research was supported by the National Science Foundation through a research grant to D. Burbank under grant 0838265 and via a Graduate Research Fellowship to R. Streit. M. Strecker was supported by Deutsche Forschungsgemeinschaft (DFG) under grant 373/21-1.

## REFERENCES

- ALLMENDINGER, R.W., RAMOS, V.A., JORDAN, T.E., PALMA, M. & ISACKS, B.L. (1983) Paleogeography and Andean structural geometry, Northwest Argentina. *Tectonics*, **2**, 1-16.
- AMIDON, W.H., LUNA, L.V., FISHER, G.B., BURBANK, D.W., KYLANDER-CLARK, A.R.C. & ALONSO, R. (2015) Provenance and tectonic implications of Orán Group foreland basin sediments, Río Iruya canyon, NW Argentina (23°S). *Basin Research*, 10.1111/bre.12139.
- BARROS, A.P., KIM, G., WILLIAMS, E. & NESBITT, S.W. (2004) Probing orographic controls in the Himalayas during the monsoon using satellite imagery. *Natural Hazards and Earth System Sciences*, **4**, 29-51.
- BOLL, A. & HERNÁNDEZ, R.M. (1986) Interpretación estructural del área Tres Cruces. *Boletín de Informaciones Petroleras, Tercera Época*, **3**, 2-14.
- BONORINO, G.G. & ABASCAL, L.D. (2012) Drainage and base-level adjustments during evolution of a late Pleistocene piggyback basin, Eastern Cordillera, Central Andes of northwestern Argentina. *Geological Society of America Bulletin*, **124**, 1858-1870.
- BOOKHAGEN, B. & STRECKER, M.R. (2008) Orographic barriers, high-resolution TRMM rainfall, and relief variations along the eastern Andes. *Geophysical Research Letters*, **35**, L06403, doi:06410.01029/02007gl032011.
- BOOKHAGEN, B. & STRECKER, M.R. (2012) Spatiotemporal trends in erosion rates across a pronounced rainfall gradient: Examples from the southern Central Andes. *Earth and Planetary Science Letters*, **327**, 97-110.
- BOSIO, P.P., POWELL, J., DEL PAPA, C. & HONGN, F. (2009) Middle Eocene deformation-sedimentation in the Luracatao Valley: Tracking the beginning of the foreland basin of northwestern Argentina. *Journal of South American Earth Sciences*, **28**, 142-154.
- BOSSI, G.E., GEORGIEFF, S.M., GAVRILOFF, I.J.C., IBANEZ, L.M. & MURUAGA, C.M. (2001) Cenozoic evolution of the intramontane Santa Maria basin, Pampean Ranges, northwestern Argentina. *Journal of South American Earth Sciences*, **14**, 725-734.
- BURBANK, D., MEIGS, A. & BROZOVIC, N. (1996) Interactions of growing folds and coeval depositional systems. *Basin Research*, **8**, 199-223.
- BURBANK, D.W. & RAYNOLDS, R.G.H. (1988) Stratigraphic keys to the timing of thrusting in terrestrial foreland basins: Applications to the Northwestern Himalaya. In: *New Perspectives in Basin Analysis* (Ed. by K. L. Kleinspehn, and Paola, C.), 331-351. Springer-Verlag, New York.
- BURBANK, D.W. (2002) Rates of erosion and their implications for exhumation. *Mineralogical Magazine*, **66**, 25-52.
- BURBANK, D.W., BOOKHAGEN, B., GABET, E.J. & PUTKONEN, J. (2012) Modern climate and erosion in the Himalaya. *Comptes Rendus Geoscience*, **344**, 610-626.
- BYWATER-REYES, S., CARRAPA, B., CLEMENTZ, M. & SCHOENBOHM, L. (2010) Effect of late Cenozoic aridification on sedimentation in the Eastern Cordillera of northwest Argentina (Angastaco basin). *Geology*, **38**, 235-238.
- CANAVAN, R.R., CARRAPA, B., CLEMENTZ, M.T., QUADE, J., DECELLES, P.G. & SCHOENBOHM, L.M. (2014) Early Cenozoic uplift of the Puna Plateau, Central Andes, based on stable isotope paleoaltimetry of hydrated volcanic glass. *Geology*, **42**, 447-450.

- CARRAPA, B., STRECKER, M.R. & SOBEL, E.R. (2006) Cenozoic orogenic growth in the Central Andes: Evidence from sedimentary rock provenance and apatite fission track thermochronology in the Fiambala Basin, southernmost Puna Plateau margin (NW Argentina). *Earth and Planetary Science Letters*, **247**, 82-100.
- CARRAPA, B., HAUER, J., SCHOENBOHM, L., STRECKER, M.R., SCHMITT, A.K., VILLANUEVA, A. & GOMEZ, J.S. (2008) Dynamics of deformation and sedimentation in the northern Sierras Pampeanas: An integrated study of the Neogene Fiambala basin, NW Argentina. *Geological Society of America Bulletin*, **120**, 1518-1543.
- CARRAPA, B., TRIMBLE, J.D. & STOCKLI, D.F. (2011) Patterns and timing of exhumation and deformation in the Eastern Cordillera of NW Argentina revealed by (U-Th)/He thermochronology. *Tectonics*, **30**, 30.
- CARRAPA, B., BYWATER-REYES, S., DECELLES, P.G., MORTIMER, E. & GEHRELS, G.E. (2012) Late Eocene-Pliocene basin evolution in the Eastern Cordillera of northwestern Argentina (25 degrees-26 degrees S): regional implications for Andean orogenic wedge development. *Basin Research*, **24**, 249-268.
- CARRAPA, B., HUNTINGTON, K.W., CLEMENTZ, M., QUADE, J., BYWATER-REYES, S., SCHOENBOHM, L.M. & CANAVAN, R.R. (2014) Uplift of the Central Andes of NW Argentina associated with upper crustal shortening, revealed by multiproxy isotopic analyses. *Tectonics*, **33**, 2013TC003461, doi: 003410.001002/002013TC003461.
- CARRAPA, B. & DECELLES, P.G. (2015) Regional exhumation and kinematic history of the central Andes in response to cyclical orogenic processes. *Geological Society of America Memoirs*, **212**, 201-213.
- CASTELLANOS, A. (1950) *El Uquiense, Sedimentos Neogenos de Uquia (Senador Perez) en la Provincia de Jujuy (Argentina)*. Universidad Nacional del Litoral, Facultad de Ciencias Matematicas Fisicas y Quimicas y Naturales, Rosario.
- COTTLE, J.M., KYLANDER-CLARK, A.R. & VRIJMOED, J.C. (2012) U-Th/Pb geochronology of detrital zircon and monazite by single shot laser ablation inductively coupled plasma mass spectrometry (SS-LA-ICPMS). *Chemical Geology*, **332**, 136-147.
- COUTAND, I., COBBOLD, P.R., DE URREIZTIETA, M., GAUTIER, P., CHAUVIN, A., GAPAIS, D., ROSSELLO, E.A. & LOPEZ-GAMUNDI, O. (2001) Style and history of Andean deformation, Puna plateau, northwestern Argentina. *Tectonics*, **20**, 210-234.
- COUTAND, I., CARRAPA, B., DEEKEN, A., SCHMITT, A.K., SOBEL, E.R. & STRECKER, M.R. (2006) Propagation of orographic barriers along an active range front: insights from sandstone petrography and detrital apatite fission-track thermochronology in the intramontane Angastaco basin, NW Argentina. *Basin Research*, **18**, 1-26.
- CRISTIANI, C., MATTEINI, M., MAZZUOLI, R., OMARINI, R. & VILLA, I.M. (2005) Petrology of Late Jurassic-Early Cretaceous Tusaquillas and Abra Laite-Aguilar Plutonic complexes (Central Andes, 23°05' S – 66°05'W): a comparison with the rift-related magmatism of NW Argentina and E Bolivia. In: *Mesozoic to Cenozoic Alkaline Magmatism in the Brazilian Plataform* (Ed. by P. Comin-Chiaramonti & C. Barros Gomez), 213-241. Editora da Universidade de São Paulo, Brazil.
- CROWLEY, J.L., SCHOENE, B. & BOWRING, S.A. (2007) U-Pb dating of zircon in the Bishop Tuff at the millennial scale. *Geology*, **35**, 1123-1126.
- DECELLES, P.G., CARRAPA, B., HORTON, B.K. & GEHRELS, G.E. (2011) Cenozoic foreland basin system in the central Andes of northwestern Argentina: Implications for



- Andean geodynamics and modes of deformation. *Tectonics*, **30**, TC6013, doi: 6010.1029/2011tc002948.
- DEEKEN, A., SOBEL, E.R., HASCHKE, M. & RILLER, U. (2005) Age of initiation and growth pattern of the Puna plateau, NW Argentina, constrained by AFT thermochronology. *Potsdam, Germany Abstract Volume, Terra Nostra*, **5** (1), 39.
- DEEKEN, A., SOBEL, E.R., COUTAND, I., HASCHKE, M., RILLER, U. & STRECKER, M.R. (2006) Development of the southern Eastern Cordillera, NW Argentina, constrained by apatite fission track thermochronology: From early Cretaceous extension to middle Miocene shortening. *Tectonics*, **25**, TC6003, doi: 6010.1029/2005tc001894.
- ECHAVARRIA, L., HERNANDEZ, R., ALLMENDINGER, R. & REYNOLDS, J. (2003) Subandean thrust and fold belt of northwestern Argentina: Geometry and timing of the Andean evolution. *AAPG Bulletin*, **87**, 965-985.
- ELGER, K., ONCKEN, O. & GLODNY, J. (2005) Plateau-style accumulation of deformation: Southern Altiplano. *Tectonics*, **24**, TC4020, doi: 4010.1029/2004tc001675.
- GABALDÓN, V., M.A. GONZALEZ, M.A. & LIZUAIN, A. (1998) *El mapa geológico, Estudio geológico integrado de la Quebrada de Humahuaca*. Servicio Geológico Minero Argentino (SEGEMAR), Buenos Aires.
- GALEWSKY, J. (2009) Rain shadow development during the growth of mountain ranges: An atmospheric dynamics perspective. *Journal of Geophysical Research-Earth Surface*, **114**, F01018, doi:01010.01029/02008JF001085.
- GALLI, C.I., COIRA, B., ALONSO, R., REYNOLDS, J., MATTEINI, M. & HAUSER, N. (2014) Tectonic controls on the evolution of the Andean Cenozoic foreland basin: Evidence from fluvial system variations in the Payogastilla Group, in the Calchaquí, Tonco and Amblayo Valleys, NW Argentina. *Journal of South American Earth Sciences*, **52**, 234-259.
- GEHRELS, G.E., VALENCIA, V.A. & RUIZ, J. (2008) Enhanced precision, accuracy, efficiency, and spatial resolution of U-Pb ages by laser ablation-multicollector-inductively coupled plasma-mass spectrometry. *Geochemistry Geophysics Geosystems*, **9**, Q03017, doi:03010.01029/02007GC001805.
- GODARD, V., TUCKER, G.E., BURCH FISHER, G., BURBANK, D.W. & BOOKHAGEN, B. (2013) Frequency-dependent landscape response to climatic forcing. *Geophysical Research Letters*, **40**, 859-863.
- GONZALEZ, M.A., PEREYRA, F., RAMALLO, E. & TCHILINGURIAN, P. (2004) Hoja Geológica 2366-IV, Ciudad Libertador General San Martín, provincias de Jujuy y Salta. *Boletín* 274, Instituto de Geología y Recursos Minerales, Servicio Geológico Minero Argentino. Buenos Aires, 109.
- GUBBELS, T.L., ISACKS, B.L. & FARRAR, E. (1993) High-level surfaces, plateau uplift, and foreland development, Bolivian central Andes. *Geology*, **21**, 695-698.
- HAIN, M.P., STRECKER, M.R., BOOKHAGEN, B., ALONSO, R.N., PINGEL, H. & SCHMITT, A.K. (2011) Neogene to Quaternary broken foreland formation and sedimentation dynamics in the Andes of NW Argentina (25 degrees S). *Tectonics*, **30**, TC2006, doi:2010.1029/2010TC002703.
- HILLEY, G.E. & STRECKER, M.R. (2005) Processes of oscillatory basin filling and excavation in a tectonically active orogen: Quebrada del Toro Basin, NW Argentina. *Geological Society of America Bulletin*, **117**, 887-901.

- HONGN, F., DEL PAPA, C., POWELL, J., PETRINOVIC, I., MON, R. & DERACO, V. (2007) Middle Eocene deformation and sedimentation in the Puna-Eastern Cordillera transition (23 degrees-26 degrees S): Control by preexisting heterogeneities on the pattern of initial Andean shortening. *Geology*, **35**, 271-274.
- HORTON, B.K. (2005) Revised deformation history of the central Andes: Inferences from Cenozoic foredeep and intermontane basins of the Eastern Cordillera, Bolivia. *Tectonics*, **24**, TC3011, doi:3010.1029/2003TC001619.
- HOUGH, B.G., GARZIONE, C.N., WANG, Z.C., LEASE, R.O., BURBANK, D.W. & YUAN, D.Y. (2011) Stable isotope evidence for topographic growth and basin segmentation: Implications for the evolution of the NE Tibetan Plateau. *Geological Society of America Bulletin*, **123**, 168-185.
- HUMPHREY, N.F. & KONRAD, S.K. (2000) River incision or diversion in response to bedrock uplift. *Geology*, **28**, 43-46.
- INSEL, N., GROVE, M., HASCHKE, M., BARNES, J.B., SCHMITT, A.K. & STRECKER, M.R. (2012) Paleozoic to early Cenozoic cooling and exhumation of the basement underlying the eastern Puna plateau margin prior to plateau growth. *Tectonics*, **31**, TC6006, doi:6010.1029/2012TC003168.
- JACKSON, S.E., PEARSON, N.J., GRIFFIN, W.L. & BELOUSOVA, E.A. (2004) The application of laser ablation-inductively coupled plasma-mass spectrometry to in situ U-Pb zircon geochronology. *Chemical Geology*, **211**, 47-69.
- JONES, C.H. (2002) User-driven integrated software lives: "Paleomag" paleomagnetism analysis on the Macintosh. *Computers & Geosciences*, **28**, 1145-1151.
- JORDAN, T.E. (1981) Thrust loads and foreland basin evolution, Cretaceous, Western United States. *AAPG Bulletin*, **65**, 2506-2520.
- JORDAN, T.E., ISACKS, B.L., ALLMENDINGER, R.W., BREWER, J.A., RAMOS, V.A. & ANDO, C.J. (1983) Andean tectonics related to geometry of subducted Nazca plate. *Geological Society of America Bulletin*, **94**, 341-361.
- JORDAN, T.E. & ALONSO, R.N. (1987) Cenozoic stratigraphy and basin tectonics of the Andes Mountains, 20°-28° South latitude. *AAPG Bulletin-American Association of Petroleum Geologists*, **71**, 49-64.
- JORDAN, T.E., FLEMINGS, P.B. & BEERS, J.A. (1988) Dating thrust-fault activity by use of foreland-basin strata. In: *New perspectives in basin analysis* (Ed. by K. L. Kleinspehn & C. Paola), 307 - 330. Springer-Verlag, New York.
- JORDAN, T.E., MPODOZIS, C., MUNOZ, N., BLANCO, N., PANANONT, P. & GARDEWEG, M. (2007) Cenozoic subsurface stratigraphy and structure of the Salar de Atacama Basin, northern Chile. *Journal of South American Earth Sciences*, **23**, 122-146.
- KIRSCHVINK, J.L. (1980) The least-squares line and plane and the analysis of paleomagnetic data. *Geophysical Journal of the Royal Astronomical Society*, **62**, 699-718.
- KIRSCHVINK, J.L., KOPP, R.E., RAUB, T.D., BAUMGARTNER, C.T. & HOLT, J.W. (2008) Rapid, precise, and high-sensitivity acquisition of paleomagnetic and rock-magnetic data: Development of a low-noise automatic sample changing system for superconducting rock magnetometers. *Geochemistry Geophysics Geosystems*, **9**, Q05Y01, doi:10.1029/2007GC001856.
- KLEINERT, K. & STRECKER, M.R. (2001) Climate change in response to orographic barrier uplift: Paleosol and stable isotope evidence from the late Neogene Santa Maria basin, northwestern Argentina. *Geological Society of America Bulletin*, **113**, 728-742.

- KLEY, J. & MONALDI, C.R. (2002) Tectonic inversion in the Santa Barbara System of the central Andean foreland thrust belt, northwestern Argentina. *Tectonics*, **21**, 18.
- LEASE, R.O., BURBANK, D.W., HOUGH, B., WANG, Z.C. & YUAN, D.Y. (2012) Pulsed Miocene range growth in northeastern Tibet: Insights from Xunhua Basin magnetostratigraphy and provenance. *Geological Society of America Bulletin*, **124**, 657-677.
- LISIECKI, L.E. & RAYMO, M.E. (2005) A Pliocene-Pleistocene stack of 57 globally distributed benthic delta O-18 records. *Paleoceanography*, **20**, PA1003, doi:10.1029/2004PA001071.
- LOURENS, L., HILGEN, F., SHACKLETON, N.J., LASKAR, J. & WILSON, D. (2004) The Neogene Period. In: *A Geologic Time Scale 2004* (Ed. by F. M. Gradstein, Ogg, J.G., Smith, A.), 409-440. Cambridge University Press, Cambridge, UK.
- LUDWIG, K.R. (2012) User's Manual for Isoplot 3.75, A Geochronological Toolkit for Microsoft Excel. *Berkeley Geochronology Center Special Publication No. 5*.
- MARQUILLAS, R.A., DEL PAPA, C. & SABINO, I.F. (2005) Sedimentary aspects and paleoenvironmental evolution of a rift basin: Salta Group (Cretaceous-Paleogene), northwestern Argentina. *International Journal of Earth Sciences*, **94**, 94-113.
- MARRETT, R. & STRECKER, M.R. (2000) Response of intracontinental deformation in the central Andes to late Cenozoic reorganization of South American Plate motions. *Tectonics*, **19**, 452-467.
- MARRETT, R.A., ALLMENDINGER, R.W., ALONSO, R.N. & DRAKE, R.E. (1994) Late Cenozoic tectonic evolution of the Puna Plateau and adjacent foreland, northwestern Argentine Andes. *Journal of South American Earth Sciences*, **7**, 179-207.
- MARSHALL, L.G., BUTLER, R.F., DRAKE, R.E. & CURTIS, G.H. (1982) Geochronology of Type Uquian (Late Cenozoic) Land Mammal Age, Argentina. *Science*, **216**, 986-989.
- McFADDEN, P.L. & McELHINNY, M.W. (1990) Classification of the reversal test in paleomagnetism. *Geophysical Journal International*, **103**, 725-729.
- MIALL, A.D. (1985) Architectural-element analysis: A new method of facies analysis applied to fluvial deposits. *Earth-Science Reviews*, **22**, 261-308.
- MIALL, A.D. (1996) *The Geology of Fluvial Deposits: Sedimentary Facies, Basin Analysis, and Petroleum Geology*. Springer, New York.
- MONTERO-LÓPEZ, C., STRECKER, M.R., SCHILDGEN, T.F., HONGN, F., GUZMÁN, S., BOOKHAGEN, B. & SUDO, M. (2014) Local high relief at the southern margin of the Andean plateau by 9 Ma: evidence from ignimbritic valley fills and river incision. *Terra Nova*, **26**, 454-460.
- MORENO, J.A. (1970) Estratigrafía y paleogeografía del Cretácico superior en la Cuenca del Noroeste Argentino, con especial mención de los Subgrupos Balbuena y Santa Barbara. *Revista de la Asociación Geológica Argentina*, **25**, 9-44.
- MORTIMER, E., CARRAPA, B., COUTAND, I., SCHOENBOHM, L., SOBEL, E.R. & GOMEZ, J.S. (2007) Fragmentation of a foreland basin in response to out-of-sequence basement uplifts and structural reactivation: El Cajon-Campo del Arenal basin, NW Argentina. *Geological Society of America Bulletin*, **119**, 637-653.
- O'REILLY, W. (1984) *Rock and Mineral Magnetism*. Blackie & Son, Glasgow.
- ORI, G.G. & FRIEND, P.F. (1984) Sedimentary basins formed and carried piggyback on active thrust sheets. *Geology*, **12**, 475-478.

- PATON, C., WOODHEAD, J.D., HELLSTROM, J.C., HERGT, J.M., GREIG, A. & MAAS, R. (2010) Improved laser ablation U-Pb zircon geochronology through robust downhole fractionation correction. *Geochemistry Geophysics Geosystems*, **11**, Q0AA06, doi:10.1029/2009GC002618.
- PEARSON, D.M., KAPP, P., DECELLES, P.G., REINERS, P.W., GEHRELS, G.E., DUCEA, M.N. & PULLEN, A. (2013) Influence of pre-Andean crustal structure on Cenozoic thrust belt kinematics and shortening magnitude: Northwestern Argentina. *Geosphere*, **9**, 1766-1782.
- PINGEL, H., STRECKER, M.R., ALONSO, R.N. & SCHMITT, A.K. (2013) Neotectonic basin and landscape evolution in the Eastern Cordillera of NW Argentina, Humahuaca Basin (similar to 24 degrees S). *Basin Research*, **25**, 554-573.
- PINGEL, H., ALONSO, R.N., MULCH, A., ROHRMANN, A., SUDO, M. & STRECKER, M.R. (2014) Pliocene orographic barrier uplift in the southern Central Andes. *Geology*, **42**, 691-694.
- POPE, R.J.J. & WILKINSON, K.N. (2005) Reconciling the roles of climate and tectonics in Late Quaternary fan development on the Spartan piedmont, Greece. In: *Alluvial Fans: Geomorphology, Sedimentology, Dynamics* (Ed. by A. Harvey, A. Mather & M. Stokes), **251**, 133-152. Geological Society, London, Special Publications.
- QUADE, J., DETTINGER, M.P., CARRAPA, B., DECELLES, P., MURRAY, K.E., HUNTINGTON, K.W., CARTWRIGHT, A., CANAVAN, R.R., GEHRELS, G. & CLEMENTZ, M. (2015) The growth of the central Andes, 22°S–26°S. *Geological Society of America Memoirs*, **212**, 277-308.
- RAMOS, V.A. (1999) Los depósitos sinorogénicos Terciarios de la región Andina. In: *Geología Argentina* (Ed. by R. Caminos), *Anales*, **29**, 651-682. Instituto de Geología y Recursos Minerales, Buenos Aires, Argentina.
- REGUERO, M.A., CANDELA, A.M. & ALONSO, R.N. (2007) Biochronology and biostratigraphy of the Uquia Formation (Pliocene-early Pleistocene, NW Argentina) and its significance in the Great American Biotic Interchange. *Journal of South American Earth Sciences*, **23**, 1-16.
- REINERS, P.W., THOMSON, S.N., VERNON, A., WILLETT, S.D., ZATTIN, M., EINHORN, J., GEHRELS, G., QUADE, J., PEARSON, D., MURRAY, K.E. & CAVAZZA, W. (2015) Low-temperature thermochronologic trends across the central Andes, 21°S–28°S. *Geological Society of America Memoirs*, **212**, 215-249.
- REYNOLDS, J.H., GALLI, C.I., HERNANDEZ, R.M., IDLEMAN, B.D., KOTILA, J.M., HILLIARD, R.V. & NAESER, C.W. (2000) Middle Miocene tectonic development of the Transition Zone, Salta Province, northwest Argentina: Magnetic stratigraphy from the Metan Subgroup, Sierra de Gonzalez. *Geological Society of America Bulletin*, **112**, 1736-1751.
- REYNOLDS, J.H., HERNANDEZ, R.M., GALLI, C.I. & IDLEMAN, B.D. (2001) Magnetostratigraphy of the Quebrada La Porcelana section, Sierra de Ramos, Salta Province, Argentina: age limits for the Neogene Oran Group and uplift of the southern Sierras Subandinas. *Journal of South American Earth Sciences*, **14**, 681-692.
- ROBINSON, R.A.J., SPENCER, J.Q.G., STRECKER, M.R., RICHTER, A. & ALONSO, R.N. (2005) Luminescence dating of alluvial fans in intramontane basins of NW Argentina. In: *Alluvial Fans: Geomorphology, Sedimentology, Dynamics* (Ed. by A. Harvey, A.

- Mather & M. Stokes), **251**, 153-168. Geological Society, London, Special Publications.
- RODRÍGUEZ FERNÁNDEZ, L.R., HEREDIA, N., SEGGIARO, R.E. & GONZÁLEZ, M.A. (1999) Estructura andina de la Cordillera Oriental en el área de la Quebrada de Humahuaca, provincia de Jujuy, NO de Argentina. *Trabajos de Geología - Universidad de Oviedo*, **21**, 321-332.
- ROHRMANN, A., STRECKER, M.R., BOOKHAGEN, B., MULCH, A., SACHSE, D., PINGEL, H., ALONSO, R.N., SCHILDGEN, T.F. & MONTERO, C. (2014) Can stable isotopes ride out the storms? The role of convection for water isotopes in models, records, and paleoaltimetry studies in the central Andes. *Earth and Planetary Science Letters*, **407**, 187-195.
- SALFITY, J.A., BRANDÁN, E.M., MONALDI, C.R. & GALLARDO, E.F. (1984) Tectónica compresiva cuaternaria en la Cordillera Oriental Argentina, latitud de Tilcara (Jujuy). *Actas del IX Congreso Geológico Argentino*, **2**, 427-434.
- SANCHO, C., PENA, J.L., RIVELLI, F., RHODES, E. & MUNOZ, A. (2008) Geomorphological evolution of the Tilcara alluvial fan (Jujuy Province, NW Argentina): Tectonic implications and palaeoenvironmental considerations. *Journal of South American Earth Sciences*, **26**, 68-77.
- SCHARER, U. (1984) The effect of initial Th-230 disequilibrium on young U-Pb ages - the Makalu case, Himalaya. *Earth and Planetary Science Letters*, **67**, 191-204.
- SCHILDGEN, T.F., YILDIRIM, C., COSENTINO, D. & STRECKER, M.R. (2014) Linking slab break-off, Hellenic trench retreat, and uplift of the Central and Eastern Anatolian plateaus. *Earth-Science Reviews*, **128**, 147-168.
- SCHOENBOHM, L.M., CARRAPA, B., MCPHERSON, H.M., PRATT, J.R., BYWATER-REYES, S. & MORTIMER, E. (2015) Climate and tectonics along the southern margin of the Puna Plateau, NW Argentina: Origin of the late Cenozoic Punaschotter conglomerates. *Geological Society of America Memoirs*, **212**, 251-260.
- SIKS, B.C. & HORTON, B.K. (2011) Growth and fragmentation of the Andean foreland basin during eastward advance of fold-thrust deformation, Puna plateau and Eastern Cordillera, northern Argentina. *Tectonics*, **30**, TC6017, doi: 6010.1029/2011TC002944.
- SKLAR, L.S. & DIETRICH, W.E. (2001) Sediment and rock strength controls on river incision into bedrock. *Geology*, **29**, 1087-1090.
- SOBEL, E.R., HILLEY, G.E. & STRECKER, M.R. (2003) Formation of internally drained contractional basins by aridity-limited bedrock incision. *Journal of Geophysical Research-Solid Earth*, **108**, 2344, doi:2310.1029/2002JB001883.
- SOBEL, E.R. & STRECKER, M.R. (2003) Uplift, exhumation and precipitation: tectonic and climatic control of Late Cenozoic landscape evolution in the northern Sierras Pampeanas, Argentina. *Basin Research*, **15**, 431-451.
- STACEY, J.S. & KRAMERS, J.D. (1975) Approximation of terrestrial lead isotope evolution by a 2-stage model. *Earth and Planetary Science Letters*, **26**, 207-221.
- STARCK, D. & ANZÓTEGUI, L.M. (2001) The late miocene climatic change—persistence of a climatic signal through the orogenic stratigraphic record in northwestern Argentina. *Journal of South American Earth Sciences*, **14**, 763-774.

- STRECKER, M.R., CERVENY, P., BLOOM, A.L. & MALIZIA, D. (1989) Late Cenozoic tectonism and landscape development in the foreland of the Andes: Northern Sierras Pampeanas (26- 28°S), Argentina. *Tectonics*, **8**, 517-534.
- STRECKER, M.R., ALONSO, R.N., BOOKHAGEN, B., CARRAPA, B., HILLEY, G.E., SOBEL, E.R. & TRAUTH, M.H. (2007) Tectonics and climate of the southern central Andes. *Annual Review of Earth and Planetary Sciences*, **35**, 747-787.
- STRECKER, M.R., ALONSO, R., BOOKHAGEN, B., CARRAPA, B., COUTAND, I., HAIN, M.P., HILLEY, G.E., MORTIMER, E., SCHOENBOHM, L. & SOBEL, E.R. (2009) Does the topographic distribution of the central Andean Puna Plateau result from climatic or geodynamic processes? *Geology*, **37**, 643-646.
- STRECKER, M.R., HILLEY, G.E., BOOKHAGEN, B. & SOBEL, E.R. (2011) Structural, Geomorphic, and Depositional Characteristics of Contiguous and Broken Foreland Basins: Examples from the Eastern Flanks of the Central Andes in Bolivia and NW Argentina. In: *Tectonics of Sedimentary Basins* (Ed. by, 508-521. John Wiley & Sons, Ltd.
- STREIT, R.L., BURBANK, D.W., STRECKER, M.R., ALONSO, R.N., COTTLE, J.M. & KYLANDER-CLARK, A.R.C. (2015) Controls on intermontane basin filling, isolation, and incision on the margin of the Puna Plateau, NW Argentina (~23°S). *Basin Research*, n/a-n/a.
- TCHILINGUIRIAN, P. & PEREYRA, F.X. (2001) Geomorfología del sector Salinas Grandes-Quebrada de Humahuaca, provincia de Jujuy. *Revista de la Asociación Geológica Argentina*, **56**, 3-15.
- TURNER, J.C.M. (1960) Estratigrafía de la Sierra de Santa Victoria y adyacencias. *Boletín Academia Nacional de Ciencias*, **41**, 163-196.
- TURNER, J.C.M. & MÉNDEZ, V. (1979). *Puna*. Segundo simposio de geología regional argentina, Córdoba, Argentina, Academia Nacional de Ciencias Córdoba.
- TURNER, J.C.M. & MON, R. (1979). *Cordillera Oriental*. Segundo simposio de geología regional argentina, Córdoba, Argentina, Academia Nacional de Ciencias Córdoba.
- UBA, C.E., STRECKER, M.R. & SCHMITT, A.K. (2007) Increased sediment accumulation rates and climatic forcing in the central Andes during the late Miocene. *Geology*, **35**, 979-982.
- UBA, C.E., KLEY, J., STRECKER, M.R. & SCHMITT, A.K. (2009) Unsteady evolution of the Bolivian Subandean thrust belt: The role of enhanced erosion and clastic wedge progradation. *Earth and Planetary Science Letters*, **281**, 134-146.
- VERA, C., HIGGINS, W., AMADOR, J., AMBRIZZI, T., GARREAUD, R., GOCHIS, D., GUTZLER, D., LETTENMAIER, D., MARENGO, J., MECHOSO, C.R., NOGUES-PAEGLE, J., DIAS, P.L.S. & ZHANG, C. (2006) Toward a unified view of the American Monsoon Systems. *Journal of Climate*, **19**, 4977-5000.
- VERMEESCH, P. (2012) On the visualisation of detrital age distributions. *Chemical Geology*, **312**, 190-194.
- WALTHER, A., ORGEIRA, M., REGUERO, M., VERZI, D., VILAS, J., ALONSO, R.N., GALLADO, E., KELLY, S. & JORDAN, T.E. (1998) Estudio Paleomagnetico, Paleontologico y Radimetrico de la Formacion Uquia (Plio-Pleistoceno) en Esquina Blanca (Jujuy). *Actas del X Congreso Latinoamericano de Geologia y VI Congreso Nacional de Geologia Economica*, **1**, 77.

- WHITMAN, D., ISACKS, B.L. & KAY, S.M. (1996) Lithospheric structure and along-strike segmentation of the Central Andean Plateau: Seismic Q, magmatism, flexure, topography and tectonics. *Tectonophysics*, **259**, 29-40.
- WIEDENBECK, M., ALLE, P., CORFU, F., GRIFFIN, W.L., MEIER, M., OBERLI, F., VONQUADT, A., RODDICK, J.C. & SPEIGEL, W. (1995) Three natural zircon standards for U-Th-Pb, Lu-Hf, trace element and REE analysis. *Geostandards Newsletter*, **19**, 1-23.
- YILDIRIM, C., SCHILDGEN, T.F., ECHTLER, H., MELNICK, D. & STRECKER, M.R. (2011) Late Neogene and active orogenic uplift in the Central Pontides associated with the North Anatolian Fault: Implications for the northern margin of the Central Anatolian Plateau, Turkey. *Tectonics*, **30**, TC5005, doi:5010.1029/2010TC002756.
- ZACHOS, J., PAGANI, M., SLOAN, L., THOMAS, E. & BILLUPS, K. (2001) Trends, rhythms, and aberrations in global climate 65 Ma to present. *Science*, **292**, 686-693.
- ZAPPETTINI, E. (1989) Geología y metalogénesis de la región comprendida entre las localidades de Santa Ana y Cobres, provincias de Jujuy y Salta, República Argentina. Tesis doctoral Thesis, Universidad de Buenos Aires, Buenos Aires.

## TABLES & FIGURES

**Table 1.** Summary of zircon U-Pb geochronology of volcanic ashes.

| Sample      | Latitude  | Longitude | Description                        | N <sup>a</sup> | Age <sup>b</sup><br>[Ma] | 2 S.D. <sup>c</sup><br>[Myr] |
|-------------|-----------|-----------|------------------------------------|----------------|--------------------------|------------------------------|
| CG210311-01 | -23.23908 | -65.55495 | @ 50 m in center section           | 30             | 3.00                     | 0.02                         |
| CG210311-02 | -23.23965 | -65.55477 | @ 80 m in center section           | 77             | 2.13                     | 0.08                         |
| CG220311-01 | -23.29084 | -65.58504 | @ 18.5 m in SW section             | 88             | 2.14                     | 0.14                         |
| CG220311-02 | -23.29497 | -65.58681 | @ 62 m in SW section               | 30             | 0.80                     | 0.02                         |
| CG250307-01 | -23.22264 | -65.55517 | base of fill, 1 km S of N section  | 42             | 3.74                     | 0.04                         |
| CG270307-02 | -23.22243 | -65.55898 | 60 m above CG250307-01             | 40             | 2.95                     | 0.02                         |
| HU190412-01 | -23.41114 | -65.38380 | @ 200 m in Río Yacoraite section   | 30             | 2.54                     | 0.06                         |
| UQ280307-01 | -23.30585 | -65.36925 | above unconformity W of Uquía      | 32             | 4.12                     | 0.05                         |
| UQ160512-01 | -23.30218 | -65.36660 | above unconformity W of Uquía      | 32             | 3.97                     | 0.05                         |
| HU240307-01 | -23.43259 | -65.37079 | above unconformity W of Huacalera  | 32             | 4.24                     | 0.08                         |
| HU180411-03 | -23.43132 | -65.37006 | above unconformity W of Huacalera  | 30             | 4.38                     | 0.11                         |
| HU080410-01 | -23.41936 | -65.37400 | above unconformity W of Huacalera  | 32             | 3.86                     | 0.04                         |
| HU190311-01 | -23.41114 | -65.38380 | above unconformity W of Huacalera  | 30             | 3.80                     | 0.05                         |
| HU210307-03 | -23.43057 | -65.36928 | below unconformity W of Huacalera  | 30             | 5.05                     | 0.14                         |
| HU230412-01 | -23.41163 | -65.32528 | fill terrace on east of Río Grande | 32             | 0.87 <sup>d</sup>        | 0.03                         |
| HU230412-02 | -23.40508 | -65.33505 | fill terrace on east of Río Grande | 32             | 2.21                     | 0.08                         |

<sup>a</sup> Number of zircons analyzed.

<sup>b</sup> Weighted average of the five youngest ages, corrected for initial Th disequilibrium and common Pb.

<sup>c</sup> 2 \* standard deviation of the five youngest ages.

<sup>d</sup> Age reported for HU230412-01 only includes four youngest ages.

**Table 2.** Fisher mean of ChRM directions of normal and reversed specimens from the Río Yacoraite section and reversal test.

|  | Decl. | Incl. | k     | N  |
|--|-------|-------|-------|----|
| <b>Geographic</b>                      |       |       |       |    |
| Normal                                 | 345.3 | -33.8 | 16.03 | 27 |
| Reversed                               | 160.2 | 40.7  | 30.9  | 59 |
| <b>Tilt-corrected</b>                  |       |       |       |    |
| Normal                                 | 359.2 | -34.5 | 16.43 | 27 |
| Reversed                               | 18.4  | 38.7  | 32.4  | 59 |
| <b>Reversal test (tilt-corrected):</b> |       |       |       |    |
| Difference between means:              |       |       | 4.27° |    |
| Critical angle (95% confidence):       |       |       | 9.29° |    |



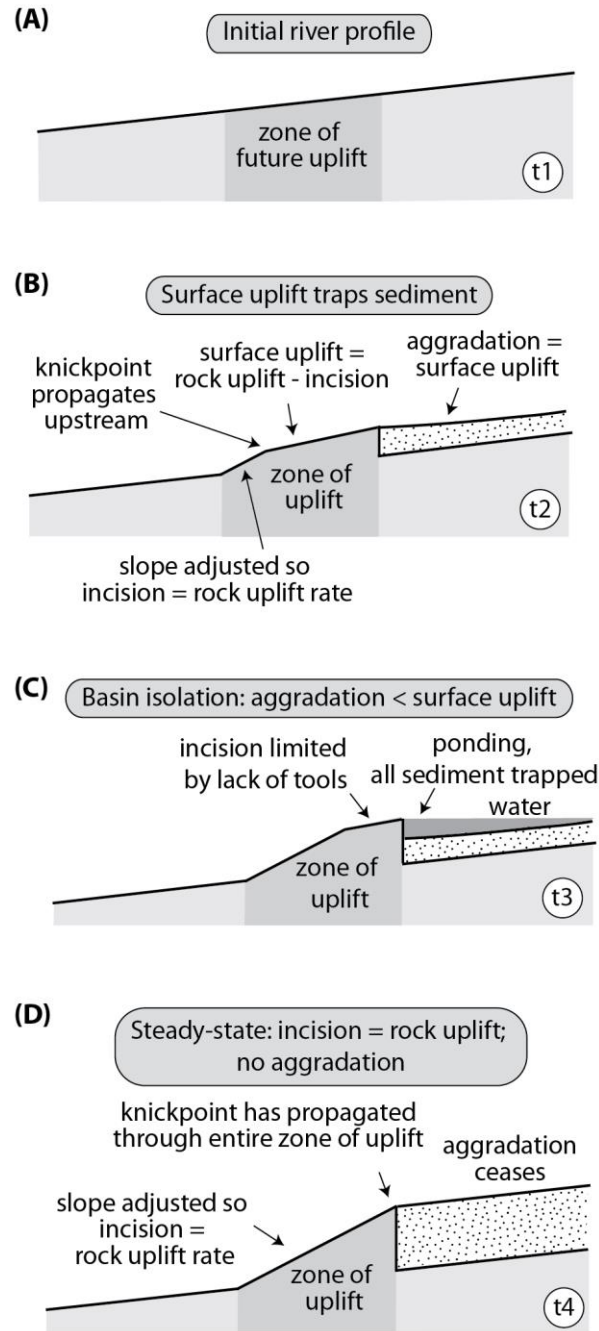


**Fig. 1.** Controls on sediment accumulation behind an uplifting barrier. (A) Initial channel profile, (B) Rock-uplift rate increases in zone of uplift (e.g. due to faulting). In the unadjusted portion of the channel, the river continues to incise at the initial rate, resulting in surface uplift of the channel. Upstream of the uplift, the river aggrades at a rate equal to the surface uplift at the upstream end of the zone of uplift. Uplift results in channel steepening and a knickpoint propagates upstream. Downstream of the knickpoint, the channel slope is adjusted to the new uplift rate. (C) If aggradation upstream of the zone of uplift is unable to keep pace with the rate of surface uplift, the channel is defeated, ponding occurs behind the uplift, and no sediment is transported out of the upstream basin. (D) Eventually, the knickpoint propagates all the way through the zone of uplift and the rate of rock uplift is once again balanced by the rate of incision along the entire profile. As a result, aggradation ceases in the upstream basin.

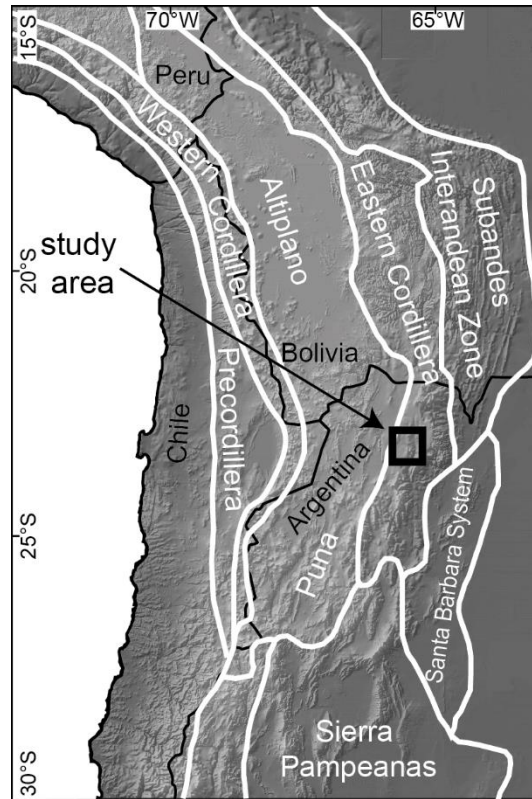


**Fig. 2.** Location of study area in relation of Andean morphotectonic provinces (Jordan *et al.*, 1983; Strecker *et al.*, 2007).



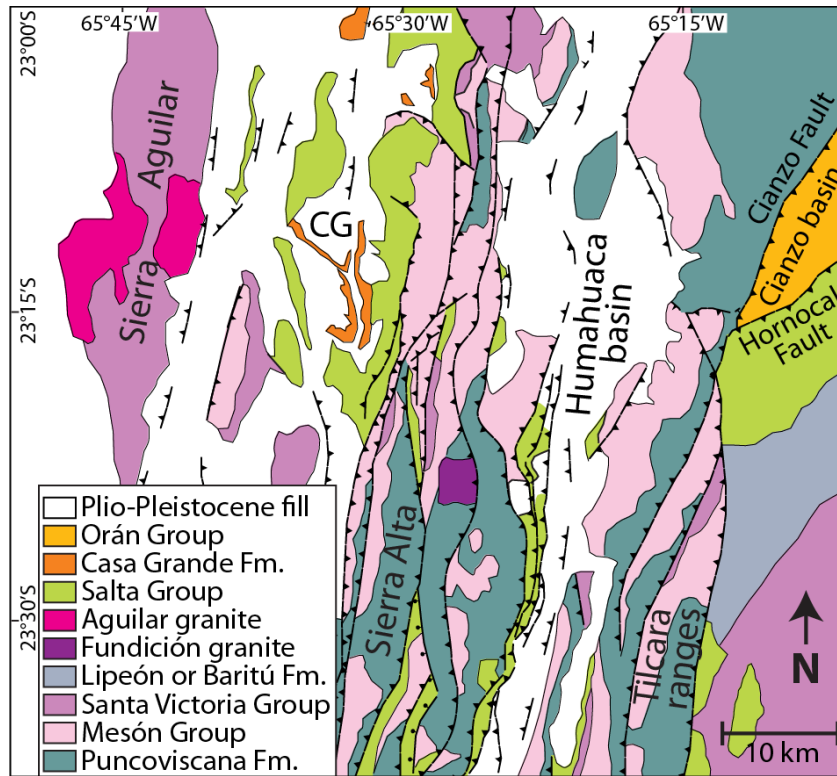


**Fig. 4.** Simplified geologic map after Gonzalez *et al.* (2004). CG = Casa Grande basin.

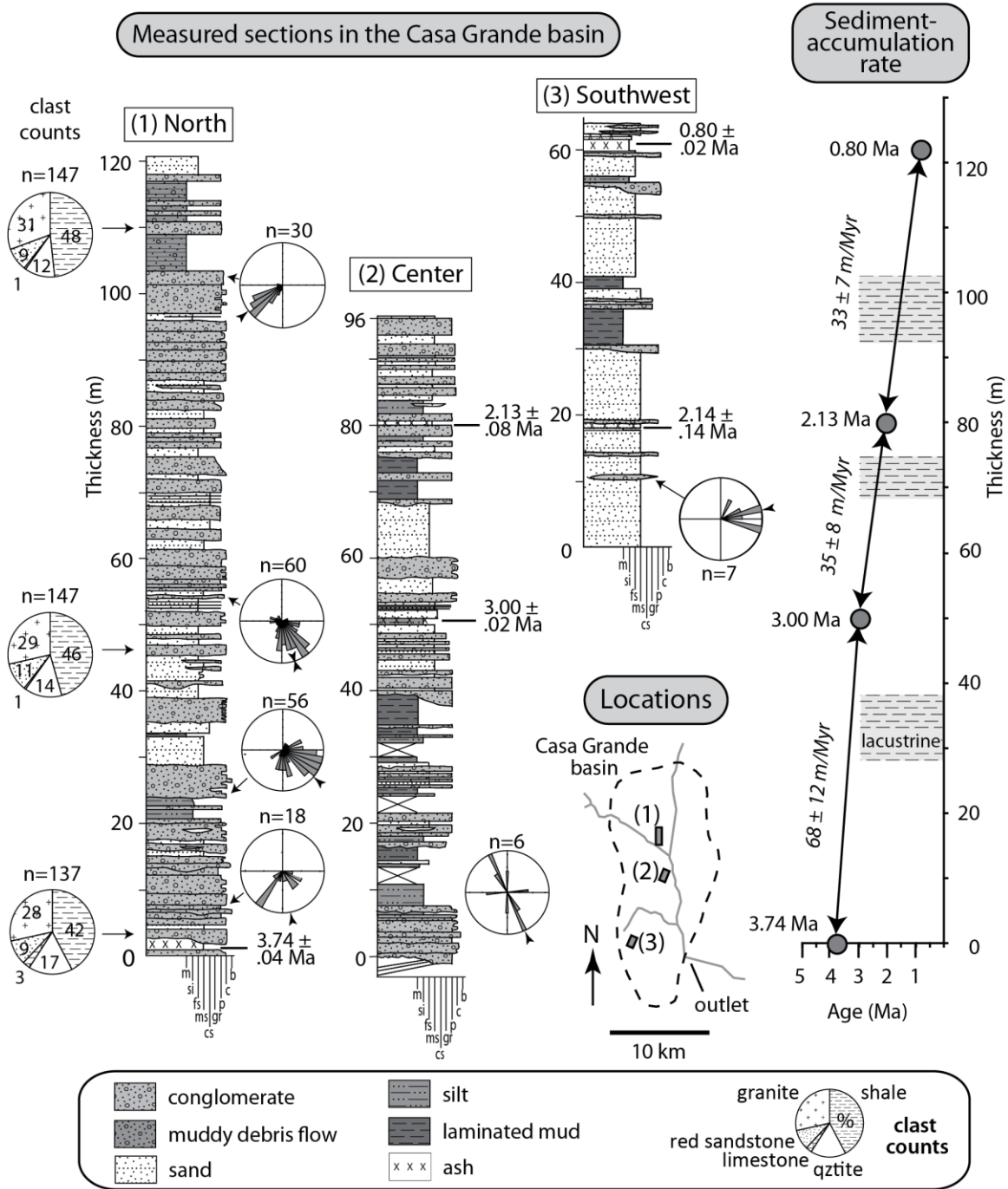


**Fig. 5.** Measured sections in the Casa Grande basin. Paleocurrents from imbrications (unidirectional) and channel margins (bidirectional). Ages from zircon U-Pb geochronology of ash layers. Grain size: m – mud, si – silt, fs – fine sand, ms – medium sand, cs – coarse sand, gr – granule, p – pebble, c – cobble, b – boulder. Average sediment-accumulation rate is given by the slope of the plot of height vs. age of ashes in measured sections. Sediment-accumulation rate decreases around 3 Ma. Light gray bars indicate intervals of lacustrine deposition within the otherwise fluvial strata.



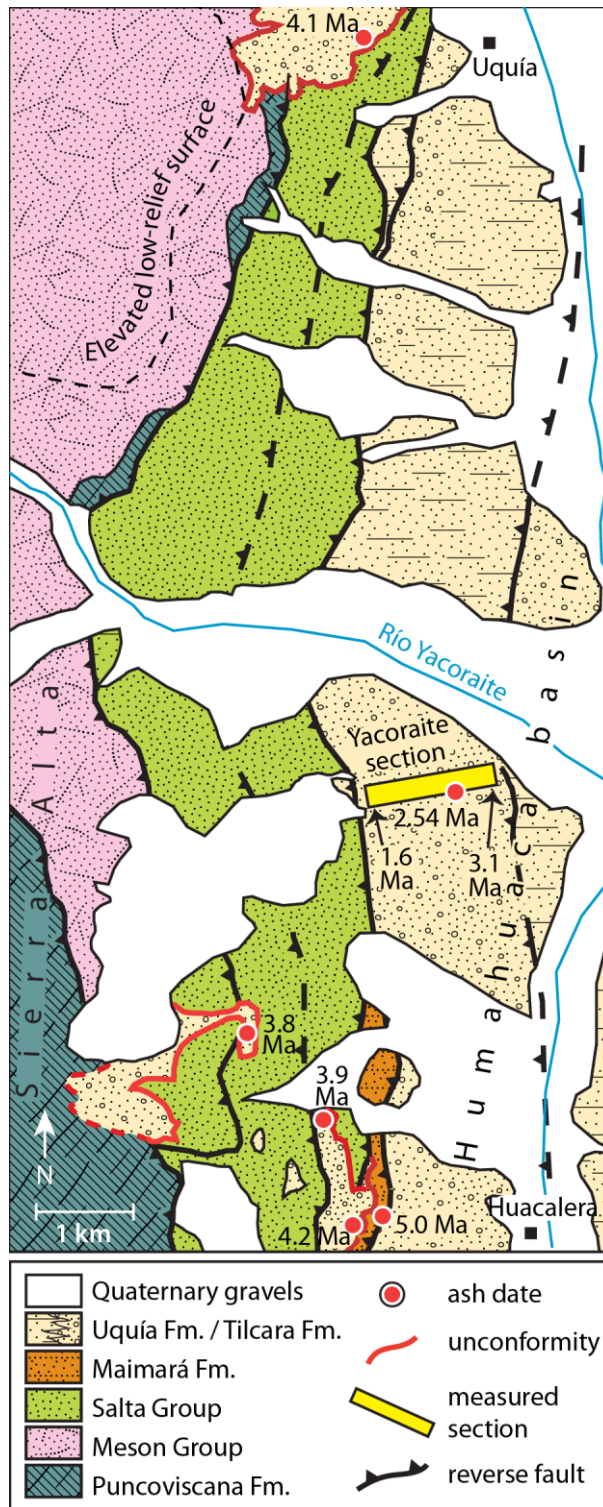


**Fig. 6.** The widespread unconformity in the Humahuaca basin is similar in age (4.2-3.8 Ma) to the unconformity at the base of the fill in the Casa Grande basin (3.74 Ma). Cross-cutting relationships indicate faults on the west side of the Humahuaca basin were active from >4.3 Ma to <1.7 Ma. See Fig. 3 for location.

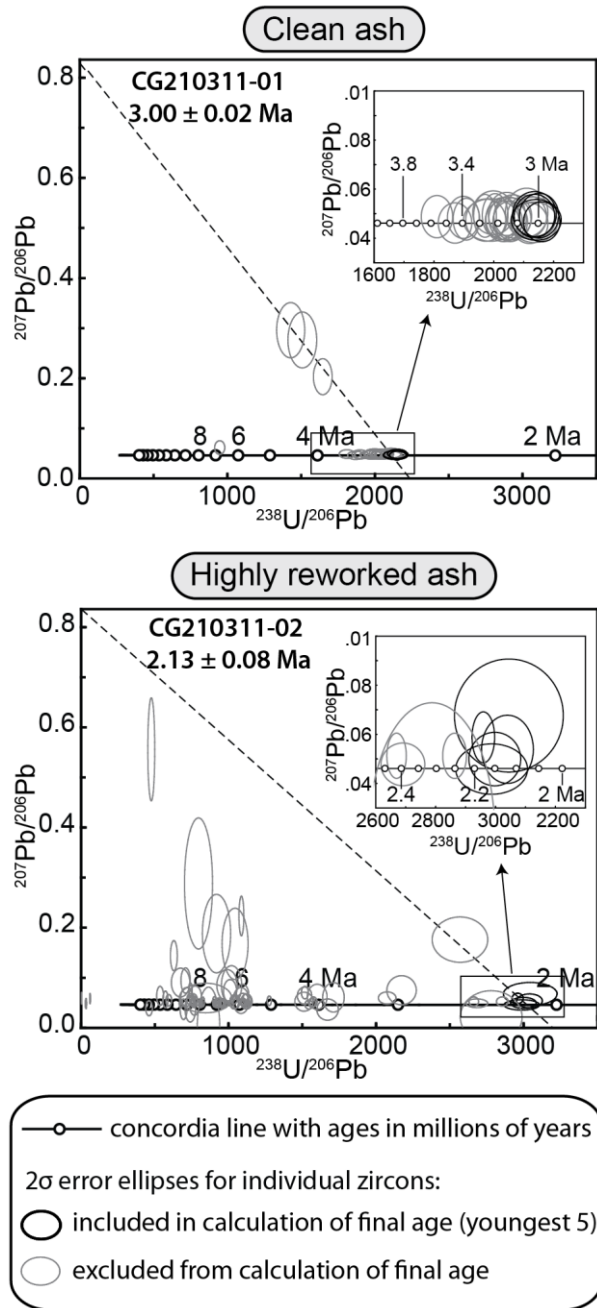


**Fig. 7.** Examples of ash data from the Casa Grande basin: a relatively pristine ash (CG210311-01, from 50 m in center section) and a highly reworked ash (CG210311-02, 80 m in center section). Plotted  $^{207}\text{Pb}/^{206}\text{Pb}$  and  $^{238}\text{U}/^{206}\text{Pb}$  ratios have been corrected for initial Th-disequilibrium using a magma Th/U ratio of  $2.5 \pm 1.5$ , and then corrected for common-Pb using an assumed a common-lead  $^{207}\text{Pb}/^{206}\text{Pb}$  ratio of 0.836. Ellipses show  $2\sigma$  error. The final age reported for each sample is the weighted average of the five youngest ages (black ellipses), and the uncertainty reported is two times the standard deviation of those five ages. Gray data points are excluded from the final age calculation.

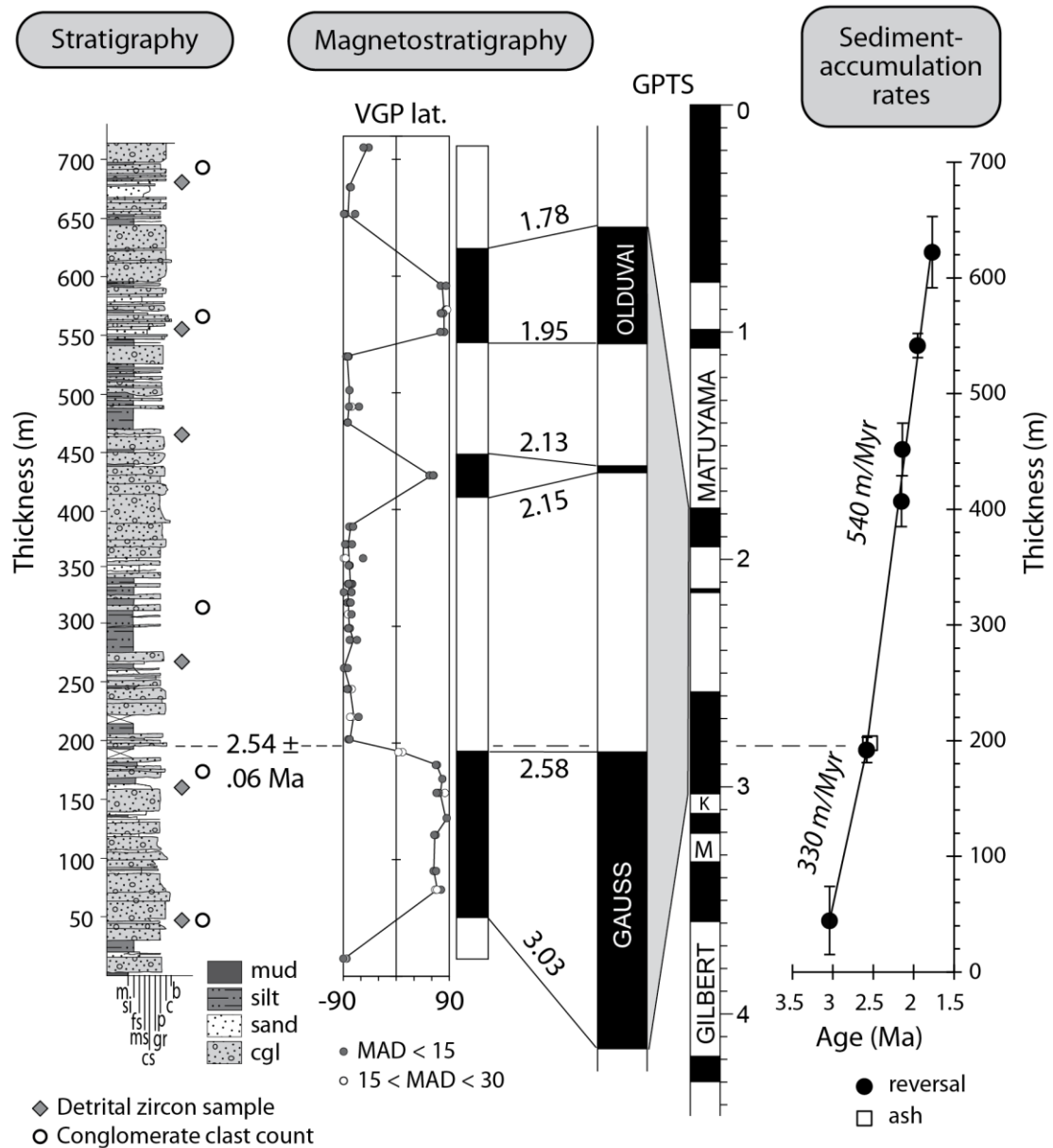


**Fig. 8.** Measured section at the mouth of the Río Yacoraité in the Humahuaca basin, including locations of detrital zircon samples and pebble clast counts. The 2.54-Ma age is from zircon U-Pb geochronology of an ash layer at 200 m in the section. Grain size: as in Fig. 4. Correlation of the magnetic polarity stratigraphy to the Geomagnetic Polarity Time Scale (GPTS) (Lourens *et al.*, 2004): Stratigraphic log of virtual geomagnetic pole (VGP) latitudes for each specimen with mean angular deviation (MAD) < 30°; gray circles are specimens with MAD < 15° and white circles are specimens with 15° < MAD < 30°. Normal and reversed magnetozones indicated by black and white bands respectively next to log of VGP latitude. Undecompressed sediment-accumulation rates are given by the slope of plot of height vs. age of reversals and the dated ash. Error bars indicate the uncertainty in the location of reversal between normal and reversed samples.



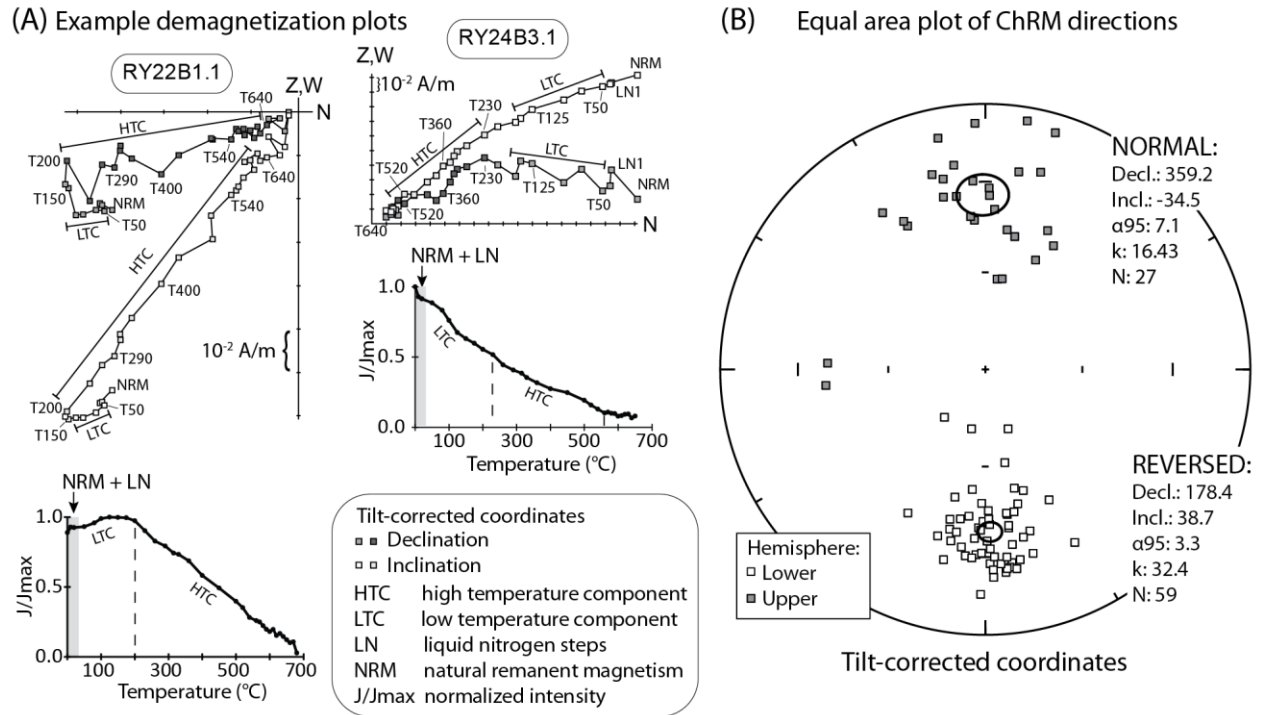


**Fig. 9.** (A) Representative orthogonal demagnetization plots for specimens from the Río Yacoraité section (upper) and decay of magnetization for same specimens (lower). In orthogonal plots, darker shading indicates points used to calculate characteristic remanent magnetization (ChRM). (B) Equal-area plot of tilt-corrected ChRM directions for each specimen. Circles indicate  $\alpha_{95}$  around the Fisher mean.

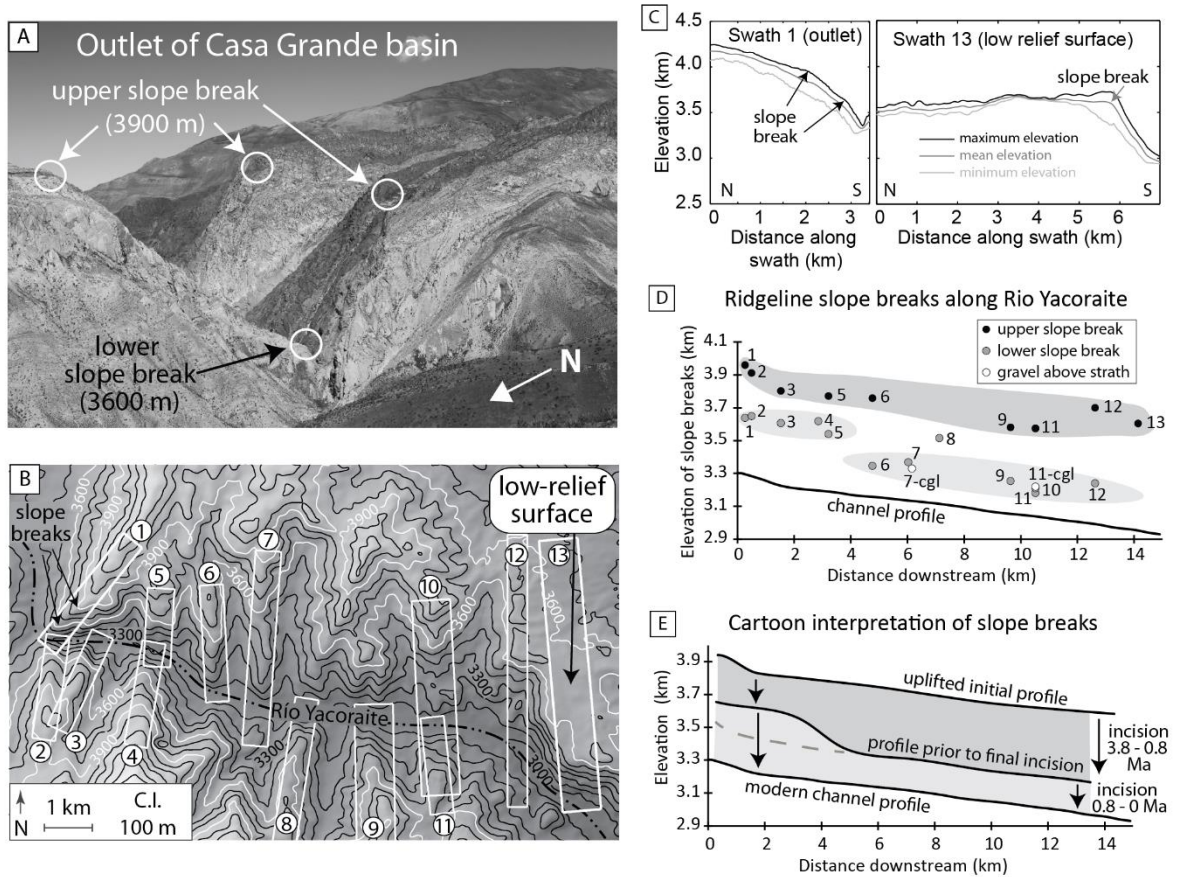


**Fig. 10.** Topographic indicators of surface uplift of the Sierra Alta relative to the level of the Río Yacoraite. (A) Field photo of the narrow gorge at the outlet of the Casa Grande basin, showing upper and lower breaks in slope on ridgelines striking perpendicular to the Río Yacoraite. Lower slope break is at about the same elevation as the top of the intermontane basin fill and is interpreted to have formed during the final incision after 0.8 Ma. Upper slope break is at an elevation 600 m above the modern river channel. (B) Topographic map of the Sierra Alta adjacent to the Río Yacoraite. White contours highlight elevations of the slope breaks at the outlet of the Casa Grande basin (3600 and 3900 m contours) and the low-relief surface on the eastern side of the Sierra Alta north of the Río Yacoraite (3600 m contour). Numbered rectangles enclose swath profiles. (C) Elevation profiles at the outlet of the Casa Grande basin and across the low-relief surface. Both the low-relief surface and the upper slope break lie ~600 m above the modern river channel and are interpreted to be related to the onset of uplift of the Sierra Alta at ~4.3 Ma. Consistent relief (600 m) suggests quite uniform rock uplift across the range. (D) Elevation of slope breaks on ridge crests along the Río Yacoraite and bases of gravels above small straths (7-cgl and 11-cgl). (E) Interpretation of slope breaks in relation to fluvial incision.

## Modern detrital zircon ages

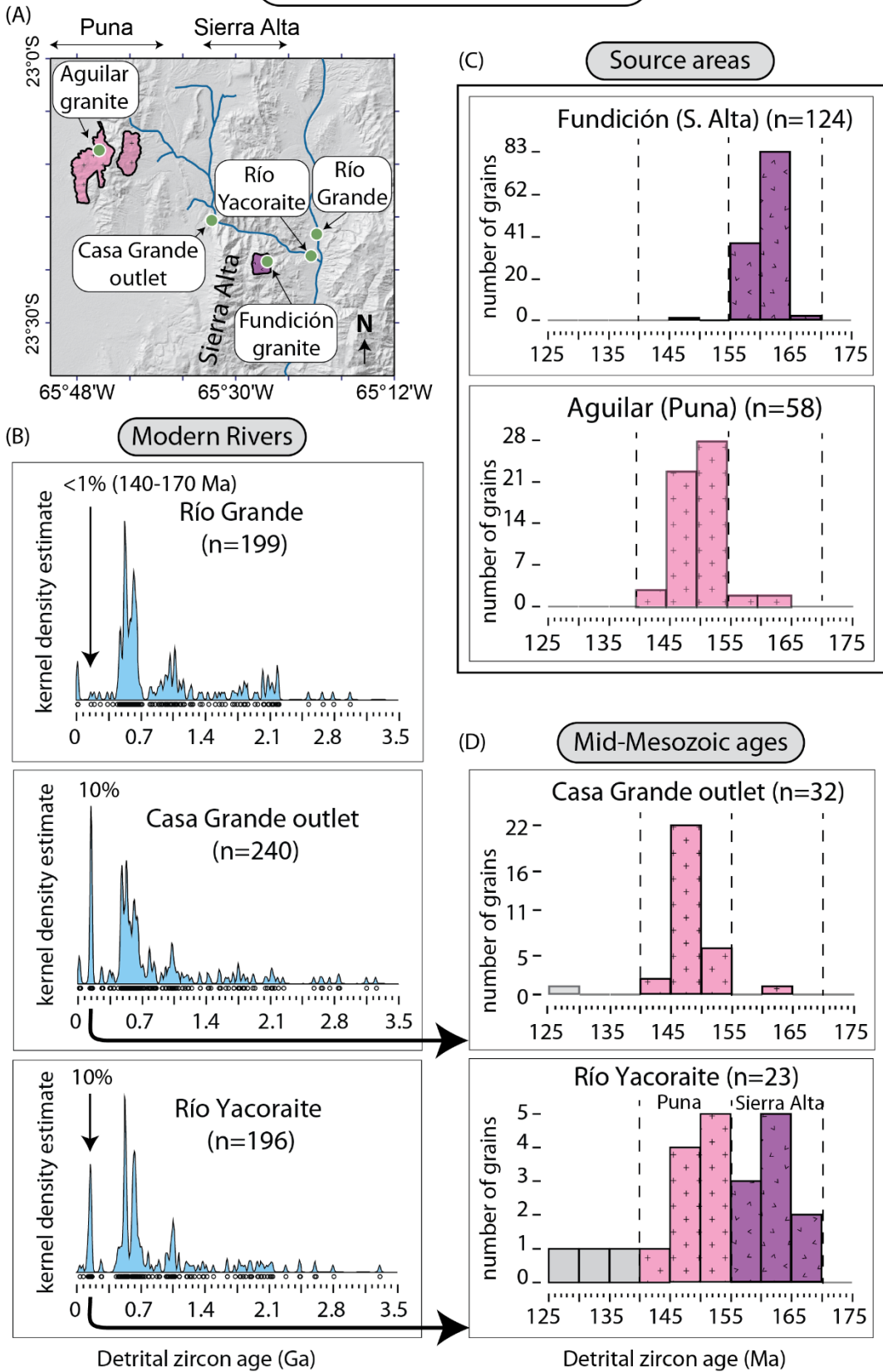


**Fig. 11.** Detrital zircon data from modern rivers used to characterize the signature of source areas on the border of the Puna Plateau (Aguilar granite) and Sierra Alta (Fundición granite). (A) Location of detrital zircon samples. (B) Kernel Density Estimation (KDE) plots (Vermeesch, 2012) of detrital zircon ages from: the Río Grande 6 km upstream of the Río Yacoraite; the outlet of the Casa Grande basin; and the Río Yacoraite 1.5 km upstream of the confluence with the Río Grande.  $n$  is the number of grains with concordant ages  $>12$  Ma. The samples from the Casa Grande basin and the Río Yacoraite have an age peak at  $\sim 150$  Ma from the Aguilar and Fundición granites that accounts for  $\sim 10\%$  of the  $>12$  Ma zircons in these samples. The Río Grande sample lacks this peak. (C) Histogram of detrital zircon ages from small catchments within the Aguilar granite or Fundición granite. Zircons from the Aguilar granite have ages between 140-155 Ma, whereas zircons from the Fundición granite have ages between 155-170 Ma. (D) Histograms of ages making up the  $\sim 150$ -Ma peak in the Casa Grande basin outlet and Río Yacoraite detrital zircon samples. As expected, zircons from the Casa Grande basin include the age of the Aguilar granite (Puna) but not the Fundición granite (Sierra Alta), and zircons from the Río Yacoraite include ages from both granites.

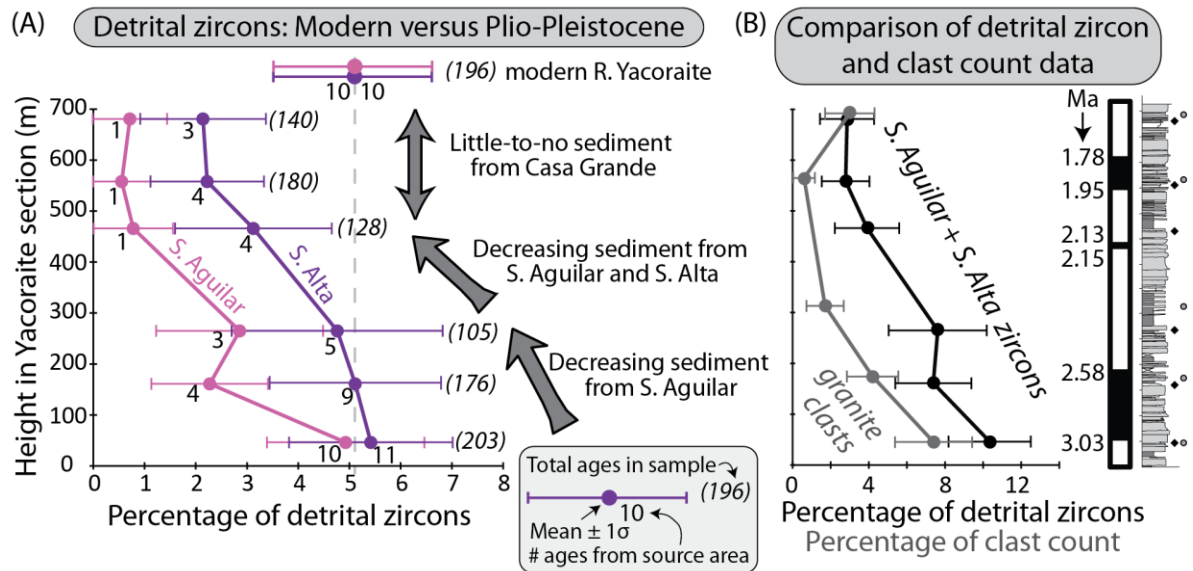


**Fig. 12.** (A) Detrital zircon provenance of sediment in the Río Yacoraite section. Pink data points indicate the percentage of grains in that sample with Aguilar granite (Sierra Aguilar) ages (140-155 Ma); purple data points indicate the percentage of grains with Fundición granite (Sierra Alta) ages (155-170 Ma). The number next to each data point is the number of zircons from that source area and the number in parentheses is the number of zircons analyzed with age  $> 12$  Ma for that sample. Above the plot, the percentages for the modern Río Yacoraite are shown for reference. (B) The percentage of granite clasts in pebble counts from the Río Yacoraite section shows the same trend as the detrital zircon data: decreasing sediment from the Sierra Aguilar and Sierra Alta relative to other sources.

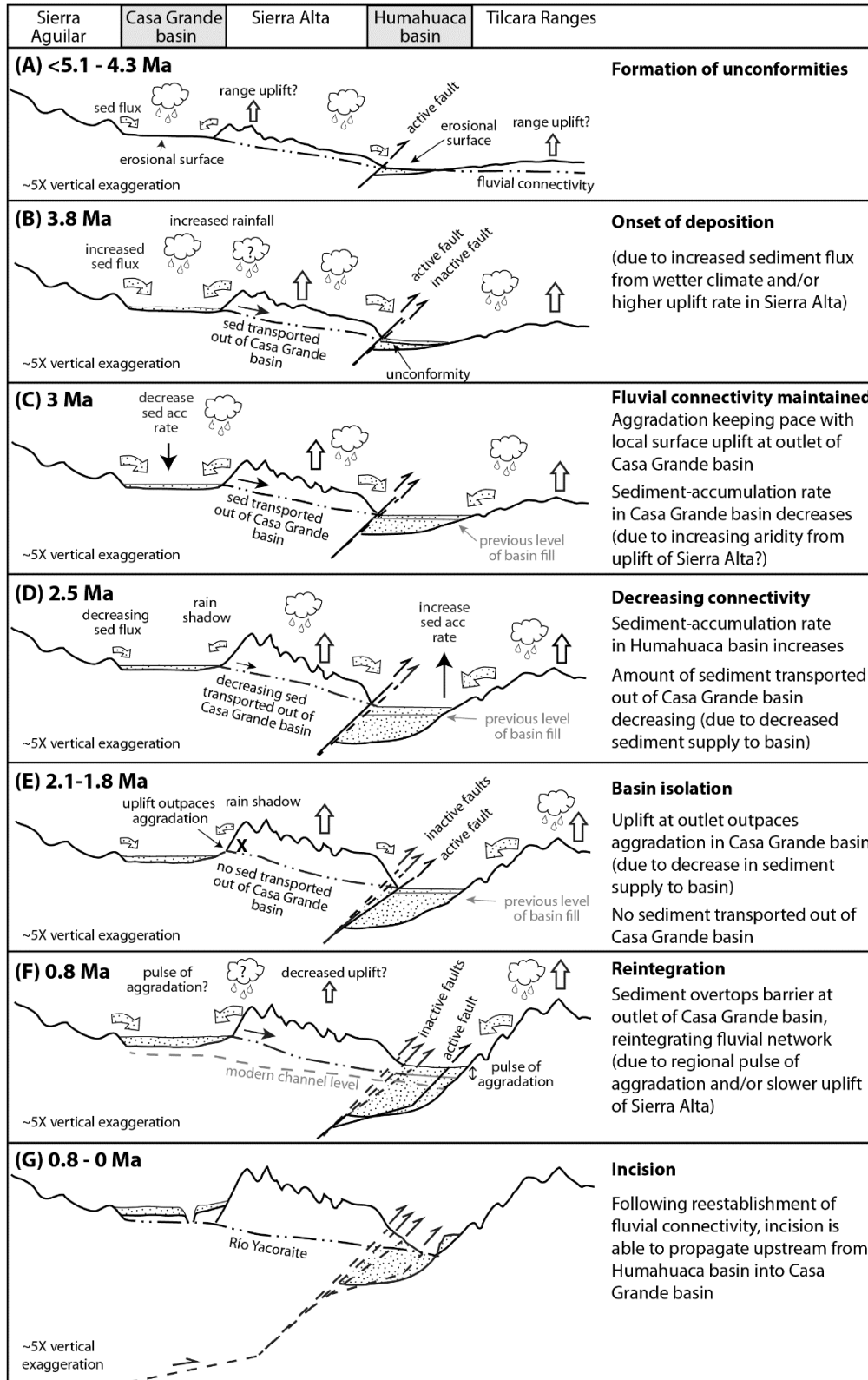


**Fig. 13.** Cartoon summary of Plio-Pleistocene history of the Casa Grande basin, highlighting timing and causes of events, such as the onset of deposition, changes in sediment-accumulation rates, basin isolation, reintegration of the fluvial network and final incision.

## **Appendices**

**Table A1.** Effect of basin geometry on sediment-accumulation rate, under constant sediment flux.

### **Supplemental files (available online)**

**Table S1.** U-Pb geochronology data. (Excel file)

**Table S2.** Magnetostratigraphy data.

**Table S3.** Detrital zircon LA-ICPMS U-Pb data. (Excel file)

## **CHAPTER 2**

### **Neogene – Quaternary stratigraphy of the northern Humahuaca basin**

#### **ABSTRACT**

The Humahuaca basin is an intermontane basin in the Eastern Cordillera of NW Argentina (23-24°S) that formed in response to a late phase of Andean mountain building during the last 5 Myr. The Humahuaca basin records the transition from a foreland basin setting to intermontane basin conditions, the integration of individual subbasins into a single basin through defeat of rivers crossing the bounding ranges to the east, and multiple cycles of filling and incision. Zircon U-Pb geochronology of ashes intercalated with the Neogene-Quaternary basin fill, including new dates from 35 sites in the northern Humahuaca basin, provides excellent time control, which allows detailed reconstruction of the spatiotemporal evolution of the northern Humahuaca subbasin, as well as comparison with the southern subbasin and other basins in the region. The integration of multiple datasets, including stratigraphic analyses, sediment-accumulation rates, paleocurrent data, and provenance data, from locations distributed throughout the northern Humahuaca basin, provides insight into the processes controlling lateral and vertical facies variations and sediment storage in intermontane basins. The synchronous onset of intermontane conditions in both the northern and southern subbasins ~4.4-4.2 Ma, which resulted in deflection of formerly eastward flow to the north in the northern subbasin and to the south in the southern subbasin, is attributed to uplift of the Tilcara Range that bounds the basin to the east. The onset of intermontane basin conditions was also coincident with the onset of deformation on the western side of the Humahuaca basin and with uplift of ranges in the Eastern Cordillera along strike ~250 km to

the south and ~100 km to the north, suggesting that this tectonism was regionally significant. In the northern subbasin, the period 2.5-2 Ma is characterized by higher sediment-accumulation rates, deposition of finer-grained sediments, and the first appearance of southward paleoflow, which we interpret to reflect ponding of the fluvial system due to channel defeat at the outlet of the northern subbasin and subsequent integration of the northern and southern subbasins. Increasing aridity in the lee of the growing ranges to the east likely reduced the stream power, and hence the river's ability to incise through the uplifting range at the outlet of the northern subbasin. Increased aridity has also been invoked as contributing to channel defeat at the outlet of the Casa Grande basin to the west and in the Santa Victoria Range to the north around the same time. Following the integration of the northern and southern subbasins, the Humahuaca basin experienced an episode of incision that created a prominent unconformity between 1.6 Ma and 0.9 Ma.

## **INTRODUCTION**

Sedimentary deposits preserved within intermontane basins record deformation, range uplift, and climatic changes during orogenic growth. In contractional orogens, as deformation propagates into the foreland, the fluvial system is episodically disrupted. Rivers that are unable to maintain their course across a growing range are deflected along it until they join or are captured by another river crossing the range. In the Eastern Cordillera of NW Argentina, such deflections commonly resulted in elongate intermontane basins with outlets to the foreland through narrow bedrock gorges. The balance of incision, uplift, and aggradation at a basin's outlet determines whether the basin maintains connectivity with the foreland or becomes isolated, which in turn can affect sediment-accumulation rates and the depositional environments occurring in the basin (Burbank *et al.*, 1996; Humphrey & Konrad, 2000;



Sobel *et al.*, 2003). This balance depends not only on local conditions at the outlet, e.g., uplift rates and bedrock erodibility, but also on upstream changes in the catchment, such as changes in climate, catchment size, or sediment supply. The sedimentary record within the basin also reflects local variations in intrabasinal deformation, sediment sources, and processes, such as stream capture, landslide damming, and alluvial fan growth.

The southern Humahuaca basin of NW Argentina records the establishment of intermontane basin conditions ~4.2 Ma (Pingel *et al.*, 2013). Pingel *et al.* (2013) suggested that lithological differences between Plio-Pleistocene deposits in the northern and southern parts of the basin represent concurrent deposition in two subbasins. This study focuses on the stratigraphy of the northern subbasin to understand what controlled segmentation and integration of these subbasins, the paleoenvironmental significance of lateral and vertical changes in sedimentary facies, and what the similarities and differences between the two subbasins can reveal about patterns of range growth and controls on basin isolation. Comparison of the timing of events in the northern Humahuaca basin with other studies from the Eastern Cordillera, Subandes, and Santa Barbara ranges allows these events to be assessed in the context of broader-scale tectonic or climatic changes.

The detailed time control provided by U-Pb dating of ash layers interbedded with the Neogene-Quaternary basin fill allows us to integrate multiple datasets from locations throughout the northern Humahuaca basin to create a more nuanced interpretation of the spatiotemporal evolution of the basin. We find that intermontane basin conditions were established at the same time (~4.4-4.2 Ma) in both subbasins, with paleoflow deflected to the north in the northern subbasin and to the south in the southern subbasin. Temporally-constrained changes in sedimentary facies, grain size, and sediment-accumulation rates

throughout the northern subbasin at ~2.5 Ma are interpreted as an episode of ponding in response to channel defeat at the basin's outlet where a bedrock river had traversed the uplifting range to the east. Ponding lasted until ~2.1 Ma, and the appearance of southward paleocurrents in the northern Humahuaca basin around that time suggest that aggradation resulted in overtopping of the drainage divide between the northern and southern subbasins and integration of the northern subbasin into the southern subbasin.

## **GEOLOGIC BACKGROUND**

The Humahuaca basin is an elongate intermontane basin located within the Eastern Cordillera of northwestern Argentina between 23°S and 24°S latitude (Figure 1). The northern part of the basin lies at 2500-3200 m elevation and is bounded by ranges exceeding 5000 m elevation. The Humahuaca basin is separated from the arid, internally-drained Puna Plateau to the west by the Sierra Alta, except in its northern region where the Río Yacoraite drains the Casa Grande basin (Fig. 1B) eastward into the Humahuaca basin. To the east, the Tilcara ranges and Sierra Hornocal separate the Humahuaca basin from the humid foreland. The Río Grande flows southward along the axis of the valley and exits into the foreland through a narrow bedrock gorge ~90 km south of the town of Humahuaca. The foreland east of the Humahuaca basin (Fig. 1A) includes the southernmost extension the thin-skinned Subandes fold-and-thrust belt, the northernmost extension of the Santa Barbara System of high-angle reverse faults (Jordan *et al.*, 1983), and a gap in significant foreland deformation between 23-23.5°S (Kley & Monaldi, 2002).

The Upper Miocene – Pleistocene deposits in the Humahuaca basin are influenced by a late phase of deformation within the Eastern Cordillera. Regionally, shortening within the Eastern Cordillera began ~40 Ma (Horton, 2005; Hongn *et al.*, 2007; Bosio *et al.*, 2009;

Carrapa & DeCelles, 2015). In southern Bolivia, deformation in the Eastern Cordillera ceased by ~10 Ma (Gubbels *et al.*, 1993) and shifted to the Subandean fold-and-thrust belt around 12-9 Ma (Echavarría *et al.*, 2003; Uba *et al.*, 2009). In northwestern Argentina (25-26°S), deformation migrated through the Eastern Cordillera between 40 Ma and 4 Ma (Carrapa *et al.*, 2011; Carrapa & DeCelles, 2015). Hain *et al.* (2011) highlight three main phases of deformation at ~13-10 Ma, ~5 Ma and <2 Ma. Deformation in the western Santa Barbara System began ~10 Ma and was coeval with uplift of the western ranges of the Eastern Cordillera (Coutand *et al.*, 2006; Deeken *et al.*, 2006; Carrapa *et al.*, 2011; Hain *et al.*, 2011; Pearson *et al.*, 2013). Uplift of the central Eastern Cordillera and greatest exhumation in the eastern ranges of the Eastern Cordillera occurred at or since ~5 Ma, and deformation of the eastern Santa Barbara System is younger than 5 Ma (Kley & Monaldi, 2002; Hain *et al.*, 2011; Pearson *et al.*, 2013). Since ~2 Ma, diachronous deformation was partitioned across the entire broken foreland (Hain *et al.*, 2011). As Carrapa *et al.* (2011) point out, the timing of deformation in the Subandes of Bolivia appears similar to that in Eastern Cordillera of northwestern Argentina.

The timing of deformation in the Humahuaca basin and bounding ranges broadly matches the overall timing of deformation in the Argentinian Eastern Cordillera. Middle Miocene exhumation and surface uplift of the Sierra Alta is recorded by ~14-Ma apatite fission-track cooling ages (Deeken *et al.*, 2005) and by the loss of western sources of detrital zircons by ~12 Ma in the Cianzo basin (Fig. 1B), which is located in Sierra Hornocal east of Humahuaca (Siks & Horton, 2011). Growth strata indicate that the Hornocal Fault, a SE-dipping reverse fault (inverted normal fault) bounding the Cianzo basin to the south and east, was active in the Late Miocene (~9 Ma) (Siks & Horton, 2011), but uplift of the Tilcara

ranges did not disrupt eastward fluvial transport until ~4.2 Ma in the southern Humahuaca basin (Pingel *et al.*, 2013). Faulting within the Humahuaca basin was active from at least 4 Ma to <90 ka (Rodríguez Fernández *et al.*, 1999; Sancho *et al.*, 2008; Pingel *et al.*, 2013; Streit *et al.*, 2015).

The Sierra Alta and Tilcara ranges expose Proterozoic to Paleogene rocks (Figure 2), including the Neoproterozoic-Lower Cambrian slates of the Puncoviscana Formation, the Cambrian quartzites of the Mesón Group, the marine sandstones and shales of the Ordovician Santa Victoria Group, and the Cretaceous-Paleogene rift-related deposits of Salta Group (Turner, 1960; Turner & Mon, 1979; Marquillas *et al.*, 2005). The Salta Group includes the Cretaceous rift-related sandstones of the Pirgua Subgroup, the Upper Cretaceous – Paleocene post-rift marine carbonates of the Balbuena Subgroup, and the fluvial and lacustrine mudstones, siltstones, and sandstones of the upper Paleocene to middle Eocene Santa Bárbara Subgroup (Moreno, 1970; Marquillas *et al.*, 2005). Additionally, the Sierra Alta contain the Fundición granite, a small Jurassic pluton (Insel *et al.*, 2012). Upper Eocene – Upper Miocene foreland and intermontane basin deposits are preserved in the Cianza basin in the Sierra Hornocal (Siks & Horton, 2011).

The Neogene to Quaternary sedimentary deposits within the Humahuaca basin comprise four main units: the Maimará Fm (Salfity *et al.*, 1984; Pingel *et al.*, 2013), the Uquía Fm (Castellanos, 1950; Marshall *et al.*, 1982; Walther *et al.*, 1998; Reguero *et al.*, 2007), the Tilcara Fm (Pingel *et al.*, 2013), and younger Quaternary conglomerates (Tchilinguirian & Pereyra, 2001; Robinson *et al.*, 2005; Sancho *et al.*, 2008; Pingel *et al.*, 2013). Previous studies indicate that the Maimará Fm comprises at least 250 m of sandstones and interbedded conglomerates that were deposited between >6 Ma and 4.2 Ma (Pingel *et al.*,

2013). Both paleocurrent data and the presence of ignimbrite clasts sourced from the Puna Plateau indicate that eastward flow of the fluvial system from the Puna into the foreland had not yet been interrupted by range uplift (Pingel *et al.*, 2013). Pingel *et al.* (2013) defined the Tilcara Fm in the southern Humahuaca basin as a separate unit from the Uquía Fm in the northern part of the basin on the basis of lithological differences between the Plio-Pleistocene deposits in these two subbasins. The Uquía Fm consists of ~250 m of fossil-bearing, light-colored sandstones, siltstones, mudstones, and uncommon conglomerates deposited between ~3 Ma and <2 Ma (Reguero *et al.*, 2007), whereas the Tilcara Fm consists of >250 m of conglomerates, fanglomerates, and some sandstones deposited between 4.2 Ma and <2.5 Ma (Pingel *et al.*, 2013). In the southern Humahuaca basin, the transition from the Maimará Fm to the Tilcara Fm at ~4.2 Ma is marked by an abrupt change in clast compositions and paleocurrent directions, as formerly eastward-flowing rivers were deflected southward by the uplift of the Tilcara ranges (Pingel *et al.*, 2013). The shift from a more humid climate to the present semi-arid to arid conditions of the Humahuaca basin is inferred to have occurred between ~3-2.5 Ma and is attributed to the Tilcara ranges attaining sufficient elevation to significantly decrease moisture transport from the east (Reguero *et al.*, 2007; Pingel *et al.*, 2014; Streit *et al.*, 2015). The top of the Tilcara Fm is truncated by an angular unconformity with overlying Quaternary conglomerates as old as ~1 Ma (Pingel *et al.*, 2013; Streit *et al.*, 2015). Basin filling and subsequent incision is recorded by fluvial fill terraces that range in age from ~800 ka to 40 ka (Tchilinguirian & Pereyra, 2001; Robinson *et al.*, 2005; Strecker *et al.*, 2007; Sancho *et al.*, 2008; Pingel *et al.*, 2013). In the sections below, we refine the delineation between the northern and southern Humahuaca subbasins and the chronology of

Plio-Pleistocene deposition in the northern subbasin, including both the interfingering the Uquía Fm with the Tilcara Fm and connectivity with the foreland to the east.

## **METHODS**

Detailed geologic field mapping in the Humahuaca basin (Figure 2) documents stratigraphic and structural relationships between Neogene-Quaternary strata, unconformities, faults, and folds. Detailed stratigraphic sections (Figure 3) were described in the Tilcara Fm and Uquía Fm at six locations between the Angosto de Perchel and Humahuaca in order to characterize the depositional environments, lateral and vertical facies variations, and paleoflow directions recorded by these deposits. In this analysis, we also include the measured section at the Río Yacoraite described in Chapter 1 (Streit et al., 2015). Paleocurrent directions were determined from the orientation of imbricated clasts, channel margins, and/or cross-bedding. In most cases, we measured the orientation of individual clasts and applied a correction for the structural dip of the bedding. To characterize spatial and temporal variations in sediment sources, conglomerate compositions were determined by counting at least 100 clasts >1 cm in size within a 1-m<sup>2</sup> area.

U-Pb dating of zircons from numerous volcanic ashes interbedded with the Neogene-Quaternary basin fill allows robust correlation between measured sections and observations from different parts of the basin, calculation of sediment-accumulation rates, and comparison of the timing of events in the Humahuaca with regional histories of deformation and intermontane basin development. Zircons were dated with laser-ablation multi-collector, inductively coupled mass spectrometry (LA-MC-ICPMS) at the University of California Santa Barbara. Measured U-Pb ratios were corrected for initial <sup>230</sup>Th disequilibrium and common lead. To minimize the effects of protracted crystal residence time in the magma

chamber or of fluvial reworking of older ashes, we use the weighted mean of a subset of the youngest ages (typically the five youngest zircons in a sample) to best approximate the depositional age. We conservatively report the uncertainty on the age as twice the standard deviation of the youngest five zircons. The details of this method are described in Chapter 1 of this dissertation (Streit *et al.*, 2015).

The Río Yacoraite section was dated using magnetostratigraphy, as described in Chapter 1 (Streit *et al.*, 2015). Oriented block samples of siltstone, mudstone, or fine sandstone were collected from 35 sites at intervals of 10-20 m where possible (Figure 3). Measurements were performed on 2-4 specimens from each site using a DC SQUID magnetometer in the Caltech paleomagnetism lab (Kirschvink *et al.*, 2008). Each sample was subjected to stepwise thermal demagnetization and the direction of its characteristic remanent magnetization and its virtual geomagnetic pole was calculated (VGP). The VGP latitudes define three normal and four reversed magnetic polarity zones through the Río Yacoraite section that we then correlated to the Geomagnetic Polarity Timescale (GPTS) (Lourens *et al.*, 2004) with the aid of one dated ash.

Sediment-accumulation rates were calculated by dividing the thickness of strata between two ashes or magnetozone boundaries by the age difference between the ashes or those magnetic reversals. Maximum (minimum) sediment-accumulation rates were calculated either by adding (subtracting) 10% to the thickness and subtracting (adding) the 2SD uncertainty of each ash to the age difference or by accounting for the uncertainty in the precise location of the reversal boundary between two sites of opposite magnetic polarity.

## **RESULTS**

## Geochronology

We report new U-Pb zircon ages for ashes from 35 locations in the Humahuaca basin (Table 1). We also refer to previously published U-Pb data for 9 additional ashes (Table 2) and the magnetostratigraphy of the Río Yacoraite section (Streit *et al.*, 2015). The ages of the newly dated ashes range from 6.3 Ma to 1.3 Ma and the average uncertainty (2SD) is 0.09 Myr. Our choice to use twice the standard deviation of the youngest 5 ages, rather than twice the standard error on the mean of those 5 ages, increased the average reported uncertainty by 0.04 Ma. An alternative method of calculating the age of each ash would to use the weighted mean of the youngest zircons forming a single population (which would typically include 10 zircons). That method would have resulted in ages that are older by 0.04 Ma on average.

## Stratigraphy of the northern Humahuaca basin

### *Maimará Formation*

In the northern Humahuaca basin, the Maimará Formation is exposed in the hanging wall of a thrust fault on the western side of the basin. The northernmost exposure of the Maimará Fm occurs 2 km north of the village of Huacalera, where this fault strand terminates and slip is transferred to another fault strand located a few hundred meters to the west (Figure 2). The base of the Maimará Formation is not exposed, but the oldest exposed strata of this formation are located west of the town of Tilcara. There, ~150 m of well-rounded pebble-cobble conglomerates with interbeds of reddish sandstone and siltstone lie below an ash (HU140412-01) dated to  $6.31 \pm 0.06$  Ma. This ash is located near the transition within the Maimará Formation from predominantly conglomerates to predominantly siltstones and sandstones, and extends the estimate for the onset of deposition of the Maimará Formation to



at least 6.5 Ma, from previous constraints of at least 6 Ma (Pingel *et al.*, 2013). Deposition of the Maimará Fm continued until ~4.3 Ma, as constrained by an outcrop west of Huacalera where a  $4.38 \pm .11$  Ma ash (HU180411-03) within the Maimará Fm (identified by the presence of well-rounded conglomerates with typical Maimará Fm clast compositions interbedded with sandstones) lies ~10 m below the contact with the Tilcara Fm, which contains a  $4.24 \pm .08$  Ma ash (HU240307-01) ~5 m above the contact.

The clast composition of the lower conglomeratic part of the Maimará Fm (12-20% Puncoviscana Fm, 71% Mesón Group, 8-10% Salta Group, 1-6% igneous) is similar to clast compositions of conglomeratic layers within the rest of the Maimará Fm in the same area (6-9% Puncoviscana Fm, 69-76% Mesón Group, 15-25% Salta Group) and to that reported by Pingel *et al.* (2013) in the southern Humahuaca basin (23.5% Puncoviscana Fm, 64.5% Mesón Group, 12% Salta Group). The upper parts of the Maimará Fm (<5 Ma) have more variable clast compositions and a greater proportion of Salta Group clasts (Figure 4). In the northern Humahuaca basin, imbricated clasts and channel margins within the Maimará Fm indicate paleoflow directions to the east and southeast (Figure 5).

#### *Tilcara Formation*

The Tilcara Fm directly overlies the Maimará Fm, and the onset of Tilcara Fm deposition is marked by an abrupt change in sedimentary facies, clast composition, and paleoflow directions. Extensive outcrops of the Tilcara Formation occur south of the Río Yacoraite, with only isolated outcrops north of the Río Yacoraite near Uquía. Stratigraphic sections spanning 4.3 Ma to 1.6 Ma between the Angosto de Perchel and the Río Yacoraite are dominated by conglomerates, except between ~2.4-2.2 Ma, when sandstones and siltstones are more prevalent north of the Angosto de Perchel (Figure 3). We assign these

finer-grained deposits to the Uquía Fm (see next subsection), which spread over a wide area and interfingered with the conglomerates of the Tilcara Fm during this period. Near Huacalera, the age of the base of the Tilcara Fm is tightly constrained by a  $4.24 \pm .08$ -Ma ash (HU240307-01) in the Tilcara Fm ~5 m above its contact with the Maimará Fm and a  $4.38 \pm .11$  Ma ash (HU180411-03) in the Maimará Fm <10 m below the contact (Table 2, ash data, Streit *et al.* (2015)). North of the Angosto de Perchel, an ash (HU220310-03) low in the Tilcara Fm is dated to  $4.42 \pm .11$  Ma.

The Tilcara Formation consists of mostly clast-supported, rounded pebble-cobble conglomerates (Figure 3). Pebble and cobble conglomerates are typically horizontally stratified and commonly sorted into weakly bedded layers ~0.2 – 1 m thick (Figure 6e). Small channel scours are commonly visible at the base of conglomerates overlying layers of silt or sand (Figure 6 c, g). We interpret these conglomerates as gravel-bedded, braided stream deposits (Miall, 1996). We interpret as debris flows the association of matrix-supported conglomerates and subangular pebble-boulder conglomerate layers interbedded with massive siltstone layers that are ~20-40 cm thick, for example, around 360-380 m and at 622 m in the Angosto de Perchel (AP) section (Figure 6h). The predominance of eastward paleoflow directions between 3.5 Ma and 2.2 Ma (Figure 5), clast compositions (Figure 4) that reflect the local lithologies exposed in the Sierra Alta (Figure 2) immediately west of the site of deposition, the rare occurrence of debris flows in addition to channel deposits, and the broad areal extent of these conglomerates suggests deposition in a fluvially dominated alluvial fan environment during that time.

North of the Angosto de Perchel, the interval from ~2.4 Ma to ~2.2 Ma is characterized by more fine-grained deposits (Uquía Fm). Within the Angosto de Perchel

(AP) section itself, however, the equivalent interval consists of interbedded pebble-cobble conglomerates and reddish siltstones (Figures 3, 6c). An ash (HU140411-01) in the lower part of this interval yielded a U-Pb age of  $2.43 \pm .12$  Ma. In the section 1.5 km north of the Angosto de Perchel (AP-N), this interval contains reddish siltstones and sandstones with 10-50 cm bedding, as well as less common pebble conglomerate layers and tan-to-reddish laminated mudstones (Figures 3, 6a). Laterally extensive beds with horizontal stratification and scarce channelization or cross-bedding suggest that these were deposited as distal sheetfloods (Miall, 1985). A  $2.39 \pm .03$  Ma ash (HU220310-01) occurs within the transition from predominantly conglomerates to predominantly siltstones and sandstones (Figure 3). South of the Arroyo Perchel, conglomerate deposition continued uninterrupted throughout this interval. There, sparse silt layers begin to be interbedded with conglomerates around 2.4 Ma ( $2.37 \pm .03$  Ma, HU070411-01), but do not constitute a significant fraction of the deposits until nearly 2.1 Ma (before  $2.11 \pm .07$  Ma, HU070411-02).

Around 2.2 Ma (after  $2.25 \pm .06$  Ma, HU220310-02), an abrupt transition from fine-grained facies back to conglomerates occurs in the Angosto de Perchel area. This conglomerate appears dark gray due to the high proportion of Puncoviscana clasts it contains (up to 80%). We interpret these clast-supported and matrix-supported, moderately-sorted, subangular pebble-cobble conglomerates as debris flow-dominated alluvial fan deposits. The upper 10 m of the measured section north of the Angosto de Perchel (AP-N), above a  $1.98 \pm .12$  Ma ash (HU160411-01), consists of fine sand with trough cross-bedding interbedded with pebble conglomerates with southward paleoflow directions and equal proportions of Puncoviscana and Mesón clasts.

Paleoflow directions (Figure 5) were inferred from channel margins and imbricated pebbles. Northward flow directions are recorded in the lower Tilcara Fm, between 4.4 Ma and 3.5 Ma, near the Angosto de Perchel. Between 3.5 – 2.2 Ma, the flow direction recorded near the Angosto de Perchel is predominantly eastward. Some southwestward flow is recorded by well-exposed channels at 590 m in the Angosto de Perchel (AP) section (~2.2 Ma). By 2 Ma, the flow direction near the Angosto de Perchel was predominantly southward. About 5-10 km farther south, between the villages of Juella and Tilcara (Figure 5), southward paleoflow directions are recorded as early as ~3 Ma. Still farther south in the southern Humahuaca basin, the southward paleoflow directions are present even in the lowermost part (~4 Ma) of the Tilcara Formation (Pingel *et al.*, 2013).

The clast composition of conglomerates (Figure 4) in the Tilcara Fm differs sharply from the Maimará Fm. Within the Tilcara Fm, typical clast compositions are roughly 40-60% Puncovicana Fm, 40-60% Mesón Group, and 0-15% Salta Group. North-south variations in clast composition between the Angosto de Perchel and Humahuaca (Figure 4) reflect the lithologies exposed in the nearby Sierra Alta, with more deeply exhumed rocks exposed in the south than in the north, i.e., mostly Puncoviscana Formation versus mostly Mesón Group (Figure 2). Clast counts also reveal a subtle overall pattern of progressive unroofing of the bounding ranges, such that the fraction of Puncoviscana Formation clasts increases upsection relative to the fraction of Mesón Group clasts between 4.4 Ma and 2 Ma (Figure 4). The extremely Puncoviscana-rich (~80%) conglomerates deposited ~2 Ma in the Angosto de Perchel area, however, could reflect the capture of a local source area in the Puncoviscana Fm, rather than an increase in the area of Puncoviscana Fm exposed in the bounding ranges. Within this overall pattern, significant variability exists on shorter timescales, e.g. the clast

count at 119 m in the north Angosto de Perchel section (Figure 4), likely reflecting variable contributions from local sediment sources, particularly Salta Group rocks exposed in the hanging walls of thrust faults on the western side of the Humahuaca basin. Conglomerate beds with anomalously high proportions of Salta Group clasts are more common 4-3.5 Ma and 2.4-2.1 Ma.

In summary, the Tilcara Fm consists of primarily clast-supported, rounded pebble-cobble conglomerates and was deposited between ~4.3 Ma and 1.6 Ma. Finer-grained deposits of the Uquía Fm interfinger with the conglomerates of the Tilcara Fm between 2.4 and 2.2 Ma. As in the southern Humahuaca basin (Pingel *et al.*, 2013), an abrupt change in both conglomerate clast compositions and paleoflow directions occurs at the contact between the Maimará Fm and the Tilcara Fm. In contrast to the Maimará Fm, Tilcara Fm conglomerates contain a relatively minor quantity of Cretaceous-Paleogene Salta Group clasts and a much greater quantity of Precambrian Puncoviscana Fm clasts. Northward paleoflow directions in the lower part of the Tilcara Fm indicate that formerly eastward fluvial transport was deflected northward in the northern Humahuaca subbasin at the same time (~4.3 Ma) that it was deflected southward in the southern Humahuaca subbasin (Pingel *et al.*, 2013). The appearance of southward paleocurrent directions in the northern subbasin by 2 Ma suggests the integration of the northern subbasin with the southern subbasin by that time.

#### *Uquía Formation*

Consisting of fluvial and lacustrine sandstones, siltstones, and mudstones, the Uquía Fm is more fine-grained than the Tilcara Fm. Deposition of the Uquía Fm occurred between ~ 3 Ma (Reguero *et al.*, 2007) and  $1.84 \pm .08$  Ma (HU040411-01), overlapping in time with

deposition of the Tilcara Fm. The most extensive outcrops of the Uquía Formation occur north of the Río Yacoraite (Figure 2), but between 2.4 and 2.2 Ma, sandstones, siltstones and mudstones of the Uquía Formation also interfinger with the conglomerates of the Tilcara Formation between the Río Yacoraite and the Angosto de Perchel (Figure 3). Stratigraphic sections east of Humahuaca (HUM-E), southwest of Humahuaca (HUM-S), and east of Huacalera (HUA-E) comprise fluvial sandstones before 2.5 Ma, predominantly lacustrine facies between 2.5 Ma and 2.1 Ma, and coarsening upward fluvial sandstones and conglomerates after 2.1 Ma (Figure 3).

Northeast of Humahuaca, ~10 m of pinkish-tan fine sandstones containing a muddy ash dated to  $2.26 \pm .12$  Ma (HU210310-02) onlap the Puncoviscana Formation. Above the tan sands lie ~40 m of light-gray laminated muds, silts, and fine sands with abundant bioturbation, as well as a few lenses of rounded pebble conglomerates and layers of pinkish silt or mud with wavy lamination, which we interpret as shallow lacustrine and shoreline deposits. The upper 20 m of this light-gray unit is exposed in the measured section east of Humahuaca (Hum-E) (Figures 3, 6b). An age of  $2.12 \pm .14$  Ma was obtained from an ash (HU210310-01) collected ~10 m below the top of this light-gray unit. Directly overlying the light-gray unit is ~5 m of bright red mudstones and siltstones, followed by reddish sandstones interbedded with pebble conglomerates, in an overall coarsening upward sequence, which we interpret as fluvial in origin. An erosional unconformity separates the Uquía Fm from overlying Quaternary conglomerates.

The section located 3 km south of the town of Humahuaca (Hum-S) (Figure 3) begins with ~40 m of tan siltstones and sandstones with a few layers of pebble conglomerate, followed by ~50 m of laminated light tan-colored mudstones with abundant bioturbation,

~100 m of red fine-coarse sands and interbedded silts and muds, ~80 m of tan mudstones and siltstones with a few marlstone layers, and finally, a >100-m-thick coarsening upwards sequence of sands and conglomerates. We interpret the tan mudstones, siltstones, and marlstones as shallow lacustrine deposits, whereas the red sandstones are interpreted as fluvial channel sands deposited by streams that flowed eastward into the shallow lake that occupied much of the northern Humahuaca basin at this time. Only a few hundred meters north of the measured section, these red sandstones are apparently absent from equivalent levels. An ash (HU290412-02) located in the middle of the bioturbated mudstones was dated to  $2.36 \pm .07$  Ma. An ash (HU290412-04) in the conglomerates at the top of the section yielded an age of  $1.32 \pm .11$  Ma. Although the unconformity between the Uquía Fm and Quaternary conglomerates is not clearly exposed at this location (where the upper part of the Uquía Fm is increasingly conglomeratic), we interpret the conglomerates that contain this ash as belonging to the Quaternary conglomerates, rather than to the Uquía Fm.

Near Huacalera, ~100 m of tan to light greenish-gray mudstones, siltstones and sandstones are exposed east of the Río Grande (Hua-E) (Figures 3, 6d). The upper part of this outcrop consists of laminated mudstones, which we interpret as lake beds. The lower part consists of fine-medium sandstones, with both planar stratification and trough cross-bedding, interbedded with well-rounded pebble conglomerates in the lowest 25 m exposed. A  $2.50 \pm .03$  Ma ash (HU310310-02) ~10 m below the top of the sandstones indicates that lacustrine deposition began ~2.5-2.4 Ma.

Between the villages of Uquía and Chucalezna (Figure 3), where the Uquía Fm was first described by Castellanos (1950), roughly 450 m of the Uquía Fm are exposed west of the Río Grande. A prominent 2-m-thick ash (UQ160311-01) within this section yielded a U-

Pb zircon age of  $2.49 \pm 0.03$  Ma, and likely corresponds to the U1 Tuff of Walther *et al.* (1998), as described by (Reguero *et al.*, 2007). Approximately 150 m of interbedded sand and conglomerate lie below this ash layer (e.g. Figure 6f) and ~300 m of grayish tan fine sand, silt, and clay lie above it. This sequence is consistent both with previous studies that placed the base of the Uquía Fm at ~3 Ma (Reguero *et al.*, 2007) and with our interpretation of a widespread shift from fluvial to lacustrine deposition within the Uquía Fm at ~2.5 Ma. An ash (UQ270307-02) ~20 m below the top of the Uquía Fm at Chucalezna was dated to  $2.23 \pm .07$  Ma. The youngest dated ash in the Uquía Fm is  $1.84 \pm .08$  Ma (HU040411-01) and lies in the footwall of a thrust fault ~ 3 km south of Chucalezna.

Overall, the Uquía Fm is more fine grained than the Tilcara Fm and was deposited between ~3 Ma (Reguero *et al.*, 2007) and <1.84 Ma (HU040411-01). Prior to 2.5 Ma, the Uquía Fm was deposited only in the northern and eastern parts of the northern Humahuaca subbasin and contained primarily fluvial sandstones with interbedded pebble conglomerate layers. From 2.5 Ma until 2.1 Ma, deposits throughout the northern subbasin were more fine-grained, as lacustrine mudstones and siltstones replaced the fluvial sandstones and conglomerates in the northern and eastern parts of the basin. Between 2.4 and 2.2 Ma, the sandstones, siltstones, and mudstones of the Uquía Fm were deposited as far south as the Angosto de Perchel, where they interfinger with the conglomerates of the Tilcara Fm.

#### *Río Yacoraite measured section*

The Río Yacoraite measured section (RY), previously presented in Chapter 1, comprises 715 m of fluvial conglomerates and siltstones and spans from ~3.1 Ma to ~1.6 Ma without any major unconformities (Figure 3). The combination of magnetostratigraphy and the dated ash in the Río Yacoraite section provides some of the best time control on events in



the Humahuaca basin. These events include a nearly two-fold increase in sediment-accumulation rates around 2.5 Ma, loss of fluvial connectivity between the Casa Grande basin and the downstream Humahuaca basin by 2.1 Ma, and an interval of finer-grained deposition from ~2.5-2.1 Ma. This section contains both Tilcara Fm and Uquía Fm deposits, but differs from nearby sections, because it reflects sediment input from the Río Yacoraite. For example, strata traced along strike ~3 km to the north exhibit pronounced fining away from the Río Yacoraite.

This section contains 5 main intervals defined by changes in grain size: mostly conglomerates prior to ~2.4 Ma, dominantly siltstone between ~2.4 and 2.2 Ma, another interval of conglomerates between ~2.2 and ~2.1, another interval of mostly siltstone with increasing abundance of conglomerate layers between 2.1 and 1.95 Ma, and interbedded conglomerates, sandstones, and siltstones between 1.95 and 1.6 Ma (Figure 3). A similar shift to more fine-grained sedimentary facies between 2.5 and 2.1 Ma occurred throughout the entire northern Humahuaca subbasin. The lower 160 m of the section consists primarily of well-rounded pebble-cobble conglomerates with some interbedded sandstones, which we assign to the Tilcara Fm. Between 160-280 m, the fraction of sandstones and siltstones interbedded with the conglomerates increases, which we interpret as an interfingering of fine-grained Uquía Fm deposits with Tilcara Fm conglomerates. Between 260-350 m, the section consists mostly of orangish siltstone, with some interbedded pebble conglomerate layers. This interval is followed by 120 m of mostly pebble-cobble conglomerates before a return to orangish siltstones and interbedded pebble conglomerates at 470 m. Above 495 m, the fraction of conglomerate relative to siltstones increases, and sandstones interbedded with the conglomerates become more common above 550 m. We consider 260 – 550 m in the section

(~2.45-1.95 Ma) to belong to the Uquía Fm, and the deposits above 550 m (~1.95 Ma) to be transitional between the Uquía Fm and the Tilcara Fm. The 120 m of conglomerates in the middle of finer-grained Uquía Fm deposits ~2.15 Ma appears to have been deposited around the same time as the red sandstones in the measured section southwest of Humahuaca (Figure 3), and therefore suggests a drop in lake levels at that time.

Finally, the provenance of detrital zircons in Río Yacoraite section records the history of fluvial connectivity with the Casa Grande basin to the west, and with ranges on the edge of the Puna Plateau that bound the Casa Grande basin (Streit *et al.*, 2015). These data show that Casa Grande basin maintained connectivity with the Humahuaca basin at 3 Ma, but became isolated from the downstream basin by 2.1 Ma and remained isolated at least until 1.7 Ma.

### *Unconformities*

Two major unconformities formed in the northern Humahuaca basin around the time of the transitions from the Maimará Fm to the Tilcara Fm (between 4.5 Ma – 3.8 Ma) and from the Uquía Fm to the Quaternary conglomerates (between 1.6 Ma – 0.8 Ma). Streit *et al.* (2015) identified an extensive ~4-Ma unconformity in both the northern Humahuaca basin and the Casa Grande basin to the west (Figure 1b). Whereas the widespread occurrence of this unconformity reflects the interplay between the onset of intrabasinal deformation and increased sediment supply basin-wide, the variation in the precise age of the deposits directly above the unconformity at different locations reflects the timing of deformation on individual structures. For example, at Huacalaera, the angular unconformity between Maimará Fm sandstones containing a 5.05 Ma ash (HU210307-03) and 4.38 ±.11 Ma (HU180411-03) sandstones and interbedded rounded pebble conglomerates of the uppermost Maimará Fm reflects erosion during tilting of the Maimará Fm, whereas west of this location, the 3.8-Ma

age directly above the unconformity with Pirgua Subgroup rocks thrust over the uppermost Maimará Fm reflects erosion in the hanging wall of a fault that was active between 4.2 and 3.8 Ma.

In the southern Humahuaca basin, Pingel *et al.* (2013) noted a pronounced regional unconformity between the Tilcara Fm (4.2 Ma - <2.5 Ma) and the oldest overlying Quaternary gravel unit (~1.06 - 0.8 Ma). Similarly, an unconformity between the Uquía Fm and Quaternary conglomerates is observed in the northern Humahuaca basin between 2.2-Ma sandstones and siltstones belonging to the Uquía Fm and 0.9-Ma Quaternary conglomerates on the east side of the Río Grande north of Huacalera (Streit *et al.*, 2015). The episode of incision that created this unconformity must have occurred after 1.6 Ma because no unconformity is observed in the Río Yacoraite (RY) measured section, which dates to ~1.6 Ma at its top (Figure 3) (Streit *et al.*, 2015). In the northernmost Humahuaca basin, an unconformity is observed between the Uquía Fm and undated overlying Quaternary conglomerates east of Humahuaca, but is not obvious in the measured section southwest of Humahuaca (Hum-S), where an ash (HU290412-04) in the gravels at the top of the top of the section yielded an age of ~1.3 Ma. It is possible that the regional unconformity between the Tilcara Fm and the Quaternary conglomerates lies below the 1.3-Ma ash, but is obscured by a gradual increase in the abundance of pebble conglomerate layers interbedded with sandstones in the upper part of the Uquía Fm, which is relatively flat-lying at this location. Alternatively, the unconformity observed east of Humahuaca could correspond to a younger unconformity between the ~1-Ma Quaternary conglomerate unit and a younger (~94-65 ka) Quaternary conglomerate unit (Robinson *et al.*, 2005; Sancho *et al.*, 2008; Pingel *et al.*, 2013).

In summary, two major unconformities exist in the northern Humahuaca basin, one around 4 Ma and one around 1 Ma. The exact age of the unconformities at different locations varies by as much as 0.5 Myr. We suggest that the ~4 Ma unconformity, which is also present in the Casa Grande basin, reflects erosion due to renewed uplift on the western side of the Humahuaca basin and in the Sierra Alta beginning ~4.5 Ma and followed by a return to deposition in response to increased sediment supply ~4 Ma (Streit *et al.*, 2015). Unconformities between the Tilcara Fm or Uquía Fm and overlying Quaternary conglomerates are observed in both the northern and southern Humahuaca basin around 1 Ma. In detail, creation of these unconformities may be diachronous, forming at different times between <1.6 Ma and >0.9 Ma at different locations.

### **Sediment-accumulation rates**

Based on dated ashes, magnetostratigraphic boundary ages, and measured sections in the northern Humahuaca basin, sediment-accumulation rates averaged over ~0.2- to ~1.1-Myr-long intervals are typically 200-400 m/Myr, with an interval of higher sediment-accumulation rates (>500 m/Myr) from 2.5-2 Ma (Figure 3, inset). We report the minimum and maximum sediment-accumulation rates calculated taking into account the uncertainties on ash ages, the precise locations of magnetozone boundaries, and measured thicknesses. Low sediment-accumulation rates between 4.38 and 3.86 Ma (ashes HU180411-03 and HU080410-01) at Huacalera (40-110 m/Myr) and between 4.36 and 4.04 Ma (ashes HU300310-01 and HU300310-02) in the section 1.5 km north of the Angosto de Perchel (30-130 m/Myr) likely reflect episodes of erosion related to local deformation. At Huacalera, these low sediment accumulation rates were calculated ~200 m east of a fault that was active at least between 4.2 and 3.9 Ma (Streit *et al.*, 2015). In the section north of the Angosto de

Perchel, the vertical separation between the 4.36-Ma ash and the 4.04-Ma ash increases to the east, suggesting deposition on eastern flank of a growing anticline. In the two sections near Angosto de Perchel, the sediment-accumulation rates increase from 170-350 m/Myr between 4.04 and 3.41 Ma (ashes HU300310-02 and HU170411-01) to 310-440 m/Myr between 3.59 and 2.48 Ma (ashes HU130411-01 and HU140411-01), and then to 410-1170 m/Myr between 2.39 and 1.98 Ma (HU220310-01 and HU160411-01). These rates are consistent with sediment-accumulation rates in the Río Yacoraite section of 230-410 m/Myr between 3.04 Ma and 2.58 Ma and 520-590 m/Myr between 2.58 Ma and 1.95 Ma (Streit *et al.*, 2015). The interval of higher sediment-accumulation rates coincides with the interval when finer-grained deposits of the Uquía Fm expanded south to interfinger with the Tilcara Fm, but high sediment-accumulation rates at this time are also observed in conglomerates farther south. Three kilometers south of the Angosto de Perchel, where the conglomerates of the Tilcara Fm lack any interfingering with the Uquía Fm, the sediment-accumulation rate estimated between 2.4 and 2.1 Ma (ashes HU070411-01 and HU070411-02) was at least 500 m/Myr. In the section southwest of Humahuaca, the average sediment-accumulation rate was 220-470 m/Myr between  $2.36 \pm 0.07$  Ma (HU290412-02) and  $1.32 \pm 0.11$  Ma (HU290412-04). It is not clear if this rate reflects high sediment-accumulation rates around 2.5-2 Ma, as found in other locations the northern Humahuaca basin, followed by lower sediment-accumulation rates related to the unconformity between the Uquía Fm and ~1-Myr-old Quaternary conglomerates (Pingel *et al.*, 2013; Streit *et al.*, 2015), or if sediment-accumulation rates were simply persistently lower in the northernmost part of the basin. In summary, average sediment-accumulation rates throughout the northern Humahuaca basin increased from ~200-400 m/Myr to >500 m/Myr around 2.5 Ma and appear to have decreased to ~200-400 m/Myr

again after ~2 Ma. Sediment-accumulation rates of <200 m/Myr appear to be related to local uplift and erosion.

## **DISCUSSION**

### **Evolution of the northern Humahuaca subbasin**

The above observations (summarized in Figure 7) of changes in sedimentary facies, paleocurrent directions, and sediment-accumulation rates, together with the chronology provided by U-Pb dating of zircons from tuff layers, illuminate the following major events in the evolution of the northern Humahuaca basin: (1) a transition from conglomerates to siltstones and sandstones in the Maimará Fm at ~6.3 Ma, (2) the transition from the Maimará Fm to the Tilcara Fm at ~4.3 Ma, (3) an episode of higher sediment-accumulation rates and fine-grained deposition throughout the northern subbasin ~2.5-2.1 Ma, (4) the integration of the northern subbasin with the southern subbasin by ~2.2 – 2 Ma, (5) the loss of connectivity with the Casa Grande basin by 2.1 Ma, and (6) the creation of a major unconformity sometime between 1.6 and 0.9 Ma. Following these events, multiple episodes of aggradation and incision are recorded by a series of Quaternary basin fills, fluvial terraces, and alluvial fan surfaces that formed between ~800 ka and 40 ka (Tchilinguirian & Pereyra, 2001; Robinson *et al.*, 2005; Strecker *et al.*, 2007; Sancho *et al.*, 2008; Pingel *et al.*, 2013). In the discussion below, we focus on the onset of deposition of the Tilcara Fm and the events that occurred ~2.5-2 Ma.

As in the southern Humahuaca basin (Pingel *et al.*, 2013), the transition from the Maimará Formation to the Tilcara Formation in the northern Humahuaca basin is marked by an abrupt change in both paleocurrent directions (Figures 5,7) and conglomerate clast

composition (Figures 4,7). Similar to the southern Humahuaca basin (Pingel *et al.*, 2013), comparison of clast counts reveals a shift from predominantly Cretaceous-Paleogene Salta Group and Cambrian Mesón Group clasts with a small fraction of Proterozoic-early Cambrian Puncoviscana Formation clasts in the Maimará Formation to compositions with about equal proportions of Mesón Group and Puncoviscana Formation clasts and a small fraction of Salta Group clasts in the Tilcara formation (Figure 4,7). One difference between the northern and southern subbasins is that paleocurrents in the northern Humahuaca basin indicate that the formerly eastward flow during the deposition of the Maimará Formation was initially deflected northward with the onset of Tilcara Formation deposition (Figure 5,7), in contrast to the southward deflection of flow in the southern Humahuaca basin (Pingel *et al.*, 2013). In the northern Humahuaca subbasin, deposition of the Tilcara Fm began ~4.3 Ma, as constrained by a  $4.42 \pm 0.11$  Ma ash low in the Tilcara Fm near the Angosto de Perchel, a  $4.24 \pm .08$  Ma ash ~10 m above the contact with the Maimará Fm near Huacalera, and a  $4.38 \pm .11$  Ma in the upper 5 m of the Maimará Fm near Huacalera. The onset of deposition of Tilcara Fm in the southern Humahuaca basin occurred at ~4.2 Ma (Pingel *et al.*, 2013). Given the uncertainties in the ages, this event may be considered synchronous throughout the Humahuaca basin, although it is also possible that the onset of deposition of the Tilcara Fm in the northern subbasin preceded deposition in the southern subbasin by 0.1-0.2 Myr.

Based on the difference in paleoflow direction between the southern and northern subbasins between 4.2 and 3.5 Ma, the drainage divide between the two subbasins is inferred to have been located south of the Angosto de Perchel and north of Tilcara. This boundary is also consistent with the maximum southern extent of Uquía Fm deposits, which between 2.4 and 2.2 Ma interfinger with the Tilcara Fm at the Angosto de Perchel, but not farther south.

Because this location does not represent a structural boundary (Figure 2), the initial creation of separate subbasins appears to have been driven by paleotopography.

The most striking difference between the northern and southern subbasins of the Humahuaca Valley is the presence of the fine-grained deposits of the Uquía Fm in the northern subbasin. Outcrops of the lower part of the Uquía Fm (>2.5 Ma) mainly occur in the area between the village of Uquía and the Río Yacoraite and are predominantly well-sorted sandstone, with interbedded siltstones and lenses of well-rounded pebble conglomerate (Figs. 2 and 3). Lateral facies variation between the coarse-grained Tilcara Fm in the southern part of the northern subbasin and the finer-grained Uquía Fm in the northern part of the subbasin may reflect downstream fining closer to the outlet of the northern subbasin and/or the northward decrease in Plio-Pleistocene faulting on the western side of the basin and, hence, less coarse-grained sediment being delivered to the northernmost part of the basin. After 2.5 Ma, there is a decrease in grain size throughout the northern Humahuaca basin (north of the Angosto de Perchel). In the northern and eastern parts of the subbasin, the upper Uquía Fm consists of lacustrine deposits. Between 2.5 and 2.2 Ma, the Uquía Fm was deposited over an expanded area, replacing the conglomerates of the Tilcara Fm on the western side of the basin between the Angosto de Perchel and the Río Yacoraite with sandstones and siltstones, which we interpret as a low-gradient fluvial system that flowed into a large, shallow lake. The loss of fluvial connectivity between the Casa Grande and Humahuaca basins also occurred at this time, and the Casa Grande basin remained isolated from the Humahuaca basin from 2.1 Ma to a least 1.6 Ma (Streit *et al.*, 2015). Farther south, in the Angosto de Perchel area, we interpret an abrupt transition back to conglomerate deposition ~2.2 Ma as the progradation of a debris-flow dominated alluvial fan. By 2 Ma, the section 1.5 km north



of Angosto de Perchel (AP-N) becomes dominated by interbedded conglomerates and sandstones recording southward paleoflow, which we interpret as gravel-bed braided river deposits from the axial river. In the northern part of the subbasin, lacustrine deposition continued until ~2.1 Ma and was followed by a coarsening upwards sequence of fluvial sandstones and conglomerates.

We propose that this interval of finer-grained deposition between ~2.5 and ~2.1 Ma was caused by channel defeat at the former northern outlet of the Humahuaca basin at ~2.5 Ma. Under this scenario, the channel defeat could have been caused by an increase in rock-uplift rates in the bounding ranges to the east and/or reduced stream power as a result of decreased precipitation in the lee of the growing ranges. Evidence for a shift to a more arid climate around this time includes a shift in the hydrogen isotopic composition of hydrated volcanic glasses in the southern Humahuaca basin that occurred between 3.5-2.5 Ma (Pingel *et al.*, 2014). Additionally the loss of fluvial connectivity of the Casa Grande basin (Fig. 1B), lying west of the Sierra Alta (Fig. 2), with the Humahuaca basin between 2.7 and 2.1 Ma has been attributed to increasing aridity and concurrent range uplift at that time (Streit *et al.*, 2015). Channel defeat would have caused ponding closest to the former outlet (in the eastern and northern parts of the northern Humahuaca subbasin) and higher sediment-accumulation rates as all sediment entering the basin remained trapped there. As the lake level and the thickness of trapped sediments rose, the gradient between the mountain front and the local base level would have decreased, resulting in finer-grained fluvial deposits as well. With sufficient aggradation, the fill would have been likely to overtop the drainage divide between the northern and southern subbasins of the Humahuaca basin, resulting initially in the capture

of the northern subbasin by the southern subbasin by 2 Ma and subsequently in incision of the northern subbasin by the newly integrated river system.

Alternatively, and although we have no paleocurrent data (Fig. 5) supporting such an interpretation, it is possible that southward axial drainage in the northern subbasin may have been established prior to 2.5 Ma. Given that the Angosto de Perchel is one of the narrowest points in the valley, obstruction of southward flow at this point could have caused the upstream ponding and rapid aggradation to the north. Such a blockage could have been caused either by structural uplift or by an alluvial fan prograding across the entire valley to dam the river near the Angosto de Perchel, one of the narrowest points in the valley. Alluvial fan progradation could also be related to the shift to semi-arid conditions in the Humahuaca basin at this time, given that fan growth may be caused by an increase in sediment supply as a result of decreased vegetation under more arid conditions (e.g., Pope & Wilkinson, 2005). Alternatively, alluvial fan progradation could be tectonically controlled, either by decreased activity on the thrust faults on the western side of the basin resulting in lower accommodation space in the footwall of these faults, or by increased rock-uplift rates in the Sierra Alta (related to increased activity on these faults) resulting in greater sediment supply to the fan. Although cross-cutting relationships with the Plio-Pleistocene basin fill indicate that faults on the western side of the basin were active between >4 Ma and <1.6 Ma (Streit *et al.*, 2015), we are not able to resolve changes in rates of thrusting with sufficient resolution to evaluate these hypotheses. Chapter 3 presents a more detailed chronology of deformation in the Humahuaca basin and its relationship to the sedimentary record.

In sum, Neogene-Quaternary deposition in the northern Humahuaca basin can be divided into four main phases: deposition of the Maimará Fm from >6.5 Ma to 4.3 Ma,

deposition of the Tilcara Fm (and the Uquía Fm in the northern part of the basin beginning ~3 Ma) from 4.3 to ~1.6 Ma, channel defeat at the northern outlet resulting in finer-grained deposits and higher sediment-accumulation rates ~2.5-2.1 Ma, and widespread deposition of conglomerates above an unconformity <1 Ma. As in the southern Humahuaca basin, paleocurrents in the Maimará Fm indicate paleoflow to the east. With the onset of deposition of the Tilcara Fm ~4.3 Ma, formerly eastward fluvial transport was deflected southward in the southern subbasin (Pingel *et al.*, 2013) and northward in the northern subbasin by the uplift of the Tilcara ranges, resulting in the creation of two subbasins. Faulting on the western side of the Humahuaca basin and renewed uplift of the Sierra Alta caused a change in conglomerate clast composition from the Maimará Fm to the Tilcara Fm. We interpret the higher sediment-accumulation rates and finer-grained deposits throughout the northern Humahuaca basin between ~2.5 – 2.1 Ma to have resulted from channel defeat at the outlet of the northern subbasin. At the end of this interval, the northern subbasin was integrated with the southern subbasin, as indicated by the appearance of southward paleocurrents by 2 Ma. Deposition of the Tilcara Fm and Uquía Fm continued until at least 1.6 Ma, and was followed by an episode of incision sometime between 1.6 and 0.9 Ma, which created the unconformity with the overlying Quaternary conglomerates.

### **Regional Context**

Regional comparison of the timing of these events suggests that some of these events reflect regionally significant changes. In the Argentinean Subandes ~90 km northeast of the northern Humahuaca basin, Amidon *et al.* (2015) describe changes in detrital zircon populations of foreland-basin sediments exposed along the Río Iruya (Fig. 1B) at ~6.3 Ma, ~4 Ma and ~2.3 Ma. They attribute the appearance of Jurassic – Neogene zircons between

6.7 and 6.0 Ma to the tectonic reactivation of the Eastern Cordillera, noting that deposition of the Maimará Fm also began around this time. Whereas deposition of the Maimará Fm reflects uplift of the ranges to the west of the Humahuaca basin, i.e., the Sierra Alta, apatite (U-Th)/He cooling ages between 5.6 - 6.1 Ma on the eastern side of the Sierra Hornocal (Reiners *et al.*, 2015) attests to exhumation of the ranges east of the Humahuaca basin during this time as well.

The onset of deposition of the Tilcara Fm in both the northern and southern Humahuaca basin at 4.4-4.2 Ma is interpreted as a response to a regional increase in rock-uplift rates. Deflection of antecedent rivers by a growing structure can also be caused by a local increase in rock-uplift rates, the exposure of more resistant lithologies, or climate change. However, the climate of the Humahuaca basin remained humid at that time (Pingel *et al.*, 2013; Pingel *et al.*, 2014), and neither the exhumation of more resistant lithologies nor changes in local uplift rates in the Tilcara ranges can explain the change in clast compositions between the Maimará Fm and the Tilcara Fm: a change that reflects uplift of the Sierra Alta. Uplift of the Sierra Alta at this time is also supported by the onset of deposition by 3.7 Ma in the Casa Grande intermontane basin on the west side of the Sierra Alta (Streit *et al.*, 2015). Additionally intrabasinal deformation on the west side of the Humahuaca basin (angular unconformity ~4.4 Ma and active faulting between 4.2 and 3.9 Ma near Huacalera (Streit *et al.*, 2015)) began around the same time as the deposition of the Tilcara Fm. An acceleration of rock uplift at ~4 Ma (between 4.3 and 3.5 Ma) is also inferred in the Santa Victoria range, >50 km north of the Tilcara ranges (Amidon *et al.*, 2015).

Increased rock-uplift rates in these ranges may relate to changing patterns of uplift and exhumation on a broader regional scale between ~4 and 5 Ma. Farther south, at ~24-

25°S, uplift and exhumation shifted westward from the western Santa Barbara System (east of Lerma Valley) into the central ranges of the Eastern Cordillera (i.e., separating the Lerma Valley from the Angastaco basin and the Quebrada del Toro to the west), which record apatite (U-Th)/He cooling ages between 3-6 Ma (Carrapa *et al.*, 2011; Hain *et al.*, 2011; Pearson *et al.*, 2013; Reiners *et al.*, 2015). (See Figure 1a for the locations of the Lerma Valley, Angastaco, and Quebrada del Toro basins). That these ranges lie approximately along strike with the Tilcara ranges (Figure 1a) and have similar cooling ages suggests relatively consistent timing of exhumation over distances of more than 300 km. Additionally, uplift of the central ranges of the Eastern Cordillera isolated the Angastaco basin from the Lerma Valley by ~ 4 Ma (Bywater-Reyes *et al.*, 2010; Carrapa *et al.*, 2011; Carrapa *et al.*, 2012), around the same time that uplift of the Tilcara ranges disrupted eastward fluvial transport from the Sierra Alta to the foreland and created the elongate Humahuaca intermontane basin in which drainage was diverted to the north or south. It is unclear whether out-of-sequence deformation in the Argentinian Subandes from ~4.5 Ma until present (Echavarría *et al.*, 2003) and in the Bolivian Subandes from ~4 Ma until 2.1 Ma (Uba *et al.*, 2009) is related to this phase of deformation in the Eastern Cordillera of NW Argentina or whether the timing is coincidental.

Whereas the onset of deposition of the Tilcara Fm at ~4.3 Ma appears to be related to regional-scale tectonics affecting patterns of deformation over hundreds of kilometers, the episode of higher sediment-accumulation rates, deposition of more fine-grained sediments in the northern Humahuaca basin 2.5 - 2.1 Ma, and reorientation of the northern Humahuaca drainage system to the south, rather than to the NE appears to have been controlled by processes acting on a smaller scale (~100 km). The timing of these events coincides with the

loss of a source of Neogene detrital zircons to the foreland basin deposits exposed along the Río Iruya (Amidon *et al.*, 2015), a loss of fluvial connectivity between the Casa Grande basin and the Humahuaca basin (Streit *et al.*, 2015), and the onset of arid conditions in the Humahuaca basin (Pingel *et al.*, 2014). Both Amidon *et al.* (2015) and Streit *et al.* (2015) attribute these events to channel defeat related to increased aridity coincident with range growth. The hypothesis that fine-grained alluvial and shallow lacustrine deposition in the northern Humahuaca basin was caused by channel defeat at the northern outlet of the basin clearly fits in this context. As the elevation of the Tilcara ranges (and the along-strike ranges to the north) reached threshold elevations for intercepting moisture from the east, increased aridity by 2.5 Ma (Pingel *et al.*, 2014) on the lee side of the range likely decreased the ability of rivers crossing the range to incise through the uplifting range. As the rate of rock uplift outpaced the rate of incision at the outlet of the basin, surface uplift of the bedrock channel resulted in its defeat. Lacustrine deposits reflect ponding upstream of this uplift. Cut off from the foreland, all of the sediment delivered to the fluvial system remained trapped in the intermontane basin, resulting in higher sediment-accumulation rates until a drainage divide to the south was overtopped by sediments and the entire Humahuaca basin was integrated into a south-flowing fluvial system.

## **CONCLUSIONS**

This study focuses on the stratigraphic evolution of the northern Humahuaca basin, including the synchronous onset of intermontane basin conditions in separate northern and southern subbasins, changes in sedimentary facies and sediment-accumulation rates associated with channel defeat at the outlet of the northern subbasin, and subsequent integration of the two subbasins. Exceptional time control provided by new U-Pb ages from

ash layers at 35 sites in the northern Humahuaca basin, combined with previously published geochronology and magnetostratigraphy (Streit *et al.*, 2015), facilitates precise correlation between stratigraphic sections distributed throughout the northern Humahuaca basin, calculations of average sediment-accumulation rates, identification of temporally constrained lateral facies variations, integration of paleocurrent and provenance data from different parts of the basin, and comparison with events in nearby regions. These data highlight the interplay of regional tectonics (increased uplift of multiple ranges in NW Argentina) and more local climate changes in the basin's history.

The onset of intermontane basin conditions in the Humahuaca basin is recorded by the deflection of a formerly east-flowing fluvial system, deposition of conglomerates, and an abrupt change in clast composition at approximately the same time (4.4-4.2 Ma) in both the northern and southern Humahuaca basin. These changes delineate the transition between the Maimará and Tilcara Formations. The existence of separate subbasins at that time is indicated by northward paleocurrents in the northern subbasin and southward paleocurrents in the southern subbasin. The indistinguishable timing (at ~4.3 Ma) of the deflection of antecedent rivers in both Humahuaca subbasins suggests that drainage reorganization was caused by an overall increase in rock-uplift rates in the Tilcara ranges, rather than along-strike growth of the range. Intrabasin deformation and renewed uplift of the Sierra Alta along the western margin of the Humahuaca basin also began around the same time. Indeed, this event appears to be related to the ~5-Ma phase of deformation that included the uplift and exhumation of ranges in the central Eastern Cordillera that lie approximately along strike with the Tilcara ranges (Bywater-Reyes *et al.*, 2010; Carrapa *et al.*, 2011; Hain *et al.*, 2011; Carrapa *et al.*, 2012; Pearson *et al.*, 2013; Reiners *et al.*, 2015).

In the southern part of the northern Humahuaca subbasin, most of the Tilcara Fm conglomerates represent east-flowing gravel-bed braided stream deposits, which were likely deposited on fluvially-dominated alluvial fans within the intermontane basin. In the northern part of the subbasin, the older strata of the Uquía Fm (>2.5 Ma) comprise fluvial sandstones, siltstones, and pebble conglomerates. Lacustrine deposits occur in the north and east of the subbasin between 2.5 – 2.1 Ma and are associated with finer-grained deposition and higher sediment-accumulation rates throughout the entire northern subbasin. These higher accumulation rates occur synchronously with a loss of connectivity both with the Casa Grande basin to the west on the edge of the Puna Plateau (Streit et al., 2015) and with the foreland to the east (Amidon et al., 2015). We interpret this interval of rapid, fine-grained aggradation as a response to channel defeat at the outlet of the northern outlet of the basin; a defeat that occurred as a result of increased aridity (likely due to the ranges to the east achieving threshold elevations to block moisture transport from the foreland), decreased stream power, and rock uplift along the eastern margins of the Humahuaca basin.

The first appearance of southward paleocurrents in the northern subbasin toward the end of this interval suggests that this event contributed to the integration of the northern and southern subbasins. The capture of the northern subbasin by the southern subbasin would have increased stream power at the southern outlet of the Humahuaca basin and therefore could have contributed to enabling the episodes of incision that occurred after 1.6 Ma.

The main events in the stratigraphic record of the northern Humahuaca subbasin can be explained in terms of changes in the balance of rock uplift and incision where rivers cross from the basin into the bounding ranges to the east. Regional increases in tectonic uplift rates appear to have driven the transition from foreland basin deposition of the Maimará Fm to



intermontane basin deposition of the Tilcara Fm ~4.3 Ma. On the other hand, the facies changes and increase in sediment-accumulation rates ~2.5 Ma likely resulted from increased aridity (and hence decreased stream power) limiting the ability of the river to incise through the uplifting range at the outlet of the northern subbasin, resulting in channel defeat and ponding. Comparison of different locations in the basin, including similarities and differences between the northern and southern subbasins and lateral facies changes within the northern subbasin, is essential to understanding the controls on intermontane basin evolution – from the establishment of intermontane basin conditions, to changes in sediment-accumulation rates and sedimentary facies through time, to the eventual integration of individual subbasins.

## REFERENCES

- AMIDON, W.H., LUNA, L.V., FISHER, G.B., BURBANK, D.W., KYLANDER-CLARK, A.R.C. & ALONSO, R. (2015) Provenance and tectonic implications of Orán Group foreland basin sediments, Río Iruya canyon, NW Argentina (23°S). *Basin Research*, 10.1111/bre.12139.
- BOSIO, P.P., POWELL, J., DEL PAPA, C. & HONGN, F. (2009) Middle Eocene deformation-sedimentation in the Luracatao Valley: Tracking the beginning of the foreland basin of northwestern Argentina. *Journal of South American Earth Sciences*, **28**, 142-154.
- BURBANK, D., MEIGS, A. & BROZOVIC, N. (1996) Interactions of growing folds and coeval depositional systems. *Basin Research*, **8**, 199-223.
- BYWATER-REYES, S., CARRAPA, B., CLEMENTZ, M. & SCHOENBOHM, L. (2010) Effect of late Cenozoic aridification on sedimentation in the Eastern Cordillera of northwest Argentina (Angastaco basin). *Geology*, **38**, 235-238.
- CARRAPA, B., TRIMBLE, J.D. & STOCKLI, D.F. (2011) Patterns and timing of exhumation and deformation in the Eastern Cordillera of NW Argentina revealed by (U-Th)/He thermochronology. *Tectonics*, **30**, 30.
- CARRAPA, B., BYWATER-REYES, S., DECELLES, P.G., MORTIMER, E. & GEHRELS, G.E. (2012) Late Eocene-Pliocene basin evolution in the Eastern Cordillera of northwestern Argentina (25 degrees-26 degrees S): regional implications for Andean orogenic wedge development. *Basin Research*, **24**, 249-268.
- CARRAPA, B. & DECELLES, P.G. (2015) Regional exhumation and kinematic history of the central Andes in response to cyclical orogenic processes. *Geological Society of America Memoirs*, **212**, 201-213.

- CASTELLANOS, A. (1950) *El Uquiense, Sedimentos Neogenos de Uquia (Senador Perez) en la Provincia de Jujuy (Argentina)*. Universidad Nacional del Litoral, Facultad de Ciencias Matematicas Fisicas y Quimicas y Naturales, Rosario.
- COUTAND, I., CARRAPA, B., DEEKEN, A., SCHMITT, A.K., SOBEL, E.R. & STRECKER, M.R. (2006) Propagation of orographic barriers along an active range front: insights from sandstone petrography and detrital apatite fission-track thermochronology in the intramontane Angastaco basin, NW Argentina. *Basin Research*, **18**, 1-26.
- DEEKEN, A., SOBEL, E.R., HASCHKE, M. & RILLER, U. (2005) Age of initiation and growth pattern of the Puna plateau, NW Argentina, constrained by AFT thermochronology. *Potsdam, Germany Abstract Volume, Terra Nostra*, **5** (1), 39.
- DEEKEN, A., SOBEL, E.R., COUTAND, I., HASCHKE, M., RILLER, U. & STRECKER, M.R. (2006) Development of the southern Eastern Cordillera, NW Argentina, constrained by apatite fission track thermochronology: From early Cretaceous extension to middle Miocene shortening. *Tectonics*, **25**, TC6003, doi: 6010.1029/2005tc001894.
- ECHAVARRIA, L., HERNANDEZ, R., ALLMENDINGER, R. & REYNOLDS, J. (2003) Subandean thrust and fold belt of northwestern Argentina: Geometry and timing of the Andean evolution. *AAPG Bulletin*, **87**, 965-985.
- GABALDÓN, V., M.A. GONZALEZ, M.A. & LIZUAIN, A. (1998) *El mapa geológico, Estudio geológico integrado de la Quebrada de Humahuaca*. Servicio Geológico Minero Argentino (SEGEMAR), Buenos Aires.
- GONZALEZ, M.A., PEREYRA, F., RAMALLO, E. & TCHILINGURIAN, P. (2004) Hoja Geológica 2366-IV, Ciudad Libertador General San Martín, provincias de Jujuy y Salta. *Boletín* 274, Instituto de Geología y Recursos Minerales, Servicio Geológico Minero Argentino. Buenos Aires, 109.
- GUBBELS, T.L., ISACKS, B.L. & FARRAR, E. (1993) High-level surfaces, plateau uplift, and foreland development, Bolivian central Andes. *Geology*, **21**, 695-698.
- HAIN, M.P., STRECKER, M.R., BOOKHAGEN, B., ALONSO, R.N., PINGEL, H. & SCHMITT, A.K. (2011) Neogene to Quaternary broken foreland formation and sedimentation dynamics in the Andes of NW Argentina (25 degrees S). *Tectonics*, **30**, TC2006, doi:2010.1029/2010TC002703.
- HONGN, F., DEL PAPA, C., POWELL, J., PETRINOVIC, I., MON, R. & DERACO, V. (2007) Middle Eocene deformation and sedimentation in the Puna-Eastern Cordillera transition (23 degrees-26 degrees S): Control by preexisting heterogeneities on the pattern of initial Andean shortening. *Geology*, **35**, 271-274.
- HORTON, B.K. (2005) Revised deformation history of the central Andes: Inferences from Cenozoic foredeep and intermontane basins of the Eastern Cordillera, Bolivia. *Tectonics*, **24**, TC3011, doi:3010.1029/2003TC001619.
- HUMPHREY, N.F. & KONRAD, S.K. (2000) River incision or diversion in response to bedrock uplift. *Geology*, **28**, 43-46.
- INSEL, N., GROVE, M., HASCHKE, M., BARNES, J.B., SCHMITT, A.K. & STRECKER, M.R. (2012) Paleozoic to early Cenozoic cooling and exhumation of the basement underlying the eastern Puna plateau margin prior to plateau growth. *Tectonics*, **31**, TC6006, doi:6010.1029/2012TC003168.
- JORDAN, T.E., ISACKS, B.L., ALLMENDINGER, R.W., BREWER, J.A., RAMOS, V.A. & ANDO, C.J. (1983) Andean tectonics related to geometry of subducted Nazca plate. *Geological Society of America Bulletin*, **94**, 341-361.

- JORDAN, T.E. & ALONSO, R.N. (1987) Cenozoic stratigraphy and basin tectonics of the Andes Mountains, 20°-28° South latitude. *AAPG Bulletin-American Association of Petroleum Geologists*, **71**, 49-64.
- KIRSCHVINK, J.L., KOPP, R.E., RAUB, T.D., BAUMGARTNER, C.T. & HOLT, J.W. (2008) Rapid, precise, and high-sensitivity acquisition of paleomagnetic and rock-magnetic data: Development of a low-noise automatic sample changing system for superconducting rock magnetometers. *Geochemistry Geophysics Geosystems*, **9**, Q05Y01, doi:10.1029/2007GC001856.
- KLEY, J. & MONALDI, C.R. (2002) Tectonic inversion in the Santa Barbara System of the central Andean foreland thrust belt, northwestern Argentina. *Tectonics*, **21**, 18.
- LOURENS, L., HILGEN, F., SHACKLETON, N.J., LASKAR, J. & WILSON, D. (2004) The Neogene Period. In: *A Geologic Time Scale 2004* (Ed. by F. M. Gradstein, Ogg, J.G., Smith, A.), 409-440. Cambridge University Press, Cambridge, UK.
- MARQUILLAS, R.A., DEL PAPA, C. & SABINO, I.F. (2005) Sedimentary aspects and paleoenvironmental evolution of a rift basin: Salta Group (Cretaceous-Paleogene), northwestern Argentina. *International Journal of Earth Sciences*, **94**, 94-113.
- MARSHALL, L.G., BUTLER, R.F., DRAKE, R.E. & CURTIS, G.H. (1982) Geochronology of Type Uquian (Late Cenozoic) Land Mammal Age, Argentina. *Science*, **216**, 986-989.
- MIALL, A.D. (1985) Architectural-element analysis: A new method of facies analysis applied to fluvial deposits. *Earth-Science Reviews*, **22**, 261-308.
- MIALL, A.D. (1996) *The Geology of Fluvial Deposits: Sedimentary Facies, Basin Analysis, and Petroleum Geology*. Springer, New York.
- MORENO, J.A. (1970) Estratigrafía y paleogeografía del Cretacico superior en la Cuenca del Noroeste Argentino, con especial mencion de los Subgrupos Balbuena y Santa Barbara. *Revista de la Asociación Geológica Argentina*, **25**, 9-44.
- PEARSON, D.M., KAPP, P., DECELLES, P.G., REINERS, P.W., GEHRELS, G.E., DUCEA, M.N. & PULLEN, A. (2013) Influence of pre-Andean crustal structure on Cenozoic thrust belt kinematics and shortening magnitude: Northwestern Argentina. *Geosphere*, **9**, 1766-1782.
- PINGEL, H., STRECKER, M.R., ALONSO, R.N. & SCHMITT, A.K. (2013) Neotectonic basin and landscape evolution in the Eastern Cordillera of NW Argentina, Humahuaca Basin (similar to 24 degrees S). *Basin Research*, **25**, 554-573.
- PINGEL, H., ALONSO, R.N., MULCH, A., ROHRMANN, A., SUDO, M. & STRECKER, M.R. (2014) Pliocene orographic barrier uplift in the southern Central Andes. *Geology*, **42**, 691-694.
- POPE, R.J.J. & WILKINSON, K.N. (2005) Reconciling the roles of climate and tectonics in Late Quaternary fan development on the Spartan piedmont, Greece. In: *Alluvial Fans: Geomorphology, Sedimentology, Dynamics* (Ed. by A. Harvey, A. Mather & M. Stokes), **251**, 133-152. Geological Society, London, Special Publications.
- REGUERO, M.A., CANDELA, A.M. & ALONSO, R.N. (2007) Biochronology and biostratigraphy of the Uquia Formation (Pliocene-early Pleistocene, NW Argentina) and its significance in the Great American Biotic Interchange. *Journal of South American Earth Sciences*, **23**, 1-16.
- REINERS, P.W., THOMSON, S.N., VERNON, A., WILLETT, S.D., ZATTIN, M., EINHORN, J., GEHRELS, G., QUADE, J., PEARSON, D., MURRAY, K.E. & CAVAZZA, W. (2015) Low-

- temperature thermochronologic trends across the central Andes, 21°S–28°S. *Geological Society of America Memoirs*, **212**, 215-249.
- ROBINSON, R.A.J., SPENCER, J.Q.G., STRECKER, M.R., RICHTER, A. & ALONSO, R.N. (2005) Luminescence dating of alluvial fans in intramontane basins of NW Argentina. In: *Alluvial Fans: Geomorphology, Sedimentology, Dynamics* (Ed. by A. Harvey, A. Mather & M. Stokes), **251**, 153-168. Geological Society, London, Special Publications.
- RODRÍGUEZ FERNÁNDEZ, L.R., HEREDIA, N., SEGGIARO, R.E. & GONZÁLEZ, M.A. (1999) Estructura andina de la Cordillera Oriental en el área de la Quebrada de Humahuaca, provincia de Jujuy, NO de Argentina. *Trabajos de Geología - Universidad de Oviedo*, **21**, 321-332.
- SALFITY, J.A., BRANDÁN, E.M., MONALDI, C.R. & GALLARDO, E.F. (1984) Tectónica compresiva cuaternaria en la Cordillera Oriental Argentina, latitud de Tilcara (Jujuy). *Actas del IX Congreso Geológico Argentino*, **2**, 427-434.
- SANCHO, C., PENA, J.L., RIVELLI, F., RHODES, E. & MUNOZ, A. (2008) Geomorphological evolution of the Tilcara alluvial fan (Jujuy Province, NW Argentina): Tectonic implications and palaeoenvironmental considerations. *Journal of South American Earth Sciences*, **26**, 68-77.
- SIKS, B.C. & HORTON, B.K. (2011) Growth and fragmentation of the Andean foreland basin during eastward advance of fold-thrust deformation, Puna plateau and Eastern Cordillera, northern Argentina. *Tectonics*, **30**, TC6017, doi: 6010.1029/2011TC002944.
- SOBEL, E.R., HILLEY, G.E. & STRECKER, M.R. (2003) Formation of internally drained contractional basins by aridity-limited bedrock incision. *Journal of Geophysical Research-Solid Earth*, **108**, 2344, doi:2310.1029/2002JB001883.
- STRECKER, M.R., ALONSO, R.N., BOOKHAGEN, B., CARRAPA, B., HILLEY, G.E., SOBEL, E.R. & TRAUTH, M.H. (2007) Tectonics and climate of the southern central Andes. *Annual Review of Earth and Planetary Sciences*, **35**, 747-787.
- STREIT, R.L., BURBANK, D.W., STRECKER, M.R., ALONSO, R.N., COTTLE, J.M. & KYLANDER-CLARK, A.R.C. (2015) Controls on intermontane basin filling, isolation, and incision on the margin of the Puna Plateau, NW Argentina (~23°S). *Basin Research*, n/a-n/a.
- TCHILINGUIRIAN, P. & PEREYRA, F.X. (2001) Geomorfología del sector Salinas Grandes-Quebrada de Humahuaca, provincia de Jujuy. *Revista de la Asociación Geológica Argentina*, **56**, 3-15.
- TURNER, J.C.M. (1960) Estratigrafía de la Sierra de Santa Victoria y adyacencias. *Boletín Academia Nacional de Ciencias*, **41**, 163-196.
- TURNER, J.C.M. & MON, R. (1979). *Cordillera Oriental*. Segundo simposio de geología regional argentina, Córdoba, Argentina, Academia Nacional de Ciencias Córdoba.
- UBA, C.E., KLEY, J., STRECKER, M.R. & SCHMITT, A.K. (2009) Unsteady evolution of the Bolivian Subandean thrust belt: The role of enhanced erosion and clastic wedge progradation. *Earth and Planetary Science Letters*, **281**, 134-146.
- WALTHER, A., ORGEIRA, M., REGUERO, M., VERZI, D., VILAS, J., ALONSO, R.N., GALLADO, E., KELLY, S. & JORDAN, T.E. (1998) Estudio Paleomagnetico, Paleontologico y Radimetrico de la Formacion Uquia (Plio-Pleistoceno) en Esquina Blanca (Jujuy). *Actas del X Congreso Latinoamericano de Geología y VI Congreso Nacional de Geología Economica*, **1**, 77.

## TABLES

**Table 1.** New U-Pb geochronology of volcanic ashes

| Sample      | Latitude  | Longitude | Description   | N* | Age †<br>[Ma] | 2 S.D. ‡<br>[Myr] |
|-------------|-----------|-----------|---|----|---------------|-------------------|
| HU210310-02 | -23.18648 | -65.33621 | Uquíá Fm northeast of Humahuaca                       | 30 | 2.26          | 0.12 <sup>a</sup> |
| HU210310-01 | -23.19466 | -65.33570 | Uquíá Fm east of Humahuaca, 10 m below red beds       | 30 | 2.12          | 0.14 <sup>b</sup> |
| HU290412-04 | -23.24532 | -65.38219 | SW of Humahuaca, cgl. at top of section               | 32 | 1.32          | 0.11              |
| HU290412-02 | -23.24677 | -65.36159 | SW of Humahuaca, tan sltst. & mdst.                   | 32 | 2.36          | 0.07              |
| UQ160311-01 | -23.32672 | -65.35571 | Uquíá Fm, prominent 2-m-thick ash                     | 30 | 2.49          | 0.03              |
| UQ270307-01 | -23.34922 | -65.35946 | Uquíá Fm, Chucalezna, near core of anticline          | 32 | 2.39          | 0.04              |
| UQ270307-02 | -23.35266 | -65.36858 | Uquíá Fm, Chucalezna, at base of 4-m cgl              | 30 | 2.23          | 0.07              |
| HU110411-01 | -23.39333 | -65.36413 | N. of Huacalera / S. of R. Yacoraite, Uquíá Fm sltst. | 30 | 2.37          | 0.05              |
| HU270412-01 | -23.41543 | -65.36675 | N. of Huacalera, 2-4 m thick ash in Maimará Fm        | 32 | 5.52          | 0.18              |
| HU240307-02 | -23.42866 | -65.37280 | Huacalera, Tilcara Fm cgl.                            | 36 | 3.01          | 0.05              |
| HU210307-02 | -23.42936 | -65.36377 | Huacalera, Uquíá Fm sst.                              | 30 | 2.36          | 0.12              |
| HU180411-01 | -23.42945 | -65.36304 | Huacalera, Uquíá Fm sst.                              | 32 | 2.49          | 0.06              |
| HU310310-02 | -23.42983 | -65.34039 | East of Huacalera, sst. 10 m below lakebeds           | 33 | 2.5           | 0.03              |
| HU120410-01 | -23.45759 | -65.37343 | West of Villa Perchel, Tilcara Fm, cgl.               | 30 | 3.06          | 0.04              |
| HU030410-01 | -23.46012 | -65.34193 | E. of Villa Perchel, Uquíá Fm tan sltst.              | 30 | 2.41          | 0.04              |
| HU010410-01 | -23.46116 | -65.38074 | W. of V. Perchel, Tilcara Fm, highest ash in valley   | 30 | 3.48          | 0.08              |
| HU220310-03 | -23.47255 | -65.37558 | North Angosto de Perchel, lowest ash in Tilcara Fm    | 30 | 4.42          | 0.11              |
| HU220310-01 | -23.47351 | -65.37217 | N. Angosto de Perchel, 157 m in footwall section      | 30 | 2.39          | 0.03              |
| HU170411-01 | -23.47353 | -65.38365 | N. Angosto de Perchel, top of hanging wall section    | 30 | 3.41          | 0.07              |
| HU220310-02 | -23.47442 | -65.37464 | N. Angosto de Perchel, 318 m in footwall section      | 30 | 2.25          | 0.06              |
| HU300310-02 | -23.47517 | -65.38228 | N. Angosto de Perchel, ~150 m hanging wall section    | 40 | 4.04          | 0.05              |
| HU160411-01 | -23.47568 | -65.37626 | N. Angosto de Perchel, near top of footwall section   | 30 | 1.98          | 0.12              |
| HU300310-01 | -23.47708 | -65.37851 | N. Angosto de Perchel, ~ 135 m hanging wall section   | 32 | 4.36          | 0.14              |
| HU140411-01 | -23.48589 | -65.37551 | Angosto de Perchel, 515 m in section                  | 30 | 2.43          | 0.12              |
| HU150411-01 | -23.48635 | -65.38034 | Angosto Perchel, Maimará, lowest ash, 1-3m thick      | 40 | 5.58          | 0.05              |
| WG220307-02 | -23.48679 | -65.36711 | Angosto de Perchel, above fault at base of section    | 32 | 3.89          | 0.12              |
| HU130411-01 | -23.48753 | -65.36845 | Angosto de Perchel, 100 m in section                  | 30 | 3.53          | 0.09              |
| WG230307-02 | -23.4898  | -65.38185 | Angosto de Perchel, Maimará Fm orange sst.            | 61 | 5.45          | 0.14              |
| HU260310-01 | -23.49119 | -65.38338 | Angosto de Perchel, Maimará Fm orange sst.            | 32 | 5.35          | 0.09              |
| HU070411-02 | -23.50688 | -65.39134 | S. of Arroyo Perchel, cgl. rich in Salta Gp. clasts   | 32 | 2.11          | 0.08              |
| HU070411-03 | -23.50737 | -65.39391 | N. of Juella, Maimará Fm cgl. to sst. transition      | 32 | 6.27          | 0.10              |
| HU070411-01 | -23.50883 | -65.38658 | S. of Arroyo Perchel, Tilcara Fm cgl.                 | 30 | 2.37          | 0.06              |
| HU120412-01 | -23.53194 | -65.40294 | S. of Juella, Maimará Fm cgl.                         | 32 | 6.42          | 0.09              |
| HU150412-01 | -23.56334 | -65.41281 | W. of Tilcara, thick ash, Maimará Fm orange v.f. sst. | 32 | 5.70          | 0.28              |
| HU140412-01 | -23.56684 | -65.42034 | W. of Tilcara, Maimará Fm cgl. to sst. transition     | 32 | 6.31          | 0.06              |

\* Number of zircons analyzed.

† Weighted average of the five youngest ages, corrected for initial Th disequilibrium and common-Pb.

‡ 2 × standard deviation of the five youngest ages.

<sup>a</sup> Weighted mean of youngest 3 grains because youngest 5 grains did not form a single population; we report 2SE of the weighted mean rather than 2 SD because this was greater.

<sup>b</sup> Weighted mean of youngest 4 grains because youngest 5 grains did not form a single population.

**Table 2.** U-Pb geochronology data from Streit *et al.* (2015) relevant to this study.

| Sample      | Latitude  | Longitude | Description  | N* Age† 2 S.D. ‡ |                   |      |
|-------------|-----------|-----------|--|------------------|-------------------|------|
|             |           |           |  | [Ma]             | [Myr]             |      |
| UQ160512-01 | -23.30218 | -65.3666  | above unconformity W of Uquía                            | 32               | 3.97              | 0.05 |
| UQ280307-01 | -23.30585 | -65.36925 | above unconformity W of Uquía                            | 32               | 4.12              | 0.05 |
| HU190412-01 | -23.3857  | -65.3594  | @ 200 m in Río Yacoraite section                         | 30               | 2.54              | 0.06 |
| HU230412-02 | -23.40508 | -65.33505 | in terrace NNE of Huacalera, sst. below unconformity     | 32               | 2.21              | 0.08 |
| HU230412-01 | -23.41163 | -65.32528 | in terrace NNE of Huacalera, cgl. above unconformity     | 32               | 0.87 <sup>a</sup> | 0.07 |
| HU080410-01 | -23.41936 | -65.37400 | Huacalera, Tilcara Fm above 2 <sup>nd</sup> unconformity | 32               | 3.86              | 0.04 |
| HU210307-03 | -23.43057 | -65.36928 | Huacalera, Maimará Fm below 1 <sup>st</sup> unconformity | 30               | 5.05              | 0.14 |
| HU180411-03 | -23.43132 | -65.37006 | Huacalera, Maimará Fm above 1 <sup>st</sup> unconformity | 30               | 4.38              | 0.11 |
| HU240307-01 | -23.43259 | -65.37079 | Huacalera, Tilcara Fm 5m above contact w /Mai. Fm        | 32               | 4.24              | 0.08 |

\* Number of zircons analyzed.

† Weighted average of the five youngest ages, corrected for initial Th disequilibrium and common-Pb.

‡ 2 × standard deviation of the five youngest ages.

<sup>a</sup> Age reported for HU230412-01 only includes four youngest ages.

## FIGURES

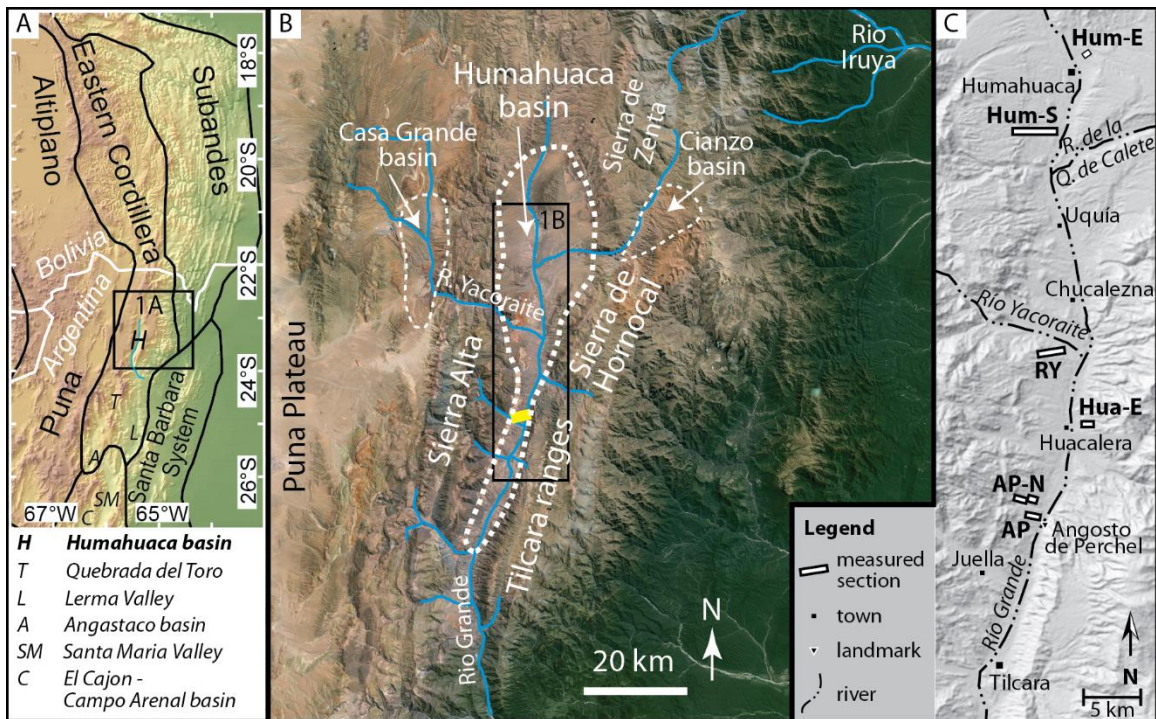


**Figure 1. Location of study area.** (A) Location of study Humahuaca basin with respect to Central Andean tectonomorphic provinces (Jordan & Alonso, 1987; Strecker *et al.*, 2007) and other intermontane basins in NW Argentina. (B) Humahuaca basin, bounding ranges, and nearby basins. Thick yellow line shows approximate boundary between northern and southern subbasins. (C) Locations of measured sections. Individual measured sections are identified with an abbreviation (bold text): Hum-E = section east of Humahuaca, Hum-S = section southwest of Humahuaca, RY = Río Yacoraite section, Hua-E = section east of Huacalera, AP-N = section 1.5 km north of the Angosto de Perchel, AP = the Angosto de Perchel section.



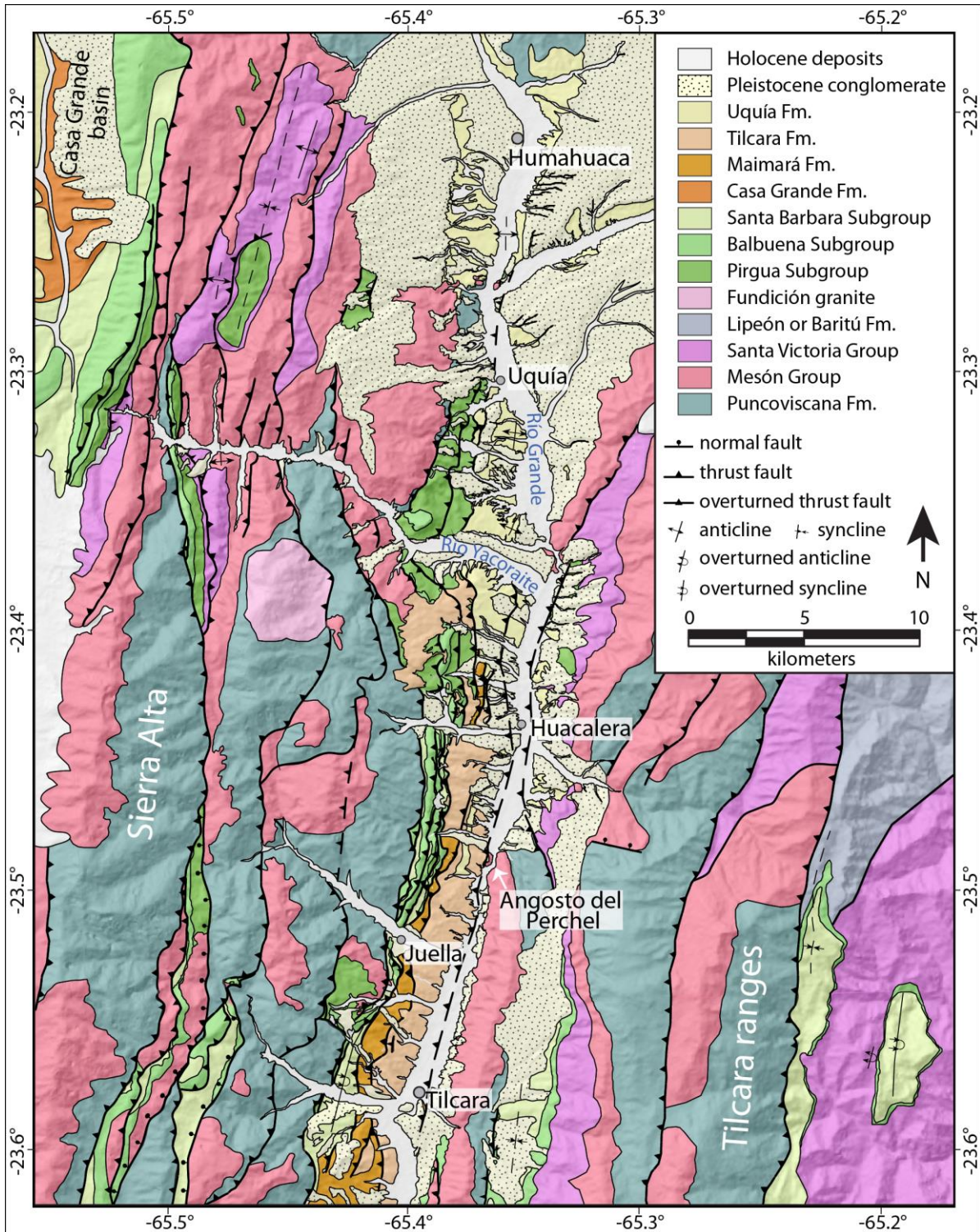


**Figure 2. Geologic map.** Based on field mapping in the Humahuaca basin and along the two transects through the Sierra Alta at the Rio Yacoraité and through the Sierra Alta and Tilcara ranges near Tilcara, and on interpretation of Google Earth satellite imagery, with reference to published maps (Gabaldón *et al.*, 1998; Rodríguez Fernández *et al.*, 1999; Gonzalez *et al.*, 2004), in the rest of Sierra Alta and Tilcara ranges.



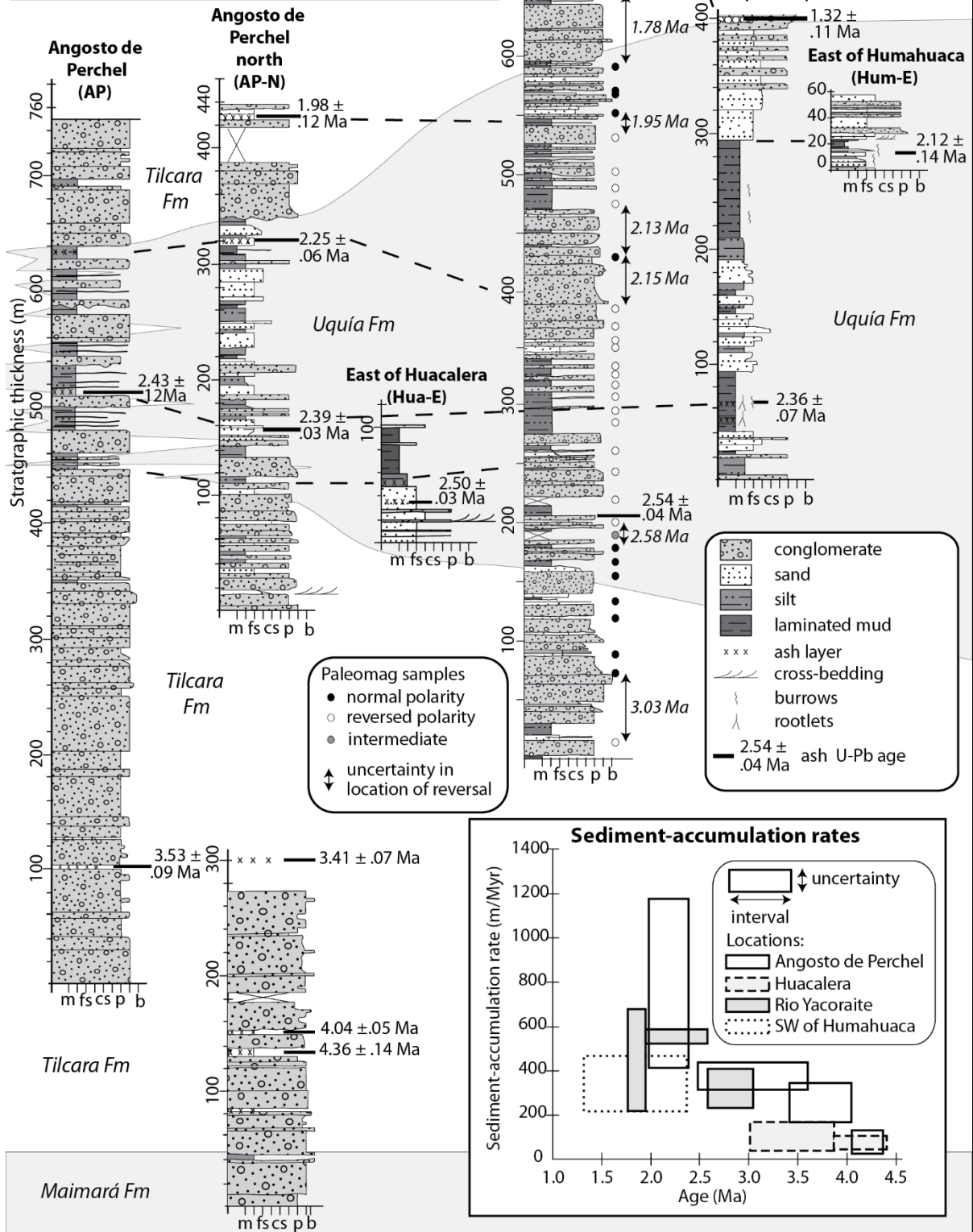
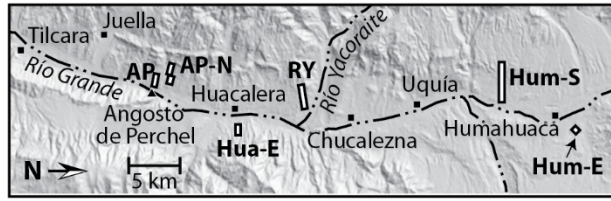


**Figure 3. Measured sections and sediment-accumulation rates.** Río Yacoraite measured section and associated data is from Streit *et al.* (2015). Locations of measured sections labelled on inset map. Ash dates are reported with  $2\sigma$  uncertainties. Dashed lines indicated correlations between sections. Gray and white background is used to indicate different stratigraphic units: Maimará Fm, Tilcara Fm, Uquíá Fm, and Quaternary conglomerates. Sediment-accumulation rates calculated by dividing the stratigraphic thickness by the age difference between two ashes or magnetic reversals; width of boxes indicate interval over which the sediment-accumulation rates are averaged and height of boxes span from minimum to maximum rates calculated based on  $2\sigma$  uncertainties on both ages and thicknesses. Note higher sediment-accumulation rates and finer-grained deposits ~2.5-2.1 Ma.

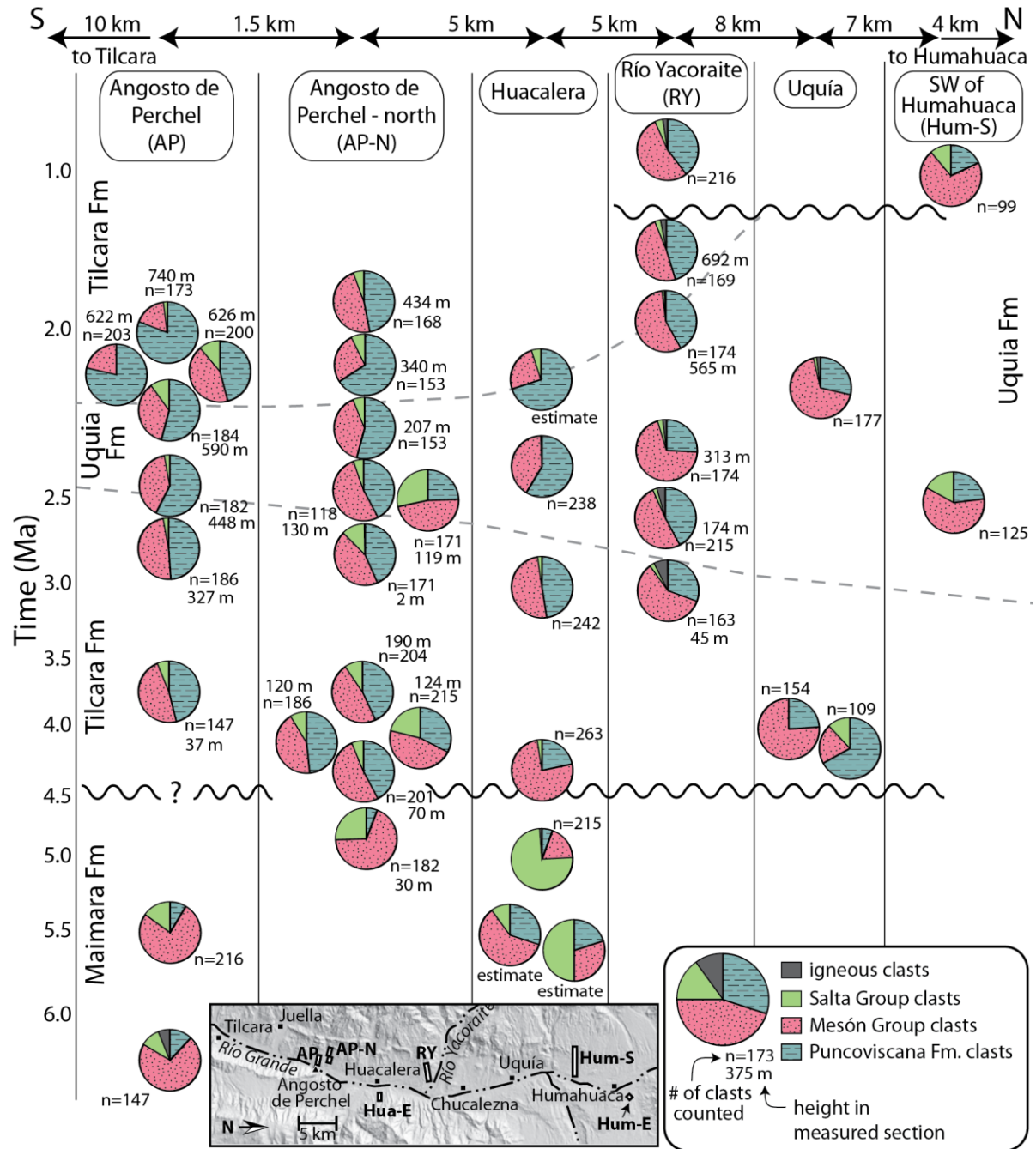


**Figure 4. Clast counts.** An abrupt increase in the abundance of Puncoviscana clasts occurs between the Maimará Fm and the Tilcara Fm North – south spatial trend in clast compositions reflect greater degree of exhumation of the Sierra Alta in the south than in the north. Increase in fraction of Puncoviscana clasts in Tilcara Fm between 4.3 Ma and 2 Ma likely reflects continuing exhumation of bounding ranges. Río Yacoraite data are from Streit *et al.* (2015).

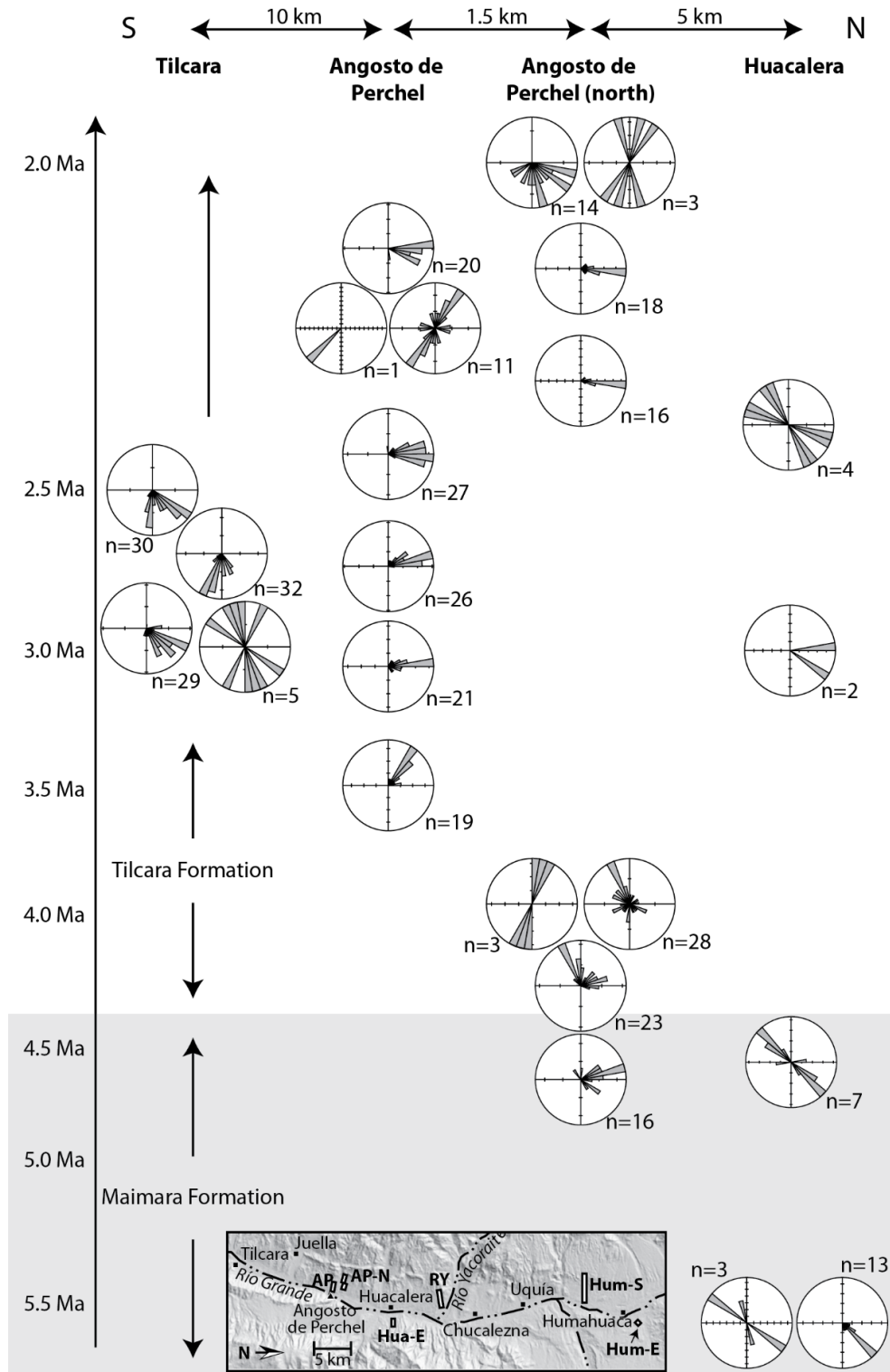


**Figure 5. Paleocurrents.** Paleocurrents inferred from channel margins (bi-directional plots), measurements of the orientation of individual moderately imbricated clasts ( $n > 4$ ), or sets of well-imbricated clasts (unidirectional plots with  $n < 5$ ). Note change from eastward paleoflow in the Maimara to initially northward paleoflow in the Tilcara formation. In the Angosto de Perchel area, southward paleoflow was established by 2 Ma, indicating integration of the northern and southern subbasins.



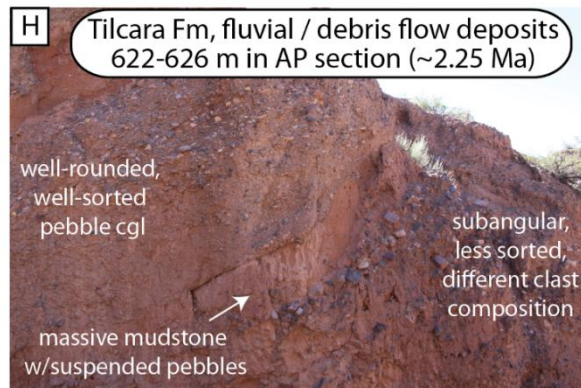
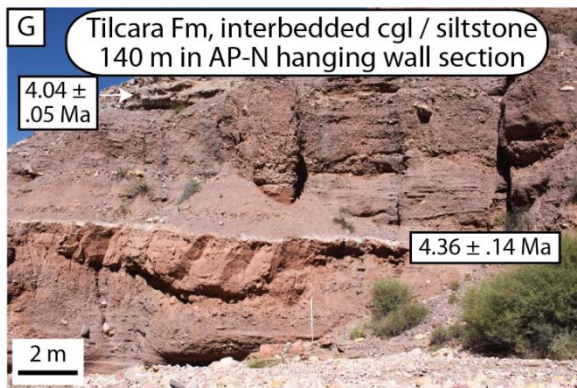
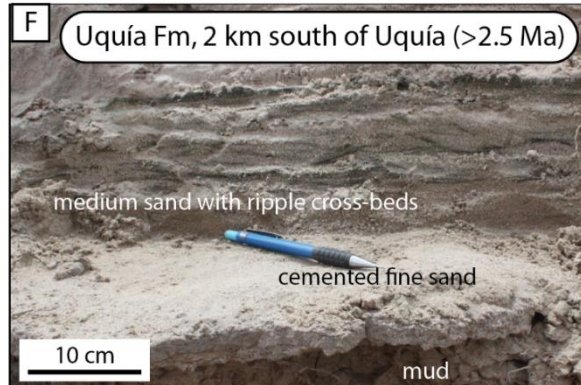
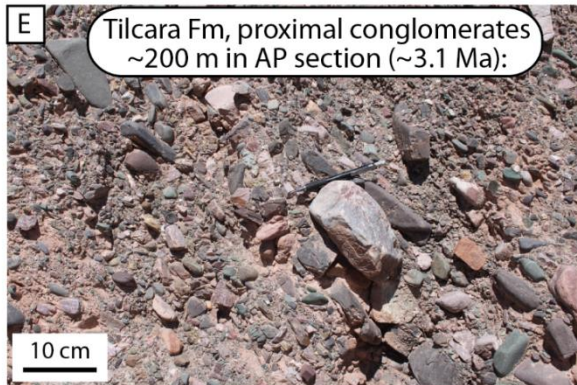
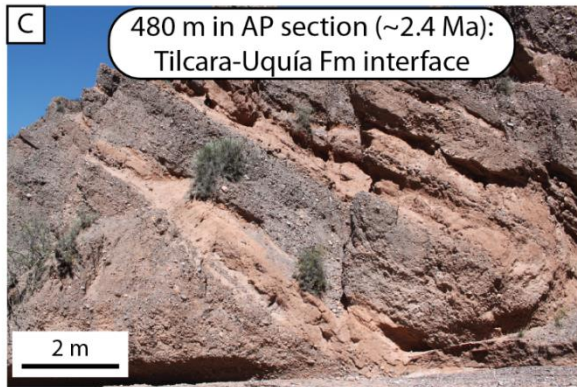
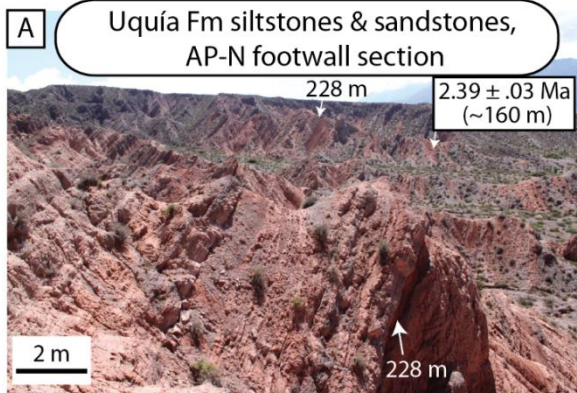


**Figure 6. Field photos of Tilcara and Uquía Formations.** (A) Uquía Fm siltstones and sandstones with 10-50 cm bedding in fine-grained interval (~2.4-2.2 Ma) of the measured section 1.5 km north of the Angosto de Perchel (AP-N). (B) Lacustrine (light gray) and fluvial (reddish) deposits of the Uquía Fm in the measured section east of Humahuaca (Hum-E). (C) Siltstones interbedded with conglomerates ~2.4 Ma in the Angosto de Perchel section (AP). (D) Lake beds in upper part (<2.5 Ma) of Uquía Fm, east of Huacalera (Hua-E). (E) Tilcara Fm in the Angosto de Perchel section (AP): moderately sorted, clast-supported rounded pebble-cobble conglomerates with weak horizontal bedding. (F) Sandstone in lower part of the Uquía Fm (>2.5 Ma), ~2km south of Uquía village. (G) Tilcara Fm in AP-N measured section: pebble-cobble conglomerate interbedded with massive siltstone – fine sandstone and ash layers. (H) Contrasting fluvial (upper) and debris flow (lower) deposits in the upper Tilcara Fm in the Angosto de Perchel measured section (AP).

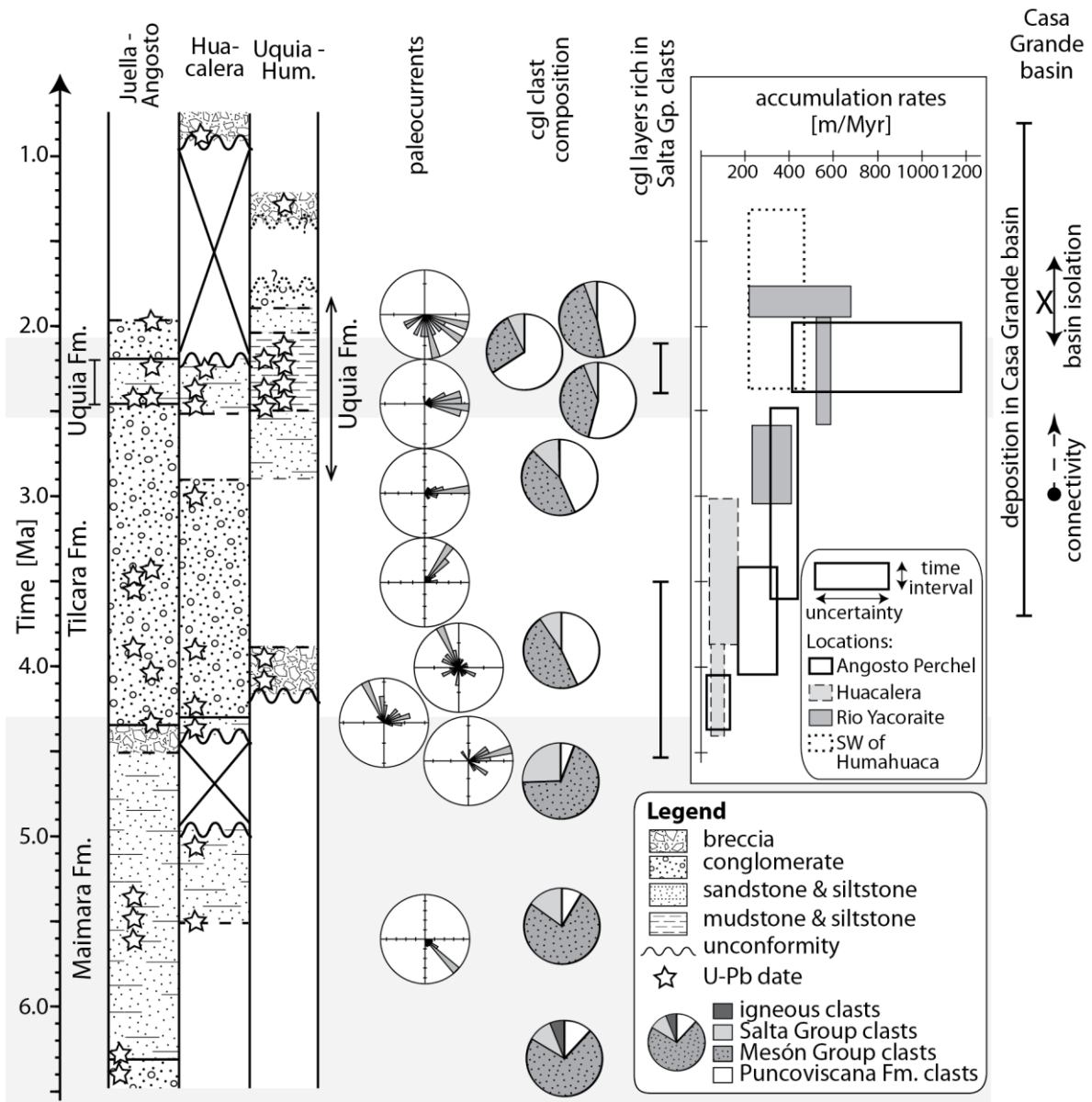


**Figure 7. Data overview.** Composite stratigraphic columns from southern (between Juella and Angosto de Perchel), central (near Huacalera), and northern (between Uquia and Humahuaca) parts of the northern subbasin. Representative paleocurrents and conglomerate clast compositions are from the Angosto de Perchel area. Stars indicate locations of radiometric dates. Transition from Maimará Fm to Tilcara Fm is characterized by abrupt changes in grain size (from silty sandstone to pebble-cobble conglomerate), paleocurrents (from east to north), and clast composition (increase in fraction of Puncoviscana clasts). Low sediment-accumulation rates and more common occurrence of conglomerate layers rich in Salta Group clasts around this time are probably related to faulting on west side of the basin. The interval between 2.5 and 2 Ma includes fine-grained deposits throughout the northern Humahuaca subbasin, an increase in sediment-accumulation rates, a greater abundance of conglomerate layers rich in Salta Group clasts, and the first observations southward paleoflow directions toward the end of this interval. Fluvial connectivity between the Casa Grande basin and the downstream Humahuaca basin was lost around the same time (by 2.1 Ma).



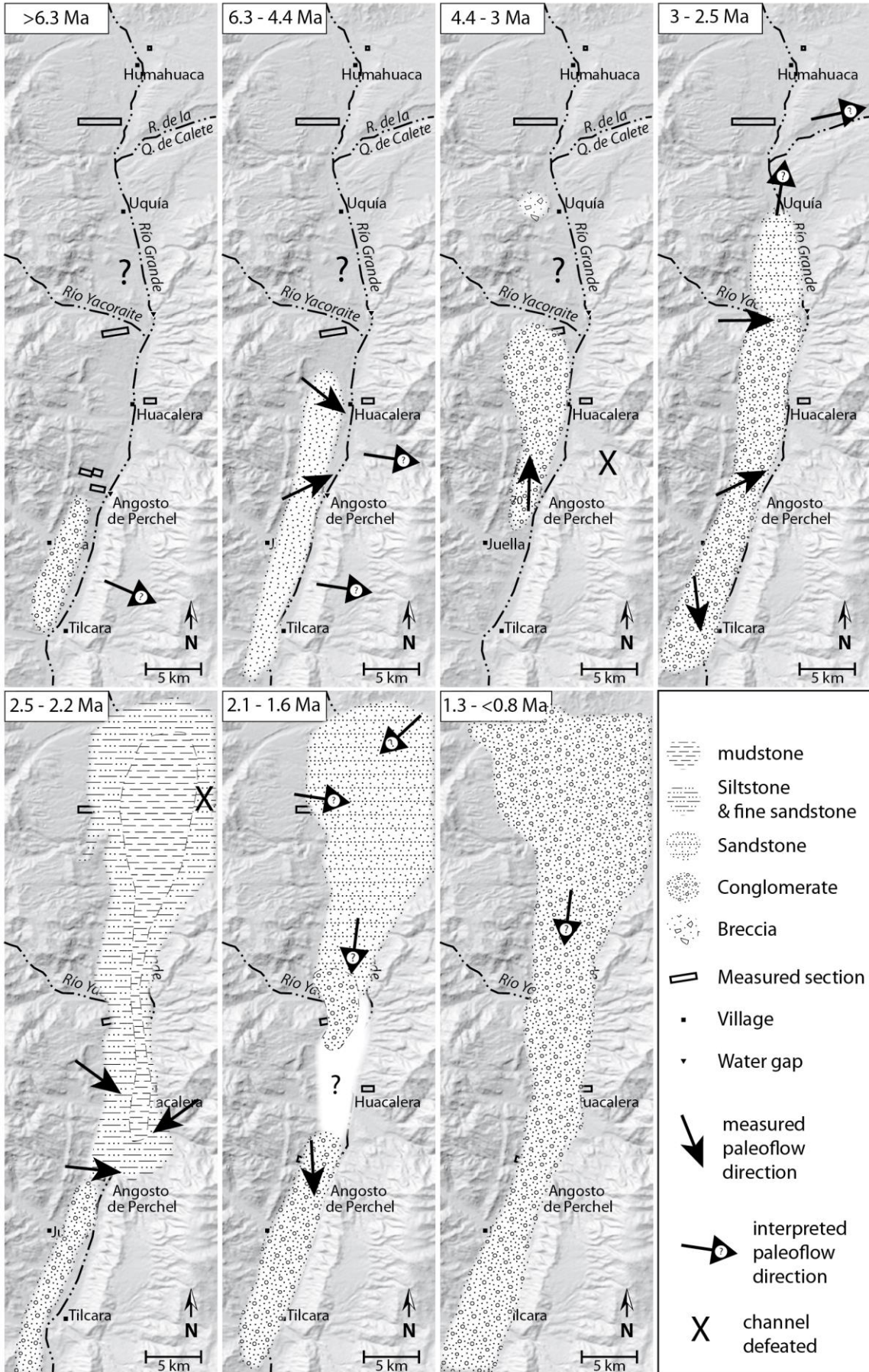




**Figure 8.** Basin evolution. (1) Deposition of lower Maimará cgl. (2) Deposition of Maimará sandstones and siltstones in east-flowing fluvial system. (3) Deposition of Tilcara Fm, paleoflow deflected northward in northern Humahuaca basin. (4) Uquía Fm fluvial sandstones deposited north of Río Yacoraite, Tilcara Fm conglomerates deposited south of Río Yacoraite. In northern Humahuaca basin (i.e. Angosto de Perchel and north) paleocurrents are primarily eastward, whereas southward paleocurrents are recorded near Tilcara (5) Finer-grained deposition throughout northern subbasin, including lacustrine deposits. Higher sediment-accumulation rates. Deposition of conglomerates continues south of Angosto de Perchel. (6) Southward paleoflow at Angosto de Perchel suggests capture of northern subbasin by southern subbasin. Coarsening upward fluvial deposits. (7) Quaternary conglomerates deposited throughout entire Humahuaca basin.

## **CHAPTER 3**

### **Neogene – Quaternary deformation in the Humahuaca basin**

#### **ABSTRACT**

The Humahuaca basin provides an excellent opportunity to explore both the controls on patterns of deformation within and at the margins of an intermontane basin in the Eastern Cordillera of NW Argentina and the relationships between this deformation and deposition in the basin. Thrust faults along the western margin of the northern Humahuaca basin expose a band of the Cretaceous-Paleogene Salta Group rocks in their hanging walls and include Neogene-Quaternary basin fill deposits in their footwalls. Inferred east-west-trending normal faults related to the Cretaceous Salta Rift result in segmentation of these north-south-trending thrust faults in the Humahuaca basin, with different styles of hanging-wall deformation along each of three segments. Multiple cross-cutting relationships with Neogene-Quaternary basin fill that contains numerous dated ash layers provides unusually tight constraints on the timing of displacement on individual faults and folds within the Humahuaca basin. Thrust faults in the basin were active from ~4.5 Ma until <1.6 Ma, coeval with the uplift of the bounding ranges to the east. Comparison with the timing of changes in sediment-accumulation rates and sedimentary facies in the basin suggests that faults in and on the western margin of the Humahuaca basin exerted a secondary control on deposition in the basin, which depended more strongly on the uplift of the bounding ranges to the east and the local climate changes associated with that uplift. The timing of deformation in the Humahuaca basin and bounding ranges is similar to the main phases of shortening and foreland fragmentation in the Eastern Cordillera and broken Salta foreland ~200 km to the south (~14 Ma, 10 Ma, ~5-4 Ma, and <2

Ma). Differences in the style and spatial distribution of deformation in these two regions may reflect differences in the position of each region relative to the Cretaceous Salta Rift and the orientation of rift-related normal faults.

## 1. INTRODUCTION

Differences in the spatiotemporal patterns of deformation and foreland basin fragmentation along the eastern flank of the southern Central Andes reflect along-strike contrasts in the pre-Andean upper crustal structure (e.g., Kley *et al.*, 1999). In the broken Salta foreland of northwest Argentina (~25°S), the Miocene contractile inversion of normal faults that developed during Cretaceous rift-basins has resulted in unsteady propagation of deformation into the foreland and the uplift of isolated ranges (Hain *et al.*, 2011; Pearson *et al.*, 2013). In contrast, farther north in the Andean foreland of Bolivia and northwest Argentina, the presence of a thick Paleozoic sedimentary cover has promoted the development of a thin-skinned fold-and-thrust belt in the Subandes (Allmendinger *et al.*, 1983). The high-elevation, high-relief ranges of the Eastern Cordillera separate the foreland from the Puna-Altiplano Plateau to the west. A contrast in the style and timing of deformation also exists between the Eastern Cordillera of NW Argentina and Bolivia. In Bolivia, deformation along thrust faults in Ordovician and Silurian rocks occurred between 40 and 15 Ma (McQuarrie, 2002; McQuarrie *et al.*, 2005), whereas the Eastern Cordillera in NW Argentina is characterized by high-angle reverse faults cutting Precambrian-Cambrian rocks, and uplift of the ranges continued until <4 Ma (Carrapa *et al.*, 2011). These contrasting styles of deformation also contribute to differences in sediment routing and storage. In the broken foreland of NW Argentina, isolated range uplift led to localized

deposition in intermontane basins (Strecker *et al.*, 2011), whereas the fold-and-thrust system in Bolivia produced extensive laterally continuous foredeep basins (Horton, 2005).

This study focuses on Late Miocene – Pleistocene deformation in the Humahuaca basin, located in the Eastern Cordillera of NW Argentina at 23-24°S latitude (Figure 1). The Humahuaca basin is one of the northernmost basins in the Argentinean Eastern Cordillera. The foreland east of the basin includes the northern limit of the thick-skinned Santa Barbara System, which is largely controlled by inversion of normal faults related to the Cretaceous Salta rift, the southern limit of the Subandean fold-and-thrust belt, and a gap in obvious foreland deformation between these two domains (Kley & Monaldi, 2002). Additionally the Humahuaca basin and its bounding ranges straddle the margin of the Cretaceous Salta Rift (Figure 1), and east-trending Cretaceous normal faults are present in the Humahuaca basin (Kley *et al.*, 2005). Given its position between these contrasting regimes, questions persist about whether the spatiotemporal patterns of deformation in the Humahuaca basin and bounding ranges are similar to those documented farther south (e.g., Carrapa *et al.*, 2011; Hain *et al.*, 2011; Pearson *et al.*, 2013), whether the lesser amount of deformation in the foreland east of Humahuaca affects the timing or amount of deformation within the basin and its bounding ranges, and what effect Cretaceous normal faults in the area had on later contractile deformation.

The timing of deformation in the Humahuaca basin is exceptionally well-constrained by U-Pb dating of ash layers interbedded with the Neogene-Quaternary strata that display cross-cutting relationships with numerous faults. This temporal framework allows the comparison of the timing of displacement on individual faults with the timing of changes in

the stratigraphic record in order to investigate the relationships between deformation and deposition in the basin.

## **2. GEOLOGIC BACKGROUND**

The central Andes of northwestern Argentina and southern Bolivia are divided into several tectonomorphic zones on the basis of morphology and structural style of deformation (Figure 1b) (Jordan *et al.*, 1983). The Puna-Altiplano plateau forms a broad area of internal drainage, high topography (4.4 km mean elevation in the Puna and 3.8 km elevation in the main Altiplano basin), and low relief (Whitman *et al.*, 1996). The plateau is bounded to the west by the magmatic arc of the Western Cordillera and to the east by the high-relief ranges of the Eastern Cordillera. Farther east, the style of foreland deformation varies along the length of the orogen, defining the tectonomorphic provinces of the Subandes (~15-23°S), the Santa Barbara System (~23-27°S), and the Sierras Pampeanas (~27-33°S). This segmentation correlates with both dip of the subducting Nazca plate (Jordan *et al.*, 1983) and older stratigraphic and structural anisotropies in the crust (Allmendinger *et al.*, 1983). The basement uplifts of the Sierras Pampeanas occur above a “flat slab” segment of the Nazca plate, whereas the Nazca plate dips 30° under the thin-skinned Subandean fold-and-thrust belt; a gradual transition in slab dip occurs between 24°S and 28°S (Jordan *et al.*, 1983; Cahill & Isacks, 1992). The position of thin-skinned fold-and-thrust-belts also correlates spatially with the occurrence of thick Paleozoic basin deposits (Allmendinger *et al.*, 1983; Kley *et al.*, 1999). Between 23.5°S and 27°S, thick-skinned deformation of the Santa Barbara System is largely controlled by inversion of normal faults related to the Cretaceous Salta rift (Kley & Monaldi, 2002). A gap in obvious foreland deformation exists between 23°S and

23.5°S (Kley & Monaldi, 2002) (Figure 1). The southern limit of thin-skinned deformation at 23°S arises from southward truncation of detachment levels in Silurian and Devonian strata (Belotti *et al.*, 1995), whereas significant reactivation of Cretaceous normal faults mainly occurs south of 23.5°S, where the trend of these faults is closer to perpendicular to the Neogene shortening direction (Kley & Monaldi, 2002).

The Humahuaca basin lies within the Eastern Cordillera of northwest Argentina between 23°S and 24°S (Figure 2). It is bounded to the west by the Sierra Alta and to the east by the Tilcara ranges, Sierra Hornocal, and Sierra de Zenta, progressively from south to north. In the southern part of the basin, the Sierra Alta separates the Humahuaca basin from the Puna plateau. In the northern part of the basin, the externally drained Casa Grande basin lies west of the Sierra Alta, and the Sierra Aguilar west of the Casa Grande basin forms the boundary between the Eastern Cordillera and the Puna plateau (Figure 2). The Sierra Alta is uplifted along a bivergent thrust and reverse fault system, with east-vergent faults throughout most of the range and west-vergent faults along the western border with the Puna plateau. The ranges east of the Humahuaca basin consist of an east-vergent thrust system (Rodríguez Fernández *et al.*, 1999). The Sierra Hornocal additionally includes the southeast-dipping Hornocal Fault, which is an inverted Cretaceous normal fault (Kley *et al.*, 2005).

These ranges bounding the Humahuaca basin expose Neoproterozoic to Paleogene rocks, including the Neoproterozoic-Lower Cambrian slates of the Puncoviscana Formation, the Cambrian quartzites of the Mesón Group, the marine sandstones and shales of the Ordovician Santa Victoria Group, and the Cretaceous-Paleogene deposits of Salta Group (Turner, 1960; Turner & Mon, 1979; Marquillas *et al.*, 2005) (Figures 3 and 4). The Salta Group includes the Cretaceous rift-related sandstones of the Pirgua Subgroup, the upper

Cretaceous – Paleocene post-rift calcareous sandstones (Lecho Fm) and marine carbonates (Yacoraite Fm) of the Balbuena Subgroup, and the fluvial and lacustrine mudstones, siltstones, and sandstones of the upper Paleocene to middle Eocene Santa Bárbara Subgroup (Moreno, 1970; Marquillas *et al.*, 2005). The study area straddles the margin of the Salta rift (Figure 1), and the variable thickness of the Pirgua Subgroup, which ranges from 0 to ~600 m throughout most of the study area and >2000 m in the hanging wall of the Hornocal Fault, is controlled by the location of Cretaceous normal faults (Rodríguez Fernández *et al.*, 1999; Kley *et al.*, 2005; Marquillas *et al.*, 2005). Upper Eocene – Upper Miocene deposits of the Oran Group are preserved in the Cianzo basin, which is bounded by the Hornocal Fault to the southeast and the Cianzo Thrust to the west (Siks & Horton, 2011).

The Neogene-Quaternary strata in the Humahuaca basin include the Maimará Fm (Salfity *et al.*, 1984; Pingel *et al.*, 2013), the Uquía Fm (Castellanos, 1950; Marshall *et al.*, 1982; Walther *et al.*, 1998; Reguero *et al.*, 2007), the Tilcara Fm (Pingel *et al.*, 2013), and younger Quaternary conglomerates (Tchilinguirian & Pereyra, 2001; Robinson *et al.*, 2005; Sancho *et al.*, 2008; Pingel *et al.*, 2013). The Maimará Fm was deposited in a foreland setting (Pingel *et al.*, 2013) between ~6.5 Ma and 4.3 Ma. The onset of deposition of the Tilcara Fm conglomerates records the establishment of intermontane basin conditions 4.4-4.2 Ma, when formerly eastward fluvial transport was deflected by uplift of the Tilcara ranges (Pingel *et al.*, 2013). The Uquía Fm comprises fluvial and lacustrine sandstones, siltstones, mudstones, and uncommon conglomerates deposited in the northern Humahuaca basin between ~3 Ma and <2 Ma (Reguero *et al.*, 2007). Quaternary conglomerates as old as 1 Ma are deposited above an unconformity with the Tilcara Fm and Uquía Fm (Pingel *et al.*, 2013; Streit *et al.*, 2015).

In the region surrounding our study, the deformation front propagated across the Eastern Cordillera from west to east between the late Eocene and the late Miocene. Late Eocene to Oligocene deformation west of the Sierra Alta is recorded by syndeformational deposits in Tres Cruces basin (Coutand *et al.*, 2001) and by K-feldspar  $^{40}\text{Ar}/^{39}\text{Ar}$  thermochronology that indicates relatively rapid exhumation and cooling ( $\sim 5^\circ\text{C}/\text{Myr}$ ) of the Sierra Aguilar 34-25 Ma (Insel *et al.*, 2012) (see Figure 2 for location of ranges). Mid-Miocene uplift and exhumation of the Sierra Alta is recorded by  $\sim 14$ -Ma apatite fission-track cooling ages in the range (Deeken *et al.*, 2006) and by changes in detrital zircon provenance in Cianzo basin, located east of Humahuaca and bounded by the Sierra Hornocal and the Sierra de Zenta (Figure 2), that indicate the loss of western sources in the Puna Plateau by  $\sim 12$  Ma (Siks & Horton, 2011). Late Miocene ( $\sim 9$  Ma) deformation in the Sierra Hornocal, along the Hornocal Fault and Cianzo Thrust, is recorded by the presence of growth strata and further changes in provenance and sedimentary facies in the Cianzo basin (Siks & Horton, 2011). Despite this earlier phase of Late Miocene deformation, Pingel *et al.* (2013) conclude that uplift of the Tilcara ranges did not disrupt eastward fluvial transport in the southern Humahuaca basin until 4.2 Ma. Farther west, a generation of out-of-sequence thrusting in the Sierra Alta occurred  $< 8.5$  Ma (Rodríguez Fernández *et al.*, 1999). Deformation within the Humahuaca basin was active from at least 4.4 Ma until  $< 90$  ka (Rodríguez Fernández *et al.*, 1999; Sancho *et al.*, 2008; Pingel *et al.*, 2013; Streit *et al.*, 2015). Deformation of the Santa Barbara System and the Zapla anticline (Figure 2) in the foreland east of the southern end of the study area is younger than 5 Ma (Reynolds *et al.*, 2000; Kley & Monaldi, 2002). To summarize, deformation propagated eastward from the Sierra Aguilar  $\sim 30$  Ma, to the Sierra Alta (west of the Humahuaca basin)  $\sim 14$  Ma, to the Sierra Hornocal (east of the Humahuaca



basin) ~9 Ma. Beginning ~5 Ma, uplift of the Tilcara ranges (east of the Humahuaca basin) began in concert with deformation in and along the western margin of the Humahuaca basin and associated renewed uplift of the Sierra Alta along, and deformation of the Santa Barbara System occurred <5 Ma. The present study focuses on the Pliocene - Quaternary phase of deformation in the Humahuaca basin and adjacent ranges.

The history of deformation in the regions to the north and south (Figure 1b) provide a broader context in which to place the structural and stratigraphic evolution of the Humahuaca basin. North of our study area, shortening within the Bolivian Eastern Cordillera occurred from 40 to 15 Ma, but then shifted into the Bolivian Subandes ~12.4 Ma (McQuarrie *et al.*, 2005; Uba *et al.*, 2009). In the Argentinian Subandes, deformation propagated across the foreland fold-and-thrust belt between 9 Ma and 2 Ma, with out-of-sequence deformation in the foreland occurring from 4.5 Ma until present (Echavarría *et al.*, 2003; Hernández & Echavarría, 2009). Provenance data from foreland basin deposits exposed along the Río Iruya, ~70 km north of study area (Figure 2), suggests tectonic reactivation of the Eastern Cordillera ~6.3 Ma and accelerated uplift of the Santa Victoria range ~4 Ma (Amidon *et al.*, 2015).

South of our study area, at 25-26°S (Figure 1), the deformation front arrived in the western Eastern Cordillera by the Late Eocene (Hongn *et al.*, 2007; Carrapa & DeCelles, 2015) and rapid exhumation of the westernmost ranges of the Eastern Cordillera occurred between ~30-15 Ma (Coutand *et al.*, 2006; Deeken *et al.*, 2006; Carrapa *et al.*, 2014b). Deformation propagated unsteadily across the broken Salta foreland, including the Eastern Cordillera and Santa Barbara System, at ~25°S in three main phases of deformation : ~13-10 Ma, ~5 Ma and <2 Ma (Hain *et al.*, 2011). Deformation in the western Santa Barbara System

began ~10 Ma and was coeval with uplift of the western ranges of the Eastern Cordillera (Coutand *et al.*, 2006; Deeken *et al.*, 2006; Carrapa *et al.*, 2011; Hain *et al.*, 2011; Pearson *et al.*, 2013). Uplift of the central Eastern Cordillera occurred ~5-4 Ma and most exhumation in the eastern ranges of the Eastern Cordillera occurred at or since 6-4 Ma (Hain *et al.*, 2011; Pearson *et al.*, 2013). Since ~2 Ma, diachronous deformation was partitioned across the entire broken foreland (Hain *et al.*, 2011).

### **3. METHODS**

#### **3.1. Geologic Mapping**

Geologic mapping (Figure 4), a magnetostratigraphy, and new radiometric dates provides constraints on the timing, amount, and style of deformation in the Humahuaca basin, Sierra Alta, and Tilcara ranges. Faults and folds displaying cross-cutting relationships with Neogene – Quaternary strata in the Humahuaca basin were mapped in the field at a 1:5,000 scale. Structural measurements in the field include ~1500 measurements of bedding orientations and 75 measurements of fault plane orientations. Two transects through the bounding ranges were mapped at a scale 1:14,000: one along the Río Yacoraite (A-A' on Figure 4) and one near the town of Tilcara (C-C'-C'' on Figure 4). Coarser mapping of the Sierra Alta and Tilcara ranges outside of these transects is based on interpretation of Google Earth satellite imagery, with reference to published studies of the area (Gabaldón *et al.*, 1998; Rodríguez Fernández *et al.*, 1999; Gonzalez *et al.*, 2004; Kley *et al.*, 2005). Ashes interbedded with the Neogene – Quaternary strata provide constraints on the timing of deformation and, in some cases, serve as marker beds that can be used to estimate the amount of displacement across a given fault.

### 3.2. Geochronology

The timing of deformation in the Humahuaca basin is constrained by zircon U-Pb geochronology from 7 newly dated ashes and 19 ashes presented in the previous two chapters of this dissertation (Table 1), as well as the magnetostratigraphy of the Río Yacoraite section presented in Chapter 1. The details of these methods are described in Chapter 1 (Streit *et al.*, 2015); a brief overview is provided below.

Zircon U-Pb geochronology was carried out with laser-ablation multi-collector inductively coupled mass spectrometry (LA-MC-ICPMS) at the University of California Santa Barbara. Measured U-Pb ratios were corrected for initial  $^{230}\text{Th}$  disequilibrium (Scharer, 1984) following the method of Crowley *et al.* (2007), and the age calculated for each analysis was corrected for common Pb using the  $^{207}\text{Pb}$  correction method with the Isoplot 3.0 Excel plug-in (Ludwig, 2012). The depositional age of each sample is approximated by the weighted mean of the five youngest concordant zircon ages to minimize the effects of protracted crystal residence time in the magma chamber or of fluvial reworking of older ashes. We conservatively report the  $2\sigma$  uncertainty on the age as twice the standard deviation of these five youngest ages.

Due to the relative paucity of ashes interbedded with the strata of the Río Yacoraite measured section, this section was dated with magnetostratigraphy (Streit *et al.*, 2015). The resulting magnetozones were correlated to the Geomagnetic Polarity Timescale (GPTS) (Lourens *et al.*, 2004) with the aid of one dated ash located just above the Gauss-Matuyama boundary.

### 3.3. Cross-sections

Geologic cross-sections (Figures 5 and 6) document the style and amount of deformation in the Humahuaca basin and bounding ranges. Cross-sections were constructed to be consistent with (i) our geologic mapping of fault and bedding orientations at the surface, (ii) the timing of activity on individual faults as constrained by cross-cutting relationships with dated ash layers, and (iii) estimates of the amount of displacement on individual faults based on the offsets both of ash layers and of stratigraphic units across faults.

The 2D kinematic modelling module of Midland Valley's Move™ software was used to construct one cross-section across the Sierra Alta, Humahuaca basin, and the western part of the Sierra Hornocal near the Río Yacoraite (along A-A') (Figure 5), and a second, shorter cross-section across the Humahuaca basin near the Angosto de Perchel (B-B') (Figure 6) (See figure 4 for locations). Iterative restoration and forward modeling of fault-parallel flow along faults and was used to balance the Río Yacoraite cross-section. Minimum depths to the main detachment under the Sierra Alta and Tilcara ranges were estimated from the maximum thickness of Puncoviscana Formation exposed in each range, combined with the stratigraphic thickness of the Cambrian-Paleogene units (Figure 3), and assuming that the top of the Santa Barbara Subgroup was near sea level prior to Andean deformation. To be consistent with previously published cross-sections in this region (Rodríguez Fernández *et al.*, 1999; Kley *et al.*, 2005), the detachment under the Tilcara ranges was constructed at a greater depth than the detachment under the Sierra Alta.

## **4. RESULTS**

### **4.1. Style of deformation in the Humahuaca basin and its bounding ranges**

#### 4.1.1. *Tilcara ranges*

The Tilcara ranges contain three main east-vergent faults that each expose 1000-4000 m of the Neoproterozoic Puncoviscana Fm in their hanging walls (Figure 4). Along transect C-C', east of Tilcara, the surface traces of these faults are spaced ~6-7 km apart and the eastern and western faults each dip 70-80° west at the surface; the middle fault is not well-exposed. At the northern end of the Tilcara ranges (transect A-A'), these faults are more closely spaced and additional fault splays are exposed (Figures 4 and 5). Cambrian quartzites overlying the Puncoviscana Fm in the hanging wall dip 30-50° west and tend to form the ridge crests of the high peaks of the range. Both gentler dips measured along the ridge crests in the Tilcara ranges and outcrop patterns observed in the satellite imagery of the Sierra Hornocal suggest broad hanging-wall anticlines.

East of these faults, Ordovician and Salta Group rocks are folded in a series of synclines and anticlines (Figure 4). Folding of the Ordovician shales and sandstones also occurs at shorter length scales (10s of meters) than mapped. Deformation and uplift extends ~45 km east of our mapped area, where a broad syncline, with anticlines on each flank forms the Valle Grande (Figure 2) (Rodríguez Fernández *et al.*, 1999).

#### 4.1.2. *Sierra Alta*

The Sierra Alta contains multiple, steeply dipping reverse faults. In our study area, most of these faults are east-vergent, with the exception of a west-vergent fault on the western edge of the range (Figures 4 and 5). Three of these east-vergent thrusts can be traced along entire length of the study area (Figure 4) where they typically display up to 3500 m of stratigraphic throw on them. An exception occurs in the transect along the Río Yacoraite, where the middle of these faults (the fault with the Fundición pluton in its hanging wall) has

<1 km of stratigraphic throw across it, and additional slip appears to have been accommodated on three relatively minor faults to its west (Figures 4 and 5). Overall, the dips of the faults within the Sierra increase from east to west, suggesting progressive rotation by forward imbrication of thrust faults.

West of Tilcara, Salta Group rocks are exposed in the hanging wall of two north-south trending normal faults (Figure 4). We interpret these two normal faults as a single normal fault that has been repeated by subsequent thrusting. Given that the Santa Barbara Subgroup (Figure 3) was involved with this normal faulting, this faulting must have occurred after the early Eocene rather than during Cretaceous rifting. In the western part of our transect along the Río Yacoraite, we interpret a fault dipping steeply west with Salta Group rocks in the hanging wall and Cambrian Meson Group rocks in the footwall to be an inverted normal fault (Figure 5). Given that it lies approximately along strike with the normal fault west of Tilcara, these could be the same normal fault.

Exhumation of the range decreases from south to north (Figure 4). In the southern portion of our field area (between the latitudes of Tilcara and Huacalera) up to 3 km of the Puncoviscana Fm are exposed in the hanging walls of these faults. North of the Río Yacoraite, the rocks exposed in the Sierra Alta consist primarily of Cambrian and Ordovician quartzites and shales as well as the rift-related sandstones and limestones of the Cretaceous-Paleogene Salta Group, with little exposure of the Puncoviscana Fm.

#### 4.1.3. *Western basin-bounding faults in the Humahuaca basin*

On the western side of the Humahuaca basin, at the eastern boundary of the Sierra Alta, a band of Cretaceous-Paleogene Salta Group rocks are thrust over the Neogene-Quaternary basin fill of the Maimará, Tilcara, and Uquía Formations (Faults C and D on

Figure 7). This system of east-vergent reverse faults can be divided into three main segments on the basis of the style of deformation (Labeled I, II, and III from south to north in Figure 7). The boundaries between these segments coincide with lateral changes in the thickness of the rift-related Pirgua Subgroup. Differences in mechanical stratigraphy arising from these thickness changes appear to be an important control on the style of deformation in the hanging wall of the main thrust. The surface dip of Fault C is similar ( $50\text{-}66^\circ$  west) along all three segments. Fault D is present only in the northern segment (III) and dips  $35\text{-}50^\circ$  west. In the following paragraphs, we describe first each segment in terms of the style of deformation (e.g., presence or absence of folding in the hanging wall and number and spacing of imbricated faults) and the Salta Group rocks present in the hanging wall; then the more complicated structures at the boundaries of these segments.

Along the southern segment (I), west of Tilcara, the Santa Barbara Subgroup is thrust over the Maimará Formation. The Salta Group rocks in the hanging wall of this fault are folded into an overturned syncline, with relatively minor displacement on a second fault that cuts the western limb of the syncline (Figures 4 and 7). Along segment I, the Pirgua Subgroup is absent, and the Balbuena Subgroup appears to lie directly above an erosional unconformity with Precambrian and Cambrian rocks. Along the central segment (II), between the village of Jueya and the southern end of Huacalera, the Salta Group rocks thrust over the Maimará and Tilcara Formations are tightly folded in the hanging walls of 3-4 closely spaced ( $\sim 200\text{-}400$  m apart) imbricated thrust faults (Figure 8a). Along this segment, the Salta Group rocks in the hanging wall include the Pirgua, Balbuena and Santa Barbara Subgroups, and the Pirgua Subgroup comprises  $\sim 200$  m of massive well-rounded cobble conglomerate composed almost entirely of quartzite clasts. Finally, the northern segment

(III), between the northern end of Huacalera and the village of Uquía, contains only two thrust sheets (Faults C and D), which carry Salta Group rocks and lack large-scale folds. Displacement on these two faults decreases to the north: ~5 km north of Uquía, ~2-Myr-old strata are folded in a broad anticline along strike with these faults, but are not faulted. The Salta Group rocks exposed in the hanging wall of the northern segment are mostly the bright red sandstones of the Pirgua Subgroup, and in some places, the overlying Balbuena Subgroup, but the Santa Barbara Subgroup is not exposed. These red sandstones are at least 450 m thick in this area, but are not found south of Huacalera. In all three segments, the band of Salta group rocks are bounded to the west by a major thrust with Paleozoic rocks (primarily Puncoviscana Formation and in places Mesón Group rocks) in the hanging wall (Fault A in Figure 7).

The regions near the boundaries between these main segments, i.e., the area west of Huacalera and the area south of Jueya, are characterized by more complicated structures. The Huacalera area (Figure 9) is of particular interest because several of the faults in this area display cross-cutting relationships with ash-bearing Neogene-Quaternary strata, providing some of our best constraints on the timing of deformation (described in the next section). On the western side of the Huacalera area (Figure 9), Fault B thrusts ~200 m of Pirgua Subgroup quartzite cobble conglomerates over other Salta Group rocks (Santa Barbara Subgroup mudstones, Balbuena Subgroup limestones, and Pirgua Subgroup sandstones) in the footwall (Figure 8d). At the southern end of the outcrop of the Pirgua cobble conglomerate, the fault between the Pirgua conglomerate and the Santa Barbara Subgroup trends east-west rather than north-south. We interpret this trend to result from a normal fault of the Cretaceous rift reactivated as a tear fault between segments II and III (Figure 8c). The Salta Group rocks in



the footwall of Fault B lie in the hanging wall of Fault C, ~900 m to the east. Also in the hanging wall of Fault C, a west-vergent backthrust places Yacoraite rocks over mudstones of the Santa Barbara Subgroup (Figure 8c). South the backthrust, in its footwall, outcrops of the Pirgua sandstone are absent and the style of deformation is similar to that in segment II: the Yacoraite formation has been tightly folded, including two well-exposed fault-propagation folds (Figures 8b and 9). East of Fault C, the southern termination of the Fault D, which thrusts Pirgua Subgroup sandstones over Plio-Pleistocene basin fill, overlaps with the northern termination of Fault E (described in more detail in the next subsection), which thrusts the Maimará Fm over the Tilcara Fm (Figure 7). We propose that the southern termination of Fault D, the backthrust in the hanging wall Fault C, and the east-west-trending fault at the southern end of the Pirgua conglomerate in the hanging wall of Fault B are all related to their position at or very near in the hanging wall of a Cretaceous normal fault (Figure 10), which segmented the Neogene-Quaternary thrusting.

The area south of Jueya marks the boundary between Segments I and II (Figure 7). Here, the hanging wall of Fault A exposes the well-rounded cobble conglomerate of the Pirgua Subgroup and the quartzites of the Cambrian Meson Group, whereas along the rest of the length of Fault A, the Precambrian Puncoviscana Fm is exposed in the hanging wall. The southern end of this area in the hanging wall of Fault A is marked by an ESE-WNW-trending shear zone in the Puncoviscana Fm at the contact with the Pirgua conglomerate. Notably, the thick cobble conglomerate of the Pirgua Subgroup is apparently not exposed south of this area in the Humahuaca basin. Thus, we interpret this shear zone as a Cretaceous rift-related normal fault that controlled the southern limit of deposition of the rounded quartzite conglomerate of the Pirgua Subgroup (Figure 10).

In sum, the suite of east-vergent thrust faults along the western margin of the Humahuaca basin are subdivided into three segments (Figure 7) that are separated by east-west-trending, rift-related faults that control the thickness of the Pirgua Subgroup in the thrusts' hanging walls (Figure 10). The northern segment (III) is characterized by the presence of the >450-m-thick bright red Pirgua sandstone and little folding. The middle segment (II) is characterized by tight folds and several closely-space thrusts. The thick bright red Pirgua sandstone is found only in the northern segment, but the lower Pirgua conglomerate is found in both the northern and central segments. The southern segment (I) contains only one thrust with Salta Group rocks in the hanging wall and the thick Pirgua deposits found in the other two segments are absent. We interpret east-west-trending faults at the boundaries between these segments as Cretaceous rift-related normal faults that control the thickness of the Pirgua Subgroup (Figure 10). We suggest that the unconformity between the Salta Group and the underlying Paleozoic rocks (Figure 10) provides a detachment horizon for Faults C and D. Hence, the style of deformation in each segment is partially controlled by the distance from the unconformity to Salta Group units with contrasting mechanical properties (see section 5.1 for further discussion).

#### 4.1.4. *Intrabasinal deformation*

Within the Humahuaca basin, the Maimará Fm, Tilcara Fm, and Uquía Fm (Figure 3) record faulting and folding since >4.4 Ma (Figure 7). In the western and central part of the basin, two main thrust faults (Faults E and F, Figure 7) accommodate east-west shortening and folding of basin strata. In the east, broad tilting records uplift of the Tilcara ranges.

Located 150 m – 1 km east of the band of thrust-displaced Salta Group rocks described in the previous section (4.1.3), Fault E thrusts Maimará Fm and overlying Tilcara

Fm strata over younger Tilcara Fm and Uquía Fm strata in the footwall (Figure 7). This fault dips 40-55° at the surface. Anticlines are common in the hanging wall, with relatively large anticlines present north of Huacalera and near the Angosto de Perchel (Figure 8e background). The total amount of exhumation of strata in the hanging wall of Fault E decreases from south to north: based on dated ashes, the age of the lowest strata exposed in the hanging wall for Fault E decreases along strike from ~6.2 Ma just north of Jueya to ~4.4 Ma in the measured section 1.5 km north of the Angosto de Perchel. In the vicinity of Huacalera (Figure 9), two fault strands appear to be related to Fault E: one that thrusts 5.5-Ma Maimará Fm strata over 3-Ma Tilcara Fm and a second more poorly exposed fault ~400 m to the east that thrusts ~3.8-Ma strata over 2.4-Ma strata.

We propose that a thrust fault that runs along the western edge of the Río Grande channel (Fault F in Figure 7) is responsible for the differential tilting of Tilcara Fm and Uquía Fm strata on the west side of the Río Grande. These strata on the west side of the Río Grande dip 20-45° to the west, whereas strata of the same age on the east side of the Río Grande near Huacalera dip <10° to the west. The fault is exposed at only a few locations: at the Angosto de Perchel, in an isolated outcrop 2 km south of the Angosto de Perchel, and on the south side of the Río Yacoraite near the confluence with the Río Grande. At the Angosto de Perchel, the fault dips 44° west at the surface. The dip of the Tilcara Fm conglomerates in the hanging wall is 30° ~200 m west of the fault and decreases to 15° ~1100 m west of the fault, dip changes that we interpret as reflecting the underlying fault flattening out at depth within the upper part of the Maimará Fm (Figure 6). From the north side of the Río Yacoraite to the southern end of the town of Uquía, the crest of a tight anticline (Figure 8g) within the Uquía Fm is aligned with the northward projection of the strike of this fault. This fault could

be the same that thrusts the Maimará strata over Quaternary gravels at the south end of Tilcara or the northward extension of the Tumbaya Fault (Salfity *et al.*, 1984; Pingel *et al.*, 2013).

In addition to these main faults, the basin fill contains evidence of deformation that we were unable to attribute to specific structures. West of the town of Huacalera, an angular unconformity that truncates the Maimará Fm records 10-15° of westward tilting of the Maimará Fm at this location prior to the deposition of the Tilcara Fm (Figure 8f). The tilted strata could represent the backlimb of an anticline, perhaps related to an early episode of folding in the future hanging wall of Fault E, or tilting could have occurred basin-wide in response to uplift of the Tilcara ranges to the east. Second, growth strata are present in the lower part of the Tilcara Fm north of the Angosto Perchel. The eastward thickening of strata between two ashes (from 2 m to 10 m over a distance of ~400 m) indicates fold growth west of this location at the time of deposition 4.3-4 Ma. Finally, the 3-10° westward tilt of lake deposits on the east side of Río Grande near Huacalera reflects relative uplift of the Tilcara ranges (as much as 500 m) since <2.5 Ma.

#### **4.2. Timing of deformation**

The zircon U-Pb geochronology of ashes interbedded with the Neogene-Quaternary basin fill at 26 sample locations, including 19 reported in the previous two chapters of this dissertation and 7 new samples (Table 1), provides constraints on the timing of faulting, folding, and differential uplift in the Humahuaca basin. Magnetostratigraphy of the Río Yacoraite measured section (Chapter 1) provides additional constraints on the timing of deformation (Streit *et al.*, 2015). The types of cross-cutting relationships used to constrain the timing of faulting include the following: (1) The youngest ash in the footwall of a thrust fault

indicates that the fault was active after that time, but tells us neither whether the fault was also active before that time nor during what interval(s) the fault was active between the deposition of the ash and present. (2) An ash that caps a fault, i.e., is present on both sides of the fault without any apparent offset, indicates that the fault has not been active since that time. (3) One or more ashes offset across a fault can be used to estimate the amount of slip on the fault over specific intervals, i.e., between the age of the older ash and the younger ash, and between the age of the younger ash and present or some other dating constraint. (4) Comparison of the elevation of an ash in the hanging wall of a fault with the elevation of nearby deposits of the same age can provide rough constraints on differential uplift due to faulting or folding since the time of ash deposition. Below, we present, in chronological order, constraints on the timing of activity on Faults A-F in the northern Humahuaca basin (Figure 7). The timing of faulting is also summarized in Figure 11. Some of the best constraints on the timing of deformation come from the area west of Huacalera (Figure 9).

Most of the displacement on faults A and B probably occurred during the earlier (Miocene) phase of deformation in the Sierra Alta, with negligible slip on these faults since 4 Ma. Fault B, which thrusts the Pirgua conglomerate over the Balbuena Subgroup west of Huacalera, has been inactive since at least  $3.80 \pm 0.05$  Ma, as indicated by a dated ash (HU190311-01) within the undeformed conglomerate above the thrust. Near Uquía, a 4.1-Ma ash (UQ280307-01) appears to be offset ~60 m vertically, which is insignificant compared to the >1.5 km of stratigraphic throw on this fault, which thrusts the Puncoviscana Fm over the Pirgua Subgroup. West of Huacalera, the same 3.8-Ma conglomerate that caps Fault B also caps Fault A ~1 km west. Hence, both faults A and B have been largely inactive since ~3.8 Ma.

The earliest unambiguous intrabasinal deformation in the northern Humahuaca basin occurred 4-5 Ma. The angular unconformity at the top of the Maimará Fm west of Huacalera indicates 10-15° of westward tilting between  $5.05 \pm 0.14$  Ma (ash HU210307-03, ~25 m below the unconformity) and  $4.38 \pm 0.11$  Ma (ash HU180411-03, <10 m above the unconformity) (Figure 8f). West of the northern end of Huacalera (Figure 9), this same unconformity lies in the footwall of Fault D, which implies displacement on Fault D after 4.3 Ma. At Huacalera, most of the displacement on Fault D likely occurred before 3.8 Ma, given that a  $3.86 (\pm .04)$ -Ma ash layer (HU080410-01) is offset <50 m vertically by this steeply dipping fault with ~2 km of slip prior to 3.8 Ma inferred from cross-section balancing. Around this time, deformation farther south is recorded by growth strata in the measured section 1.5 km north of Angosto de Perchel. The growth strata are well delineated by two ash layers whose vertical separation increases to the east and north, suggesting a growing fold southwest of this location. The lower ash (HU300310-01) is  $4.04 \pm .05$  Ma and the upper ash (HU300310-02) is  $4.36 \pm .14$  Ma.

After 3.8 Ma, the locus of deformation west of Huacalera backstepped from Fault D to Fault C, ~500 m to the west (Figure 9). Most of the slip on Fault C occurred after 3 Ma. Comparison of the offsets of a 3-Ma ash (HU240307-02 and HU190310-01) and the 3.8-Ma ash (HU080410-01 and HU190311-01) across Fault C suggests that ~100-200 m of slip occurred on this fault between 3.8 and 3 Ma, and ~800 m of slip has occurred on the fault since 3 Ma. Most of the deformation in the hanging wall of Fault C (in the footwall of Fault B) probably occurred prior to 3 Ma. For example, at Huacalera (Figure 9), the backthrust in the hanging wall of Fault C appears to be capped by conglomerates that we correlate with nearby conglomerates containing a 3-Ma ash (HU190310-01) and is also truncated by Fault

C to the east. A minor thrust fault (probably 10s – 100s of meters total displacement) in the hanging wall of C cuts these conglomerates. In segment II (south of Huacalera), the imbricated thrusts and tight folds in the hanging wall of fault C (Figure 8A) do not display cross-cutting relationships with the basin fill, but it is possible that the 4.5- to 4-Ma growth strata in the Angosto de Perchel area are related to growth of these folds.

Shortening farther east in the Humahuaca basin, on Faults E and F, occurred < 2 Ma. At Huacalera, Fault E includes 2 strands: one with the Maimará Fm (~5-4.4 Ma, HU210307-03 and HU180411-03) in its hanging wall and Tilcara Fm (3.8 – 2.9 Ma, HU180411-02 and HU200310-01) in its footwall, and the other ~250 m to the east, with Uquía Fm (<2.5 Ma, HU180411-01 and HU210307-02) in the footwall and 3.8 – 2.9 Ma Tilcara Fm in the hanging wall (Figure 9). We estimate ~600 m of slip on the western strand since 2.9 Ma and ~1700 m of slip on the eastern strand since 2.36 Ma. Farther south, near the Angosto de Perchel (Figure 8e), Fault E is represented by a single fault strand with Maimará Fm and Tilcara Fm (4.3 – 3 Ma) in the hanging wall and a  $1.98 \pm .12$  Ma ash (HU160411-01) in the footwall. Thus we conclude that Fault E was active <2 Ma. Growth of the anticline in the hanging wall of Fault E at the Angosto de Perchel appears to have begun significantly earlier, as indicated by a  $3.43 \pm .09$  Ma ash (HU290311-01) dipping ~60° SSE in the forelimb of this anticline above an angular unconformity with nearly vertical strata of the Maimará Fm that are overturned to the NNW (Figure 8e background). Approximately 2 km north of Huacalera, Fault E appears to die out (Figure 7). North of this point, Fault D, which sits ~1 km farther west, was active as recently as 1.6 Ma (the age at the top of the Río Yacoraite measured section in the footwall of this fault), where a fault with Tilcara Fm conglomerates in its hanging wall truncates this measured section. Nonetheless, even near the Río Yacoraite

section, much of the displacement on Fault D occurred prior to 3.8 Ma, as indicated by the presence of a  $3.85 \pm 0.1$  Ma ash (HU120411-01) above an unconformity with the Pirgua sandstone in the hanging wall of Fault D, as also seen in the Huacalera area ~3 km to the south. Fault F (Figure 7) is constrained to have been active  $<1.8$  Ma based on the  $1.84 \pm 0.08$  Ma ash (HU040411-01) in the footwall of this fault south of the Río Yacoraite. Farther south in the Humahuaca basin, faults that may be equivalent to Fault F were active more recently than 1.8 Ma. In the southern Humahuaca basin, a 1-Ma conglomerate dips  $10\text{-}15^\circ$  west above an angular unconformity with Tilcara Fm conglomerates that dip  $20\text{-}30^\circ$  west (Pingel *et al.*, 2013). Additionally, the thrust fault that cuts the alluvial fan south of Tilcara has ~15-20 m of vertical displacement since ~85 ka (Salfity *et al.*, 1984; Sancho *et al.*, 2008).

Based on these cross-cutting relationships with multiple dated ashes, the following sequence of faulting in the Humahuaca basin can be established (Figures 7 and 11). Following an earlier period of late Miocene deformation in the bounding ranges, Pliocene-Pleistocene deformation in the Humahuaca basin and at its western margin began ~4.5 Ma. Significant slip on Faults A and B had ceased by ~4 Ma, and it is likely that much of the slip on these faults occurred during the late Miocene phase of deformation. Strata of the Maimará Fm were tilted  $10\text{-}15^\circ$  west between 5 and 4.4 Ma. Between 4.3 and 3.9 Ma, Fault D thrust Cretaceous Pirgua Fm rocks over Pliocene Tilcara Fm strata. By 3 Ma, the locus of deformation stepped back ~500 m to the west, to fault C. On the eastern side of the Humahuaca basin, the  $5\text{-}10^\circ$  westward dip of 2.5 Myr-old lakebeds suggests ~500 m of uplift of the Tilcara ranges since 2.5 Ma. Finally, dated ashes in the footwall blocks of Faults D, E, and F indicate that these faults were active sometime after 1.6 Ma, 2.0 Ma, and 1.8 Ma, respectively.



### 4.3. Geologic cross-sections

A cross-section across the Sierra Alta, Humahuaca basin, and western part of the Tilcara ranges was constructed for the transect along the Río Yacoraite (Figure 5). Based on the maximum thicknesses of the Puncoviscana Fm exposed in the Sierra Alta and Tilcara ranges, we estimate a minimum detachment depth of 6 to 7 km b.s.l. under both ranges. Based on comparison with published sections (Rodríguez Fernández *et al.*, 1999; Kley *et al.*, 2005), we chose to put the detachment at 7 km b.s.l. in the Sierra Alta and 10 km b.s.l. in the Tilcara ranges/Sierra Hornocal. In our reconstruction, we assume that deformation occurred first in the Sierra Alta, then on the faults within the Tilcara ranges, and lastly on the faults within the Humahuaca basin. This sequencing is certainly an oversimplification, given that continued growth of the Tilcara ranges caused minor tilting (5-10°) of the lakebeds on the east side of the Humahuaca basin after 2.5 Ma, and it is likely that at least some out-of-sequence deformation occurred within the Sierra Alta (Rodríguez Fernández *et al.*, 1999). Nonetheless, most of the deformation probably occurred in this order. Siks and Horton (2011) infer that faults within the Sierra Hornocal were active at ~9 Ma, and the fact that apatite (U-Th)/He cooling ages between 5.6 - 6.1 Ma on the eastern side of the Sierra Hornocal (Reiners *et al.*, 2015) lie in the footwall of these faults suggests that exhumation of the ranges east of the Humahuaca basin was accommodated on structures that lie deeper and/or farther east than the faults shown in our cross-section. In the Sierra Alta, topographic analysis of hillslope profiles flanking the Río Yacoraite suggests that most of the Plio-Pleistocene uplift of the Sierra Alta was due to the faulting on the eastern margin of the range, rather than faulting within the range (Streit *et al.*, 2015).

We used the MOVE software to balance the eastern part of the cross-section (our labelled faults A-F and faults within the Tilcara ranges). The western part of the cross-section remains schematic; better constraints on the sequence of thrusting and additional structural data from the area to the west would be required to balance this part of the section, which includes an inverted normal fault and west-vergent thrust faults in addition to east-vergent thrusts. Our cross-section (Figure 5) implies ~2000 m of slip on Fault A and ~5000 m of slip on Fault B. Next, 1000-2000 m of slip on each of the faults in the Tilcara ranges would have resulted in tilting strata in the Humahuaca basin ~25° west. Faults C and D sole into a detachment at the base of the Salta Group, consistent with the observation that the Pirgua Subgroup in the hanging wall of Fault D is nearly parallel to the dip of the fault and with the presence of tight folds in the Salta Group in the hanging wall of Fault C along Segment II (Figure 8a). The sequence of faulting on Faults C, D, and F in the model followed the constraints on timing of deformation discussed above, but more total slip than estimated from cross-cutting relationships with ashes was needed to bring the Pirgua Subgroup to the surface at the correct location. This cross-section construction implies 2000 m of slip on Fault D, followed by 1500 m of slip on Fault C, another 3000 m of slip on Fault D and 500 m of slip on Fault F. Note that Fault F does not reach the surface here and this slip is translated into fold growth in the Uquía Fm (Figures 5 and 8G). Overall, ~7 km of shortening was accommodated on Faults C, D, and F since ~5 Ma.

A shorter schematic cross-section in the Angosto de Perchel area illustrates some key aspects of the structure in this area (Figure 6). In contrast to the northern section, imbricated thrusts and tight folds involving the Pirgua, Balbuena, and Santa Barbara Subgroups are found in the hanging wall of Fault C (Figure 8a), which here also branches from a

detachment at the base of the Salta Group. Fault E, which thrusts the Maimará Fm over the Tilcara Fm, is interpreted to originate from the same detachment level as Fault C, but with only enough displacement to expose the Maimará Fm, rather than the Salta Group, at the surface. Fault F comes to the surface along Río Grande and tilts the Tilcara Fm and the Uquía Fm west in its hanging wall. Given that the Tilcara Fm dips nearly parallel to the fault plane close to the fault and that the dip of the strata in the hanging wall decreases away from the fault, we constructed Fault F as a listric thrust fault with a detachment near the base of the Tilcara Fm. Based on this cross-section, we estimate ~900 m of slip on Fault F and ~1200 m of slip on fault E in the Angosto de Perchel area.

#### **4.4. Comparison of timing and patterns of deformation with the stratigraphic record**

As discussed in the previous chapters of this dissertation, the stratigraphic records of the Humahuaca and Casa Grande basins highlight changes at ~4.4-3.7 Ma and ~2.5-2.1 Ma. Here we compare the timing of these events with the timing of deformation in the Humahuaca basin (Figure 11). The ~4 Ma events include the abrupt changes in paleoflow direction, clast composition, and facies between the Maimará Fm and the overlying Tilcara Fm 4.3 Ma and the onset of deposition in the Casa Grande basin 3.7 Ma. The eastward paleoflow recorded in the Maimará Fm was deflected to the north in northern Humahuaca subbasin (north of the Angosto de Perchel) and to the south in the southern Humahuaca subbasin (south of Jueya) by uplift of the Tilcara ranges (Pingel *et al.*, 2013; Streit *et al.*, 2015). At the same time, grain size increased from predominantly sandstones and siltstones in the Maimará Fm to predominantly pebble-cobble conglomerates in the Tilcara Fm, and conglomerate clast compositions abruptly increased in abundance of Puncoviscana Fm and decreased in abundance of Salta Group clasts. These changes in clast composition and grain

size are attributed to renewed uplift and progressive unroofing of the Sierra Alta. The onset of deposition in the Casa Grande basin by 3.7 Ma is also related to the uplift of the Sierra Alta, but likely resulted from the combined effects of this uplift (which helped create a piggyback basin behind it (Ori & Friend, 1984)) and associated climatic changes, specifically a hypothesized increase in sediment supply due to orographically enhanced precipitation (Bookhagen & Strecker, 2008; Streit *et al.*, 2015).

The constraints on the timing of deformation in and adjacent to the Humahuaca basin supports the hypothesis that the changes in its stratigraphic record ~4 Ma result from uplift of the Tilcara ranges and Sierra Alta due to renewed deformation on faults underlying those ranges. Intrabasinal deformation in the Humahuaca basin around this time (Figure 11) includes the tilting of the Maimará Fm at Huacalera between 5 and 4.4 Ma, displacement on fault D sometime between 4.3 and 3.8 Ma, and fold growth on the west side of the basin inferred from the presence of growth strata between 4.4 and 4 Ma. Additionally, the greater abundance of cobble-boulder conglomerate layers with anomalously high fractions of Salta Group clasts 4.5 – 3.5 Ma in the western part of the basin between Tilcara and the Angosto de Perchel indicates a local source of Salta Group clasts and suggests exhumation in the hanging wall of fault C at this time. When compared to younger strata, lower sediment-accumulation rates (~100-300 m/Myr) at Huacalera and the Angosto de Perchel between 4.5 and 3.5 Ma appear to be related to deposition in the hanging walls of active faults or on the flanks of growing folds.

The interval between 2.5 and 2.1 Ma is characterized by higher sediment-accumulation rates (>500 m/Myr) and more fine-grained deposition, including lakebeds, in the northern Humahuaca subbasin (north of the Angosto de Perchel). These changes are

attributed to channel defeat and ponding at the northern outlet of the Humahuaca basin as a result of increased aridity in the rain shadow of the actively uplifting Tilcara ranges.

Previously the paleo-Río Grande may have flowed to the NE out of the northern Humahuaca basin into the Río Iruya (Fig. 1). Provenance changes in the Iruya at ~2.3 Ma are consistent with the defeat of a river that had been draining the eastern Puna Plateau (Amidon *et al.*, 2015). The loss of fluvial connectivity from Casa Grande basin to Humahuaca basin between 2.7 and 2.1 Ma, as recorded by detrital zircon provenance at the mouth of the Río Yacoraite, is also attributed to increasing aridity (Streit *et al.*, 2015). North of the Angosto de Perchel, the first southward paleocurrents are recorded at the end of this interval, suggesting that more rapid sediment-accumulation during this interval may have allowed the fill to overtop the drainage divide between the northern and southern Humahuaca subbasins, resulting in the integration of a single basin with flow towards the southern outlet.

The constraints on the timing of faulting that may have occurred around 2.5-2 Ma are not tight enough to definitively establish a relationship (nor absence of a relationship) between deformation and the changes in the sedimentary system between 2.5-2 Ma. Based on the offset of dated ashes at Huacalera, we know that fault C was active around 3 Ma and later. Additionally, between Tilcara and the Angosto de Perchel, conglomerate layers rich in Salta Group clasts suggest that fault C was likely active around 2.4-2.1 Ma. On the other hand, dated ashes in the footwalls of the faults farther east in the basin (fault F, fault E south of Huacalera, and fault D north of Huacalera) indicate these faults were active after 2 Ma, but do not indicate precisely when. If a shift in the location of deformation did in fact occur soon after 2 Ma, it is possible to speculate that faulting in center of basin had been suppressed by sediment loading during the interval of high accumulation rates and that integration of the

northern and southern subbasins ~2.1 Ma resulted in the removal of a substantial volume of sediment, thereby reducing the lithostatic load on faults in the center of the basin and making slip on these faults more favorable.

## **5. DISCUSSION**

The Humahuaca basin provides an excellent opportunity to explore the controls on the patterns of deformation within and at the margins of an intermontane basin. Multiple cross-cutting relationships with Neogene-Quaternary basin fill that contains dated ash layers provide unusually tight constraints on the timing of displacement on individual faults and folds within the basin.

The style and timing of deformation of the Humahuaca basin and its bounding ranges varies across five zones from west to east: the Sierra Alta, the basin-bounding faults on the western margin of the Humahuaca basin, the intrabasinal faults, faults within the Tilcara ranges, and faulting and folding on the east side of the Tilcara ranges. This easternmost zone is outside of our study area, but likely played a role in the uplift of the Tilcara ranges, which in the southern Humahuaca basin disrupted formerly eastward fluvial transport into the foreland around 4.2 Ma (Pingel *et al.*, 2013). In the discussion below, we focus on deformation both on the western margin of and within the northern Humahuaca basin, where we have the most structural data and the best constraints on timing of deformation.

### **5.1. Controls on the style of deformation in the Humahuaca basin**

Thrust faults along the western margin of the northern Humahuaca basin expose a band of the Cretaceous-Paleogene Salta Group rocks in their hanging walls and include Neogene-Quaternary basin fill deposits in their footwalls. This set of faults can be divided

into three segments in the northern Humahuaca basin based on variations in the style of deformation along strike (Figure 7). Along the southern segment (I), a syncline in the Santa Barbara and Balbuena Subgroups lies in the hanging wall of a single reverse fault (Fault C). In the central segment (II), the hanging wall of fault C comprises three closely-spaced imbricated faults and tightly folded Salta Group rocks, including the cobble conglomerate of the Pirgua Subgroup, the carbonates and interbedded shales of the Balbuena Subgroup, and the siltstones of the Santa Barbara Subgroup. The northern segment (III) contains only two thrust sheets (Faults C and D), which mostly consist of the bright red Pirgua sandstone and lack large-scale folds. The boundaries between these three segments coincide with WNW-striking Cretaceous normal faults that control the thickness of the rift-related Pirgua Subgroup in the hanging wall. At Huacalera, the boundary between the northern and central segments marks the southern limit of the bright red Pirgua sandstones, and the area south of Jueya, the boundary between the central and southern segments, marks the southern limit of the Pirgua cobble conglomerate.

We propose that these normal faults and the associated graben-filling strata (Figure 10) influence the style of deformation along this band of Salta Group rocks in three ways. First, these faults control lateral changes in the thickness of units with different mechanical properties. The interbedded carbonates and shales of the Balbuena Subgroup form tight folds via flexural slip between these layers, whereas the thick cobble conglomerate of the Pirgua Subgroup forms multiple shear zones several meters-thick with highly fractured clasts, and deformation of the Pirgua sandstones appears to be localized on discrete faults with little folding or shearing in the hanging wall. Second, the unconformity at the base of the Salta Group appears to serve as a detachment horizon for Faults C and D. Thus, the depth to the

detachment is deepest in the northern segment (III) and shallowest in the southern segment (I). Activation of these potential detachment horizons may have been favored by the ~25° westward tilting of strata in the Humahuaca basin by earlier thrusting on the faults in the Tilcara range, as suggested by the cross-section constructed near the Río Yacoraite. Third, these normal faults were reactivated as tear faults between the segments.

## **5.2. Relationships between faulting and deposition**

Faults in and on the western margin of the Humahuaca basin exert a secondary control on deposition in the basin; the primary control being the uplift of Tilcara ranges to the east and local climate changes associated with that uplift. Uplift of the Tilcara ranges deflected formerly eastward paleoflow to create an elongate intermontane basin ~4.3 Ma (Pingel *et al.*, 2013). After 4.3 Ma, the rate of sediment-accumulation and the basin's fluvial connectivity with the foreland depended both on the balance of rock uplift in the Tilcara ranges and the river's ability to incise through the range at the outlet(s) of the basin and on subsidence driven by thrust loading along the basin's western margin. The interval of fine-grained deposition and high sediment-accumulation rates in the northern Humahuaca subbasin resulted when increased aridity in the rain shadow of the uplifting Tilcara ranges (Pingel *et al.*, 2014) apparently reduced the river's ability to incise through the uplifting range, causing ponding in the northern subbasin. Such aridification can occur even in the face of regional increases in precipitation (Fedorov *et al.*, 2013), when rain shadows intensify in the lee of growing orographic barriers (Bookhagen & Strecker, 2008).

Faults on the western side of the Humahuaca basin exert key controls on deposition in Casa Grande basin and on some aspects of transition from the Maimará Fm to the Tilcara Fm. Displacement on these faults caused renewed uplift of the Sierra Alta, which promoted



deposition in the Casa Grande basin beginning ~3.8 Ma (Streit *et al.*, 2015) and drove distinct compositional contrasts between the Maimará Fm and Tilcara Fm as the Humahuaca basin was cut off from sources on the Puna Plateau ~4.3 Ma (Pingel *et al.*, 2013).

Within the Humahuaca basin, these faults on the western margin of the Humahuaca basin can both influence local sediment-accumulation rates near the fault and affect local sediment sources. In the first case, even though basin-wide sediment-accumulation rates depend primarily on the balance between uplift and incision at the outlet through the Tilcara ranges, local sediment-accumulation rates near an active fault within the basin will depend on whether deposition is occurring in the hanging wall or footwall of the fault. For example, the relatively low sediment-accumulation rates in the Huacalera area around 4 Ma may be a result of some continued uplift and erosion in the hanging wall of fault D. In the second case, faulting can affect local sources of sediment to the basin by exposing different lithologies in the hanging wall, by increasing the rate at which coarse material is shed from the hanging wall into the basin, or by modulating the evolution of tributary catchment areas via changes in rock-uplift rate. For example, stratigraphic intervals with a greater abundance of conglomerate layers rich in Salta Group clasts seem to broadly correlate with independent evidence for activity on faults with Salta Group in their hanging walls. More speculatively, the Puncoviscana-dominated conglomerate that was deposited in the Angosto de Perchel area around 2.1 Ma could be related to decreased activity on western faults, as deformation shifted into the basin, allowing streams to incise through the uplifted Salta Group rocks and increase the catchment size to include more Puncoviscana Fm.

Both the stratigraphy and deformation vary along strike in the intermontane Humahuaca basin. Between 4.3 and 2.1 Ma, the basin fill was apparently deposited in two

subbasins, which can be distinguished by the maximum extent of Uquía Fm deposits (2.5-2.1 Ma) and by the initial deflection ~4.3 Ma of flow to the south in the southern subbasin (Pingel *et al.*, 2013) and to the north in the northern subbasin (Chapter 2). The faults on the western margin of the Humahuaca basin (Faults A-D), are divided into three segments along strike by Cretaceous normal faults as discussed above. This structural segmentation, however, does not appear to control the divide between the northern and southern Humahuaca subbasins. That divide occurs in the middle of fault segment II between (Jueya and the Angosto de Perchel), rather than at one of the boundaries between the fault segments, i.e., west of Huacalera or NW of Tilcara. Another north-south change in deformation in the Humahuaca basin is a decrease in the amount of exhumation on faults E and F (Figure 7) from south to north. The age of the oldest strata exposed in the hanging wall of fault E decreases from 6.4 Ma west of Tilcara to 4.4 Ma. In the hanging wall of fault F, at the Angosto de Perchel, an ash (WG220307-02) within 1 m of the fault was dated to  $3.9 \pm 0.12$  Ma and an ash (HU130411-01) 100 m stratigraphically higher in the section was dated to  $3.5 \pm 0.09$  Ma, whereas the lowest reversal in the Río Yacoraite magnetostratigraphic section is 3.04 Ma such that the base of the oldest strata lying above fault F (and 75 m below the reversal) are likely to be no older than 3.1 Ma (Streit *et al.*, 2015). Farther north of the Río Yacoraite, fault F is not seen at the surface, and instead Uquía Fm (~3-2.5 Ma) strata form a tight anticline along strike with the fault. The decrease in exhumation from south to north along faults E and F suggests that these faults propagated northward through time. The amount of exhumation in the Sierra Alta also decreases from south to north, with up to 3 km of the Precambrian Puncovsicana Fm exposed south of the Río Grande and mostly Cambrian and Ordovician strata exposed north of the Río Yacoraite. This northward decrease in

exhumation could result from more of the deformation north of the Río Yacoraite being taken up east of the Humahuaca basin, perhaps on the Hornocal Fault. The north-to-south increase in uplift of the Sierra Alta could have contributed to north-to-south increase in grain size in the northern Humahuaca basin, i.e., mostly Tilcara Fm conglomerates south of Río Yacoraite and mostly Uquía Fm sandstones and siltstones north of the Río Yacoraite, because areas with greater relief and/or greater rock uplift rates would have provided more coarse-grained material.

### **5.3. How intrabasinal/basin margin deformation is recorded in sedimentary record**

The manner in which deformation is recorded in the basin fill depends in part on the relative rates of sediment-accumulation and structural uplift within the basin. If the basin-wide sediment-accumulation rate is high relative to the rate of uplift in the hanging wall of a thrust or reverse fault, then deposition and preservation of sediment in the hanging wall is more likely. In this case, syndeformational strata with interbedded ashes may be preserved in both the hanging wall and footwall, and can be used to calculate the amount of offset across the fault over different time intervals. For example, at Huacalera, the offsets of two ashes across fault C, provide an estimate of ~200 m of slip between 3.8 Ma and 3 Ma (~1 km/Myr) and ~1000 m of slip since 3 Ma. If basin-wide sediment-accumulation rates are lower than the rock-uplift rate in the hanging wall, no sediment will be deposited in the hanging wall. In this case, ashes preserved high in the footwall indicate that faulting was active after the deposition of the ash, but do not provide further constraints on the timing of deformation. Higher rock-uplift rates are also more likely to produce more sediment from sources in the hanging wall of the thrust. The more common occurrence of cobble-boulder conglomerate layers with an unusually high abundance of Salta Group clasts during the intervals 4.5-3.5

Ma and 2.4-2.1 Ma likely reflects higher rock-uplift rates on faults with Salta Group rocks in their hanging walls, i.e., faults C or D.

Intrabasinal deformation can also be recorded by growth strata. The only instance of growth strata that we observed in the Humahuaca basin was near the Angosto de Perchel, where we observed eastward thickening of conglomerates between two ash layers. Given the persistent syndeformational deposition, growth strata likely exist at other locations, but their identification is obscured by the difficulty of following bedding in the conglomerates of the Tilcara Fm over sufficient distances to identify changes in thickness. The dips of strata in the hanging wall of fault F do decrease away from the fault, which could be interpreted as growth strata. However, given the lack of clear stratal thickening, we instead interpret this as folding that reflects the underlying geometry of the fault. Growth strata are typically associated with fold growth, so it is not surprising that we observe growth strata in an area with folding in the hanging wall of fault C (segment II).

#### **5.4. Relationship to regional spatiotemporal patterns of deformation**

The timing of deformation in the Humahuaca basin and bounding ranges is similar to the timing of the main phases of deformation in the broken Salta foreland ~ 200 km to the south (~24.5-27°S). In both areas, deformation arrived at the border between the eastern margin of the Puna plateau and the Eastern Cordillera, e.g., the Sierra Aguilar west of the Sierra Alta, in the Late Eocene (Coutand *et al.*, 2001; Deeken *et al.*, 2006; Hongn *et al.*, 2007; del Papa *et al.*, 2013; Carrapa *et al.*, 2014b; Carrapa & DeCelles, 2015). Exhumation of the western ranges of the Eastern Cordillera, e.g., the Sierra Alta west of the Humahuaca basin and the ranges west of the Angastaco basin, occurred around ~15-10 Ma (Coutand *et al.*, 2006; Deeken *et al.*, 2006; Mortimer *et al.*, 2007; Pratt *et al.*, 2008; Carrapa *et al.*, 2011;

Insel *et al.*, 2012). Around 10 Ma, the deformation front of the broken foreland jumped ~75 km east to the Metán range and the Mojotoro range east of Salta (Hain *et al.*, 2011; Pearson *et al.*, 2013), and deformation in the Humahuaca area stepped ~15 km east into the Sierra de Hornocal (Siks & Horton, 2011). In both regions, this eastward shift in deformation involved the reactivation of Cretaceous normal faults as high-angle reverse faults. In the Salta foreland, deformation then propagated westward (Pearson *et al.*, 2013). Most of the exhumation of the ranges west of Salta occurred after 4-6 Ma (although deformation in this area is recognized as early as 10 Ma), and uplift of the central ranges of the Eastern Cordillera ~5-4 Ma compartmentalized the Salta foreland into discrete depozones (Bywater-Reyes *et al.*, 2010; DeCelles *et al.*, 2011; Hain *et al.*, 2011; Pearson *et al.*, 2013). The timing of exhumation and uplift of the ranges east of the Humahuaca basin is similar: apatite (U-Th)/He ages from the eastern side of the Sierra Hornocal record exhumation 5.6-6 Ma (Reiners *et al.*, 2015) and uplift of the Tilcara ranges compartmentalized the Humahuaca intermontane basin from the foreland 4.2-4.2 Ma (Pingel *et al.*, 2013). The uplift of the Tilcara ranges at this time was coeval with the deformation within the Humahuaca basin that this study focuses on. Uplift of the Tilcara ranges continued at least until <2.5 Ma and deformation within the northern Humahuaca basin continued at least until 1.6 Ma, with some deformation occurring as recently as ~85 ka (Salfity *et al.*, 1984; Sancho *et al.*, 2008). Most evidence of faulting in the Humahuaca basin clusters around 4.5-3.5 Ma on its western margin of the basin and <2 Ma in its center, 1-2 km farther east (Figure 11). This apparent clustering could truly reflect two pulses of deformation or could be an artifact of how deformation is recorded in the sedimentary record. The interpretation of a separate, younger pulse of deformation would match the timing of the final <2 Ma phase of deformation in the

broken Salta foreland, in which deformation was distributed across the entire foreland, including the eastern ranges of the Santa Barbara System (Hain *et al.*, 2011). Although the timing of deformation in the Humahuaca area is similar to the timing of deformation in the Salta area, deformation in the Salta area was distributed over a width of ~150 km, whereas in the Humahuaca area, deformation spanned ~75 km. In the broken Salta foreland, foreland deformation spread across the Cretaceous Salta rift (Figure 1), where inversion of normal faults promoted uplift of isolated ranges. In the Humahuaca area, on the other hand, a lack of favorably oriented normal faults in the foreland (Kley & Monaldi, 2002) apparently resulted in deformation remaining localized in the Eastern Cordillera for the most part.

The late Miocene-Quaternary deformation in the Humahuaca basin could be considered a phase of “out-of-sequence” deformation, because earlier deformation had already occurred to the east in the Sierra Hornocal and farther east in the foreland <100 km to the north by ~9 Ma (Echavarría *et al.*, 2003; Siks & Horton, 2011). Considering that deformation in the Humahuaca area appears to be more closely tied to the broken foreland to the south than to the fold-and-thrust belt farther north, an “out-of-sequence” characterization may be inappropriate (Strecker *et al.*, 2011). Uplift on structures east of our field area resulted in significant uplift and exhumation of the Tilcara ranges during Plio-Pleistocene deformation, but this phase of deformation in the Humahuaca basin appears to have contributed less to shortening and uplift than did the earlier phase of Miocene deformation in the Sierra Alta.

Structural inheritance, especially related to the normal faults of the Cretaceous Salta rift, is an important control on the structural evolution of the Eastern Cordillera at a variety of scales. At the scale of tectonomorphic provinces, the extent of the Salta rift and the

distribution of normal faults controls the extent of the Santa Barbara System and the style of deformation within this province. At the scale of individual basins and ranges, inversion of normal faults striking perpendicular to the direction of shortening control the uplift of isolated ranges and the creation of intermontane basins in the broken Salta foreland. In the range east of the Humahuaca basin, inversion of the Hornocal Fault with a vertical displacement of ~6500 m led to the development of intermontane basin conditions in the Cianzo basin ~9 Ma (Kley *et al.*, 2005; Siks & Horton, 2011). Within the Humahuaca basin, the presence of normal faults controls lateral variations in the style of deformation over length scales of a few kilometers. Because the Humahuaca basin straddles the margin of an arm of the Salta rift (Figure 1) (Marquillas *et al.*, 2005), it contains E-W-trending normal faults, as well as N-S-trending normal faults. The steepness of the faults in the Sierra Alta may be related to reactivation of crustal weaknesses along the SSW-striking margin of the Salta rift. Within the Humahuaca basin, rift-related sediment thickness and mechanical properties related to WNW-striking normal faults control both the segmentation and deformational character of SSW-striking thrust faults on the western margin of the basin.

## **6. CONCLUSIONS**

This study provides exceptional time control on a series of closely spaced thrust faults in the Humahuaca basin in the Eastern Cordillera of NW Argentina. Detailed geologic mapping reveals along-strike variations in the style of deformation, which appear to be controlled by segmentation due to E-W-trending Cretaceous normal faults of the Salta Rift. To provide insight into the relationship between deposition and both intrabasinal deformation and uplift of the bounding ranges, new constraints on the timing, style, and amount of

deformation are combined with the stratigraphic record of changes in fluvial connectivity across the bounding ranges, sediment-accumulation rates, and depositional environments. Dozens of U-Pb dates on volcanic ashes interbedded with the basin fill provide clear temporal constraints on the structural and stratigraphic evolution of the Humahuaca basin. Comparison of the Humahuaca basin's history with the development of the Eastern Cordillera and foreland deformation in nearby regions reveals broad similarities between the timing of deformation in the Humahuaca basin and the broken Salta foreland at ~25°S. Key findings of this study include the following:

1. Individual faults in the Humahuaca basins are constrained to have been active from ~4.5 Ma until <1.6 Ma, coeval with the uplift of the Tilcara range to the east.
2. The variation in the style of deformation in the Humahuaca basin and the bounding ranges depends on the depth to the detachment of the thrust faults, the mechanical properties of the rocks in the hanging wall, and the influence of pre-existing weaknesses and heterogeneities in the crust related to Cretaceous rifting. In particular, the style of deformation (e.g., the presence or absence of folding, and deformation along a single fault versus multiple faults) in the hanging walls of thrust faults on the western margin of the basin varies along strike due to segmentation by E-W-trending Cretaceous normal faults. These inferred normal faults controlled the thickness of the rift-related Pirgua Subgroup in their hanging walls. Because these faults apparently originate from a detachment near the base of the Salta Group, this variation in the thickness of the Pirgua Subgroup conspires with the contrasting mechanical properties of the different subgroups of the Salta Group to create different styles of deformation in each of the three segments.



3. Faulting along the Humahuaca basin's western margin drove uplift of the Sierra Alta that contributed to changes in clast composition and grain size between the Maimará Fm and the Tilcara Fm ~4.3 Ma and resulted in sediment accumulation in the Casa Grande basin, west of the Humahuaca basin, from 3.8 to 0.8 Ma. On the other hand, faulting within the Humahuaca basin itself was only a secondary control on deposition in the basin because accommodation space was more strongly controlled by the balance of uplift and incision at the outlet of the basin, where the river traversed the ranges to the east prior to channel defeat ~2.5 Ma.
4. The timing of deformation in the Humahuaca basin and bounding ranges matches the timing of deformation in the Eastern Cordillera and broken foreland ~200 km to the south (~24-27°S). Deformation at the boundary between the Puna Plateau and the Eastern Cordillera (Sierra Aguilar in the Humahuaca area) occurred in the Late Eocene – Oligocene, and the main phase of exhumation of the western ranges of the Eastern Cordillera (Sierra Alta) occurred ~14 Ma. Deformation subsequently shifted eastward into the easternmost ranges of the Eastern Cordillera (Tilcara ranges and Sierra Hornocal) ~10 Ma. Approximately ~5 Ma, deformation stepped back into the central Eastern Cordillera (deformation in the Humahuaca basin) and range uplift (Tilcara ranges) compartmentalized intermontane basins from the foreland. A final phase of deformation < 2 Ma included deformation across the entire broken foreland at ~25°S and a subtle shift in the location of deformation within the Humahuaca basin. The narrower width over which deformation occurred in the Humahuaca basin compared to the Salta foreland results from its position on the margin of the Salta rift.

## REFERENCES

- ALLMENDINGER, R.W., RAMOS, V.A., JORDAN, T.E., PALMA, M. & ISACKS, B.L. (1983) Paleogeography and Andean structural geometry, Northwest Argentina. *Tectonics*, **2**, 1-16.
- AMIDON, W.H., LUNA, L.V., FISHER, G.B., BURBANK, D.W., KYLANDER-CLARK, A.R.C. & ALONSO, R. (2015) Provenance and tectonic implications of Orán Group foreland basin sediments, Río Iruya canyon, NW Argentina (23°S). *Basin Research*, 10.1111/bre.12139.
- BARROS, A.P., KIM, G., WILLIAMS, E. & NESBITT, S.W. (2004) Probing orographic controls in the Himalayas during the monsoon using satellite imagery. *Natural Hazards and Earth System Sciences*, **4**, 29-51.
- BELOTTI, H.J., SACCAVINO, L.L. & SCHACHNER, G.A. (1995) Structural Styles and Petroleum Occurrence in the Sub-Andean Fold and Thrust Belt of Northern Argentina. In: *Petroleum Basins of South America: AAPG Memoir 62* (Ed. by A. J. Tankard, R. S. Soruco & H. J. Welsink), 545-555.
- BOLL, A. & HERNÁNDEZ, R.M. (1986) Interpretación estructural del área Tres Cruces. *Boletín de Informaciones Petroleras, Tercera Época*, **3**, 2-14.
- BONORINO, G.G. & ABASCAL, L.D. (2012) Drainage and base-level adjustments during evolution of a late Pleistocene piggyback basin, Eastern Cordillera, Central Andes of northwestern Argentina. *Geological Society of America Bulletin*, **124**, 1858-1870.
- BOOKHAGEN, B. & STRECKER, M.R. (2008) Orographic barriers, high-resolution TRMM rainfall, and relief variations along the eastern Andes. *Geophysical Research Letters*, **35**, L06403, doi:06410.01029/02007gl032011.
- BOOKHAGEN, B. & STRECKER, M.R. (2012) Spatiotemporal trends in erosion rates across a pronounced rainfall gradient: Examples from the southern Central Andes. *Earth and Planetary Science Letters*, **327**, 97-110.
- BOSIO, P.P., POWELL, J., DEL PAPA, C. & HONGN, F. (2009) Middle Eocene deformation-sedimentation in the Luracatao Valley: Tracking the beginning of the foreland basin of northwestern Argentina. *Journal of South American Earth Sciences*, **28**, 142-154.
- BOSSI, G.E., GEORGIEFF, S.M., GAVRILOFF, I.J.C., IBANEZ, L.M. & MURUAGA, C.M. (2001) Cenozoic evolution of the intramontane Santa Maria basin, Pampean Ranges, northwestern Argentina. *Journal of South American Earth Sciences*, **14**, 725-734.
- BURBANK, D., MEIGS, A. & BROZOVIC, N. (1996) Interactions of growing folds and coeval depositional systems. *Basin Research*, **8**, 199-223.
- BURBANK, D.W. & RAYNOLDS, R.G.H. (1988) Stratigraphic keys to the timing of thrusting in terrestrial foreland basins: Applications to the Northwestern Himalaya. In: *New Perspectives in Basin Analysis* (Ed. by K. L. Kleinspehn, and Paola, C.), 331-351. Springer-Verlag, New York.
- BURBANK, D.W. (2002) Rates of erosion and their implications for exhumation. *Mineralogical Magazine*, **66**, 25-52.
- BURBANK, D.W., BOOKHAGEN, B., GABET, E.J. & PUTKONEN, J. (2012) Modern climate and erosion in the Himalaya. *Comptes Rendus Geoscience*, **344**, 610-626.
- BYWATER-REYES, S., CARRAPA, B., CLEMENTZ, M. & SCHOENBOHM, L. (2010) Effect of late Cenozoic aridification on sedimentation in the Eastern Cordillera of northwest Argentina (Angastaco basin). *Geology*, **38**, 235-238.

- CAHILL, T. & ISACKS, B.L. (1992) Seismicity and shape of the subducted Nazca plate. *Journal of Geophysical Research-Solid Earth*, **97**, 17503-17529.
- CANAVAN, R.R., CARRAPA, B., CLEMENTZ, M.T., QUADE, J., DECELLES, P.G. & SCHOENBOHM, L.M. (2014) Early Cenozoic uplift of the Puna Plateau, Central Andes, based on stable isotope paleoaltimetry of hydrated volcanic glass. *Geology*, **42**, 447-450.
- CARRAPA, B., STRECKER, M.R. & SOBEL, E.R. (2006) Cenozoic orogenic growth in the Central Andes: Evidence from sedimentary rock provenance and apatite fission track thermochronology in the Fiambala Basin, southernmost Puna Plateau margin (NW Argentina). *Earth and Planetary Science Letters*, **247**, 82-100.
- CARRAPA, B., HAUER, J., SCHOENBOHM, L., STRECKER, M.R., SCHMITT, A.K., VILLANUEVA, A. & GOMEZ, J.S. (2008) Dynamics of deformation and sedimentation in the northern Sierras Pampeanas: An integrated study of the Neogene Fiambala basin, NW Argentina. *Geological Society of America Bulletin*, **120**, 1518-1543.
- CARRAPA, B., TRIMBLE, J.D. & STOCKLI, D.F. (2011) Patterns and timing of exhumation and deformation in the Eastern Cordillera of NW Argentina revealed by (U-Th)/He thermochronology. *Tectonics*, **30**, 30.
- CARRAPA, B., BYWATER-REYES, S., DECELLES, P.G., MORTIMER, E. & GEHRELS, G.E. (2012) Late Eocene-Pliocene basin evolution in the Eastern Cordillera of northwestern Argentina (25 degrees-26 degrees S): regional implications for Andean orogenic wedge development. *Basin Research*, **24**, 249-268.
- CARRAPA, B., HUNTINGTON, K.W., CLEMENTZ, M., QUADE, J., BYWATER-REYES, S., SCHOENBOHM, L.M. & CANAVAN, R.R. (2014a) Uplift of the Central Andes of NW Argentina associated with upper crustal shortening, revealed by multiproxy isotopic analyses. *Tectonics*, **33**, 2013TC003461, doi: 003410.001002/002013TC003461.
- CARRAPA, B., REYES-BYWATER, S., SAFIPOUR, R., SOBEL, E.R., SCHOENBOHM, L.M., DECELLES, P.G., REINERS, P.W. & STOCKLI, D. (2014b) The effect of inherited paleotopography on exhumation of the Central Andes of NW Argentina. *Geological Society of America Bulletin*, **126**, 66-77.
- CARRAPA, B. & DECELLES, P.G. (2015) Regional exhumation and kinematic history of the central Andes in response to cyclical orogenic processes. *Geological Society of America Memoirs*, **212**, 201-213.
- CASTELLANOS, A. (1950) *El Uquiense, Sedimentos Neogenos de Uquia (Senador Perez) en la Provincia de Jujuy (Argentina)*. Universidad Nacional del Litoral, Facultad de Ciencias Matematicas Fisicas y Quimicas y Naturales, Rosario.
- COTTLE, J.M., KYLANDER-CLARK, A.R. & VRIJMOED, J.C. (2012) U-Th/Pb geochronology of detrital zircon and monazite by single shot laser ablation inductively coupled plasma mass spectrometry (SS-LA-ICPMS). *Chemical Geology*, **332**, 136-147.
- COUTAND, I., COBBOLD, P.R., DE URREZTIETA, M., GAUTIER, P., CHAUVIN, A., GAPAIS, D., ROSSELLO, E.A. & LOPEZ-GAMUNDI, O. (2001) Style and history of Andean deformation, Puna plateau, northwestern Argentina. *Tectonics*, **20**, 210-234.
- COUTAND, I., CARRAPA, B., DEEKEN, A., SCHMITT, A.K., SOBEL, E.R. & STRECKER, M.R. (2006) Propagation of orographic barriers along an active range front: insights from sandstone petrography and detrital apatite fission-track thermochronology in the intramontane Angastaco basin, NW Argentina. *Basin Research*, **18**, 1-26.

- CRISTIANI, C., MATTEINI, M., MAZZUOLI, R., OMARINI, R. & VILLA, I.M. (2005) Petrology of Late Jurassic-Early Cretaceous Tusaquillas and Abra Laite-Aguilar Plutonic complexes (Central Andes, 23°05' S – 66°05'W): a comparison with the rift-related magmatism of NW Argentina and E Bolivia. In: *Mesozoic to Cenozoic Alkaline Magmatism in the Brazilian Plataform* (Ed. by P. Comin-Chiaramonti & C. Barros Gomez), 213-241. Editora da Universidade de São Paulo, Brazil.
- CROWLEY, J.L., SCHOENE, B. & BOWRING, S.A. (2007) U-Pb dating of zircon in the Bishop Tuff at the millennial scale. *Geology*, **35**, 1123-1126.
- DECELLES, P.G., CARRAPA, B., HORTON, B.K. & GEHRELS, G.E. (2011) Cenozoic foreland basin system in the central Andes of northwestern Argentina: Implications for Andean geodynamics and modes of deformation. *Tectonics*, **30**, TC6013, doi: 6010.1029/2011tc002948.
- DEEKEN, A., SOBEL, E.R., HASCHKE, M. & RILLER, U. (2005) Age of initiation and growth pattern of the Puna plateau, NW Argentina, constrained by AFT thermochronology. *Potsdam, Germany Abstract Volume, Terra Nostra*, **5** (1), 39.
- DEEKEN, A., SOBEL, E.R., COUTAND, I., HASCHKE, M., RILLER, U. & STRECKER, M.R. (2006) Development of the southern Eastern Cordillera, NW Argentina, constrained by apatite fission track thermochronology: From early Cretaceous extension to middle Miocene shortening. *Tectonics*, **25**, TC6003, doi: 6010.1029/2005tc001894.
- DEL PAPA, C., HONGN, F., POWELL, J., PAYROLA, P., DO CAMPO, M., STRECKER, M.R., PETRINOVIC, I., SCHMITT, A.K. & PEREYRA, R. (2013) Middle Eocene-Oligocene broken-foreland evolution in the Andean Calchaqui Valley, NW Argentina: insights from stratigraphic, structural and provenance studies. *Basin Research*, **25**, 574-593.
- ECHAVARRIA, L., HERNANDEZ, R., ALLMENDINGER, R. & REYNOLDS, J. (2003) Subandean thrust and fold belt of northwestern Argentina: Geometry and timing of the Andean evolution. *AAPG Bulletin*, **87**, 965-985.
- ELGER, K., ONCKEN, O. & GLODNY, J. (2005) Plateau-style accumulation of deformation: Southern Altiplano. *Tectonics*, **24**, TC4020, doi: 4010.1029/2004tc001675.
- FEDOROV, A.V., BRIERLEY, C.M., LAWRENCE, K.T., LIU, Z., DEKENS, P.S. & RAVELO, A.C. (2013) Patterns and mechanisms of early Pliocene warmth. *Nature*, **496**, 43-+.
- GABALDÓN, V., M.A. GONZALEZ, M.A. & LIZUAIN, A. (1998) *El mapa geológico, Estudio geológico integrado de la Quebrada de Humahuaca*. Servicio Geológico Minero Argentino (SEGEMAR), Buenos Aires.
- GALEWSKY, J. (2009) Rain shadow development during the growth of mountain ranges: An atmospheric dynamics perspective. *Journal of Geophysical Research-Earth Surface*, **114**, F01018, doi:01010.01029/02008JF001085.
- GALLI, C.I., COIRA, B., ALONSO, R., REYNOLDS, J., MATTEINI, M. & HAUSER, N. (2014) Tectonic controls on the evolution of the Andean Cenozoic foreland basin: Evidence from fluvial system variations in the Payogastilla Group, in the Calchaquí, Tonco and Amblayo Valleys, NW Argentina. *Journal of South American Earth Sciences*, **52**, 234-259.
- GEHRELS, G.E., VALENCIA, V.A. & RUIZ, J. (2008) Enhanced precision, accuracy, efficiency, and spatial resolution of U-Pb ages by laser ablation-multicollector-inductively coupled plasma-mass spectrometry. *Geochemistry Geophysics Geosystems*, **9**, Q03017, doi:03010.01029/02007GC001805.

- GODARD, V., TUCKER, G.E., BURCH FISHER, G., BURBANK, D.W. & BOOKHAGEN, B. (2013) Frequency-dependent landscape response to climatic forcing. *Geophysical Research Letters*, **40**, 859-863.
- GONZALEZ, M.A., PEREYRA, F., RAMALLO, E. & TCHILINGURIAN, P. (2004) Hoja Geológica 2366-IV, Ciudad Libertador General San Martín, provincias de Jujuy y Salta. *Boletín* 274, Instituto de Geología y Recursos Minerales, Servicio Geológico Minero Argentino. Buenos Aires, 109.
- GUBBELS, T.L., ISACKS, B.L. & FARRAR, E. (1993) High-level surfaces, plateau uplift, and foreland development, Bolivian central Andes. *Geology*, **21**, 695-698.
- HAIN, M.P., STRECKER, M.R., BOOKHAGEN, B., ALONSO, R.N., PINGEL, H. & SCHMITT, A.K. (2011) Neogene to Quaternary broken foreland formation and sedimentation dynamics in the Andes of NW Argentina (25 degrees S). *Tectonics*, **30**, TC2006, doi:2010.1029/2010TC002703.
- HERNÁNDEZ, R. & ECHAVARRIA, L. (2009) Faja plegada y corrida subandina del noroeste argentino: estratigrafía, geometría y cronología de la deformación. *Revista de la Asociación Geológica Argentina*, **65**, 068-080.
- HILLEY, G.E. & STRECKER, M.R. (2005) Processes of oscillatory basin filling and excavation in a tectonically active orogen: Quebrada del Toro Basin, NW Argentina. *Geological Society of America Bulletin*, **117**, 887-901.
- HONGN, F., DEL PAPA, C., POWELL, J., PETRINOVIC, I., MON, R. & DERACO, V. (2007) Middle Eocene deformation and sedimentation in the Puna-Eastern Cordillera transition (23 degrees-26 degrees S): Control by preexisting heterogeneities on the pattern of initial Andean shortening. *Geology*, **35**, 271-274.
- HORTON, B.K. (2005) Revised deformation history of the central Andes: Inferences from Cenozoic foredeep and intermontane basins of the Eastern Cordillera, Bolivia. *Tectonics*, **24**, TC3011, doi:3010.1029/2003TC001619.
- HOUGH, B.G., GARZIONE, C.N., WANG, Z.C., LEASE, R.O., BURBANK, D.W. & YUAN, D.Y. (2011) Stable isotope evidence for topographic growth and basin segmentation: Implications for the evolution of the NE Tibetan Plateau. *Geological Society of America Bulletin*, **123**, 168-185.
- HUMPHREY, N.F. & KONRAD, S.K. (2000) River incision or diversion in response to bedrock uplift. *Geology*, **28**, 43-46.
- INSEL, N., GROVE, M., HASCHKE, M., BARNES, J.B., SCHMITT, A.K. & STRECKER, M.R. (2012) Paleozoic to early Cenozoic cooling and exhumation of the basement underlying the eastern Puna plateau margin prior to plateau growth. *Tectonics*, **31**, TC6006, doi:6010.1029/2012TC003168.
- JACKSON, S.E., PEARSON, N.J., GRIFFIN, W.L. & BELOUSOVA, E.A. (2004) The application of laser ablation-inductively coupled plasma-mass spectrometry to in situ U-Pb zircon geochronology. *Chemical Geology*, **211**, 47-69.
- JONES, C.H. (2002) User-driven integrated software lives: "Paleomag" paleomagnetism analysis on the Macintosh. *Computers & Geosciences*, **28**, 1145-1151.
- JORDAN, T.E. (1981) Thrust loads and foreland basin evolution, Cretaceous, Western United States. *AAPG Bulletin*, **65**, 2506-2520.
- JORDAN, T.E., ISACKS, B.L., ALLMENDINGER, R.W., BREWER, J.A., RAMOS, V.A. & ANDO, C.J. (1983) Andean tectonics related to geometry of subducted Nazca plate. *Geological Society of America Bulletin*, **94**, 341-361.

- JORDAN, T.E. & ALONSO, R.N. (1987) Cenozoic stratigraphy and basin tectonics of the Andes Mountains, 20°-28° South latitude. *AAPG Bulletin-American Association of Petroleum Geologists*, **71**, 49-64.
- JORDAN, T.E., FLEMINGS, P.B. & BEERS, J.A. (1988) Dating thrust-fault activity by use of foreland-basin strata. In: *New perspectives in basin analysis* (Ed. by K. L. Kleinspehn & C. Paola), 307 - 330. Springer-Verlag, New York.
- JORDAN, T.E., MPODOZIS, C., MUNOZ, N., BLANCO, N., PANANONT, P. & GARDEWEG, M. (2007) Cenozoic subsurface stratigraphy and structure of the Salar de Atacama Basin, northern Chile. *Journal of South American Earth Sciences*, **23**, 122-146.
- KIRSCHVINK, J.L. (1980) The least-squares line and plane and the analysis of paleomagnetic data. *Geophysical Journal of the Royal Astronomical Society*, **62**, 699-718.
- KIRSCHVINK, J.L., KOPP, R.E., RAUB, T.D., BAUMGARTNER, C.T. & HOLT, J.W. (2008) Rapid, precise, and high-sensitivity acquisition of paleomagnetic and rock-magnetic data: Development of a low-noise automatic sample changing system for superconducting rock magnetometers. *Geochemistry Geophysics Geosystems*, **9**, Q05Y01, doi:10.1029/2007GC001856.
- KLEINERT, K. & STRECKER, M.R. (2001) Climate change in response to orographic barrier uplift: Paleosol and stable isotope evidence from the late Neogene Santa Maria basin, northwestern Argentina. *Geological Society of America Bulletin*, **113**, 728-742.
- KLEY, J., MONALDI, C.R. & SALFITY, J.A. (1999) Along-strike segmentation of the Andean foreland: causes and consequences. *Tectonophysics*, **301**, 75-94.
- KLEY, J. & MONALDI, C.R. (2002) Tectonic inversion in the Santa Barbara System of the central Andean foreland thrust belt, northwestern Argentina. *Tectonics*, **21**, 18.
- KLEY, J., ROSSELLO, E.A., MONALDI, C.R. & HABIGHORST, B. (2005) Seismic and field evidence for selective inversion of Cretaceous normal faults, Salta rift, northwest Argentina. *Tectonophysics*, **399**, 155-172.
- LEASE, R.O., BURBANK, D.W., HOUGH, B., WANG, Z.C. & YUAN, D.Y. (2012) Pulsed Miocene range growth in northeastern Tibet: Insights from Xunhua Basin magnetostratigraphy and provenance. *Geological Society of America Bulletin*, **124**, 657-677.
- LISIECKI, L.E. & RAYMO, M.E. (2005) A Pliocene-Pleistocene stack of 57 globally distributed benthic delta O-18 records. *Paleoceanography*, **20**, PA1003, doi:10.1029/2004PA001071.
- LOURENS, L., HILGEN, F., SHACKLETON, N.J., LASKAR, J. & WILSON, D. (2004) The Neogene Period. In: *A Geologic Time Scale 2004* (Ed. by F. M. Gradstein, Ogg, J.G., Smith, A.), 409-440. Cambridge University Press, Cambridge, UK.
- LUDWIG, K.R. (2012) User's Manual for Isoplot 3.75, A Geochronological Toolkit for Microsoft Excel. *Berkeley Geochronology Center Special Publication No. 5*.
- MARQUILLAS, R.A., DEL PAPA, C. & SABINO, I.F. (2005) Sedimentary aspects and paleoenvironmental evolution of a rift basin: Salta Group (Cretaceous-Paleogene), northwestern Argentina. *International Journal of Earth Sciences*, **94**, 94-113.
- MARRETT, R. & STRECKER, M.R. (2000) Response of intracontinental deformation in the central Andes to late Cenozoic reorganization of South American Plate motions. *Tectonics*, **19**, 452-467.

- MARRETT, R.A., ALLMENDINGER, R.W., ALONSO, R.N. & DRAKE, R.E. (1994) Late Cenozoic tectonic evolution of the Puna Plateau and adjacent foreland, northwestern Argentine Andes. *Journal of South American Earth Sciences*, **7**, 179-207.
- MARSHALL, L.G., BUTLER, R.F., DRAKE, R.E. & CURTIS, G.H. (1982) Geochronology of Type Uquian (Late Cenozoic) Land Mammal Age, Argentina. *Science*, **216**, 986-989.
- McFADDEN, P.L. & McELHINNY, M.W. (1990) Classification of the reversal test in paleomagnetism. *Geophysical Journal International*, **103**, 725-729.
- MCQUARRIE, N. (2002) The kinematic history of the central Andean fold-thrust belt, Bolivia: Implications for building a high plateau. *Geological Society of America Bulletin*, **114**, 950-963.
- MCQUARRIE, N., HORTON, B.K., ZANDT, G., BECK, S. & DECELLES, P.G. (2005) Lithospheric evolution of the Andean fold-thrust belt, Bolivia, and the origin of the central Andean plateau. *Tectonophysics*, **399**, 15-37.
- MIALL, A.D. (1985) Architectural-element analysis: A new method of facies analysis applied to fluvial deposits. *Earth-Science Reviews*, **22**, 261-308.
- MIALL, A.D. (1996) *The Geology of Fluvial Deposits: Sedimentary Facies, Basin Analysis, and Petroleum Geology*. Springer, New York.
- MONTERO-LÓPEZ, C., STRECKER, M.R., SCHILDGEN, T.F., HONGN, F., GUZMÁN, S., BOOKHAGEN, B. & SUDO, M. (2014) Local high relief at the southern margin of the Andean plateau by 9 Ma: evidence from ignimbritic valley fills and river incision. *Terra Nova*, **26**, 454-460.
- MORENO, J.A. (1970) Estratigrafía y paleogeografía del Cretácico superior en la Cuenca del Noroeste Argentino, con especial mención de los Subgrupos Balbuena y Santa Barbara. *Revista de la Asociación Geológica Argentina*, **25**, 9-44.
- MORTIMER, E., CARRAPA, B., COUTAND, I., SCHOENBOHM, L., SOBEL, E.R. & GOMEZ, J.S. (2007) Fragmentation of a foreland basin in response to out-of-sequence basement uplifts and structural reactivation: El Cajon-Campo del Arenal basin, NW Argentina. *Geological Society of America Bulletin*, **119**, 637-653.
- O'REILLY, W. (1984) *Rock and Mineral Magnetism*. Blackie & Son, Glasgow.
- ORI, G.G. & FRIEND, P.F. (1984) Sedimentary basins formed and carried piggyback on active thrust sheets. *Geology*, **12**, 475-478.
- PATON, C., WOODHEAD, J.D., HELLSTROM, J.C., HERGT, J.M., GREIG, A. & MAAS, R. (2010) Improved laser ablation U-Pb zircon geochronology through robust downhole fractionation correction. *Geochemistry Geophysics Geosystems*, **11**, Q0AA06, doi:10.1029/2009GC002618.
- PEARSON, D.M., KAPP, P., DECELLES, P.G., REINERS, P.W., GEHRELS, G.E., DUCEA, M.N. & PULLEN, A. (2013) Influence of pre-Andean crustal structure on Cenozoic thrust belt kinematics and shortening magnitude: Northwestern Argentina. *Geosphere*, **9**, 1766-1782.
- PINGEL, H., STRECKER, M.R., ALONSO, R.N. & SCHMITT, A.K. (2013) Neotectonic basin and landscape evolution in the Eastern Cordillera of NW Argentina, Humahuaca Basin (similar to 24 degrees S). *Basin Research*, **25**, 554-573.
- PINGEL, H., ALONSO, R.N., MULCH, A., ROHRMANN, A., SUDO, M. & STRECKER, M.R. (2014) Pliocene orographic barrier uplift in the southern Central Andes. *Geology*, **42**, 691-694.

- POPE, R.J.J. & WILKINSON, K.N. (2005) Reconciling the roles of climate and tectonics in Late Quaternary fan development on the Spartan piedmont, Greece. In: *Alluvial Fans: Geomorphology, Sedimentology, Dynamics* (Ed. by A. Harvey, A. Mather & M. Stokes), **251**, 133-152. Geological Society, London, Special Publications.
- PRATT, J.R., SCHOENBOHM, L.A., MORTIMER, E. & SCHMITT, A. (2008) Basin Compartmentalization in the Sierra Pampeanas of Northwestern Argentina: Case-study of the El Cajón Basin., Ohio State University.
- QUADE, J., DETTINGER, M.P., CARRAPA, B., DECELLES, P., MURRAY, K.E., HUNTINGTON, K.W., CARTWRIGHT, A., CANAVAN, R.R., GEHRELS, G. & CLEMENTZ, M. (2015) The growth of the central Andes, 22°S–26°S. *Geological Society of America Memoirs*, **212**, 277-308.
- RAMOS, V.A. (1999) Los depósitos sinorogénicos Terciarios de la región Andina. In: *Geología Argentina* (Ed. by R. Caminos), *Anales*, **29**, 651-682. Instituto de Geología y Recursos Minerales, Buenos Aires, Argentina.
- REGUERO, M.A., CANDELA, A.M. & ALONSO, R.N. (2007) Biochronology and biostratigraphy of the Uquia Formation (Pliocene-early Pleistocene, NW Argentina) and its significance in the Great American Biotic Interchange. *Journal of South American Earth Sciences*, **23**, 1-16.
- REINERS, P.W., THOMSON, S.N., VERNON, A., WILLETT, S.D., ZATTIN, M., EINHORN, J., GEHRELS, G., QUADE, J., PEARSON, D., MURRAY, K.E. & CAVAZZA, W. (2015) Low-temperature thermochronologic trends across the central Andes, 21°S–28°S. *Geological Society of America Memoirs*, **212**, 215-249.
- REYNOLDS, J.H., GALLI, C.I., HERNANDEZ, R.M., IDLEMAN, B.D., KOTILA, J.M., HILLIARD, R.V. & NAESER, C.W. (2000) Middle Miocene tectonic development of the Transition Zone, Salta Province, northwest Argentina: Magnetic stratigraphy from the Metan Subgroup, Sierra de Gonzalez. *Geological Society of America Bulletin*, **112**, 1736-1751.
- REYNOLDS, J.H., HERNANDEZ, R.M., GALLI, C.I. & IDLEMAN, B.D. (2001) Magnetostratigraphy of the Quebrada La Porcelana section, Sierra de Ramos, Salta Province, Argentina: age limits for the Neogene Oran Group and uplift of the southern Sierras Subandinas. *Journal of South American Earth Sciences*, **14**, 681-692.
- ROBINSON, R.A.J., SPENCER, J.Q.G., STRECKER, M.R., RICHTER, A. & ALONSO, R.N. (2005) Luminescence dating of alluvial fans in intramontane basins of NW Argentina. In: *Alluvial Fans: Geomorphology, Sedimentology, Dynamics* (Ed. by A. Harvey, A. Mather & M. Stokes), **251**, 153-168. Geological Society, London, Special Publications.
- RODRÍGUEZ FERNÁNDEZ, L.R., HEREDIA, N., SEGGIARO, R.E. & GONZÁLEZ, M.A. (1999) Estructura andina de la Cordillera Oriental en el área de la Quebrada de Humahuaca, provincia de Jujuy, NO de Argentina. *Trabajos de Geología - Universidad de Oviedo*, **21**, 321-332.
- ROHRMANN, A., STRECKER, M.R., BOOKHAGEN, B., MULCH, A., SACHSE, D., PINGEL, H., ALONSO, R.N., SCHILDGEN, T.F. & MONTERO, C. (2014) Can stable isotopes ride out the storms? The role of convection for water isotopes in models, records, and paleoaltimetry studies in the central Andes. *Earth and Planetary Science Letters*, **407**, 187-195.



- SALFITY, J.A., BRANDÁN, E.M., MONALDI, C.R. & GALLARDO, E.F. (1984) Tectónica compresiva cuaternaria en la Cordillera Oriental Argentina, latitud de Tilcara (Jujuy). *Actas del IX Congreso Geológico Argentino*, **2**, 427-434.
- SANCHO, C., PENA, J.L., RIVELLI, F., RHODES, E. & MUNOZ, A. (2008) Geomorphological evolution of the Tilcara alluvial fan (Jujuy Province, NW Argentina): Tectonic implications and palaeoenvironmental considerations. *Journal of South American Earth Sciences*, **26**, 68-77.
- SCHARER, U. (1984) The effect of initial Th-230 disequilibrium on young U-Pb ages - the Makalu case, Himalaya. *Earth and Planetary Science Letters*, **67**, 191-204.
- SCHILDGEN, T.F., YILDIRIM, C., COSENTINO, D. & STRECKER, M.R. (2014) Linking slab break-off, Hellenic trench retreat, and uplift of the Central and Eastern Anatolian plateaus. *Earth-Science Reviews*, **128**, 147-168.
- SCHOENBOHM, L.M., CARRAPA, B., MCPHERSON, H.M., PRATT, J.R., BYWATER-REYES, S. & MORTIMER, E. (2015) Climate and tectonics along the southern margin of the Puna Plateau, NW Argentina: Origin of the late Cenozoic Punaschotter conglomerates. *Geological Society of America Memoirs*, **212**, 251-260.
- SIKS, B.C. & HORTON, B.K. (2011) Growth and fragmentation of the Andean foreland basin during eastward advance of fold-thrust deformation, Puna plateau and Eastern Cordillera, northern Argentina. *Tectonics*, **30**, TC6017, doi: 6010.1029/2011TC002944.
- SKLAR, L.S. & DIETRICH, W.E. (2001) Sediment and rock strength controls on river incision into bedrock. *Geology*, **29**, 1087-1090.
- SOBEL, E.R., HILLEY, G.E. & STRECKER, M.R. (2003) Formation of internally drained contractional basins by aridity-limited bedrock incision. *Journal of Geophysical Research-Solid Earth*, **108**, 2344, doi:2310.1029/2002JB001883.
- SOBEL, E.R. & STRECKER, M.R. (2003) Uplift, exhumation and precipitation: tectonic and climatic control of Late Cenozoic landscape evolution in the northern Sierras Pampeanas, Argentina. *Basin Research*, **15**, 431-451.
- STACEY, J.S. & KRAMERS, J.D. (1975) Approximation of terrestrial lead isotope evolution by a 2-stage model. *Earth and Planetary Science Letters*, **26**, 207-221.
- STARCK, D. & ANZÓTEGUI, L.M. (2001) The late miocene climatic change—persistence of a climatic signal through the orogenic stratigraphic record in northwestern Argentina. *Journal of South American Earth Sciences*, **14**, 763-774.
- STRECKER, M.R., CERVENY, P., BLOOM, A.L. & MALIZIA, D. (1989) Late Cenozoic tectonism and landscape development in the foreland of the Andes: Northern Sierras Pampeanas (26- 28°S), Argentina. *Tectonics*, **8**, 517-534.
- STRECKER, M.R., ALONSO, R.N., BOOKHAGEN, B., CARRAPA, B., HILLEY, G.E., SOBEL, E.R. & TRAUTH, M.H. (2007) Tectonics and climate of the southern central Andes. *Annual Review of Earth and Planetary Sciences*, **35**, 747-787.
- STRECKER, M.R., ALONSO, R., BOOKHAGEN, B., CARRAPA, B., COUTAND, I., HAIN, M.P., HILLEY, G.E., MORTIMER, E., SCHOENBOHM, L. & SOBEL, E.R. (2009) Does the topographic distribution of the central Andean Puna Plateau result from climatic or geodynamic processes? *Geology*, **37**, 643-646.
- STRECKER, M.R., HILLEY, G.E., BOOKHAGEN, B. & SOBEL, E.R. (2011) Structural, Geomorphic, and Depositional Characteristics of Contiguous and Broken Foreland Basins: Examples from the Eastern Flanks of the Central Andes in Bolivia and NW

- Argentina. In: *Tectonics of Sedimentary Basins* (Ed. by, 508-521. John Wiley & Sons, Ltd.
- STREIT, R.L., BURBANK, D.W., STRECKER, M.R., ALONSO, R.N., COTTLE, J.M. & KYLANDER-CLARK, A.R.C. (2015) Controls on intermontane basin filling, isolation, and incision on the margin of the Puna Plateau, NW Argentina (~23°S). *Basin Research*, n/a-n/a.
- TCHILINGUIRIAN, P. & PEREYRA, F.X. (2001) Geomorfología del sector Salinas Grandes-Quebrada de Humahuaca, provincia de Jujuy. *Revista de la Asociación Geológica Argentina*, **56**, 3-15.
- TURNER, J.C.M. (1960) Estratigrafía de la Sierra de Santa Victoria y adyacencias. *Boletín Academia Nacional de Ciencias*, **41**, 163-196.
- TURNER, J.C.M. & MÉNDEZ, V. (1979). *Puna*. Segundo simposio de geología regional argentina, Córdoba, Argentina, Academia Nacional de Ciencias Córdoba.
- TURNER, J.C.M. & MON, R. (1979). *Cordillera Oriental*. Segundo simposio de geología regional argentina, Córdoba, Argentina, Academia Nacional de Ciencias Córdoba.
- UBA, C.E., STRECKER, M.R. & SCHMITT, A.K. (2007) Increased sediment accumulation rates and climatic forcing in the central Andes during the late Miocene. *Geology*, **35**, 979-982.
- UBA, C.E., KLEY, J., STRECKER, M.R. & SCHMITT, A.K. (2009) Unsteady evolution of the Bolivian Subandean thrust belt: The role of enhanced erosion and clastic wedge progradation. *Earth and Planetary Science Letters*, **281**, 134-146.
- VERA, C., HIGGINS, W., AMADOR, J., AMBRIZZI, T., GARREAUD, R., GOCHIS, D., GUTZLER, D., LETTENMAIER, D., MARENGO, J., MECHOSO, C.R., NOGUES-PAEGLE, J., DIAS, P.L.S. & ZHANG, C. (2006) Toward a unified view of the American Monsoon Systems. *Journal of Climate*, **19**, 4977-5000.
- VERMEESCH, P. (2012) On the visualisation of detrital age distributions. *Chemical Geology*, **312**, 190-194.
- VIRAMONTE, J.G., REYNOLDS, J.H., DELPAPA, C. & DISALVO, A. (1994) The Corte-Blanco garnetiferous tuff: a distinctive late Miocene marker bed in northwestern Argentina applied to magnetic polarity stratigraphy in the Río Yacones, Salta Province. *Earth and Planetary Science Letters*, **121**, 519-531.
- WALTHER, A., ORGEIRA, M., REGUERO, M., VERZI, D., VILAS, J., ALONSO, R.N., GALLADO, E., KELLY, S. & JORDAN, T.E. (1998) Estudio Paleomagnetico, Paleontologico y Radimetrico de la Formacion Uquia (Plio-Pleistoceno) en Esquina Blanca (Jujuy). *Actas del X Congreso Latinoamericano de Geologia y VI Congreso Nacional de Geologia Economica*, **1**, 77.
- WHITMAN, D., ISACKS, B.L. & KAY, S.M. (1996) Lithospheric structure and along-strike segmentation of the Central Andean Plateau: Seismic Q, magmatism, flexure, topography and tectonics. *Tectonophysics*, **259**, 29-40.
- WIEDENBECK, M., ALLE, P., CORFU, F., GRIFFIN, W.L., MEIER, M., OBERLI, F., VONQUADT, A., RODDICK, J.C. & SPEIGEL, W. (1995) Three natural zircon standards for U-Th-Pb, Lu-Hf, trace element and REE analysis. *Geostandards Newsletter*, **19**, 1-23.
- YILDIRIM, C., SCHILDGEN, T.F., ECHTLER, H., MELNICK, D. & STRECKER, M.R. (2011) Late Neogene and active orogenic uplift in the Central Pontides associated with the North Anatolian Fault: Implications for the northern margin of the Central Anatolian Plateau, Turkey. *Tectonics*, **30**, TC5005, doi:5010.1029/2010TC002756.

- ZACHOS, J., PAGANI, M., SLOAN, L., THOMAS, E. & BILLUPS, K. (2001) Trends, rhythms, and aberrations in global climate 65 Ma to present. *Science*, **292**, 686-693.
- ZAPPETTINI, E. (1989) Geología y metalogénesis de la región comprendida entre las localidades de Santa Ana y Cobres, provincias de Jujuy y Salta, República Argentina. Tesis doctoral Thesis, Universidad de Buenos Aires, Buenos Aires.

## TABLES

**Table 1.** Summary of zircon U-Pb geochronology of volcanic ashes relevant to deformation in the Humahuaca basin.

| Sample                     | Latitude  | Longitude | Description                                     | N <sup>a</sup> | Age <sup>b</sup><br>[Ma] | 2 S.D. <sup>c</sup><br>[Myr] |
|----------------------------|-----------|-----------|---|----------------|--------------------------|------------------------------|
| <b>New data</b>            |           |           |   |                |                          |                              |
| HU280412-01                | -23.27142 | -65.37376 | Near Calete, uplifted west of Faults B, C, D    | 32             | 2.44                     | 0.07                         |
| HU040411-01                | -23.38328 | -65.35414 | Río Yacoraite footwall of fault F               | 30             | 1.84                     | 0.08                         |
| HU120411-01                | -23.39525 | -65.37186 | Above unconformity in h. wall of Fault D        | 32             | 3.85                     | 0.1                          |
| HU190310-01                | -23.42206 | -65.38231 | Huacalera – hanging wall Fault C                | 30             | 2.96                     | 0.04                         |
| HU180411-02                | -23.43    | -65.36547 | Huacalera – h. wall of Fault E eastern strand   | 32             | 3.78                     | 0.23                         |
| HU200310-01                | -23.43308 | -65.3688  | Huacalera – footwall Fault E western strand     | 36             | 2.91                     | 0.05                         |
| HU290311-01                | -23.4885  | -65.3791  | Angosto Perchel – anticline, h. wall of Fault E | 30             | 3.43                     | 0.09                         |
| <b>Data from Chapter 1</b> |           |           |   |                |                          |                              |
| UQ280307-01                | -23.30585 | -65.36925 | Uquía, capping Fault B                          | 32             | 4.12                     | 0.05                         |
| HU190311-01                | -23.41114 | -65.3838  | Huacalera – h. wall Fault C; capping Fault B    | 30             | 3.8                      | 0.05                         |
| HU080410-01                | -23.41936 | -65.374   | Huacalera – covering Fault D; Fault C f. wall   | 32             | 3.86                     | 0.04                         |
| HU210307-03                | -23.43057 | -65.36928 | Huacalera – below angular unconformity          | 30             | 5.05                     | 0.14                         |
| HU180411-03                | -23.43132 | -65.37006 | Huacalera – above angular unconformity          | 30             | 4.38                     | 0.11                         |
| HU240307-01                | -23.43259 | -65.37079 | Huacalera – footwall of Fault D                 | 32             | 4.24                     | 0.08                         |
| <b>Data from Chapter 2</b> |           |           |   |                |                          |                              |
| HU290412-02                | -23.24677 | -65.36159 | W of Humahuaca – broad anticline                | 32             | 2.36                     | 0.07                         |
| UQ270307-02                | -23.35266 | -65.36858 | Chuculezna – footwall of Fault D                | 30             | 2.23                     | 0.07                         |
| HU270412-01                | -23.41543 | -65.36675 | N of Huacalera – in h.wall anticline of Fault E | 32             | 5.52                     | 0.18                         |
| HU240307-02                | -23.42866 | -65.3728  | Huacalera – footwall of Fault C                 | 36             | 3.01                     | 0.05                         |
| HU210307-02                | -23.42936 | -65.36377 | Huacalera – footwall, eastern strand of Fault E | 30             | 2.36                     | 0.12                         |
| HU180411-01                | -23.42945 | -65.36304 | Huacalera – footwall, eastern strand of Fault E | 32             | 2.49                     | 0.06                         |
| HU310310-02                | -23.42983 | -65.34039 | East of R. Grande – lakebeds dipping 5-12° W    | 33             | 2.5                      | 0.03                         |
| HU120410-01                | -23.45759 | -65.37343 | S of Tropic of Capricorn, h. wall of Fault E    | 30             | 3.06                     | 0.04                         |
| HU030410-01                | -23.46012 | -65.34193 | East of Río Grande – silts dipping ~5° W        | 30             | 2.41                     | 0.04                         |
| HU170411-01                | -23.47353 | -65.38365 | Angosto Perchel (north) – Fault C footwall      | 30             | 3.41                     | 0.07                         |
| HU300310-02                | -23.47517 | -65.38228 | Angosto Perchel (north) growth strata – upper   | 40             | 4.04                     | 0.05                         |
| HU160411-01                | -23.47568 | -65.37626 | Angosto Perchel (north) – Fault E footwall      | 30             | 1.98                     | 0.12                         |
| HU300310-01                | -23.47708 | -65.37851 | Angosto Perchel (north) growth strata – lower   | 32             | 4.36                     | 0.14                         |

<sup>a</sup> Number of zircons analyzed.

<sup>b</sup> Weighted average of the five youngest ages, corrected for initial Th disequilibrium and common-Pb.

<sup>c</sup> 2 × standard deviation of the five youngest ages.

## FIGURES

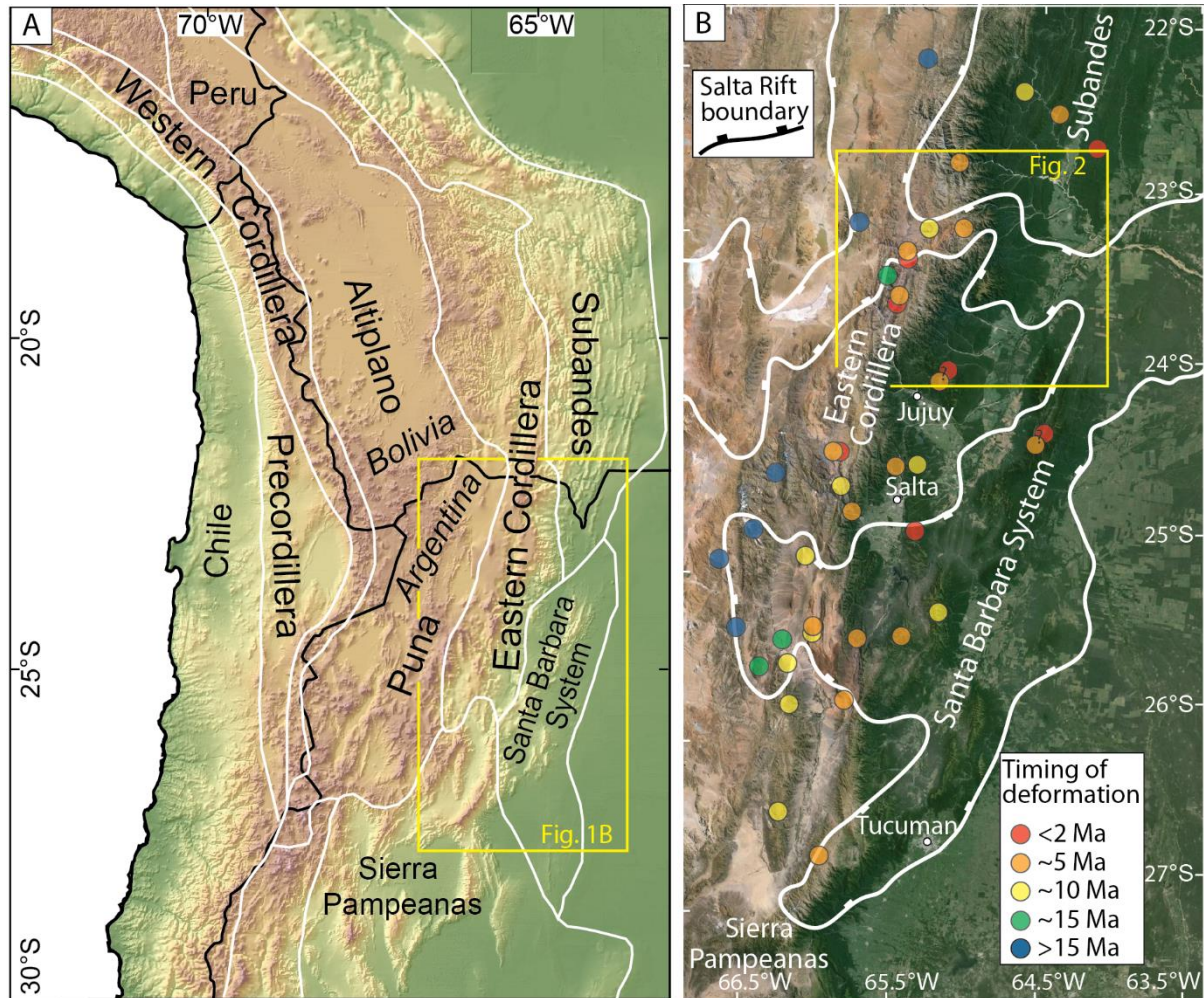


**Figure 1.** Regional setting. (A) Tectonomorphic provinces (Jordan *et al.*, 1983). (B) Salta Rift boundary (Marquillas *et al.*, 2005), and timing of deformation (Viramonte *et al.*, 1994; Marrett & Strecker, 2000; Reynolds *et al.*, 2001; Echavarría *et al.*, 2003; Sobel & Strecker, 2003; Hilley & Strecker, 2005; Coutand *et al.*, 2006; Deeken *et al.*, 2006; Hongn *et al.*, 2007; Bywater-Reyes *et al.*, 2010; Carrapa *et al.*, 2011; Hain *et al.*, 2011; Siks & Horton, 2011; Bonorino & Abascal, 2012; Carrapa *et al.*, 2012; Insel *et al.*, 2012; del Papa *et al.*, 2013; Pearson *et al.*, 2013; Pingel *et al.*, 2013; Carrapa *et al.*, 2014b; Amidon *et al.*, 2015; Reiners *et al.*, 2015; Streit *et al.*, 2015).



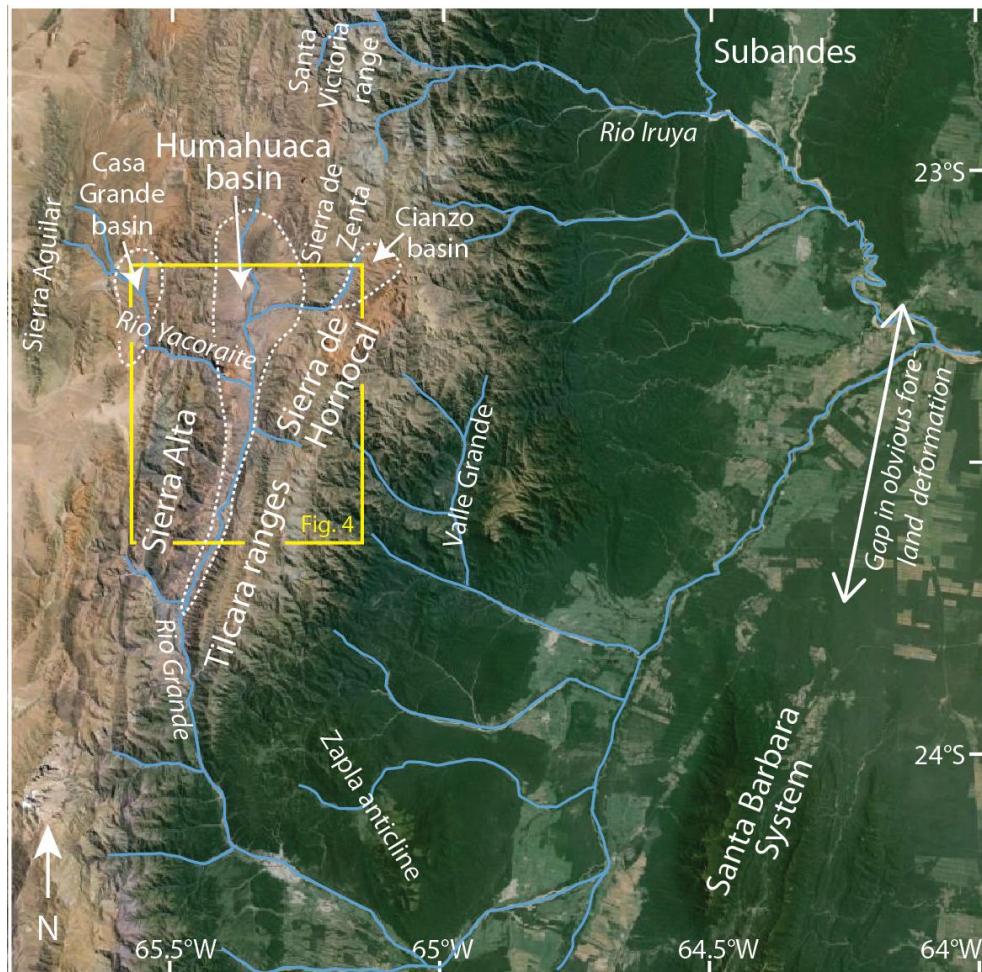


**Figure 2.** Location of Humahuaca basin, Sierra Alta, Tilcara ranges, Sierra de Hornocal, and nearby features referenced in the text (Casa Grande basin, Cianzo basin, Valle Grande, Río Iruya, Santa Victoria range). Yellow box shows location of the geologic map in Figure 4.

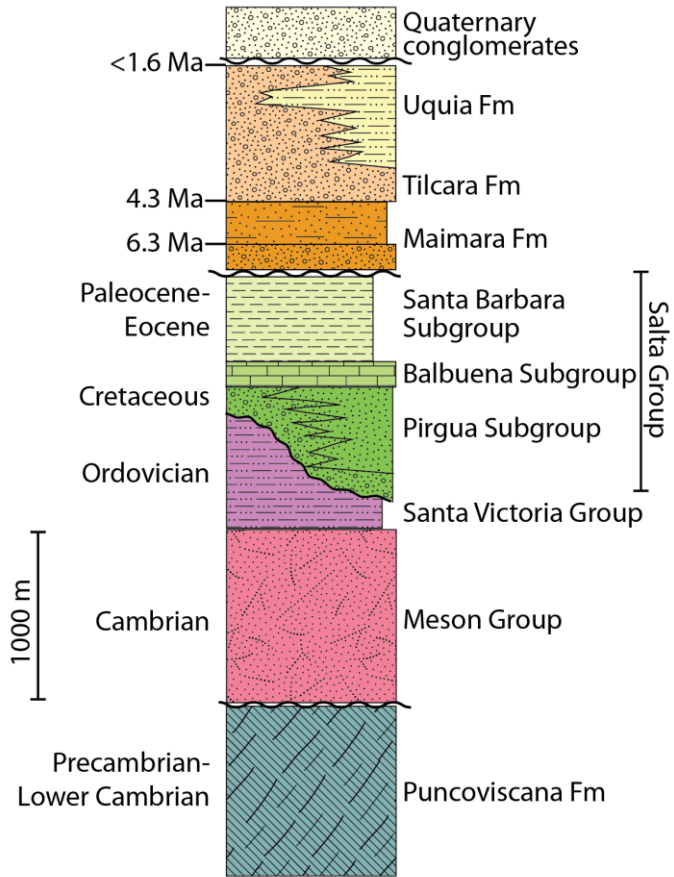


**Figure 3.** Simplified stratigraphic column of the Humahuaca basin, Sierra Aguilar, and Tilcara ranges.



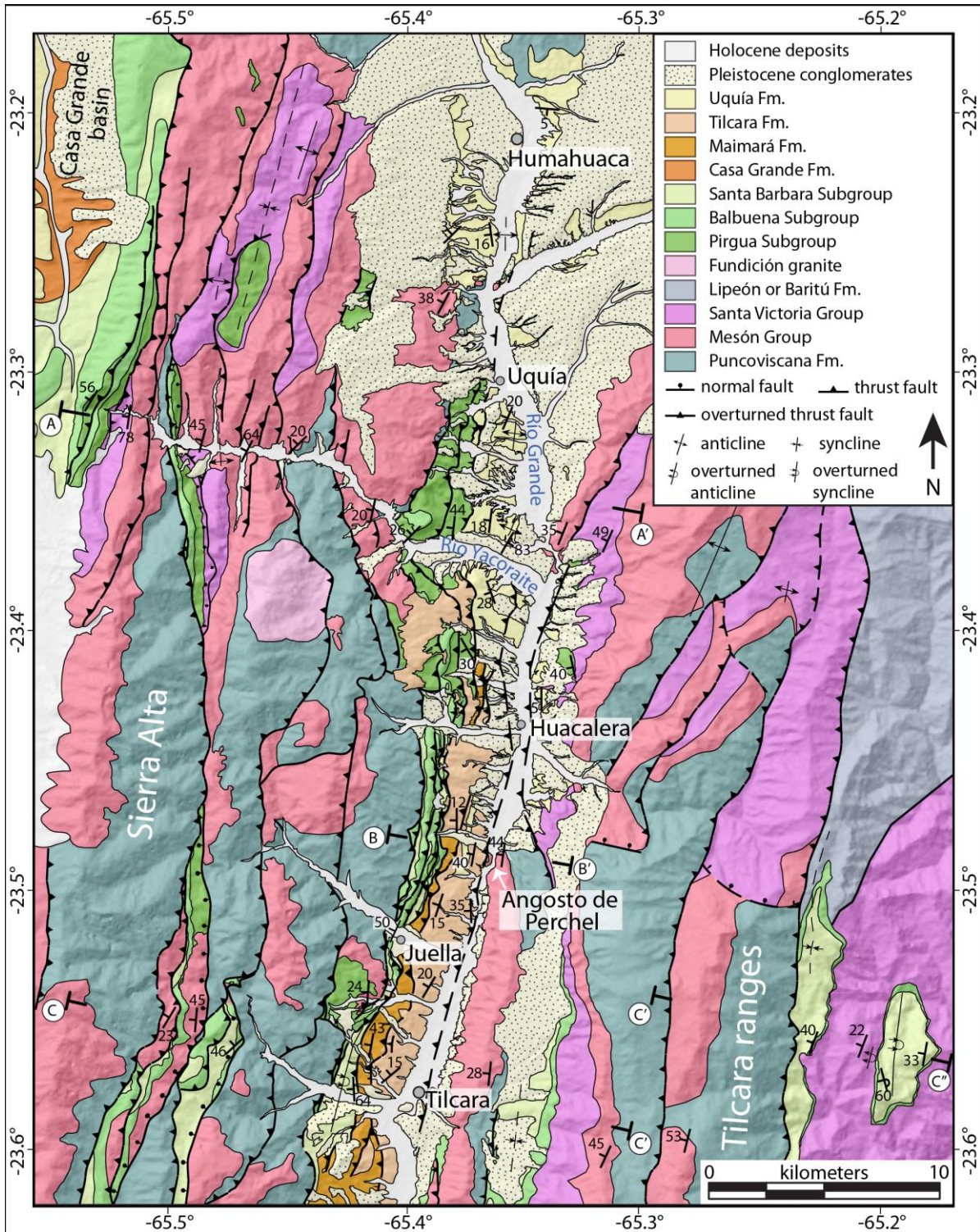


**Figure 4.** Geologic map. Based on field mapping in the Humahuaca basin and along the two transects at the Río Yacoraité and near Tilcara, and on interpretation of Google Earth satellite imagery, with reference to published maps (Gabaldón *et al.*, 1998; Rodríguez Fernández *et al.*, 1999; Gonzalez *et al.*, 2004), in the rest of Sierra Alta and Tilcara ranges.



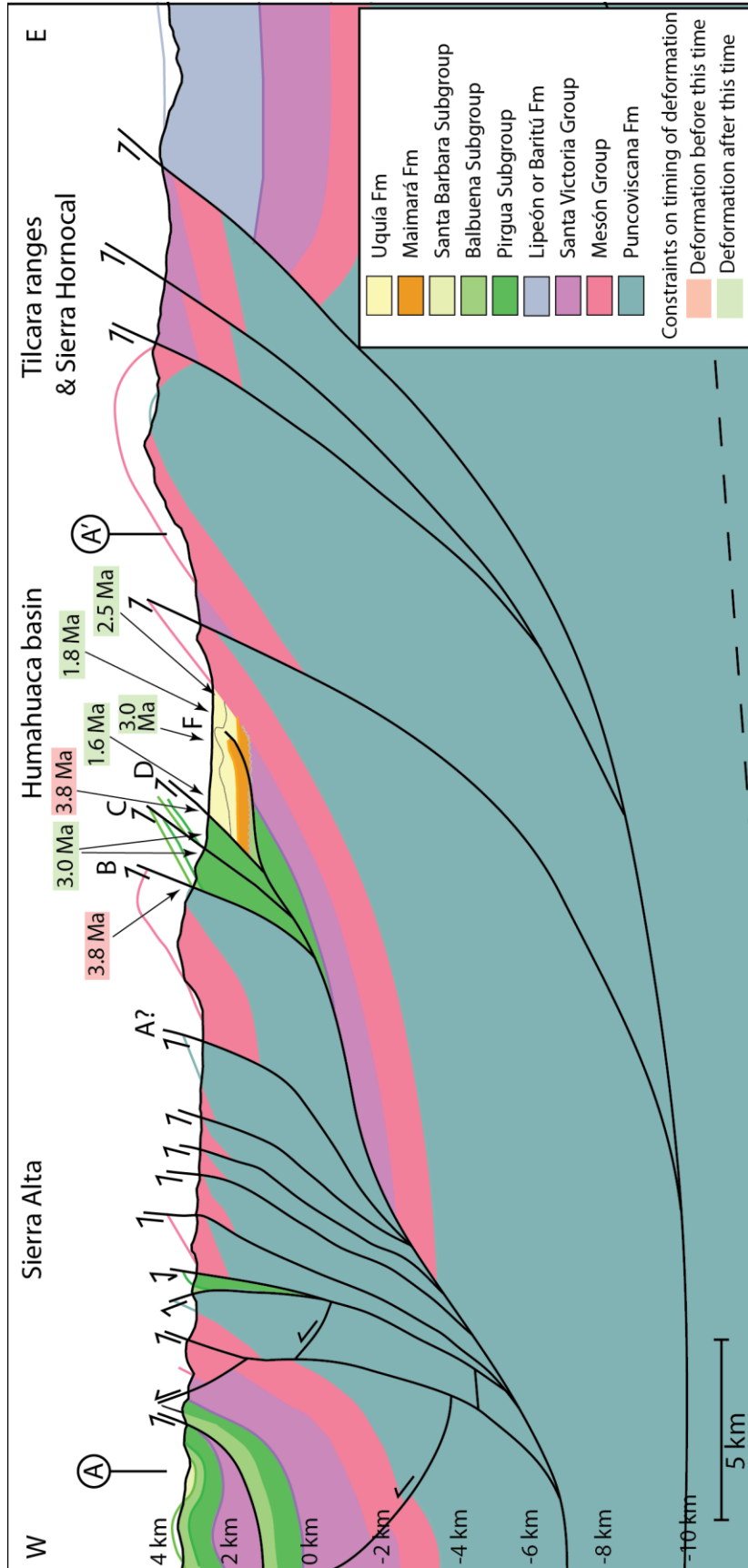


**Figure 5.** Geologic cross-section at the Río Yacoraité. Balanced cross-section was constructed using 2D kinematic modelling module of Midland Valley's Move™ software. Constraints on timing of deformation from U-Pb dating of ash layers and from magnetostratigraphy are shown in red and green boxes. Green boxes indicate that deformation occurred sometime after that date (e.g., tilted strata or dated ash high in footwall). Red boxes indicate that deformation occurred sometime before that date (e.g., strata that cap a fault and are not offset by the fault).

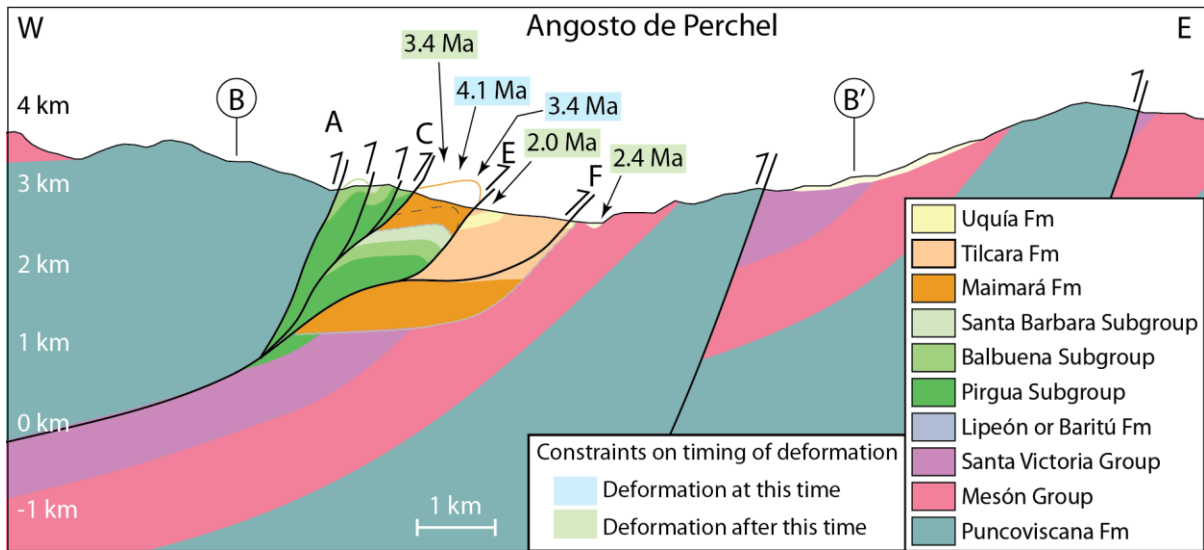


**Figure 6.** Geologic cross-section at the Angosto de Perchel. Schematic cross-section illustrates along strike variation in the style of deformation on the western margin of the Humahuaca basin. Along segment II of these faults (this section), Fault C contains closely spaced imbricated faults and tight folds. Additionally, the amount of slip on Fault F is greater at the Angosto de Perchel than near the Río Yacoraite. Radiometric constraints on timing of deformation are shown in blue and green boxes. Green boxes indicate that deformation occurred sometime after that date (e.g., tilted strata or dated ash high in footwall). Blue boxes indicate that deformation was ongoing at that time (e.g., growth strata present).



**Figure 7.** Simplified map of faults in the Humahuaca basin. Fault colors: yellow = Fault B, red = Fault C, orange = faults in hanging wall of Fault C, blue = Fault D, green = Fault E, purple = Fault F. Segments of faults on western margin of basin are labeled (I, II, III) on the left. White circles indicate sample locations that provide constraints on timing of deformation. Age labels on faults indicate when that fault was active: > means fault was not active after that time; < means the fault was active sometime after that time (but could have been active before then as well).



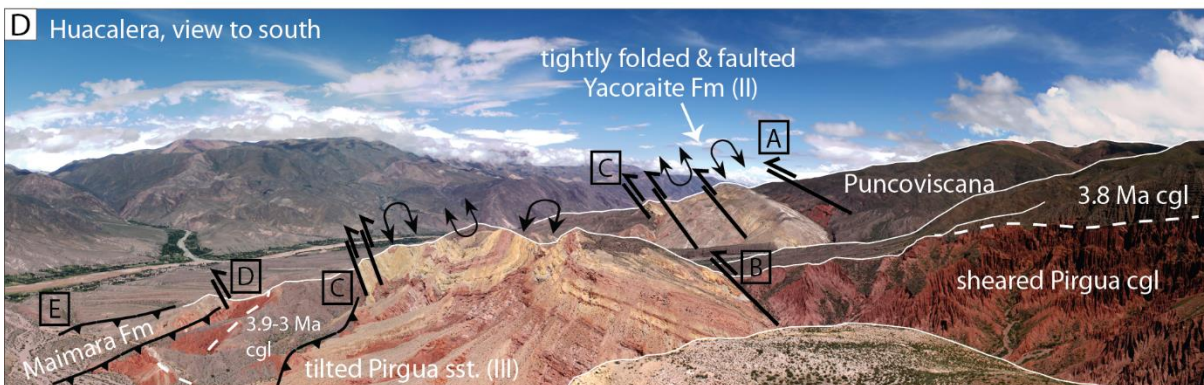
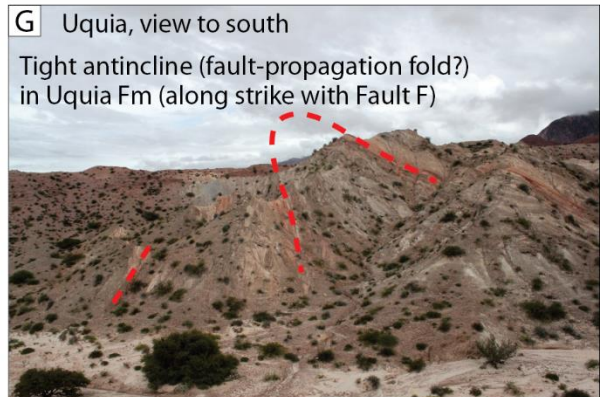
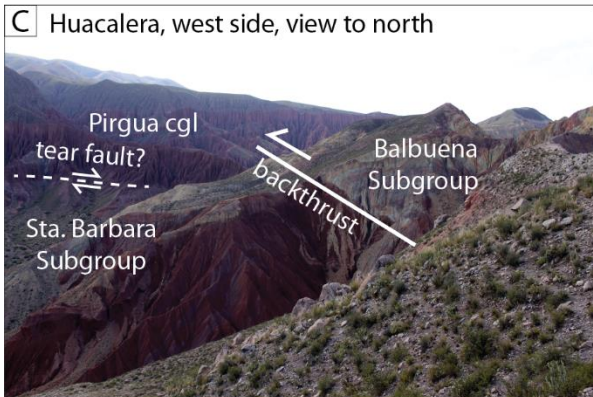
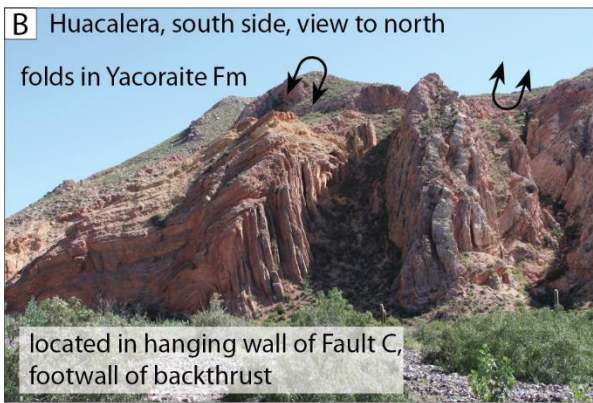
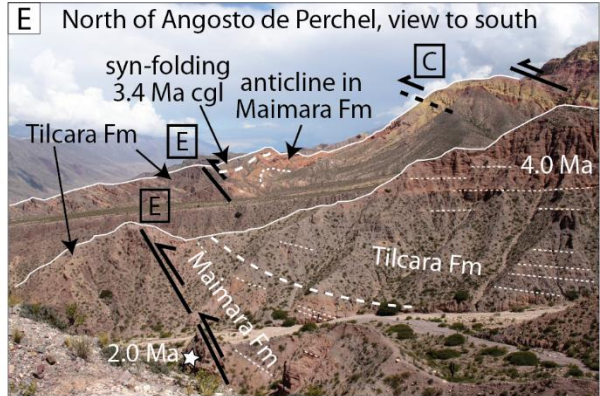
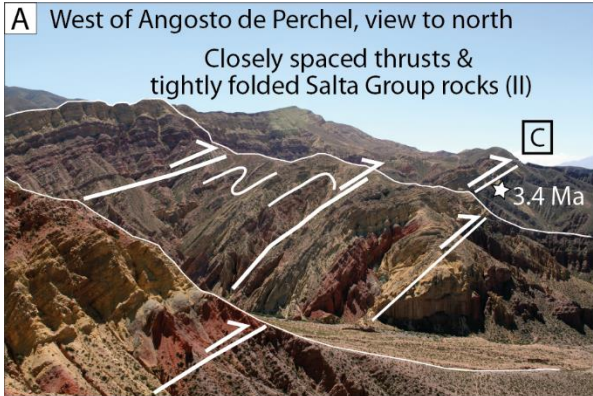


**Figure 8.** Field photos. (A) Closely-spaced thrusts and tightly folded Salta Group strata in the hanging wall of Fault C. Typical of the central segment (segment II) of the thrusts carrying Salta Group rocks on the western margin of the Humahuaca basin. (B) The Yacoraite Fm (Balbuena Subgroup) tends to form tight folds, such as the ones seen here in the hanging wall of Fault C at Huacalera. (C) Backthrust of Balbuena Subgroup over Santa Barbara Subgroup in the hanging wall of fault C at Huacalera. In background, an east-west-striking fault between the Pirgua cobble conglomerate and the Santa Barbara Fm. We interpret this as a Cretaceous normal fault that has been reactivated as an oblique tear fault. (D) Faulting and in the area west of Huacalera, which forms the boundary between the northern (III) and central (II) segments of the faults on the western margin of the basin. Note the contrasting styles of hanging wall deformation between the different members of the Salta Group: the Balbuena Subgroup (Yacoraite Fm) forms tight folds, the Pirgua conglomerate develops multiple shear zones, visible as somewhat lighter-colored bands, and the Pirgua sandstone typically lacks tight folds. The southern end of Fault D and the northern end of Fault E overlap in this area (lower left corner of the photo). Additionally, cross-cutting relationships between the faults in this area and a 3.9 – 3 Ma conglomerate containing dated ashes (lower left of photo) provide constraints on the timing of deformation. (E) Fault E thrusts the Maimará Fm and overlying Tilcara Fm (4.3 – 3.4 Ma) over younger (2.0 Ma) Tilcara Fm strata. (F) Angular unconformity at the top of the Maimará Fm indicates 10-15° westward tilting at Huacalera between 5-4.4 Ma. (G) Tight anticline in the Uquía Fm interpreted as fault propagation fold related to Fault F.

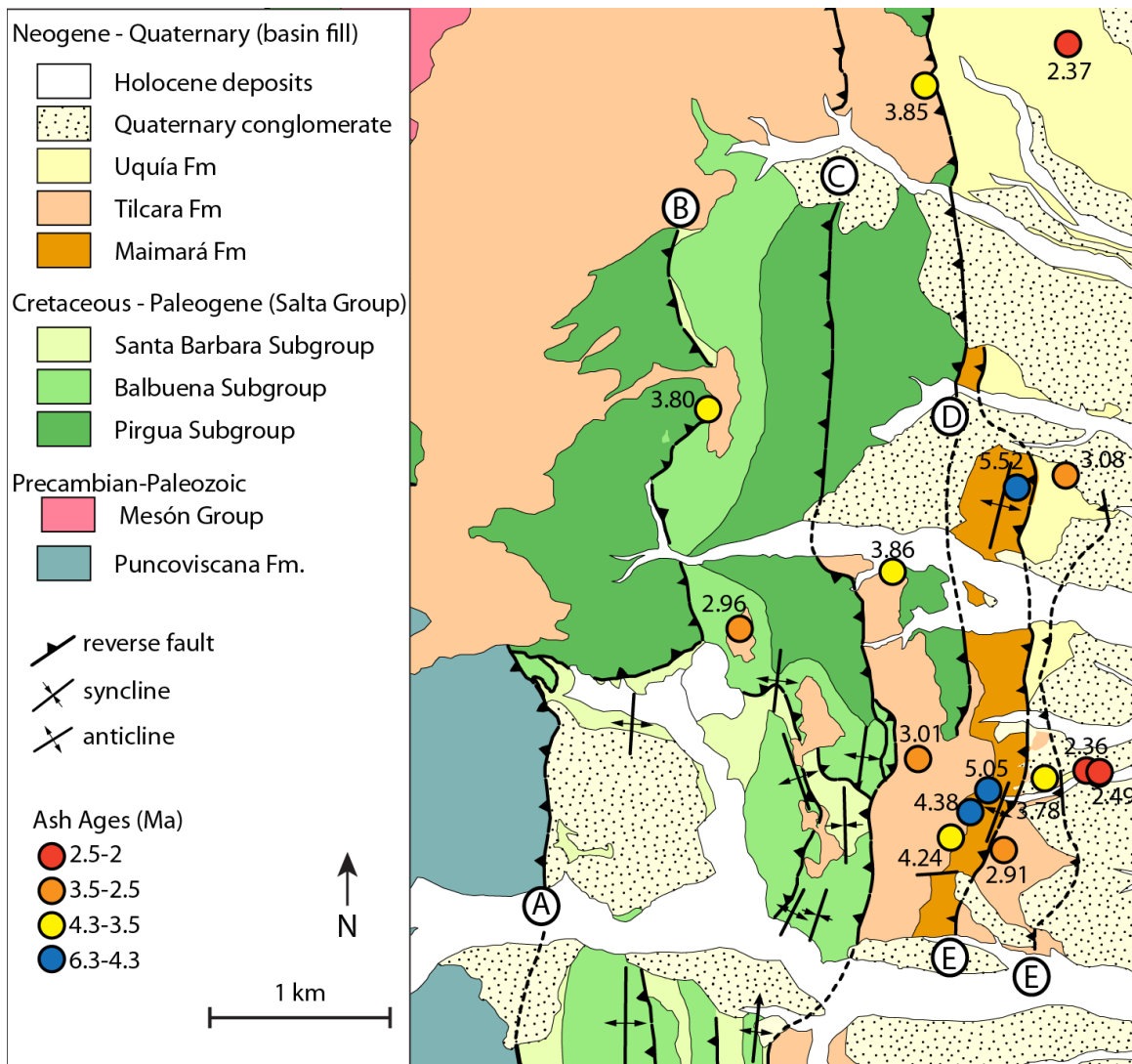


**Figure 9.** More detailed geologic map of Huacalera area. Note more complicated structure at this boundary between northern and central segments of faults on western margin of the basin. Colored circles show the location and zircon U-Pb age of ashes used to constrain timing of deformation.



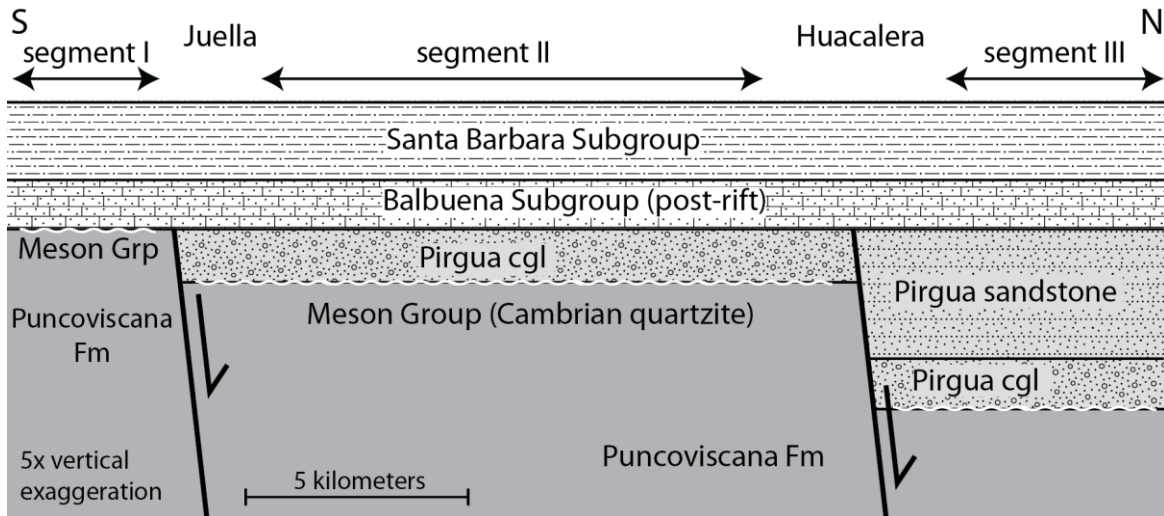


**Figure 10.** Structural inheritance of cretaceous rifting. Along the western margin of the Humahuaca basin, segmentation of faults with Salta Group (Pirgua, Balbuena, and Santa Barbara Subgroups) rocks in their hanging wall is related to Cretaceous rift-related normal faults. These normal faults create boundaries between the major segments of the Humahuaca fault system and control both the thickness of Pirgua Subgroup deposits and the depth to the potential detachment horizon at the unconformity (white wavy line) between the Salta Group and underlying Paleozoic rocks.



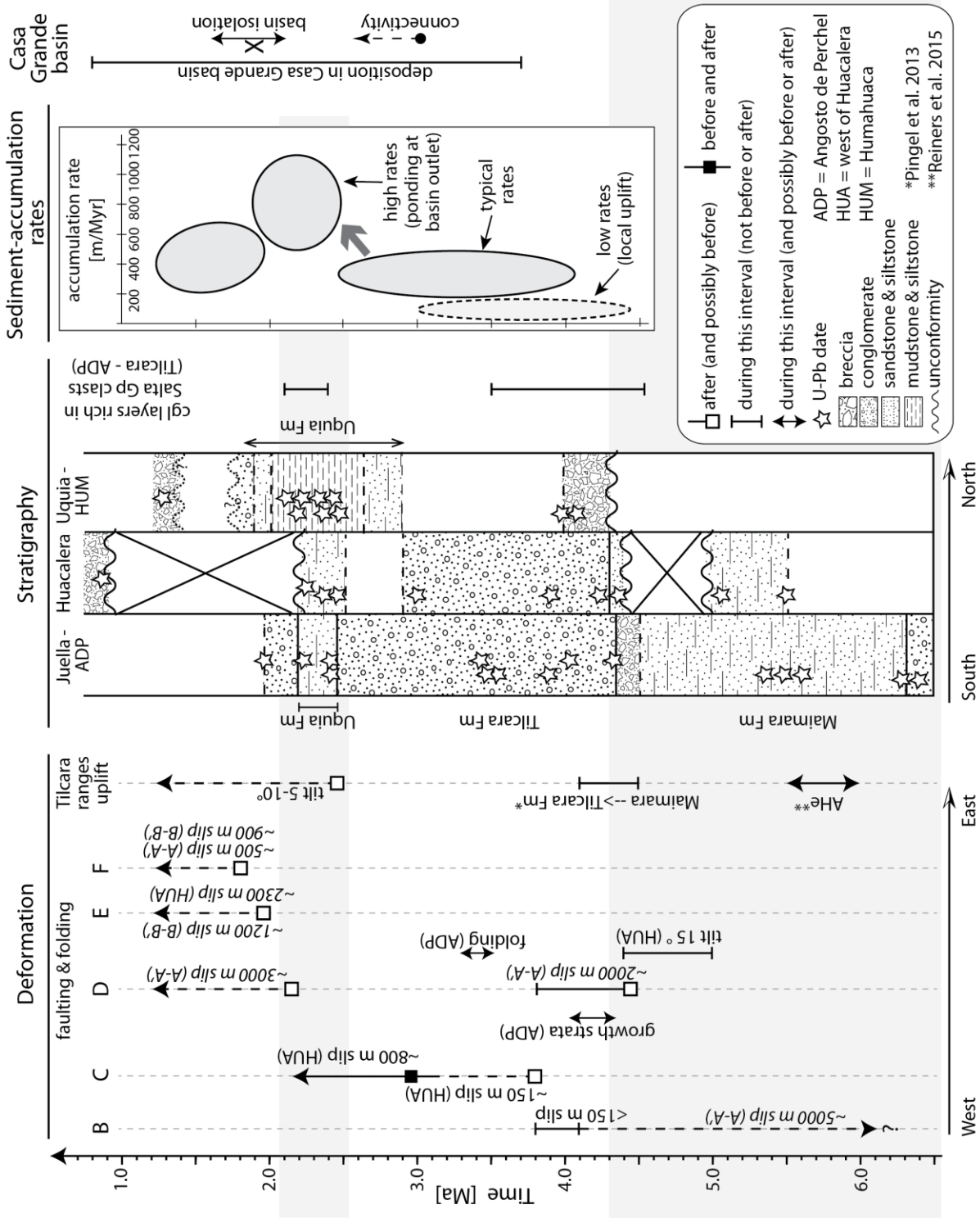


Figure 11. Timing of deformation in relation to other events in the Humahuaca basin.

## Appendix A

Effect of basin geometry on sediment-accumulation rate, under constant sediment flux.

| Initial basin width                         | Slope of basin sides | Sediment accumulation from 0-1Myr | Sediment accumulation from 1-2Myr | % change in vertical sediment-accumulation rate |
|---|----------------------|-----------------------------------|-----------------------------------|---|
| Basin geometry: isosceles trapezoidal prism |                      |                                   |                                   |   |
| 1 km  | 1°                   | 50 m                              | 24 m                              | -52.3%  |
|   | 5°                   | 50 m                              | 31 m                              | -37.2%  |
|   | 15°                  | 50 m                              | 39 m                              | -21.9%  |
|   | 30°                  | 50 m                              | 44 m                              | -13%  |
| 5 km  | 1°                   | 50 m                              | 31 m                              | -37.2%  |
|   | 5°                   | 50 m                              | 42 m                              | -15.9%  |
|   | 15°                  | 50 m                              | 47 m                              | -6.5%   |
|   | 30°                  | 50 m                              | 48 m                              | -3.2%   |
| 10 km                                       | 1°                   | 50 m                              | 36 m                              | -27.7%  |
|   | 5°                   | 50 m                              | 45 m                              | -9.3%   |
|   | 15°                  | 50 m                              | 48 m                              | -3.5%   |
|   | 30°                  | 50 m                              | 49 m                              | -1.7%   |
| 10 km                                       | 1°                   | 100 m                             | 63 m                              | -37.2%  |
|   | 5°                   | 100 m                             | 84 m                              | -15.9%  |
|   | 15°                  | 100 m                             | 93 m                              | -6.5%   |
|   | 30°                  | 100 m                             | 97 m                              | -3.2%   |
| Basin geometry: Conical frustrum            |                      |                                   |                                   |   |
| 1 km  | 1°                   | 50 m                              | 15 m                              | -69.6%  |
|   | 5°                   | 50 m                              | 22 m                              | -55.3%  |
|   | 15°                  | 50 m                              | 32 m                              | -36.4%  |
|   | 30°                  | 50 m                              | 38 m                              | -23.1%  |
| 5 km  | 1°                   | 50 m                              | 22 m                              | -55.4%  |
|   | 5°                   | 50 m                              | 36 m                              | -27.6%  |
|   | 15°                  | 50 m                              | 44 m                              | -12.2%  |
|   | 30°                  | 50 m                              | 47 m                              | -6.3%   |
| 10 km                                       | 1°                   | 50 m                              | 28 m                              | -44.1%  |
|   | 5°                   | 50 m                              | 41 m                              | -17.1%  |
|   | 15°                  | 50 m                              | 47 m                              | -6.7%   |
|   | 30°                  | 50 m                              | 48 m                              | -3.3%   |

## **Appendix B**

### **Supplemental files available online:**

**Table S1.** LA-ICPMS zircon U-Pb geochronology data from ashes. (Excel file)

**Table S2.** Magnetostratigraphy data. (Excel file)

**Table S3.** Detrital zircon LA-ICPMS U-Pb data. (Excel file)

**Table S4.** Structural data: bedding and fault plane orientations. (Excel file)